RL-TR-95-215
Final Technical Report
October 1995

RADAR SIGNAL DETECTION AND ESTIMATION USING TIME-FREQUENCY DISTRIBUTIONS

Syracuse University

Pramod K. Varshney, Donald D. Weiner, and Tzeta Tsao

19960304 087

Rome Laboratory
Air Force Materiel Command
Rome, New York

DTIC QUALITY INSPECTED 1

This report has been reviewed by the Rome Laboratory Public Affairs Office (PA) and is releasable to the National Technical Information Service (NTIS). At NTIS, it will be releasable to the general public, including foreign nations.

RL-TR-95- 215 has been reviewed and is approved for publication.

APPROVED: *Stanley E. Borek*

STANLEY E. BOREK
Project Engineer

FOR THE COMMANDER: *Donald W. Hanson*

DONALD W. HANSON
Director of Surveillance & Photonics

REPORT DOCUMENTATION PAGE

Public reporting burden for this collection of information is estimated to average 1 hour per response, including the time for reviewing instructions, searching existing data sources, gathering and maintaining the data needed, and completing and reviewing the collection of information. Send comments regarding this burden estimate or any other aspect of this collection of information, including suggestions for reducing this burden, to Washington Headquarters Services, Directorate for Information Operations and Reports, 1215 Jefferson Davis Highway, Suite 1204, Arlington, VA 22202-4302, and to the Office of Management and Budget, Paperwork Reduction Project (0704-0188), Washington, DC 20503.

1. AGENCY USE ONLY (Leave Blank)	2. REPORT DATE October 1995	3. REPORT TYPE AND DATES COVERED Final May 93 – May 94

4. TITLE AND SUBTITLE

RADAR SIGNAL DETECTION AND ESTIMATION USING TIME-FREQUENCY DISTRIBUTIONS

6. AUTHOR(S)

Pramod K. Varshney, Donald D. Weiner, and Tzeta Tsao

5. FUNDING NUMBERS

C - F30602-93-C-0155
PE - 61102F
PR - 2304
TA - E8
WU - P9

7. PERFORMING ORGANIZATION NAME(S) AND ADDRESS(ES)

Syracuse University
Electrical and Computer Engineering Department
Syracuse NY 13244

8. PERFORMING ORGANIZATION REPORT NUMBER

N/A

9. SPONSORING/MONITORING AGENCY NAME(S) AND ADDRESS(ES)

Rome Laboratory/OCSA
26 Electronic Pky
Rome NY 13441-4514

10. SPONSORING/MONITORING AGENCY REPORT NUMBER

RL-TR-95-215

11. SUPPLEMENTARY NOTES

Rome Laboratory Project Engineer: Stanley E. Borek/OCSA/(315) 330-7013

12a. DISTRIBUTION/AVAILABILITY STATEMENT

Approved for public release; distribution unlimited.

12b. DISTRIBUTION CODE

13. ABSTRACT (Maximum 200 words)

This report addresses the issues related to the applications of time-frequency distributions in radar signal detection and parameter estimation problems. The Wigner-Ville distribution, the ambiguity function, and the time-frequency correlation function are the time-frequency distributions considered. The analysis considers a number of alternative radar receiver structures based on discrete time-frequency distributions. Various forms of the discrete ambiguity function and the discrete Wigner-Ville distribution are studied and their properties analyzed. New interpolation formulas are developed. Derivations of receivers based on the discrete time-frequency distribution display the potential for aliasing. The effects of aliasing on the optimality of these receivers are analyzed. Sampling criteria to prevent aliasing are determined and schemes to reduce the sampling requirement are devised. Since digital devices are of fixed register length, the signals processed are quantized and the arithmetic performed is of finite precision. The effect of the related quantization error from these devices in discrete time-frequency distribution based receivers is analyzed. Issues concerning the effect of coefficient quantization due to either storage or in-place computation in the fast Fourier transform (FFT) are discussed and clarified. A bound on the mean-square magnitude of the discrete ambiguity function is developed. Simulations are utilized to verify and validate the results.

14. SUBJECT TERMS

Aliasing, Sampling criteria, Quantization error, Time-frequency distributions, Radar signal detection, Parameter estimation, Wigner-Ville distribution, Ambiguity function, (see reverse)

15. NUMBER OF PAGES
208

16. PRICE CODE

17. SECURITY CLASSIFICATION OF REPORT UNCLASSIFIED	18. SECURITY CLASSIFICATION OF THIS PAGE UNCLASSIFIED	19. SECURITY CLASSIFICATION OF ABSTRACT UNCLASSIFIED	20. LIMITATION OF ABSTRACT UL

14. (Cont'd)

Time-frequency correlation function, Radar receiver structures

Contents

List of Figures

iv

Glossary

The principal symbols used in this report are defined below. In many cases different subscripts are given to an existing symbol to reflect the particular condition considered. Since this modification is usually obvious, the resulting symbol may not be included here.

B One-sided bandwidth of a complex signal

$\tilde{b}$ Complex Gaussian random variable describing target reflection

β Bistatic angle

c Wave propagation speed

$\delta(t)$ Dirac delta function

δ_{ij} Kronecker delta function

E_t Energy of a signal

$e_{\tilde{s}}$ Error of quantizing $\tilde{s}$

ϵ Jitter noise in a coefficient

f_c Carrier frequency

f_{D_a} Actual Doppler shift of the target return

f_{D_H} Hypothesized Doppler shift

γ	Threshold
$I(\cdot)$	Modified Bessel function
$J(\cdot)$	Bessel function
Λ	Likelihood ratio
λ	Wave length
μ^2	Signal sample power
$\tilde{n}$	Noise complex envelope
$\tilde{\Phi}_i$	ith basis function in Karhunen-Loeve expansion
$\phi_{\tilde{s}}(\cdot)$	Continuous time-frequency correlation function of $\tilde{s}(t)$
$\phi_{\tilde{s}_1\tilde{s}_2}(\cdot)$	Continuous cross-time-frequency correlation function of $\tilde{s}_1(t)$ and $\tilde{s}_2(t)$
$\hat{\phi}_{\hat{S}}(\cdot)$	Discrete time-frequency correlation function of $\tilde{s}(t)$ in the frequency-domain
$\hat{\phi}_{\tilde{s}}(\cdot)$	Discrete time-frequency correlation function of $\tilde{s}(t)$ in the time-domain
$\bar{\phi}_{\hat{S}_1\hat{S}_2}(\cdot)$	Symmetric form of the discrete cross-time-frequency correlation function of $\tilde{s}_1(t)$ and $\tilde{s}_2(t)$ in the frequency-domain
$\bar{\phi}_{\tilde{s}_1\tilde{s}_2}(\cdot)$	Symmetric form of the discrete cross-time-frequency correlation function of $\tilde{s}_1(t)$ and $\tilde{s}_2(t)$ in the time-domain
$\check{\phi}_{\hat{S}_1\hat{S}_2}(\cdot)$	Discrete time-frequency correlation function of $\tilde{s}_1(t)$ and $\tilde{s}_2(t)$ by zero padding $\hat{\phi}_{\hat{S}_1\hat{S}_2}(\cdot)$
$\check{\phi}_{\tilde{s}_1\tilde{s}_2}(\cdot)$	Discrete time-frequency correlation function of $\tilde{s}_1(t)$ and $\tilde{s}_2(t)$ by zero padding $\hat{\phi}_{\tilde{s}_1\tilde{s}_2}(\cdot)$

$\hat{\phi}_{\hat{S}_1 \hat{S}_2}(\cdot)$ Discrete cross-time-frequency correlation function of $\tilde{s}_1(t)$ and $\tilde{s}_2(t)$ in frequency-domain

$\hat{\phi}_{\tilde{s}_1 \tilde{s}_2}(\cdot)$ Discrete cross-time-frequency correlation function of $\tilde{s}_1(t)$ and $\tilde{s}_2(t)$ in the time-domain

$\tilde{r}$ Complex envelope of the received signal

$\tilde{S}(f)$ Fourier transform of $\tilde{s}(t)$

$\tilde{s}(t)$ Complex envelope of a continuous signal

$\tilde{s}_T(t)$ Complex envelope of the transmitted signal

$\tilde{s}_R(t)$ Complex envelope of the target return

$\hat{\boldsymbol{S}}$ Column vector of discrete Fourier transform of $\tilde{\boldsymbol{s}}$

$\tilde{\boldsymbol{s}}$ Column vector of samples of $\tilde{s}(t)$

σ_n^2 Noise variance

T Signal duration

T_s Sampling period

τ_a Actual delay of the target return

τ_H Hypothesized delay

$\theta_{\tilde{s}}(\cdot)$ Continuous ambiguity function of $\tilde{s}(t)$

$\theta_{\tilde{s}_1 \tilde{s}_2}(\cdot)$ Continuous cross-ambiguity function of $\tilde{s}_1(t)$ and $\tilde{s}_2(t)$

$\hat{\theta}_{\hat{S}}(\cdot)$ Discrete ambiguity function of $\tilde{s}(t)$ in frequency-domain

$\hat{\theta}_{\tilde{s}}(\cdot)$ Discrete ambiguity function of $\tilde{s}(t)$ in the time-domain

$\bar{\theta}_{\hat{S}_1\hat{S}_2}(\cdot)$ Symmetric form of the discrete cross-ambiguity function of $\tilde{s}_1(t)$ and $\tilde{s}_2(t)$ in frequency-domain

$\bar{\theta}_{\tilde{s}_1\tilde{s}_2}(\cdot)$ Symmetric form of the discrete cross-ambiguity function of $\tilde{s}_1(t)$ and $\tilde{s}_2(t)$ in time-domain

$\hat{\theta}_{\hat{S}_1\hat{S}_2}(\cdot)$ Discrete cross-ambiguity function of $\tilde{s}_1(t)$ and $\tilde{s}_2(t)$ in the frequency-domain

$\hat{\theta}_{\tilde{s}_1\tilde{s}_2}(\cdot)$ Discrete cross-ambiguity function of $\tilde{s}_1(t)$ and $\tilde{s}_2(t)$ in the time-domain

$W_{\tilde{s}}(\cdot)$ Continuous Wigner-Ville distribution of $\tilde{s}(t)$

$W_{\tilde{s}_1\tilde{s}_2}(\cdot)$ Continuous cross-Wigner-Ville distribution of $\tilde{s}_1(t)$ and $\tilde{s}_2(t)$

$\hat{W}_{\hat{S}}(\cdot)$ Discrete Wigner-Ville distribution of $\tilde{s}(t)$ in frequency-domain

$\hat{W}_{\tilde{s}}(\cdot)$ Discrete Wigner-Ville distribution of $\tilde{s}(t)$ in the time-domain

$\bar{W}_{\hat{S}_1\hat{S}_2}(\cdot)$ Symmetric form of the discrete cross-Wigner-Ville distribution of $\tilde{s}_1(t)$ and $\tilde{s}_2(t)$ in the frequency-domain

$\bar{W}_{\tilde{s}_1\tilde{s}_2}(\cdot)$ Symmetric form of the discrete cross-Wigner-Ville distribution of $\tilde{s}_1(t)$ and $\tilde{s}_2(t)$ in the time-domain

$\check{W}_{\hat{S}_1\hat{S}_2}(\cdot)$ Discrete Wigner-Ville distribution of $\tilde{s}_1(t)$ and $\tilde{s}_2(t)$ by zero padding $\bar{\phi}_{\hat{S}_1\hat{S}_2}(\cdot)$

$\check{W}_{\tilde{s}_1\tilde{s}_2}(\cdot)$ Discrete Wigner-Ville distribution of $\tilde{s}_1(t)$ and $\tilde{s}_2(t)$ by zero padding $\bar{W}_{\tilde{s}_1\tilde{s}_2}(\cdot)$

$\hat{W}_{\hat{S}_1\hat{S}_2}(\cdot)$ Discrete cross-Wigner-Ville distribution of $\tilde{s}_1(t)$ and $\tilde{s}_2(t)$ in the frequency-domain

$\hat{W}_{\tilde{s}_1\tilde{s}_2}(\cdot)$ Discrete cross-Wigner-Ville distribution of $\tilde{s}_1(t)$ and $\tilde{s}_2(t)$ in the time-domain

Chapter 1

Introduction

In recent years considerable effort has been devoted to the analysis and application of time-frequency distributions, for example, [1], [2] and the references listed therein. This type of signal representation characterizes signals over the time-frequency plane. Ideally, it gives a temporal localization of a signal's spectral components and combines time-domain and frequency-domain analyses. The time-frequency correlation function [3] and the Wigner-Ville distribution [4] belong to the class of quadratic time-frequency distributions. The magnitude square of a time-frequency correlation function is the ambiguity function [5]. This work considers several important issues arising with application of the ambiguity function and Wigner-Ville distribution to radar signal detection and estimation. The analysis is from a radar receiver structure standpoint.

It is shown in the literature [6]-[10] that a receiver based on the Wigner-Ville distribution presents an alternative to the conventional receiver. A conventional receiver is built in such a manner that it performs matched-filtering of the received signal. It is proposed that the receiver be built in such a manner that it performs matched-filtering of the Wigner-Ville distribution of the received signal, i.e., the Wigner-Ville distribution of the reference signal is matched to the Wigner-Ville distribution of the received signal. This alternative not only retains the optimality but also possesses other merits. For example, the receiver based

1

on the Wigner-Ville distribution will enable the estimation of unknown parameters when the problem is not completely specified. In addition, noise suppression using time-variant filtering in such receivers, when the signal waveshape is unknown, is more effective [7]. It has also been proposed that the optimum receiver can be built based on the time-frequency correlation function [11]. This receiver is computationally more tractable for linear *fm* signals. However, the proposed forms of the above alternative receivers still suffer from the drawback that the test statistic is calculated inefficiently since it is calculated point by point in the hypothesized delay-Doppler plane.

While digital processing is the trend in practice, research efforts devoted to the subject of finding a better structure for the receiver have been mostly addressed to the continuous case. In the work that considered or utilized discrete signals, for example, [13] and [9], the optimal form of the receiver was either not of concern or not successfully derived, although the discrete Wigner-Ville distribution itself has received a lot of attention [13]-[15]. It appears that aliasing effects are the major hindrance to the development of the optimum discrete receiver. Therefore, a receiver based on the discrete Wigner-Ville distribution, which allows a more efficient computation of the test statistic has yet to be derived. Furthermore, the possibilities of implementing receivers based on other types of discrete time-frequency distributions still need to be explored.

Since discrete receivers are in fact implemented with digital devices of finite register length, the signals processed are quantized and the arithmetic performed are of finite precision. The effects of quantization and finite precision arithmetic can be viewed 'as introducing additional noise sources. Therefore, an assessment of how much more noise will be introduced in the discrete time-frequency distribution based receivers is needed to complete the analysis for such receivers.

This report is organized as follows. In the first section of this chapter, we derive the target model assumed throughout the entire work. In Section 2 of this chapter, we present

the derivation of the ambiguity function from the basic principles of detection and estimation theory to give a better understanding of its role in radar applications. In Section 3 of this chapter, we introduce the Wigner-Ville distribution and derive some of its properties pertaining to the development of alternative structures for the continuous signal optimum receiver. In concluding this chapter, we discuss the advantages of a time-frequency formulation of the optimum receiver.

Chapter 2 is devoted to derivation of various versions of the discrete ambiguity function and Wigner-Ville distribution. This chapter starts with a review of the problem of radar detection and estimation using sampled signals. This analysis will serve as a basis for building the optimum discrete receiver. As a direct result, it shows the manner in which the discrete ambiguity function arises from the conventional optimum discrete receiver. Then, to prevent degradation of receiver performance we consider the sampling criteria needed to ensure that aliasing does not occur with regard to the discrete ambiguity function. Also, we propose an interpolation formula which is simpler than those found in the references to transform between the discrete and continuous ambiguity function. Attention is then turned to a review of derivations of various versions of the discrete Wigner-Ville distribution. Sampling criteria and interpolation formulas are studied. A new interpolation formula that is simpler than the one found in the references is also derived for the discrete Wigner-Ville distribution. The interpolation formulas proposed in this work are restrictive in the sense that they can only be used to recover the alias-free portions of the respective time-frequency distributions. The interpolation formulas are considered only for the sake of completeness, and are not needed for the optimum receiver.

In Chapter 3, we consider a variety of alternative realizations to the optimum discrete receiver. Derivation of the optimum discrete Wigner-Ville distribution based receiver is presented and a technique for eliminating undesired aliasing is introduced. Then we consider a second implementation of the optimum receiver based on the discrete time-frequency auto-

correlation function whose squared magnitude is the ambiguity function; this latter method has computational advantages over the one based on the discrete Wigner-Ville distribution.

Having derived various forms of the optimum discrete receiver, we proceed in Chapter 4 to analyze quantization effect in these receivers. The result is useful for analyzing the computational error when calculating with finite precision arithmetic the discrete ambiguity function, time-frequency correlation function, and Wigner-Ville distribution.

Finally, in Chapter 5 we present a summary and discussion of results developed herein.

1.1   Slowly Fluctuating Point Target

Ambiguity functions are typically derived assuming a slowly fluctuating point target. The model associated with such a target is developed here.

Assume a target has scatterers distributed over the range interval (R_1, R_2), in the propagation direction of an electromagnetic pulse. Let t_i denote the instant at which the leading edge of the pulse reaches range R_i where $i = 1, 2$. We assume the time origin to correspond to the instant at which the leading edge of the pulse appears at the transmitting antenna. If T denotes the time duration of the transmitted pulse, we say that the target can be modeled as a point target provided

$$t_2 - t_1 \ll T, \tag{1.1}$$

or equivalently,

$$R_2 - R_1 \ll n\lambda \tag{1.2}$$

where n is the number of complete cycles of the carrier in the transmitted pulse, and λ is the wavelength. It should be noted that, if the transmitted waveform consists of a sequence of several pulses, n still refers to the number of carrier cycles in one pulse. For convenience, some people use the more restrictive condition

$$R_2 - R_1 \ll \lambda \tag{1.3}$$

4

in order to define a point target.

To examine the significance of the term "slowly fluctuating", assume that the transmitted pulse is given by

$$s_T(t) = \sqrt{2} \text{Re} \left\{ \sqrt{E_t} \tilde{s}(t) \exp(j2\pi f_c t) \right\} \tag{1.4}$$

where $\text{Re}\{\cdot\}$ denotes the real part operation, $\tilde{s}(t)$ is the complex envelope of the transmitted pulse, and f_c is the carrier frequency. Let the complex envelope be normalized such that

$$\int_{-\infty}^{\infty} |\tilde{s}|^2 \, dt = 1. \tag{1.5}$$

Then, the energy of the transmitted signal is equal to E_t.

For a monostatic radar, assume that a point target is located at range R_a with radial velocity V_a. Let the point target consist of a rough surface with K scatterers. The received waveform due to the reflection from the ith scatterer can be approximated by [5]

$$s_i(t) = \sqrt{2} \text{Re} \left\{ \sqrt{E_t} g_i \exp(j\theta_i) \tilde{s}(t - \tau_a) \exp[j2\pi(f_c + f_{D_a})(t - \tau_a)] \right\} \tag{1.6}$$

where g_i and θ_i denote the attenuation and phase, respectively, incurred in the reflection process, $\tau_a = 2R_a/c$ denotes the round-trip time delay and

$$f_{D_a} = \frac{2V_a}{c} f_c \tag{1.7}$$

is the shift in the carrier frequency due to radial velocity of the target. In this expression f_{D_a} is called the Doppler shift. Summing the returns from the K scatterers, the total received waveform is

$$
\begin{aligned}
s_R(t) &= \sum_{i=1}^{K} s_i(t) \\
&= \sqrt{2} \text{Re} \left\{ \sqrt{E_t} \left[\sum_{i=1}^{K} g_i \exp(j\theta_i) \right] \tilde{s}(t - \tau_a) \exp[j2\pi(f_c + f_{D_a})(t - \tau_a)] \right\} \\
&= \sqrt{2} \text{Re} \left\{ \sqrt{E_t} \tilde{b} \tilde{s}(t - \tau_a) \exp[j2\pi(f_c + f_{D_a})(t - \tau_a)] \right\}
\end{aligned}
\tag{1.8}
$$

where the operations of summation and real part have been interchanged and

$$\tilde{b} = \sum_{i=1}^{K} g_i \exp(j\theta_i) = \sum_{i=1}^{K} \tilde{g}_i. \tag{1.9}$$

Assuming that the complex random numbers $\tilde{g}_i$ are statistically independent, that none of the scatterers are dominant and that K is sufficiently large, we can use a central limit theorem argument to conclude that $\tilde{b}$ is a zero-mean complex Gaussian random variable. It follows that $|\tilde{b}|$ is a Rayleigh distributed random variable and the phase of $\tilde{b}$ is a uniformly distributed random variable. Absorbing the constant factors $\exp(-j2\pi f_{D_a}\tau_a)$ and $\exp(-j2\pi f_c\tau_a)$ into the phase component of $\tilde{b}$, the total received signal becomes

$$s_R(t) = \sqrt{2}\text{Re}\left\{\sqrt{E_t}\tilde{b}\tilde{s}(t-\tau_a)\exp[j2\pi(f_c+f_{D_a})t]\right\}. \tag{1.10}$$

The point target is defined to be slowly fluctuating provided that $\tilde{b}$ remains constant while the target is illuminated by the transmitted pulse of duration T. Having defined what is meant by a slowly fluctuating point target, we now show how the ambiguity function arises in the radar detection and parameter estimation problems.

1.2 Ambiguity Function

In detection problems, we are interested in determining whether a slowly fluctuating point target, at range R with radial velocity V, is located at the point

$$\left(\tau_H = \frac{2R}{c}, f_{D_H} = \frac{2V}{c}f_c\right) \tag{1.11}$$

in the delay-Doppler plane. In the absence of a target, the complex envelope of the received waveform is assumed to be

$$\tilde{r}(t) = \tilde{n}(t), \quad \tau_H \le t \le \tau_H + T \tag{1.12}$$

where $\tilde{n}(t)$ denotes the complex envelope of a Gaussian white noise process. On the other hand, if a slowly fluctuating point target is located at the point (τ_H, f_{D_H}) in the delay-Doppler plane, the complex envelope of the received waveform is

$$\tilde{r}(t) = \sqrt{E_t}\tilde{b}\tilde{s}(t-\tau_H)\exp(j2\pi f_{D_H}t) + \tilde{n}(t), \quad \tau_H \le t \le \tau_H + T. \tag{1.13}$$

6

Hence, given the two hypotheses

$$H_0: \quad \tilde{r}(t) = \tilde{n}(t)$$
$$H_1: \quad \tilde{r}(t) = \sqrt{E_t}\tilde{b}\tilde{s}(t - \tau_H)\exp(j2\pi f_{D_H}t) + \tilde{n}(t) \quad \tau_H \leq t \leq \tau_H + T \qquad (1.14)$$

we wish to determine the Neyman-Pearson receiver, i.e., the receiver that maximizes the detection probability for a specified false alarm probability when detecting a slowly fluctuating point target at the hypothesized point (τ_H, f_{D_H}) in the delay-Doppler plane.

For this purpose, it is convenient to expand $\tilde{r}(t)$ in a Karhunen-Loeve expansion as given by

$$\tilde{r}(t) = \sum_{i=1}^{\infty} \tilde{r}_i\tilde{\Phi}_i(t), \quad \tau_H \leq t \leq \tau_H + T. \qquad (1.15)$$

Because $\tilde{b}$ is a complex Gaussian random variable and $\tilde{n}(t)$ is a complex white Gaussian random process, the coefficients

$$\tilde{r}_i = \int_{\tau_H}^{\tau_H+T} \tilde{r}(t)\tilde{\Phi}_i^*(t)dt \qquad (1.16)$$

are statistically independent complex Gaussian random variables. In addition, since the noise is white, the basis functions $\tilde{\Phi}_i(t)$ can be chosen from any set which is complete and orthonormal over the interval $\tau_H \leq t \leq \tau_H + T$. For convenience, let the first basis function be

$$\tilde{\Phi}_1(t) = \tilde{s}(t - \tau_H)\exp(j2\pi f_{D_H}t). \qquad (1.17)$$

The first coefficient in the expansion of $\tilde{r}(t)$ is then

$$\tilde{r}_1 = \int_{\tau_H}^{\tau_H+T} \tilde{r}(t)\tilde{s}^*(t - \tau_H)\exp(-j2\pi f_{D_H}t)dt = \begin{cases} \tilde{n}_1 & : H_0 \\ \sqrt{E_t}\tilde{b} + \tilde{n}_1 & : H_1 \end{cases} \qquad (1.18)$$

where

$$\tilde{n}_1 = \int_{\tau_H}^{\tau_H+T} \tilde{n}(t)\tilde{s}^*(t - \tau_H)\exp(-j2\pi f_{D_H}t)dt \qquad (1.19)$$

is the first coefficient in the Karhunen-Loeve expansion of the complex white noise process. Let

$$E\left[|\tilde{n}_1|^2\right] = \sigma_n^2 \text{ and } E\left[|\tilde{b}|^2\right] = 2\sigma_b^2. \qquad (1.20)$$

7

It follows that the conditional probability density functions of $\tilde{r}_1$ are given by

$$p_{\tilde{r}_1|H_0}(\tilde{R}_1|H_0) = \frac{1}{\pi\sigma_n^2}\exp\left(-\frac{|\tilde{R}_1|^2}{\sigma_n^2}\right) \tag{1.21}$$

and

$$p_{\tilde{r}_1|H_1}(\tilde{R}_1|H_1) = \frac{1}{\pi(2\sigma_b^2 E_t + \sigma_n^2)}\exp\left(-\frac{|\tilde{R}_1|^2}{2\sigma_b^2 E_t + \sigma_n^2}\right). \tag{1.22}$$

The remaining orthonormal functions in the basis set can be selected in any convenient manner. For $i > 1$, the ith coefficient in the Karhunen-Loeve expansion of $\tilde{r}(t)$ is

$$\tilde{r}_i = \begin{cases} \tilde{n}_i & H_0 \\ \tilde{n}_i & H_1 \end{cases}, i > 1 \tag{1.23}$$

where $\tilde{n}_i$ is the ith coefficient in the Karhunen-Loeve expansion of $\tilde{n}(t)$. Since $\tilde{n}(t)$ is a complex Gaussian white noise process, $\tilde{n}_i$, $i > 1$, is statistically independent of $\tilde{n}_1$. Also, by assumption, $\tilde{n}_i$ is statistically independent of $\tilde{b}$. Thus, $\tilde{r}_i$, $i > 1$, contains no information either about the target return or the noise coefficient $\tilde{n}_1$. It follows that $\tilde{r}_1$ is a sufficient statistic. The log likelihood ratio is given by

$$\ln\left[\frac{p_{\tilde{r}_1|H_1}(\tilde{R}_1|H_1)}{p_{\tilde{r}_1|H_0}(\tilde{R}_1|H_0)}\right] = \ln\left(\frac{\sigma_n^2}{2\sigma_b^2 E_t + \sigma_n^2}\right) + \frac{2\sigma_b^2 E_t}{\sigma_n^2(2\sigma_b^2 E_t + \sigma_n^2)}\left|\tilde{R}_1\right|^2. \tag{1.24}$$

Because the constants can be combined with the threshold, the Neyman-Pearson receiver performs the likelihood ratio test

$$\left|\tilde{R}_1\right|^2 \underset{H_0}{\overset{H_1}{\underset{<}{>}}} \gamma \tag{1.25}$$

where the threshold γ is selected so as to achieve a specified false alarm probability.

The above test maximizes the detection probability under a false alarm probability constraint assuming that a slowly fluctuating point target is located at the point (τ_H, f_{D_H}) in the delay-Doppler plane. However, the target may actually be located at the point (τ_a, f_{D_a}). The complex envelope of the received waveform is then

$$\tilde{r}(t) = \sqrt{E_t}\tilde{b}\tilde{s}(t - \tau_a)\exp(j2\pi f_{D_a}t) + \tilde{n}(t). \tag{1.26}$$

8

Hence,

$$\tilde{r}_1 = \int_{\tau_H}^{\tau_H+T} \tilde{r}(t)\tilde{s}^*(t-\tau_H)\exp[-j2\pi(f_{D_H}-f_{D_a})t)dt$$

$$= \sqrt{E_t}\tilde{b}\int_{\tau_H}^{\tau_H+T} \tilde{s}(t-\tau_a)\tilde{s}^*(t-\tau_H)\exp(-j2\pi f_{D_H}t)dt$$

$$+ \int_{\tau_H}^{\tau_H+T} \tilde{n}(t)\tilde{s}^*(t-\tau_H)\exp(-j2\pi f_{D_H}t)dt. \tag{1.27}$$

It follows that

$$|\tilde{r}_1|^2 = E_t|\tilde{b}|^2 \left|\int_{\tau_H}^{\tau_H+T} \tilde{s}(t-\tau_a)\tilde{s}^*(t-\tau_H)\exp[-j2\pi(f_{D_H}-f_{D_a})t]dt\right|^2$$

$$+ \{\text{terms involving } \tilde{n}(t)\}. \tag{1.28}$$

Excluding the noise terms and the multiplicative factor $E_t|\tilde{b}|^2$, the ambiguity function of $\tilde{s}(t)$ is defined to be

$$\theta_{\tilde{s}}(\tau_H,\tau_a,f_{D_H},f_{D_a}) = \left|\int_{\tau_H}^{\tau_H+T} \tilde{s}(t-\tau_a)\tilde{s}^*(t-\tau_H)\exp[-j2\pi(f_{D_H}-f_{D_a})t]dt\right|^2. \tag{1.29}$$

Because $\tilde{s}(t)$ is zero outside the interval $0 \leq t \leq T$, the range of integration may be extended from $-\infty$ to ∞. Hence, the ambiguity function is commonly expressed as

$$\theta_{\tilde{s}}(\tau_H,\tau_a,f_{D_H},f_{D_a}) = \left|\int_{-\infty}^{\infty} \tilde{s}(t-\tau_a)\tilde{s}^*(t-\tau_H)\exp[-j2\pi(f_{D_H}-f_{D_a})t]dt\right|^2. \tag{1.30}$$

The function inside the magnitude signs is defined as the time-frequency autocorrelation function of $\tilde{s}(t)$, which will be denoted as $\phi_{\tilde{s}}(\tau_H,\tau_a,f_{D_H},f_{D_a})$,

$$\phi_{\tilde{s}}(\tau_H,\tau_a,f_{D_H},f_{D_a}) = \int_{-\infty}^{\infty} \tilde{s}(t-\tau_a)\tilde{s}^*(t-\tau_H)\exp[-j2\pi(f_{D_H}-f_{D_a})t]dt. \tag{1.31}$$

With a direct application of the generalized Parseval's theorem, it is also possible to express the ambiguity function in the frequency-domain. The generalized Parseval's theorem is given as follows. If $\tilde{S}_1(f)$ and $\tilde{S}_2(f)$ denote the Fourier transform of the two complex signals $\tilde{s}_1(t)$ and $\tilde{s}_2(t)$, respectively, then

$$\int_{-\infty}^{\infty} \tilde{s}_1(t)\tilde{s}_2^*(t)dt = \int_{-\infty}^{\infty} \tilde{S}_1(f)\tilde{S}_2^*(f)df. \tag{1.32}$$

9

The above relationship can be derived by a substitution of the definition of the Fourier transform to its right-hand side. Thus, denoting $\tilde{S}(f)$ as the Fourier transform of $\tilde{s}(t)$ and using Parseval's theorem, we have

$$\phi_{\tilde{s}}(\tau_H, \tau_a, f_{D_H}, f_{D_a}) = \exp[j2\pi(f_{D_a}\tau_a - f_{D_H}\tau_H)]$$

$$\cdot \int_{-\infty}^{\infty} \tilde{S}(f - f_{D_a})\tilde{S}^*(f - f_{D_H})\exp[j2\pi f(\tau_H - \tau_a)]df. \qquad (1.33)$$

Hence,

$$\theta_{\tilde{s}}(\tau_H, \tau_a, f_{D_H}, f_{D_a}) = \left| \int_{-\infty}^{\infty} \tilde{S}(f - f_{D_a})\tilde{S}^*(f - f_{D_H})\exp[j2\pi f(\tau_H - \tau_a)]dt \right|^2. \qquad (1.34)$$

Clearly, to minimize the likelihood that a target will be detected at the point (τ_H, f_{D_H}) when it is actually located at the point (τ_a, f_{D_a}), it is desirable that $\theta_{\tilde{s}}(\cdot)$ be an impulse located at (τ_a, f_{D_a}).

The ambiguity function is also related to the parameter estimation problem for a slowly fluctuating point target where the complex envelope of the received signal is again assumed to be of the form

$$\tilde{r}(t) = \sqrt{E_t}\tilde{b}\tilde{s}(t - \tau_H)\exp(j2\pi f_{D_H}t) + \tilde{n}, \quad \tau_H \leq t \leq \tau_H + T \qquad (1.35)$$

and τ_H and f_{D_H} are unknown nonrandom parameters that we wish to estimate.

Because the unknown parameters are nonrandom, we use a maximum likelihood estimation procedure. The maximum likelihood estimates are those values of τ_H and f_{D_H} at which the likelihood function is a maximum. In fact, the likelihood function and the likelihood ratio for the simple binary detection problem are identical [5]. Therefore, from (1.24), the log likelihood function is

$$\ln L\left(\tau_H, f_{D_H}\right) = \ln\left(\frac{\sigma_n^2}{2\sigma_b^2 E_t + \sigma_n^2}\right) + \frac{2\sigma_b^2 E_t}{\sigma_n^2(2\sigma_b^2 E_t + \sigma_n^2)}\left|\tilde{R}_1\left(\tau_H, f_{D_H}\right)\right|^2 \qquad (1.36)$$

where, from (1.18),

$$\tilde{R}_1\left(\tau_H, f_{D_H}\right) = \int_{\tau_H}^{\tau_H+T} \tilde{r}(t)\tilde{s}^*(t - \tau_H)\exp(-j2\pi f_{D_H}t)dt. \qquad (1.37)$$

10

Since the log likelihood function is maximized by maximizing $\left|\tilde{R}_1(\tau_H, f_{D_H})\right|^2$, the maximum likelihood estimates of τ_H and f_{D_H} are those values of τ_H and f_{D_H} at which $\left|\tilde{R}_1(\tau_H, f_{D_H})\right|^2$ is maximum.

As in the detection problem, the ambiguity function is defined by excluding terms involving noise. If the actual values of delay and Doppler are τ_a and f_{D_a}, respectively, the ambiguity function is found to be

$$\theta_{\tilde{s}}(\tau_H, \tau_a, f_{D_H}, f_{D_a}) = \left| \int_{-\infty}^{\infty} \tilde{s}(t - \tau_a)\tilde{s}^*(t - \tau_H) \exp[-j2\pi(f_{D_H} - f_{D_a})t]dt \right|^2 \qquad (1.38)$$

which is identical to that obtained in the detection problem. Hence, the time-frequency autocorrelation function is also of the same form as before. Clearly, to minimize the estimation errors, it is desirable that $\theta_{\tilde{s}}(\cdot)$ be an impulse located at (τ_a, f_{D_a}).

There is an important variation of the ambiguity function given in the foregoing discussion. Letting $\tau' = \tau_H - \tau_a$ and $f'_D = f_{D_H} - f_{D_a}$, the ambiguity function can also be put in the form

$$\theta_{\tilde{s}}(\tau', f'_D) = \left| \int_{-\infty}^{\infty} \tilde{s}(t)\tilde{s}^*(t - \tau') \exp(-j2\pi f'_D t)dt \right|^2 . \qquad (1.39)$$

That is, the ambiguity function is defined in terms of the differences between hypothesized and actual delay and between hypothesized and actual Doppler shift. In particular, letting $z = t - \tau'/2$ gives

$$\theta_{\tilde{s}}(\tau', f'_D) = \left| \int_{-\infty}^{\infty} \tilde{s}\left(z + \frac{\tau'}{2}\right) \tilde{s}^*\left(z - \frac{\tau'}{2}\right) \exp(-j2\pi f'_D z)dz \right|^2 \qquad (1.40)$$

The above form of the ambiguity function is what one commonly finds in references, and is called the symmetric form. It was shown in [16], however, that ambiguity functions in the form of either $\theta_{\tilde{s}}(\tau_H, \tau_a, f_{D_H}, f_{D_a})$ or $\theta_{\tilde{s}}(\tau', f'_D)$ do not convey sufficient information for the signal designer in bistatic radar applications. The ambiguity function for a bistatic radar was developed there. The analyses given in this work concentrate on the application to a monostatic radar, but the results can be extended to the bistatic case by applying the results from [16].

The notion of ambiguity function can also be extended and defined for two different signals. Define the cross ambiguity function of $\tilde{s}_1(t)$ and $\tilde{s}_2(t)$ as

$$\theta_{\tilde{s}_1\tilde{s}_2}(\tau, f_D) = \left| \int_{-\infty}^{\infty} \tilde{s}_1(t)\tilde{s}_2^*(t-\tau)\exp(-j2\pi f_D t)dt \right|^2. \qquad (1.41)$$

Also, the function inside the magnitude signs is defined as the time-frequency cross-correlation function of $\tilde{s}_1(t)$ and $\tilde{s}_2(t)$, which is denoted as $\phi_{\tilde{s}_1\tilde{s}_2}(\tau, f_D)$,

$$\phi_{\tilde{s}_1\tilde{s}_2}(\tau, f_D) = \int_{-\infty}^{\infty} \tilde{s}_1(t)\tilde{s}_2^*(t-\tau)\exp(-j2\pi f_D t)dt. \qquad (1.42)$$

With the above generalization, the statistic calculated by the receiver can be viewed as the cross ambiguity function between $\tilde{r}(t)$ and $\tilde{s}(t)$. By letting $\tilde{s}_r(t) = \tilde{s}(t-\tau_a)\exp(j2\pi f_{D_a}t)$, the ambiguity function $\theta_{\tilde{s}}(\tau_H, \tau_a, f_{D_H}, f_{D_a})$ can also be expressed as $\theta_{\tilde{s}_r\tilde{s}}(\tau_H, f_{D_H})$. This extension will be found useful in Chapter 2. It is also possible to express the cross ambiguity function in the frequency-domain. Denoting the Fourier transforms of $\tilde{s}_i(t)$ by $\tilde{S}_i(f)$, $i = 1, 2$, and using the generalized Parseval's theorem, we have

$$\phi_{\tilde{s}_1\tilde{s}_2}(\tau, f_D) = \exp(-j2\pi f_D \tau) \int_{-\infty}^{\infty} \tilde{S}_1(f)\tilde{S}_2^*(f-f_D)\exp(j2\pi f\tau)df. \qquad (1.43)$$

It follows that

$$\theta_{\tilde{s}_1\tilde{s}_2}(\tau, f_D) = \left| \int_{-\infty}^{\infty} \tilde{S}_1(f)\tilde{S}_2^*(f-f_D)\exp(j2\pi f\tau)df \right|^2. \qquad (1.44)$$

Rather than simply defining the ambiguity function, as is done in most references, we have shown that the ambiguity function arises naturally in both the detection and parameter estimation problems. In both applications, it is desirable to choose a waveform for $\tilde{s}(t)$ such that the shape of the ambiguity function approximates an impulse. As shown in the literature [17], however, the total volume under the ambiguity function is invariant to the choice of signal. The implication of this result is that, if we change the signal in order to narrow the main peak and improve accuracy, we then must check to see where the displaced volume reappears in the $\tau_H - f_{D_H}$ plane and check the effect on system performance. In other words, an assessment of the ambiguity function of a signal is needed to determine whether

this signal is suitable for a certain situation. The use of the ambiguity function in a radar operation is depicted in Figure 1.1.

1.3 Wigner-Ville Distribution

Unlike the ambiguity function, which has its origin in radar signal detection and parameter estimation problems as shown in previous section, the Wigner-Ville distribution was first introduced in the field of quantum mechanics as a bilinear distribution of two functions representing position and momentum [4]. Due to its importance in quantum mechanics, the Wigner-Ville distribution has been well studied and its properties derived [18],[19]. This distribution has found extensive use in optics, where it can be calculated directly by analog methods [20],[21]. Recently, the Wigner-Ville distribution has been examined for use in the field of signal analysis and processing, where it represents a bilinear time-frequency distribution [13]. Other applications include pattern recognition [22] and signal classification [23]. It should be pointed out that different versions of this distribution have been proposed. In this work, however, we define the Wigner-Ville distribution in terms of signal complex envelopes [8],[24], instead of real signals.

The Wigner-Ville distribution of two continuous signals, $\tilde{s}_1(t)$ and $\tilde{s}_2(t)$, is defined by

$$W_{\tilde{s}_1 \tilde{s}_2}(t, f) = \int_{-\infty}^{\infty} \tilde{s}_1 \left(t + \frac{\tau}{2} \right) \tilde{s}_2^* \left(t - \frac{\tau}{2} \right) \exp(-j2\pi f \tau) d\tau. \tag{1.45}$$

When $\tilde{s}_1(t) = \tilde{s}_2(t)$, the Wigner-Ville distribution (1.45) is called the auto-Wigner-Ville distribution. Otherwise it is called the cross-Wigner-Ville distribution. Letting $\tau' = \tau/2$, the Wigner-Ville distribution can also be rewritten in the form

$$W_{\tilde{s}_1 \tilde{s}_2}(t, f) = 2 \int_{-\infty}^{\infty} \tilde{s}_1(t + \tau') \tilde{s}_2^*(t - \tau') \exp(-j4\pi f \tau') d\tau. \tag{1.46}$$

Using the generalized Parseval's theorem, the Wigner-Ville distribution can be expressed in
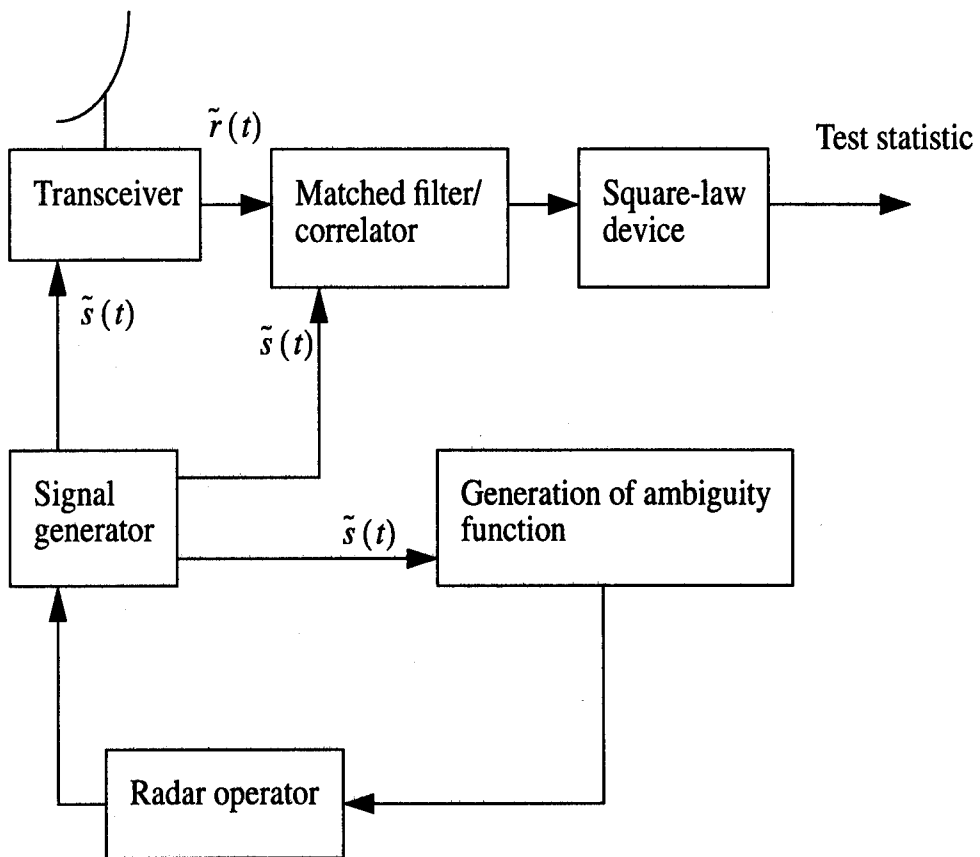
$\tilde{r}(t)$: Complex envelope of the received signal

$\tilde{s}(t)$: Complex envelope of the reference signal

Figure 1.1: Radar application of ambiguity function

the frequency-domain as

$$W_{\tilde{s}_1 \tilde{s}_2}(t, f) = 2 \int_{-\infty}^{\infty} \tilde{S}_1(f + \nu)\tilde{S}_2^*(f - \nu)\exp(j4\pi\nu t)d\tau. \tag{1.47}$$

Generalization of the correlator based receiver to one based on the Wigner-Ville distribution is due to Moyal's formula. It states that the magnitude-square of the inner product of two signals, say $\tilde{s}_1(t)$ and $\tilde{s}_2(t)$, is equivalent to the inner product of the Wigner-Ville distributions of $\tilde{s}_1(t)$ and $\tilde{s}_2(t)$. That is,

$$\left| \int_{-\infty}^{\infty} \tilde{s}_1(t)\tilde{s}_2^*(t)dt \right|^2 = \int_{-\infty}^{\infty} \int_{-\infty}^{\infty} W_{\tilde{s}_1}(t, f)W_{\tilde{s}_2}^*(t, f)dtdf. \tag{1.48}$$

The above result can be shown by substituting the definition of the Wigner-Ville distribution given by (1.45) into the right-hand side of (1.48) yielding

$$\int_{-\infty}^{\infty} \int_{-\infty}^{\infty} W_{\tilde{s}_1}(t, f)W_{\tilde{s}_2}^*(t, f)dtdf$$
$$= \int_{-\infty}^{\infty} \int_{-\infty}^{\infty} \left\{ \int_{-\infty}^{\infty} \tilde{s}_1\left(t + \frac{\tau_1}{2}\right)\tilde{s}_1^*\left(t - \frac{\tau_1}{2}\right)\exp(-j2\pi f\tau_1)d\tau_1 \right\}$$
$$\cdot \left\{ \int_{-\infty}^{\infty} \tilde{s}_2\left(t + \frac{\tau_2}{2}\right)\tilde{s}_2^*\left(t - \frac{\tau_2}{2}\right)\exp(-j2\pi f\tau_2)d\tau_2 \right\}^* dtdf. \tag{1.49}$$

Assuming the order of integration is interchangeable,

$$\int_{-\infty}^{\infty} \int_{-\infty}^{\infty} W_{\tilde{s}_1}(t, f)W_{\tilde{s}_2}^*(t, f)dtdf$$
$$= \int_{-\infty}^{\infty} \int_{-\infty}^{\infty} \int_{-\infty}^{\infty} \tilde{s}_1\left(t + \frac{\tau_1}{2}\right)\tilde{s}_1^*\left(t - \frac{\tau_1}{2}\right)\tilde{s}_2^*\left(t + \frac{\tau_2}{2}\right)\tilde{s}_2\left(t - \frac{\tau_2}{2}\right)$$
$$\cdot \left\{ \int_{-\infty}^{\infty} \exp[j2\pi f(\tau_2 - \tau_1)]df \right\} d\tau_1 d\tau_2 dt. \tag{1.50}$$

The term in the braces is the inverse Fourier transform of a Dirac delta function occurring at $\tau_2 - \tau_1$. That is,

$$\int_{-\infty}^{\infty} \exp[j2\pi f(\tau_2 - \tau_1)]df = \delta(\tau_2 - \tau_1) \tag{1.51}$$

where $\delta(\cdot)$ denotes the Dirac delta function. Utilizing (1.51) and integrating over τ_2 gives

$$\int_{-\infty}^{\infty} \int_{-\infty}^{\infty} W_{\tilde{s}_1}(t, f)W_{\tilde{s}_2}^*(t, f)dtdf$$
$$= \int_{-\infty}^{\infty} \int_{-\infty}^{\infty} \tilde{s}_1\left(t + \frac{\tau_1}{2}\right)\tilde{s}_1^*\left(t - \frac{\tau_1}{2}\right)\tilde{s}_2^*\left(t + \frac{\tau_1}{2}\right)\tilde{s}_2\left(t - \frac{\tau_1}{2}\right)d\tau_1 dt. \tag{1.52}$$

15

The left-hand side of (1.48) can then be obtained by letting $u = t + \tau_1/2$ and $v = t - \tau_1/2$. When $\tilde{s}_1(t) = \tilde{r}(t)$ and $\tilde{s}_2(t) = \tilde{s}(t - \tau_H)\exp(j2\pi f_{D_H}t)$, it is obvious that the left-hand side of (1.48) is the optimum radar detection and estimation scheme derived in Section 1.2. By calculating the left-hand side of (1.48) for various values of τ_H and f_{D_H}, the radar receiver performs detection and estimation simultaneously. On the other hand, as indicated by the right-hand side of (1.48), the optimum reception procedure can be equivalently implemented by matched filtering the received signal's Wigner-Ville distribution and the reference Wigner-Ville distributions. Hence, the optimality of the receiver based on the continuous Wigner-Ville distribution is established. However, the Moyal's formula for discrete time/frequency signals derived in the literature does not appear to result in an optimum discrete receiver. This problem is addressed in Chapter 3.

Moyal's formula can be further extended by using the following relationship between the Wigner-Ville distribution and the time-frequency correlation function. Taking the two-dimensional Fourier transform of the Wigner-Ville distribution gives

$$
\begin{aligned}
\int_{-\infty}^{\infty} & \int_{-\infty}^{\infty} W_{\tilde{s}_1}(t, f) \exp(-j2\pi vt) \exp(j2\pi fu) dt df \\
&= \int_{-\infty}^{\infty} \int_{-\infty}^{\infty} \left\{ \int_{-\infty}^{\infty} \tilde{s}_1\left(t + \frac{\tau}{2}\right) \tilde{s}_1^*\left(t - \frac{\tau}{2}\right) \exp(-j2\pi f\tau) d\tau \right\} \\
&\quad \cdot \exp(-j2\pi vt) \exp(j2\pi fu) dt df \\
&= \int_{-\infty}^{\infty} \int_{-\infty}^{\infty} \tilde{s}_1\left(t + \frac{\tau}{2}\right) \tilde{s}_1^*\left(t - \frac{\tau}{2}\right) \exp(-j2\pi vt) d\tau dt \\
&\quad \cdot \left\{ \int_{-\infty}^{\infty} \exp[j2\pi f(u - \tau)] df \right\}
\end{aligned}
\tag{1.53}
$$

where it is assumed that the order of integration is interchangeable. The term in the braces is the inverse Fourier transform of a Dirac delta occurring at $u - \tau$. Therefore, integrating over τ and f gives

$$
\begin{aligned}
\int_{-\infty}^{\infty} & \int_{-\infty}^{\infty} W_{\tilde{s}_1}(t, f) \exp(-j2\pi vt) \exp(j2\pi fu) dt df \\
&= \int_{-\infty}^{\infty} \tilde{s}_1\left(t + \frac{u}{2}\right) \tilde{s}_1^*\left(t - \frac{u}{2}\right) \exp(-j2\pi vt) dt \\
&= \exp(j\pi vu)\phi_{\tilde{s}_1}(u, v).
\end{aligned}
\tag{1.54}
$$

16

It follows that

$$\int_{-\infty}^{\infty}\int_{-\infty}^{\infty}\phi_{\tilde{s}_1}(u,v)\phi_{\tilde{s}_2}^*(u,v)dudv$$

$$= \int_{-\infty}^{\infty}\int_{-\infty}^{\infty}\left\{\int_{-\infty}^{\infty}\int_{-\infty}^{\infty}W_{\tilde{s}_1}(t_1,f_1)\exp(-j2\pi vt_1)\exp(j2\pi f_1 u)dt_1 df_1\right\}$$

$$\cdot\left\{\int_{-\infty}^{\infty}\int_{-\infty}^{\infty}W_{\tilde{s}_2}(t_2,f_2)\exp(-j2\pi vt_2)\exp(j2\pi f_2 u)dt_2 df_2\right\}^* dudv. \qquad (1.55)$$

Assuming the order of integration is interchangeable and integrating the exponential terms over u and v gives

$$\int_{-\infty}^{\infty}\int_{-\infty}^{\infty}\phi_{\tilde{s}_1}(u,v)\phi_{\tilde{s}_2}^*(u,v)dudv$$

$$= \int_{-\infty}^{\infty}\int_{-\infty}^{\infty}\int_{-\infty}^{\infty}\int_{-\infty}^{\infty}W_{\tilde{s}_1}(t_1,f_1)W_{\tilde{s}_2}^*(t_2,f_2)\delta(t_1-t_2)\delta(f_1-f_2)dt_1 dt_2 df_1 df_2$$

$$= \int_{-\infty}^{\infty}\int_{-\infty}^{\infty}W_{\tilde{s}_1}(t_1,f_1)W_{\tilde{s}_2}^*(t_1,f_1)dt_1 df_1 \qquad (1.56)$$

Comparing (1.56) and (1.48), it is clear that the optimum receiver can also be implemented in the form of the inner product of the time-frequency autocorrelation functions of $\tilde{r}(t)$ and $\tilde{s}(t-\tau_H)\exp(j2\pi f_{D_H}t)$. This is the form under development in [11]. In Chapter 3, we will apply the discrete version of (1.56) to the discrete time/frequency distribution based radar receiver.

1.4 Rationale for Using the Time-Frequency Distribution Based Receiver

Application of time-frequency distributions to signal processing has been the focus of considerable research in recent years. In particular, the use of time-frequency distributions in radar reception has been considered. A time-frequency distribution based radar receiver processes the time-frequency distribution of the signal instead of the signal itself. One of the major advantages of performing radar reception based on time-frequency distributions is that it transfers detection and estimation procedures into time-frequency space, where feature selection and time-variant filtering are more readily carried out [25].

Among the various types of time-frequency distributions considered, a receiver based on the Wigner-Ville distribution has been shown to be also optimal in the Neyman-Pearson sense. Such a receiver has advantages over the conventional one when the problem is not completely specified because it enables estimation of the unknowns. In addition, noise suppression is easier when the signal waveshape is unknown. An example of application of the Wigner-Ville distribution based receiver involves underwater detection [9] where the sound emitted from the engine of an underwater vehicle cannot be determined a priori. Another example deals with detection of a maneuvering target [10]. In a recent paper [11] it is shown that a receiver based on the time-frequency correlation function is also optimal. This choice of implementation has the advantage that it is computationally more tractable for linear *fm* signals. The use of such a receiver is demonstrated through the detection of iceberg fragments.

However, as mentioned earlier, implementation of the receiver based on the time-frequency distribution has been restricted to the continuous case. Digital implementation of the optimum radar receiver based on the time-frequency distribution is derived in Chapter 3 of this work. Further considerations regarding the advantage of using a time-frequency distribution based receiver are also given there.

Chapter 2

Discrete Versions of the Ambiguity Function and Wigner-Ville Distribution

In this chapter we consider the discrete ambiguity function and the discrete Wigner-Ville distribution. In Section 2.1, we review the problem of radar detection and estimation using sampled signals. This analysis serves as a basis for implementing the optimum discrete receiver. As a direct result, Section 2.2 shows the manner in which the discrete ambiguity function arises from the conventional optimum discrete receiver. We then derive the sampling criteria to prevent aliasing in the discrete ambiguity function that may result in degradation of receiver performance. Also, we propose an interpolation formula to recover the continuous ambiguity function from the discrete one. This interpolation formula is simpler than the one found in the literature [16]; however, it can only be used to recover that portion of the continuous ambiguity function corresponding to the alias-free region of the discrete ambiguity function. In Section 2.3, attention is turned to the review of derivations of various versions of the discrete Wigner-Ville distribution. Sampling criteria and interpolation formulas are given. A new interpolation formula that is simpler than the one found in [14] is derived; however, it can only be used to recover that portion of the continuous Wigner-Ville distribution corresponding to the alias-free region of the discrete Wigner-Ville distribution.

19

2.1 Radar Detection and Estimation Using Sampled Signals

In this section, we review radar detection and estimation problems where the observation consists of discrete samples obtained by uniformly sampling the received signal. The sampling process is assumed to be performed at the output of the synchronous (I,Q) detector. Let $\sqrt{E_t}\tilde{s}(t)$ denote the complex envelope of the transmitted waveform such that

$$\int_{-\infty}^{\infty} |\tilde{s}(t)|^2 \, dt = 1. \tag{2.1}$$

Thus, the transmitted energy is E_t. Here, we assume that $\tilde{s}(t)$ has *essentially* both limited duration, $[0, T)$, and bandwidth, $(-B, B)$. By *essentially* it is meant that the signal simultaneously has negligible energy outside $[0, T)$ in time and outside $(-B, B)$ in spectrum [26]. When the transmitted signal is narrowband and the target is non-maneuvering, the complex envelope of the reflected signal $\tilde{s}_R(t)$ from a slowly fluctuating point target can be approximated by

$$\tilde{s}_R(t) = \tilde{b}\sqrt{E_t}\tilde{s}(t - \tau_a) \exp[j2\pi f_{D_a}(t - \tau_a)] \tag{2.2}$$

where $\tilde{b}$ is a complex Gaussian random variable used to describe the reflective characteristics of the target, τ_a is the round-trip delay, and f_{D_a} is the Doppler shift. The complex variable $\tilde{b}$ can be expressed in terms of its envelope and its phase, $\tilde{b} = |\tilde{b}| \exp(j\psi)$. The envelope of $\tilde{b}$ is Rayleigh distributed with its first two moments given by

$$E\left[|\tilde{b}|\right] = \sqrt{\frac{\pi}{2}}\sigma_b \tag{2.3}$$

and

$$E\left[|\tilde{b}|^2\right] = 2\sigma_b^2. \tag{2.4}$$

The phase of $\tilde{b}$ is uniform. The term $\exp(-j2\pi f_{D_a}\tau_a)$ on the right hand side of (2.2) can be absorbed into the phase of $\tilde{b}$ such that

$$\tilde{s}_R(t) = \tilde{b}\sqrt{E_t}\tilde{s}(t - \tau_a) \exp[j2\pi f_{D_a}t]. \tag{2.5}$$

Note that this target return model was shown in [16] to be appropriate for both monostatic and bistatic radar systems.

When the receiver is implemented digitally, the received signal is sampled prior to the detection and/or estimation procedure taking place. The design of the sampling process should account for the fact that the target return is a time delayed and perhaps a frequency shifted version of the transmitted signal. The observation should last longer than the signal duration to account for uncertainty in the signal delay. Assume that a total of N samples are taken and $N \geq T/T_s$, where T_s is the sampling period. Let $N_1 = T/T_s$ and $N_0 = N - N_1$. The interval $N_0 T_s$ represents the predicted maximum delay. Also, the bandwidth of the A/D converter should be able to accommodate both the bandwidth and Doppler shift of the transmitted signal. It is assumed that the maximum Doppler shift to be encountered is known and the bandwidth of the A/D converter is greater than the sum of the signal bandwidth and the maximum Doppler shift so that no distortion will occur to the received signal spectrum in the sampling process. The aforementioned assumptions about the observation duration and the bandwidth of the A/D converter are assumed to hold true throughout this work. The observation obtained is a sequence of random variables $\tilde{r}_1, \cdots, \tilde{r}_N$ which are equal to the sums of samples of the target return and noise when the target is present, while they consist of only noise samples in the absence of the target. Denote the observation sequence by the vector $\tilde{\boldsymbol{r}}$, where $\tilde{\boldsymbol{r}}^T = [\tilde{r}_1, \cdots, \tilde{r}_N]$. Also denote the sequences of the target return samples and the noise by the vectors $\tilde{\boldsymbol{s}}_R$ and $\tilde{\boldsymbol{n}}$, respectively. In particular, the elements of $\tilde{\boldsymbol{s}}_R$ are

$$\tilde{s}_R(kT_s) = \tilde{b}\sqrt{E_t}\,\tilde{s}(kT_s - \tau_a)\exp[j2\pi f_{D_a}kT_s], \quad k = 0, 1, ..., N - 1. \tag{2.6}$$

Assume that the noise samples are independent and identically distributed Gaussian random variables with zero mean and variance σ_n^2.

Before deriving the optimum discrete receiver, we recall that the problems of detecting a target and estimating the delay and Doppler shift in the target return were treated separately in Section 1.2, where we dealt with continuous signals. The continuous ambiguity function

was shown to be associated with both the optimum detection procedure and the optimum estimation procedure. The derivation of the optimum discrete receiver and the discrete ambiguity function can follow a manner similar to that presented in Section 1.2. However, it is also possible to carry out the analysis with a different approach by forming a composite hypothesis test and combining it with a generalized likelihood-ratio test [5]. With this alternative, the detection and estimation problems are combined into one formulation. This approach is useful in reflecting the nature of radar operation where detection and estimation are performed simultaneously. The need to perform detection and estimation simultaneously is due to the fact that estimation of delay and Doppler shift in the target return is meaningful only after a target return is detected, but a reliable detection requires the knowledge of the delay and Doppler of the target return.

The composite hypothesis-testing problem is formulated as

$$H_1 : \; \tilde{r} = \tilde{s}_R + \tilde{n}$$

$$H_0 : \; \tilde{r} = \tilde{n}. \tag{2.7}$$

In this formulation, H_0 is a simple hypothesis and H_1 is a composite one in which $\tilde{b}$, τ_a, and f_{D_a} in the target return are unknown. Among these unknown parameters, $\tilde{b}$ is a random variable with a known probability density function over which it can be averaged [5]. The procedure of averaging $\tilde{b}$ over its probability density function will be given in the following paragraph where we evaluate the generalized likelihood ratio. The rest of the unknown parameters τ_a and f_{D_a} are nonrandom and their values need to be estimated. The estimates of τ_a and f_{D_a} are obtained from maximum likelihood estimates. Denoting the hypothesized values of τ_a and f_{D_a} by τ_H and f_{D_H}, respectively, the maximum likelihood estimates of τ_a and f_{D_a} are those τ_H and f_{D_H} that maximize the conditional probability density function $p_{\tilde{r}|H_1,\tau_H,f_{D_H}}(\cdot)$. Denote the maximum likelihood estimates of τ_a and f_{D_a} by $\hat{\tau}_H$ and $\hat{f}_{D_H}$,

22

respectively. Then the generalized likelihood-ratio test for (2.7) is given by

$$\frac{p_{\tilde{r}|H_1,\hat{\tau}_H,\hat{f}_{D_H}}(\tilde{R}\,|\,\hat{\tau}_H,\hat{f}_{D_H})}{p_{\tilde{r}|H_0}(\tilde{R})} \begin{array}{c} H_1 \\ > \\ < \\ H_0 \end{array} \gamma \qquad (2.8)$$

where γ is the threshold.

In the test (2.8), $p_{\tilde{r}|H_0}(\cdot)$ is simply the probability density function of the noise, i.e.,

$$p_{\tilde{r}|H_0}(\tilde{R}) = \frac{1}{(2\pi\sigma_n^2)^{N/2}} \exp\left(\frac{\tilde{R}^\dagger \tilde{R}}{-2\sigma_n^2}\right) \qquad (2.9)$$

where "$\dagger$" denotes the Hermitian transpose. To obtain an expression for the conditional probability density function in the numerator of (2.8), we recall that $p_{\tilde{r}|H_1,\hat{\tau}_H,\hat{f}_{D_H}}(\cdot)$ is the maximum of $p_{\tilde{r}|H_1,\tau_H,f_{D_H}}(\cdot)$ as a function of τ_H and f_{D_H}; therefore, we need to find $p_{\tilde{r}|H_1,\tau_H,f_{D_H}}(\cdot)$ first. Denote the hypothesized target return vector by $\tilde{s}_H$, the elements of which are

$$\tilde{s}_H(kT_s) = \tilde{s}(kT_s - \tau_H)\exp[j2\pi f_{D_H}kT_s], \quad k = 0,1,...,N-1. \qquad (2.10)$$

Then, the conditional probability density function of $\tilde{r}$ given the unknown parameters can be expressed as

$$p_{\tilde{r}|\psi,|\tilde{b}|,\tau_H,f_{D_H}}(\tilde{R}\,|\,\Psi,|\tilde{B}|,\tau_H,f_{D_H}) = \frac{1}{(2\pi\sigma_n^2)^{N/2}} \exp\left[\frac{\left|\tilde{R} - \sqrt{E_t}|\tilde{B}|e^{j\Psi}\tilde{s}_H\right|^2}{-2\sigma_n^2}\right]. \qquad (2.11)$$

Using the a priori probability density function of $\tilde{b}$, we have

$$p_{\tilde{r}|H_1,\tau_H,f_{D_H}}(\tilde{R}\,|\,\tau_H,f_{D_H}) = \int_{\mathcal{X}_{|\tilde{b}|}}\int_{\mathcal{X}_\psi} p_{\tilde{r}}(\tilde{R}\,|\,\Psi,|\tilde{B}|,\tau_H,f_{D_H})p_\psi(\Psi)p_{|\tilde{b}|}(|\tilde{B}|)d\Psi d|\tilde{B}| \qquad (2.12)$$

where $\mathcal{X}_{|\tilde{b}|}$ and $\mathcal{X}_\psi$ denote the domains of the random variables $|\tilde{b}|$ and ψ, respectively. Carrying out the integrations on the right-hand side of (2.12), we have

$$p_{\tilde{r}|H_1,\tau_H,f_{D_H}}(\tilde{R}\,|\,\tau_H,f_{D_H})$$
$$= \int_0^\infty \int_{-\pi}^\pi \left(\frac{1}{(2\pi\sigma_n^2)^{N/2}} \exp\left[\frac{\left|\tilde{R} - \sqrt{E_t}|\tilde{B}|e^{j\Psi}\tilde{s}_H\right|^2}{-2\sigma_n^2}\right]\right)\left(\frac{1}{2\pi}\right)$$

23

$$
\cdot \left[\frac{|\tilde{B}|}{2\sigma_b^2} \exp\left(\frac{-|\tilde{B}|^2}{4\sigma_b^2} \right) \right] d\Psi d|\tilde{B}|
$$

$$
= \frac{\exp\left(\frac{-|\tilde{\boldsymbol{R}}|^2}{2\sigma_n^2} \right)}{4\pi\sigma_b^2 \left(2\pi\sigma_n^2 \right)^{N/2}} \int_0^\infty |\tilde{B}| \exp\left[\frac{-|\tilde{B}|^2}{4\sigma_b^2} \right]
$$

$$
\cdot \int_{-\pi}^{\pi} \exp\left[\frac{|\sqrt{E_t}\tilde{B}\tilde{\boldsymbol{s}}_H|^2 - 2\sqrt{E_t}|\tilde{B}|\mathrm{Re}\{e^{-j\Psi}\tilde{\boldsymbol{s}}_H^\dagger\tilde{\boldsymbol{R}}\}}{-2\sigma_n^2} \right] d\Psi d|\tilde{B}|. \tag{2.13}
$$

Denoting the phase of $\tilde{\boldsymbol{s}}_H^\dagger\tilde{\boldsymbol{r}}$ by ψ', we have

$$
p_{\tilde{\boldsymbol{r}}|H_1,\tau_H,f_{D_H}}\left(\tilde{\boldsymbol{R}} \,\middle|\, \tau_H, f_{D_H} \right)
$$

$$
= \frac{\exp\left(\frac{-|\tilde{\boldsymbol{R}}|^2}{2\sigma_n^2} \right)}{4\pi\sigma_b^2 \left(2\pi\sigma_n^2 \right)^{N/2}} \int_0^\infty |\tilde{B}| \exp\left[\frac{-|\tilde{B}|^2}{4\sigma_b^2} \right]
$$

$$
\cdot \int_{-\pi}^{\pi} \exp\left[\frac{|\sqrt{E_t}\tilde{B}\tilde{\boldsymbol{s}}_H|^2 - 2\sqrt{E_t}|\tilde{B}|\mathrm{Re}\{e^{j(\psi'-\Psi)}\left|\tilde{\boldsymbol{s}}_H^\dagger\tilde{\boldsymbol{R}}\right|\}}{-2\sigma_n^2} \right] d\Psi d|\tilde{B}|
$$

$$
= \frac{\exp\left(\frac{-|\tilde{\boldsymbol{R}}|^2}{2\sigma_n^2} \right)}{4\pi\sigma_b^2 \left(2\pi\sigma_n^2 \right)^{N/2}} \int_0^\infty |\tilde{B}| \exp\left[\frac{2\sigma_b^2 E_t|\tilde{\boldsymbol{s}}_H|^2 + \sigma_n^2}{-4\sigma_b^2\sigma_n^2}|\tilde{B}|^2 \right]
$$

$$
\cdot \int_{-\pi}^{\pi} \exp\left[\sqrt{E_t}\frac{-|\tilde{B}|\left|\tilde{\boldsymbol{s}}_H^\dagger\tilde{\boldsymbol{R}}\right|\cos(\psi'-\Psi)}{\sigma_n^2} \right] d\Psi d|\tilde{B}|
$$

$$
= \frac{\exp\left(\frac{-|\tilde{\boldsymbol{R}}|^2}{2\sigma_n^2} \right)}{4\pi\sigma_b^2 \left(2\pi\sigma_n^2 \right)^{N/2}} \int_0^\infty |\tilde{B}| \exp\left[\frac{2\sigma_b^2 E_t|\tilde{\boldsymbol{s}}_H|^2 + \sigma_n^2}{-4\sigma_b^2\sigma_n^2}|\tilde{B}|^2 \right]
$$

$$
\cdot 2\pi I_0\left(\frac{\sqrt{E_t}|\tilde{B}|\left|\tilde{\boldsymbol{s}}_H^\dagger\tilde{\boldsymbol{R}}\right|}{\sigma_n^2} \right) d|\tilde{B}| \tag{2.14}
$$

where $I_0(\cdot)$ is the modified Bessel function of the first kind of order zero. Denoting the multiplier in front of $|\tilde{B}|^2$ in the exponential term by α, we have

$$
p_{\tilde{\boldsymbol{r}}|H_1,\tau_H,f_{D_H}}\left(\tilde{\boldsymbol{R}} \,\middle|\, \tau_H, f_{D_H} \right)
$$

$$
= \frac{\exp\left(\frac{-|\tilde{\boldsymbol{R}}|^2}{2\sigma_n^2} \right)}{2\sigma_b^2 \left(2\pi\sigma_n^2 \right)^{N/2}} \int_0^\infty |\tilde{B}| \exp\left[-\alpha|\tilde{B}|^2 \right] I_0\left(\frac{\sqrt{E_t}|\tilde{B}|\left|\tilde{\boldsymbol{s}}_H^\dagger\tilde{\boldsymbol{R}}\right|}{\sigma_n^2} \right) d|\tilde{B}|
$$

$$
= \frac{\exp\left(\frac{-|\tilde{\boldsymbol{R}}|^2}{2\sigma_n^2} \right)}{4\alpha\sigma_b^2 \left(2\pi\sigma_n^2 \right)^{N/2}} \exp\left[\frac{E_t\left|\tilde{\boldsymbol{s}}_H^\dagger\tilde{\boldsymbol{R}}\right|^2}{4\alpha\sigma_n^4} \right]. \tag{2.15}
$$

In deriving (2.15), the identity [27]

$$\int_0^\infty x e^{-\alpha x^2} I_\nu(\beta x) J_\nu(\gamma x) dx = \frac{1}{2\alpha} \exp\left(\frac{\beta^2 - \gamma^2}{4\alpha}\right) J_\nu(\frac{\beta\gamma}{2\alpha}) \qquad (2.16)$$

was utilized where $J_\nu(\cdot)$ is the Bessel function of order ν. It should be pointed out that in the application of (2.16) to (2.15) both ν and γ were zero, and the fact that $J_0(0) = 1$ was also used. The last relationship in (2.15) indicates that $p_{\tilde{r}|H_1,\tau_H,f_{D_H}}(\cdot)$ is a monotonic increasing function in $|\tilde{s}_H^\dagger \tilde{r}|^2$. Therefore, the values $\hat{\tau}_H$ and $\hat{f}_{D_H}$ at which $|\tilde{s}_H^\dagger \tilde{r}|^2$ attains its maximum are precisely those values that maximize $p_{\tilde{r}|H_1,\tau_H,f_{D_H}}(\cdot)$.

Thus, the generalized likelihood ratio given in (2.8) can be written as

$$\frac{p_{\tilde{r}|H_1,\hat{\tau}_H,\hat{f}_{D_H}}(\tilde{R}|\hat{\tau}_H,\hat{f}_{D_H})}{p_{\tilde{r}|H_0}(\tilde{R})} = \frac{1}{4\alpha\sigma_b^2} \exp\left[\frac{E_t \left|\hat{s}_H^\dagger \tilde{R}\right|^2}{4\alpha\sigma_n^4}\right] \qquad (2.17)$$

where $\hat{s}_H$ is the hypothesized target return with $\hat{\tau}_H$ and $\hat{f}_{D_H}$ as its parameters. From (2.17), it is seen that $|\tilde{s}_H^\dagger \tilde{r}|^2$ can be used as a sufficient statistic in performing the generalized likelihood ratio test. Therefore, discrete radar detection and estimation problems can be solved by computing $|\tilde{s}_H^\dagger \tilde{r}|^2$ and comparing it with a threshold to determine the presence or absence of the target at (τ_H, f_{D_H}). The estimates $\hat{\tau}_H$ and $\hat{f}_{D_H}$ are determined by maximizing $|\tilde{s}_H^\dagger \tilde{r}|^2$ over all possible parameter values.

2.2 Discrete Ambiguity Function

The detection and estimation procedure developed in the previous section requires processing of the statistic $|\tilde{s}_H^\dagger \tilde{r}|^2$, which is a function of the parameters τ_H and f_{D_H}. Based on this statistic, receivers are conventionally implemented with a discrete matched filter/correlator followed by a square law device. As in the continuous case, a discrete ambiguity function can be defined and used to analyze such receivers. In this section, we present a number of definitions of the discrete ambiguity function that have appeared in the literature [28],[29]. Also, we consider the sampling criteria that prevent aliasing in the discrete ambiguity function

which can result in degradation of receiver performance. We then derive an interpolation formula which is simpler than the one found in the literature [16] to recover the continuous ambiguity function from the discrete ambiguity function.

2.2.1 Time-domain Representation

In this subsection we show the relationship between the time-domain representation of the discrete ambiguity function and the time-domain realization of the conventional discrete receiver as well as the relationships among various forms of the discrete ambiguity function.

When the target is present, the statistic processed by the discrete receiver can be written as

$$
\begin{aligned}
|\tilde{\boldsymbol{s}}_H^\dagger \tilde{\boldsymbol{r}}|^2 &= \left|\tilde{\boldsymbol{s}}_H^\dagger \left(\boldsymbol{s}_R + \tilde{\boldsymbol{n}}\right)\right|^2 \\
&= |\tilde{\boldsymbol{s}}_H^\dagger \tilde{\boldsymbol{s}}_R|^2 + |\tilde{\boldsymbol{s}}_H^\dagger \tilde{\boldsymbol{n}}|^2 + 2\mathrm{Re}\{\tilde{\boldsymbol{s}}_R^\dagger \tilde{\boldsymbol{s}}_H \tilde{\boldsymbol{s}}_H^\dagger \tilde{\boldsymbol{n}}\} \\
&= E_t|\tilde{b}|^2 \left|\sum_{k=0}^{N-1} \tilde{s}(kT_s - \tau_a)\tilde{s}^*(kT_s - \tau_H)\exp[j2\pi(f_{D_a} - f_{D_H})kT_s]\right|^2 \\
&\quad + \{\text{terms involving noise}\}
\end{aligned}
\tag{2.18}
$$

where, as noted before, N is the number of samples obtained. Excluding the multiplier $E_t|\tilde{b}|^2$, we denote the first term in the last relationship of (2.18) as $\hat{\theta}_{\tilde{s}}(\tau_H, \tau_a, f_{D_H}, f_{D_a})$, and the function inside the magnitude as $\hat{\phi}_{\tilde{s}}(\tau_H, \tau_a, f_{D_H}, f_{D_a})$. That is,

$$
\begin{aligned}
|\tilde{\boldsymbol{s}}_H^\dagger \tilde{\boldsymbol{r}}|^2 &= E_t|\tilde{b}|^2 \left|\sum_{k=0}^{N-1} \tilde{s}(kT_s - \tau_a)\tilde{s}^*(kT_s - \tau_H)\exp[j2\pi(f_{D_a} - f_{D_H})kT_s]\right|^2 \\
&\quad + \{\text{terms involving noise}\} \\
&= E_t|\tilde{b}|^2 \left|\hat{\phi}_{\tilde{s}}(\tau_H, \tau_a, f_{D_H}, f_{D_a})\right|^2 + \{\text{terms involving noise}\} \\
&= E_t|\tilde{b}|^2 \hat{\theta}_{\tilde{s}}(\tau_H, \tau_a, f_{D_H}, f_{D_a}) + \{\text{terms involving noise}\}.
\end{aligned}
\tag{2.19}
$$

Clearly, if the receiver is a direct-form realization of $|\tilde{\boldsymbol{s}}_H^\dagger \tilde{\boldsymbol{r}}|^2$, the function $\hat{\phi}_{\tilde{s}}(\cdot)$ represents a scaled version of the matched filter's response to the sampled target return in the absence of noise, and $\hat{\theta}_{\tilde{s}}(\cdot)$ represents a scaled version of the receiver's output. Thus, both of these

functions provide a measure of ambiguity inherent in the sampled radar signal when it is applied to the aforementioned receiver. For this reason, $\hat{\phi}_{\tilde{s}}(\cdot)$ was defined as the discrete ambiguity function of the signal $\tilde{s}$ in [28], and was used to assess the performance of the receiver. In this work, however, we will adhere to the convention in previous chapters and consider $\hat{\theta}_{\tilde{s}}(\cdot)$ as the discrete ambiguity function and $\hat{\phi}_{\tilde{s}}(\cdot)$ the discrete time-frequency autocorrelation function.

In practice, only discrete values of the estimators τ_H and f_{D_H} are used when the receiver is implemented digitally. The statistic generated by the receiver is of the form

$$\Lambda(n\triangle_\tau, m\triangle_f) \triangleq \left| \sum_{k=0}^{N-1} \tilde{r}(kT_s)\tilde{s}^*(kT_s - n\triangle_\tau) \exp[-j2\pi m\triangle_f kT_s] \right|^2 \qquad (2.20)$$

where n and m are integers, $\triangle_\tau$ is the step size in τ_H, and $\triangle_f$ in f_{D_H}. The step size $\triangle_\tau$ is set equal to T_s so that $\tilde{s}^*(\cdot)$ can be evaluated at all available samples. In addition, the step size of $\triangle_f$ is set equal to $1/(NT_s)$ in order that fast Fourier transform procedure can be employed. The resulting receiver computes

$$\Lambda\left(nT_s, \frac{m}{NT_s}\right) = \left| \sum_{k=0}^{N-1} \tilde{r}(kT_s)\tilde{s}^*(kT_s - nT_s) \exp\left(-j2\pi \frac{mk}{N}\right) \right|^2. \qquad (2.21)$$

The range of nT_s in (2.21) is restricted to $[0, N_0 T_s]$ since the length of observation is N, and $N_0 T_s = NT_s - T$ is the predicted maximum delay. The range of m/N is restricted to -1/2 and 1/2 because of the frequency-domain periodicity which occurs with discrete-time processing. It should be pointed out that receivers implemented in the form of (2.21) are useful in generating statistics for different values of Doppler at a fixed delay (that is, slices in frequency). Figure 2.1 depicts the block diagram of this receiver.

Since the reference signal at the receiver is zero outside $[0, (N-1)T_s]$, we can extend the bounds of the summation in (2.21) to infinity, and the discrete time-frequency autocorrelation function associated with (2.21) can be explicitly expressed as

$$\hat{\phi}_{\tilde{s}}\left(nT_s, \tau_a, \frac{m}{NT_s}, f_{D_a}\right)$$

$$= \sum_{k=-\infty}^{\infty} \tilde{s}(kT_s - \tau_a)\tilde{s}^*(kT_s - nT_s) \exp\left[-j2\pi \left(\frac{m}{NT_s} - f_{D_a}\right) kT_s\right]. \qquad (2.22)$$

27

$\tilde{r}(t)$ $\tilde{r}$ $\tilde{s}^{\dagger}\tilde{r}$ Test statistic

Sampling device	Cross mutiply	FFT	Magnitude square

$\tilde{s}$
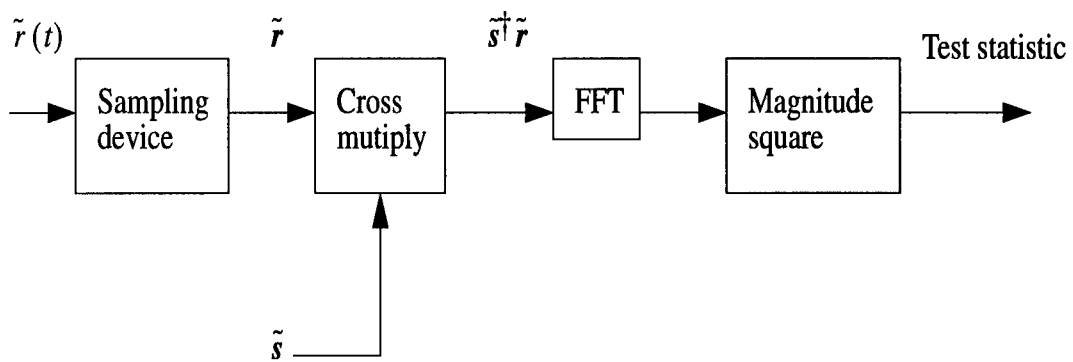
Figure 2.1: Time-domain realization of the conventional receiver

When τ_a is an integral multiple of T_s, say $\tau_a = pT_s$, and f_{D_a} is an integral multiple of $1/(NT_s)$, say $f_{D_a} = q/(NT_s)$, we have

$$\hat{\phi}_{\tilde{s}}\left(nT_s, pT_s, \frac{m}{NT_s}, \frac{q}{NT_s}\right)$$
$$= \sum_{k=-\infty}^{\infty} \tilde{s}(kT_s - pT_s)\tilde{s}^*(kT_s - nT_s)\exp\left[-j2\pi\frac{(m-q)k}{N}\right]. \qquad (2.23)$$

By setting $k' = k - p$, we have

$$\hat{\phi}_{\tilde{s}}\left(nT_s, pT_s, \frac{m}{NT_s}, \frac{q}{NT_s}\right)$$
$$= \exp\left[-j2\pi\frac{(m-q)p}{N}\right]\sum_{k'=-\infty}^{\infty} \tilde{s}(k'T_s)\tilde{s}^*(k'T_s - (n-p)T_s)\exp\left[-j2\pi\frac{(m-q)k'}{N}\right].$$
$$\qquad (2.24)$$

It follows that

$$\hat{\theta}_{\tilde{s}}\left(nT_s, pT_s, \frac{m}{NT_s}, \frac{q}{NT_s}\right)$$
$$= \left|\sum_{k=-\infty}^{\infty} \tilde{s}(kT_s)\tilde{s}^*(kT_s - (n-p)T_s)\exp\left[-j2\pi\frac{(m-q)k}{N}\right]\right|^2. \qquad (2.25)$$

Clearly, the ambiguity function given in (2.25) can be used for signal design purposes.

As in the continuous case, we can also generalize the notion of discrete ambiguity function to discrete cross-ambiguity function. The discrete time-frequency cross-correlation function of the two discrete-time signals $\tilde{s}_1$ and $\tilde{s}_2$ is defined as

$$\hat{\phi}_{\tilde{s}_1\tilde{s}_2}\left(nT_s, \frac{m}{NT_s}\right) = \sum_{k=-\infty}^{\infty} \tilde{s}_1(kT_s)\tilde{s}_2^*(kT_s - nT_s)\exp\left(-j2\pi\frac{mk}{N}\right) \qquad (2.26)$$

and the discrete cross-ambiguity function is defined as the magnitude square of (2.26). In this manner the test statistic (2.21) can be viewed as the cross-ambiguity function of $\tilde{r}$ and $\tilde{s}$. Denoting $\tilde{s}(t - \tau_a)\exp(j2\pi f_{D_a}t)$ by $\tilde{s}_r(t)$, (2.22) can also be expressed as a time-frequency cross-correlation function such that

$$\hat{\phi}_{\tilde{s}_r\tilde{s}}\left(nT_s, \frac{m}{NT_s}\right) = \sum_{k=-\infty}^{\infty} \tilde{s}_r(kT_s)\tilde{s}^*(kT_s - nT_s)\exp\left(-j2\pi\frac{mk}{N}\right). \qquad (2.27)$$

It should be noted that the discrete ambiguity function is sometimes only defined in the form of (2.25). In the context of radar detection and estimation, however, the parameters τ_a and f_{D_a} are continuous and the discrete form of (2.25) does not give an exact representation of the receiver's response. It is for this reason that we will use in the following analysis the definition of cross-ambiguity function of $\hat{s}_r$ and $\tilde{s}$ as given by the magnitude square of (2.27) to better describe the continuous nature of τ_a and f_{D_a}.

Finally, when n in (2.26) is an even number, say $n = 2u$, we can express the cross-correlation function as

$$\hat{\phi}_{\tilde{s}_1 \tilde{s}_2}\left(2uT_s, \frac{m}{NT_s}\right) = \sum_{k=-\infty}^{\infty} \tilde{s}_1(kT_s)\tilde{s}_2^*(kT_s - 2uT_s)\exp\left(-j2\pi\frac{mk}{N}\right)$$

$$= \exp\left(-j2\pi\frac{mu}{N}\right)\sum_{k=-\infty}^{\infty} \tilde{s}_1(kT_s + uT_s)\tilde{s}_2^*(kT_s - uT_s)\exp\left(-j2\pi\frac{mk}{N}\right). \quad (2.28)$$

The last relationship of (2.28) is defined as the symmetrical form of the discrete time-frequency cross-correlation function of the time samples. Denoting the symmetrical form of the discrete time-frequency cross-correlation function of the time samples as $\bar{\phi}_{\tilde{s}_1 \tilde{s}_2}(\cdot)$, we have

$$\bar{\phi}_{\tilde{s}_1 \tilde{s}_2}\left(uT_s, \frac{m}{NT_s}\right)$$

$$= \exp\left(-j2\pi\frac{mu}{N}\right)\sum_{k=-\infty}^{\infty} \tilde{s}_1(kT_s + uT_s)\tilde{s}_2^*(kT_s - uT_s)\exp\left(-j2\pi\frac{mk}{N}\right). \quad (2.29)$$

Hence the symmetrical form of the ambiguity function in the time-domain is defined as

$$\bar{\theta}_{\tilde{s}_1 \tilde{s}_2}\left(uT_s, \frac{m}{NT_s}\right) = \left|\sum_{k=-\infty}^{\infty} \tilde{s}_1(kT_s + uT_s)\tilde{s}_2^*(kT_s - uT_s)\exp\left(-j2\pi\frac{mk}{N}\right)\right|^2. \quad (2.30)$$

The discrete ambiguity function is sometimes defined in the form of (2.30) because of its resemblance to the symmetrical form ambiguity function of the continuous case. However, it is seen from the derivation that $\bar{\theta}_{\tilde{s}_1 \tilde{s}_2}(\cdot)$ is the special case of $\hat{\theta}_{\tilde{s}_1 \tilde{s}_2}(\cdot)$ where τ_a is an even integer multiple of T_s.

2.2.2 Frequency-domain Representation

The receiver can also be implemented in the frequency-domain. This result is due to the convolution theorem, which states that the discrete Fourier transform of the product of two sequences is equal to constant times the convolution between the discrete Fourier transforms of those two sequences. The exact value of the constant in the convolution theorem depends on how the discrete Fourier transform is defined. Note that the sufficient statistic calculated in the manner specified by (2.21) can be viewed as taking the magnitude square of the discrete Fourier transform of the product of the sequences $\{\tilde{r}(kT_s)\}$ and $\{\tilde{s}^*(kT_s - nT_s)\}$. From the convolution theorem, it is equivalent to the calculation of the magnitude square of constant times the convolution of the discrete Fourier transform of $\{\tilde{r}(kT_s)\}$ with that of $\{\tilde{s}^*(kT_s - nT_s)\}$.

For simplicity of notation and to follow the convention in the literature, we denote the Fourier transforms of signals by capital letters. The discrete Fourier transform of the sequence $\{\tilde{r}(kT_s)\}$ can be obtained by

$$\hat{R}\left(\frac{l}{NT_s}\right) = T_s \sum_{k=0}^{N-1} \tilde{r}(kT_s) \exp\left(-j2\pi\frac{lk}{N}\right), \text{ for all integer } l. \qquad (2.31)$$

The discrete Fourier transform of the sequence $\{\tilde{s}^*(kT_s - nT_s)\}$ can be obtained from that of $\{\tilde{s}^*(kT_s)\}$. The discrete Fourier transform of the sequence $\{\tilde{s}^*(kT_s)\}$ with N_0 zeros appended is

$$\hat{G}\left(\frac{l}{NT_s}\right) = T_s \sum_{k=0}^{N-1} \tilde{s}^*(kT_s) \exp\left(-j2\pi\frac{lk}{N}\right), \text{ for all integer } l. \qquad (2.32)$$

Note that

$$\hat{S}^*\left(\frac{l}{NT_s}\right) = T_s \sum_{k=0}^{N-1} \tilde{s}^*(kT_s) \exp\left(j2\pi\frac{lk}{N}\right) = \hat{G}\left(\frac{-l}{NT_s}\right), \text{ for all integer } l. \qquad (2.33)$$

Thus,

$$\hat{S}^*\left(\frac{l}{NT_s}\right) = \hat{G}\left(\frac{l}{NT_s}\right), \text{ for all integer } l. \qquad (2.34)$$

The discrete Fourier transform of the time shifted sequence $\{\tilde{s}^*(kT_s - nT_s)\}$ is

$$
\begin{aligned}
\hat{G}_{(n)}\left(\frac{l}{NT_s}\right) &= T_s \sum_{k=0}^{N-1} \tilde{s}^*(kT_s - nT_s) \exp\left(-j2\pi\frac{lk}{N}\right) \\
&= T_s \exp\left(-j2\pi\frac{ln}{N}\right) \sum_{k=0}^{N-1} \tilde{s}^*(kT_s) \exp\left(-j2\pi\frac{lk}{N}\right) \\
&= \exp\left(-j2\pi\frac{ln}{N}\right) \hat{G}\left(\frac{l}{NT_s}\right) \\
&= \exp\left(-j2\pi\frac{ln}{N}\right) \hat{S}^*\left(\frac{-l}{NT_s}\right)
\end{aligned}
\tag{2.35}
$$

for $0 \le n \le N_0$. Convolving $\hat{R}[l/(nT_s)]$ and $\hat{G}_{(n)}[l/(nT_s)]$, we have

$$
\sum_{l=0}^{N-1} \hat{R}\left(\frac{l}{NT_s}\right) \hat{G}_{(n)}\left(\frac{l-m}{NT_s}\right) = \sum_{l=0}^{N-1} \hat{R}\left(\frac{l}{NT_s}\right) \hat{S}^*\left(\frac{l-m}{NT_s}\right) \exp\left[j2\pi\frac{(l-m)n}{N}\right]
\tag{2.36}
$$

for $0 \le n \le N_0$. As mentioned earlier, the statistic (2.21) can equivalently be computed by taking the magnitude square of constant times (2.36). Due to the form of the discrete Fourier transform used here, the value of the constant is $1/(NT_s^2)$. Thus, for the region $0 \le n \le N_0$ and $-1/2 \le m/N < 1/2$ the receiver can also be implemented such that it calculates

$$
\Lambda\left(nT_s, \frac{m}{NT_s}\right) = \left| \frac{1}{NT_s^2} \sum_{l=0}^{N-1} \hat{R}\left(\frac{l}{NT_s}\right) \hat{S}^*\left(\frac{l-m}{NT_s}\right) \exp\left(j2\pi\frac{ln}{N}\right) \right|^2 .
\tag{2.37}
$$

It should be pointed out that a receiver implemented in the form of (2.37) is useful in generating the test statistic for different values of delay at fixed Doppler (that is, slices in time). Figure 2.2 depicts the block diagram of the receiver in which the statistic is computed as shown in (2.37).

From the linearity property of Fourier transforms it is clear that the Fourier transform of the received signal is the sum of the Fourier transforms of the target return and the noise when the target is present. Therefore, following the same approach as that used in deriving the time-domain representation of the discrete ambiguity function, it is also possible to derive a frequency-domain representation of the ambiguity function for the receiver (2.37) by ignoring those terms in (2.37) containing noise. Specifically, let $\hat{S}_r(\cdot)$ denote the Fourier transform of

32
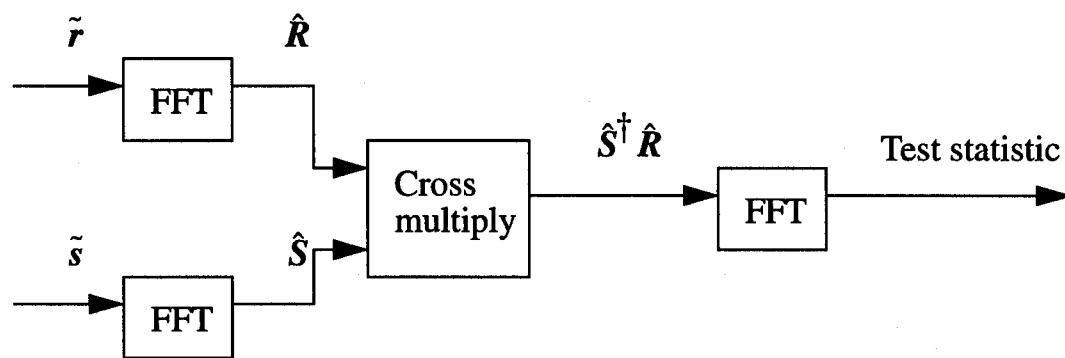
Figure 2.2: Frequency-domain realization of the conventional receiver

the scaled discrete-time samples of the target return $\{\tilde{s}(kT_s - \tau_a)\exp(j2\pi f_{D_a}kT_s)\}$. Then

$$\hat{S}_r\left(\frac{l}{NT_s}\right) = T_s \sum_{k=0}^{N-1} \{\tilde{s}(kT_s - \tau_a)\exp(j2\pi f_{D_a}kT_s)\} \exp\left(-j2\pi\frac{lk}{N}\right) \qquad (2.38)$$

for all integer l. Also, denote the Fourier transform of $\tilde{s}(t - \tau_a)\exp(j2\pi f_{D_a}t)$ by $\tilde{S}_r(\cdot)$. Then

$$\tilde{S}_r(f) = \int_{-\infty}^{\infty} \tilde{s}(t - \tau_a)\exp(j2\pi f_{D_a}t)\exp(-j2\pi ft)dt$$
$$= \exp[-j2\pi(f - f_{D_a})\tau_a]\tilde{S}(f - f_{D_a}). \qquad (2.39)$$

The discrete time-frequency cross correlation function in terms of the samples of the Fourier transforms of the discrete-time samples of the target return and of the reference signal can be defined in the form

$$\hat{\phi}_{\hat{S}_r\hat{S}}\left(nT_s, \frac{m}{NT_s}\right) = \frac{1}{NT_s^2} \sum_{l=0}^{N-1} \hat{S}_r\left(\frac{l}{NT_s}\right)\hat{S}^*\left(\frac{l-m}{NT_s}\right)\exp\left[j2\pi\frac{(l-m)n}{N}\right] \qquad (2.40)$$

where n, m are integers. From the generalized Parseval's theorem for the discrete Fourier transform, the discrete time-frequency correlation function thus defined is equivalent to (2.27) for $0 \leq n \leq N_0$ and $-1/2 \leq m/N < 1/2$. The generalized Parseval's theorem for the discrete Fourier transform is given as follows. If $\hat{S}_1$ and $\hat{S}_2$ denote the discrete Fourier transform of $\tilde{s}_1$ and $\tilde{s}_2$, respectively, then

$$\sum_{k=0}^{N-1} \tilde{s}_1(kT_s)\tilde{s}_2^*(kT_s) = \frac{1}{NT_s^2} \sum_{l=0}^{N-1} \hat{S}_1\left(\frac{l}{NT_s}\right)\hat{S}_2^*\left(\frac{l}{NT_s}\right) \qquad (2.41)$$

The above relationship can be derived by a direct substitution of the definition of the discrete Fourier transformation. An extension of (2.41) is given in Section 3 of Appendix A, where we consider the relationship between the inner product of continuous signals and inner product of discrete signals. Finally, using (2.41), we have

$$\hat{\phi}_{\hat{S}_r\hat{S}}\left(nT_s, \frac{m}{NT_s}\right) = \hat{\phi}_{\tilde{s}_r\tilde{s}}\left(nT_s, \frac{m}{NT_s}\right) \qquad (2.42)$$

for $0 \leq n \leq N_0$ and $-1/2 \leq m/N < 1/2$.

When $0 \leq \tau_a \leq N_0 T_s$, τ_a is an integral multiple of T_s, say $\tau_a = pT_s$, and f_{D_a} is an integral multiple of $1/(NT_s)$, say $f_{D_a} = q/(NT_s)$, we have from (2.38)

$$\hat{S}_r\left(\frac{l}{NT_s}\right) = T_s \sum_{k=-\infty}^{\infty} \tilde{s}(kT_s - pT_s) \exp\left[-j2\pi\frac{(l-q)k}{N}\right]$$

$$= \exp\left[-j2\pi\frac{(l-q)p}{N}\right] \hat{S}\left(\frac{l-q}{NT_s}\right). \tag{2.43}$$

In this case,

$$\hat{\phi}_{\hat{S}_r\hat{S}}\left(nT_s, \frac{m}{NT_s}\right)$$

$$= \frac{1}{NT_s^2} \exp\left(j2\pi\frac{qp-mn}{N}\right) \sum_{l=0}^{N-1} \hat{S}\left(\frac{l-q}{NT_s}\right) \hat{S}^*\left(\frac{l-m}{NT_s}\right) \exp\left[j2\pi\frac{l(n-p)}{N}\right]$$

$$= \frac{1}{NT_s^2} \exp\left(-j2\pi\frac{(m-q)n}{N}\right) \sum_{l=-q}^{N-q-1} \hat{S}\left(\frac{l}{NT_s}\right) \hat{S}^*\left(\frac{l-(m-q)}{NT_s}\right)$$

$$\cdot \exp\left[j2\pi\frac{l(n-p)}{N}\right]$$

$$= \frac{1}{NT_s^2} \exp\left(-j2\pi\frac{(m-q)n}{N}\right) \left\{\sum_{l=-q}^{-1} + \sum_{l=0}^{N-q-1}\right\} \hat{S}\left(\frac{l}{NT_s}\right) \hat{S}^*\left(\frac{l-(m-q)}{NT_s}\right)$$

$$\cdot \exp\left[j2\pi\frac{l(n-p)}{N}\right]. \tag{2.44}$$

Since $\hat{S}(\cdot)$ is periodic with period $1/T_s$, $\hat{S}[l/(NT_s)] = \hat{S}[(l+N)/(NT_s)]$. Also, $\exp(j2\pi k/N) = \exp[j2\pi(k+N)/N]$. It follows that

$$\hat{\phi}_{\hat{S}_r\hat{S}}\left(nT_s, \frac{m}{NT_s}\right)$$

$$= \frac{1}{NT_s^2} \exp\left(-j2\pi\frac{(m-q)n}{N}\right)$$

$$\cdot \sum_{l=-q}^{-1} \hat{S}\left(\frac{l+N}{NT_s}\right) \hat{S}^*\left(\frac{l+N-(m-q)}{NT_s}\right) \exp\left[j2\pi\frac{(l+N)(n-p)}{N}\right]$$

$$+ \frac{1}{NT_s^2} \exp\left(-j2\pi\frac{(m-q)n}{N}\right)$$

$$\cdot \sum_{l=0}^{N-q-1} \hat{S}\left(\frac{l}{NT_s}\right) \hat{S}^*\left(\frac{l-(m-q)}{NT_s}\right) \exp\left[j2\pi\frac{l(n-p)}{N}\right]$$

$$= \frac{1}{NT_s^2} \exp\left(-j2\pi\frac{(m-q)n}{N}\right)$$

$$\cdot \sum_{l=0}^{N-1} \hat{S}\left(\frac{l}{NT_s}\right) \hat{S}^*\left(\frac{l-(m-q)}{NT_s}\right) \exp\left[j2\pi\frac{l(n-p)}{N}\right] \qquad (2.45)$$

and

$$\hat{\theta}_{\hat{S}_r\hat{S}}\left(nT_s, \frac{m}{NT_s}\right) = \left|\frac{1}{NT_s^2}\sum_{l=0}^{N-1} \hat{S}\left(\frac{l}{NT_s}\right) \hat{S}^*\left(\frac{l-(m-q)}{NT_s}\right) \exp\left[j2\pi\frac{l(n-p)}{N}\right]\right|^2. \qquad (2.46)$$

The ambiguity function given in the form of (2.46) can be generated using one set of signal samples along with the fast Fourier transform. Therefore, it is useful in design of the transmitted waveform. The advantages of (2.25) and (2.46) are presented in [29], and they will also be discussed in the next subsection after we examine the sampling criteria.

When m in (2.40) is an even number, say $m = 2v$, we have

$$\hat{\phi}_{\hat{S}_r\hat{S}}\left(nT_s, \frac{2v}{NT_s}\right)$$
$$= \frac{1}{NT_s^2}\sum_{l=0}^{N-1} \hat{S}_r\left(\frac{l}{NT_s}\right) \hat{S}^*\left(\frac{l-2v}{NT_s}\right) \exp\left[j2\pi\frac{(l-2v)n}{N}\right]$$
$$= \frac{1}{NT_s^2}\left\{\sum_{l=v}^{N-1} + \sum_{l=N}^{N+v-1}\right\} \hat{S}_r\left(\frac{l+v}{NT_s}\right) \hat{S}^*\left(\frac{l-v}{NT_s}\right) \exp\left[j2\pi\frac{(l-v)n}{N}\right]. \qquad (2.47)$$

Since $\hat{S}_r$, $\hat{S}$, and $\exp(j2\pi k/N)$ are periodic, we have

$$\hat{\phi}_{\hat{S}_r\hat{S}}\left(nT_s, \frac{2v}{NT_s}\right)$$
$$= \frac{1}{NT_s^2}\sum_{l=v}^{N-1} \hat{S}_r\left(\frac{l+v}{NT_s}\right) \hat{S}^*\left(\frac{l-v}{NT_s}\right) \exp\left[j2\pi\frac{(l-v)n}{N}\right]$$
$$+ \frac{1}{NT_s^2}\sum_{l=N}^{N+v-1} \hat{S}_r\left(\frac{l+v-N}{NT_s}\right) \hat{S}^*\left(\frac{l-v-N}{NT_s}\right) \exp\left[j2\pi\frac{(l-v-N)n}{N}\right]$$
$$= \frac{1}{NT_s^2}\sum_{l=0}^{N-1} \hat{S}_r\left(\frac{l+v}{NT_s}\right) \hat{S}^*\left(\frac{l-v}{NT_s}\right) \exp\left[j2\pi\frac{(l-v)n}{N}\right] \qquad (2.48)$$

The last equality in (2.48) is defined as the symmetrical form of the discrete time-frequency correlation function of the frequency samples. That is, denoting the symmetrical form of the discrete time-frequency correlation function of the frequency samples by $\bar{\phi}_{\hat{S}_r\hat{S}}(\cdot)$, we have

$$\bar{\phi}_{\hat{S}_r\hat{S}}\left(nT_s, \frac{m}{NT_s}\right) = \frac{1}{NT_s^2}\sum_{l=0}^{N-1} \hat{S}_r\left(\frac{l+m}{NT_s}\right) \hat{S}^*\left(\frac{l-m}{NT_s}\right) \exp\left[j2\pi\frac{(l-m)n}{N}\right] \qquad (2.49)$$

36

where $0 \leq n \leq N_0$ and $-1/2 \leq q/N < 1/2$. The magnitude square of (2.49) is defined as the symmetrical form of the discrete ambiguity function in the frequency-domain. It is sometimes used as the definition of the discrete ambiguity function in the frequency-domain. However, it is clear that $\bar{\phi}_{\hat{S}_r,\hat{S}}(\cdot)$ is a special case of $\hat{\phi}_{\hat{S}_r,\hat{S}}(\cdot)$ where f_{D_H} is an even integer multiple of $1/(NT_s)$.

2.2.3 Relationship between Discrete and Continuous Ambiguity Functions

In the previous subsection, the discrete time-frequency correlation functions and discrete ambiguity functions in the time-domain and in the frequency-domain were defined. These ambiguity functions can be used to examine the resolution capability of the transmitted signal waveforms. In the following, we examine the relationships between the discrete forms of ambiguity function and their continuous counterparts.

Sampling criteria

From Chapter 1 the time-frequency correlation function of the continuous signals $\tilde{s}_r(t)$ and $\tilde{s}(t)$ is defined as

$$\phi_{\tilde{s}_r,\tilde{s}}(\tau_H, f_{D_H}) = \int_{-\infty}^{\infty} \tilde{s}_r(t)\tilde{s}^*(t - \tau_H) \exp(-j2\pi f_{D_H} t)dt \qquad (2.50)$$

and its magnitude square is defined as the ambiguity function $\theta_{\tilde{s}_r,\tilde{s}}(\tau_H, f_{D_H})$. Using the generalized Parseval's theorem, the equivalent form of (2.50) in frequency-domain is given by

$$\phi_{\tilde{s}_r,\tilde{s}}(\tau_H, f_{D_H}) = \exp(-j2\pi f_{D_H}\tau_H) \int_{-\infty}^{\infty} \tilde{S}_r(f)\tilde{S}^*(f - f_{D_H}) \exp(j2\pi f\tau_H)df. \qquad (2.51)$$

Since it was assumed that the lowpass signal $\tilde{s}(t)$ has a duration of T and a double-sided bandwidth of $2B$, $\phi_{\tilde{s}_r,\tilde{s}}(\cdot)$ has an extent of $2T$ in the τ_H domain, centered around τ_a, and an

37

extent of $4B$ in the f_{D_H} domain, centered around f_{D_a}. In the following discussion we use $\phi_{\tilde{s}_r\tilde{s}}(\cdot)$ and $\phi_{\tilde{S}_r\tilde{S}}(\cdot)$ to distinguish whether the continuous time-frequency correlation function is defined in the time-domain or in the frequency-domain; however, it should be clear that they are equal to each other.

From (2.27), we have

$$\hat{\phi}_{\tilde{s}_r\tilde{s}}\left(nT_s, \frac{m}{NT_s}\right) = \sum_{k=-\infty}^{\infty} \tilde{s}_r(kT_s)\tilde{s}^*(kT_s - nT_s)\exp\left(-j2\pi\frac{mk}{N}\right)$$

$$= \sum_{k=-\infty}^{\infty}\left\{\int_{-\infty}^{\infty}\tilde{s}_r(t)\tilde{s}^*(t-nT_s)\exp\left(-j2\pi\frac{mt}{NT_s}\right)\delta(t-kT_s)dt\right\}$$

$$= \int_{-\infty}^{\infty}\tilde{s}_r(t)\tilde{s}^*(t-nT_s)\exp\left(-j2\pi\frac{mt}{NT_s}\right)\left\{\sum_{k=-\infty}^{\infty}\delta(t-kT_s)\right\}dt \qquad (2.52)$$

where it was assumed that the order of the integration and summation are interchangeable. The term in the braces of the last relationship of (2.52) can be evaluated using Poisson's sum formula, which is given by

$$\sum_{k=-\infty}^{\infty}\delta(t-kT_s) = \frac{1}{T_s}\sum_{k=-\infty}^{\infty}\exp\left(\frac{j2\pi kt}{T_s}\right). \qquad (2.53)$$

Hence,

$$\hat{\phi}_{\tilde{s}_r\tilde{s}}\left(nT_s, \frac{m}{NT_s}\right)$$

$$= \int_{-\infty}^{\infty}\tilde{s}_r(t)\tilde{s}^*(t-nT_s)\exp\left(-j2\pi\frac{mt}{NT_s}\right)\left\{\frac{1}{T_s}\sum_{k=-\infty}^{\infty}\exp\left(\frac{j2\pi kt}{T_s}\right)\right\}dt$$

$$= \frac{1}{T_s}\sum_{k=-\infty}^{\infty}\left\{\int_{-\infty}^{\infty}\tilde{s}_r(t)\tilde{s}^*(t-nT_s)\exp\left[-j2\pi\frac{(m-kN)t}{NT_s}\right]dt\right\}$$

$$= \frac{1}{T_s}\sum_{k=-\infty}^{\infty}\phi_{\tilde{s}_r\tilde{s}}\left(nT_s, \frac{m-kN}{NT_s}\right). \qquad (2.54)$$

The discrete ambiguity function $\hat{\theta}_{\tilde{s}_r\tilde{s}}(\cdot)$ is the magnitude square of (2.54), thus,

$$\hat{\theta}_{\tilde{s}_r\tilde{s}}\left(nT_s, \frac{m}{NT_s}\right) = \left|\frac{1}{T_s}\sum_{k=-\infty}^{\infty}\phi_{\tilde{s}_r\tilde{s}}\left(nT_s, \frac{m-kN}{NT_s}\right)\right|^2$$

$$= \frac{1}{T_s^2}\theta_{\tilde{s}_r\tilde{s}}\left(nT_s, \frac{m}{NT_s}\right) + \left|\frac{1}{T_s}\sum_{\substack{k=-\infty\\k\neq 0}}^{\infty}\phi_{\tilde{s}_r\tilde{s}}\left(nT_s, \frac{m-kN}{NT_s}\right)\right|^2$$

$$+2\mathrm{Re}\left\{\frac{1}{T_s^2}\phi_{\tilde{s}_r\tilde{s}}^*\left(nT_s,\frac{m}{NT_s}\right)\cdot\sum_{\substack{k=-\infty\\k\neq 0}}^{\infty}\phi_{\tilde{s}_r\tilde{s}}\left(nT_s,\frac{m-kN}{NT_s}\right)\right\} \quad (2.55)$$

The above relationship indicates that the discrete ambiguity function $\hat{\theta}_{\tilde{s}_r\tilde{s}}(\cdot)$ consists of aliasing terms that are separated from each other by integral multiples of $1/T_s$ in the frequency dimension. Recall that $\phi_{\tilde{s}_r\tilde{s}}(\cdot)$ has an extent of $4B$ in the frequency dimension. Thus, to prevent aliasing in (2.55), the samples used in calculating $\hat{\theta}_{\tilde{s}_r\tilde{s}}(\cdot)$ need to be obtained at a rate greater than twice the Nyquist rate of the transmitted signal. Otherwise, the missing samples need to be obtained by interpolation when $2B < 1/T_s < 4B$.

Example 2.1

As an example, we consider the effects of aliasing in the time-domain auto-ambiguity function of the complex envelope

$$\tilde{s}(t) = \sqrt{2B}\frac{\sin 2\pi Bt}{2\pi Bt} = \sqrt{2B}\mathrm{sinc}(2Bt). \quad (2.56)$$

The discrete ambiguity function obtained at different sampling rates is shown in Figures 2.4 through 2.6. Because of the presence of the sinc function, $\tilde{s}(t)$ is bandlimited to a double-sided bandwidth of $2B$ Hertz. By means of a straightforward calculation, the continuous ambiguity function of $\tilde{s}(t)$ is found to be

$$\theta_{\tilde{s}}(\tau, f_D) = \left|\mathrm{rect}\left(\frac{f_D}{4B}\right)\frac{(2B-|f_D|)}{2B}\mathrm{sinc}\left[\tau(2B-|f_D|)\right]\right|^2. \quad (2.57)$$

The result is plotted in Figure 2.3 for $B = 1$. The discrete ambiguity function $\hat{\theta}_{\tilde{s}}(\tau, f_D)$ obtained with a sampling frequency equal to twice the Nyquist rate is shown in Figure 2.4. Note the periodicity of $\hat{\theta}_{\tilde{s}}(\tau, f_D)$ along the frequency axis and the lack of aliasing. When the sampling rate is dropped to 1.8 and 1.5 times the Nyquist rate, noticeable aliasing occurs, as shown in Figures 2.5 and 2.6. Aliasing becomes more severe as the sampling rate is decreased. $\square$
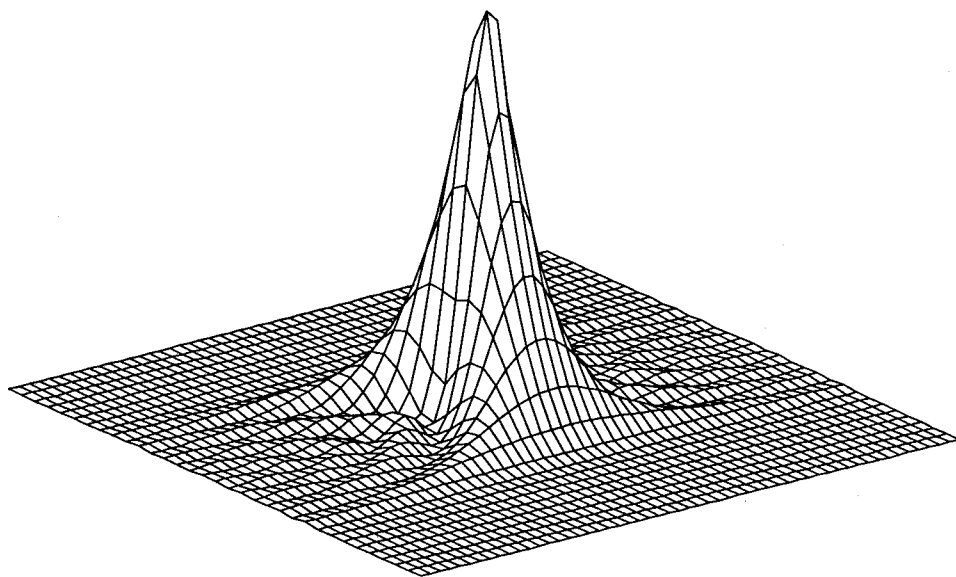
Figure 2.3: Continuous ambiguity function
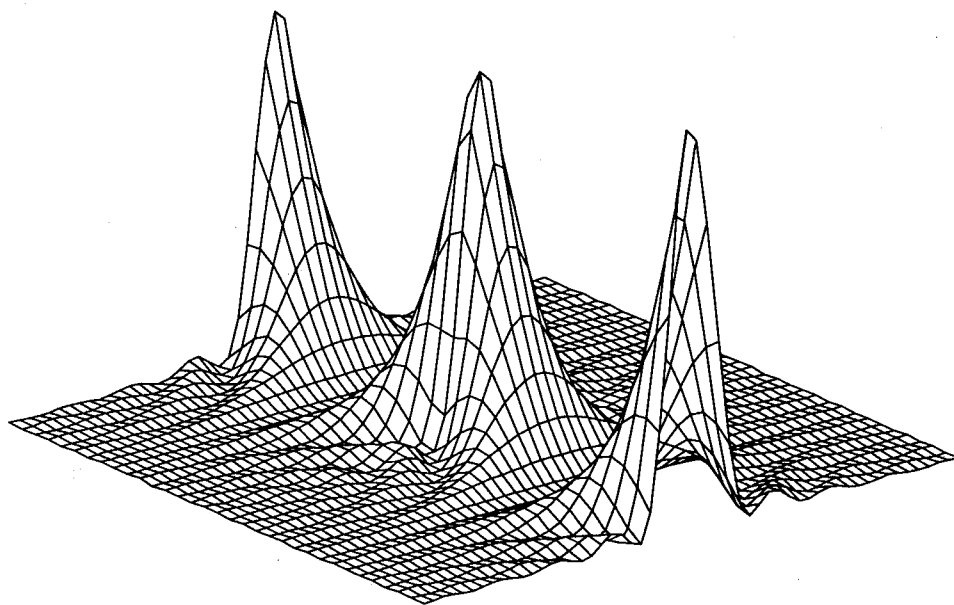
Figure 2.4: Discrete ambiguity function when the signal is sampled at twice Nyquist rate
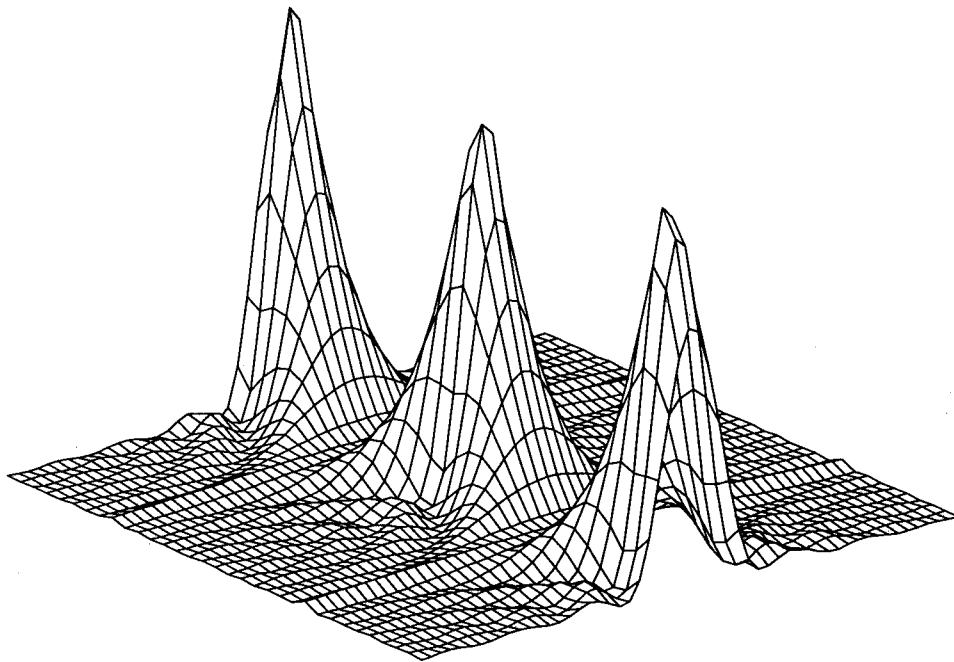
Figure 2.5: Discrete ambiguity function when the signal is sampled at 1.8 times the Nyquist rate
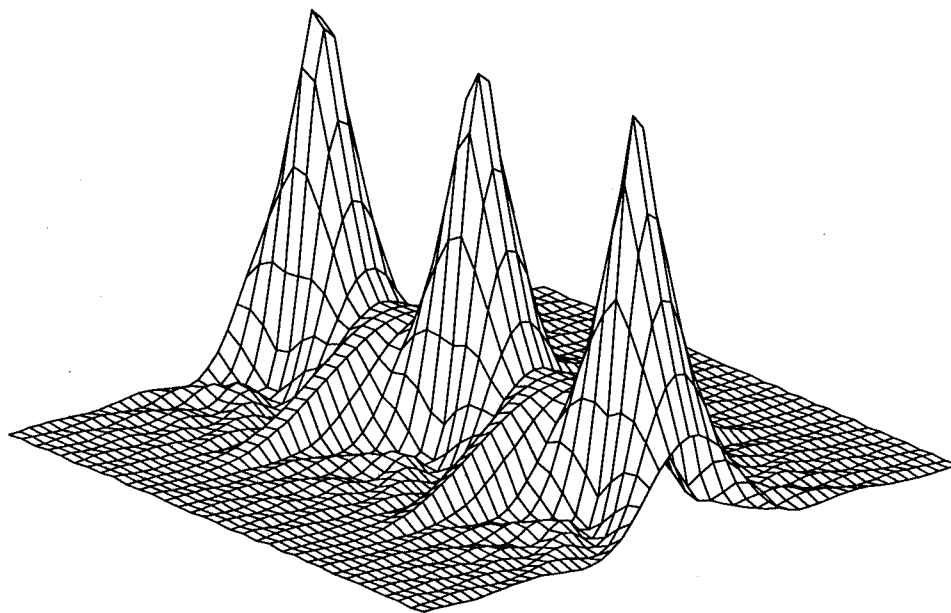
Figure 2.6: Discrete ambiguity function when the signal is sampled at 1.5 times the Nyquist rate

When the receiver is implemented in the form of (2.21), the statistic calculated by the receiver is

$$\Lambda\left(nT_s, \frac{m}{NT_s}\right) = E_t|\tilde{b}|^2\hat{\theta}_{\tilde{s}_r\tilde{s}}\left(nT_s, \frac{m}{NT_s}\right) + \{\text{noise terms}\}$$

$$= \frac{E_t|\tilde{b}|^2}{T_s^2}\theta_{\tilde{s}_r\tilde{s}}\left(nT_s, \frac{m}{NT_s}\right) + E_t|\tilde{b}|^2\left|\frac{1}{T_s}\sum_{\substack{k=-\infty \\ k\neq 0}}^{\infty}\phi_{\tilde{s}_r\tilde{s}}\left(nT_s, \frac{m-kN}{NT_s}\right)\right|^2$$

$$+ 2E_t|\tilde{b}|^2\text{Re}\left\{\frac{1}{T_s^2}\phi_{\tilde{s}_r\tilde{s}}^*\left(nT_s, \frac{m}{NT_s}\right) \cdot \sum_{\substack{k=-\infty \\ k\neq 0}}^{\infty}\phi_{\tilde{s}_r\tilde{s}}\left(nT_s, \frac{m-kN}{NT_s}\right)\right\}$$

$$+ \{\text{noise terms}\} \quad . \tag{2.58}$$

The last equality in (2.58) indicates that aliasing will be present in $\Lambda(\cdot)$ when the received signal is sampled at the Nyquist rate. Each of the aliasing terms has an extension of $4B$ in the frequency dimension, and each is separated from the others by an integral multiple of $1/T_s$ in the frequency dimension. Thus, the samples used in calculating the statistic $\Lambda(\cdot)$ in the form of (2.21) need to be obtained either at a rate greater than twice the Nyquist rate of the transmitted signal, or by interpolation when $2B < 1/T_s < 4B$. Otherwise, degradation in receiver performance as compared to that of the continuous case will occur due to aliasing in the ambiguity function. A sampling rate less than twice the Nyquist rate can be used only when the resulting aliasing can be tolerated in the specific application.

As shown earlier, the statistic can also be evaluated in the frequency-domain in the form of (2.37). Since $\hat{S}(\cdot)$ and $\exp(j2\pi k/N)$ are both periodic with period $1/T_s$, $\hat{\phi}_{\hat{S}_r\hat{S}}(\cdot)$ is also periodic with period $1/T_s$. Therefore, following the same procedure used in deriving the sampling criteria for the test statistic calculated in the time-domain, we can conclude that signal samples used to generate the test statistic in the manner specified by (2.37) need also be obtained at twice the Nyquist rate.

It should be pointed out that sampling at twice the Nyquist rate is sometimes unachievable because of hardware limitations. With the following example, we illustrate a simple procedure for raising the sampling rate by a factor of two.

44

Example 2.2

Consider the complex signal

$$\tilde{s}(t) = \sqrt{2B}\frac{\sin 2\pi B(t - t_m)}{2\pi B(t - t_m)} = \sqrt{2B}\text{sinc}[2B(t - t_m)]. \qquad (2.59)$$

Let $B = 1$ Hertz and $t_m = 0.8$ sec. The value of B indicates that the Nyquist rate is 2 Hertz, and the value of t_m indicates that $\tilde{s}(t)$ peaks at $t = 0.8$ sec. Assume that the signal duration is *essentially* limited to the interval from 0 to 1.6 sec., which covers about 94% of the signal's energy. Also assume that two sets of samples are obtained; one set is obtained at a sampling rate of 2.5 Hertz and the other is obtained at 5 Hertz. One period of the discrete Fourier transform magnitude for the two sets of samples is plotted in Figures 2.7 and 2.8, respectively. Comparing these two figures, it is seen that the Fourier transform of the samples with the higher sampling rate can be approximated by zero-padding the Fourier transform of the samples with the lower sampling rate. The quality of the approximation depends on the accuracy of the assumptions concerning the duration and bandwidth of the signal. Thus, the receiver in the form of (2.37) is more suitable when sampling at twice the Nyquist rate is physically unattainable since a higher sampling rate can be approximated by augmenting with zeros the discrete Fourier transforms of the received samples and reference. This procedure will be considered further in the next chapter where we discuss alternative forms of the discrete receiver. □

As mentioned before, the discrete ambiguity function in the form (2.46) has been utilized to examine the ambiguity function of the transmitted signal at an early signal design stage and thus to show whether the signal is suitable for the intended radar application. In this assessment, (2.46) is calculated for the region which covers $[0, NT_s]$ in the delay domain and an interval equal to $1/T_s$ in length in the Doppler domain. Recall from the previous discussion that the discrete ambiguity function has aliasing terms separated from each other by integral multiples of $1/T_s$ in the Doppler dimension, and each of the aliasing terms has an extent of $4B$ in the Doppler dimension. In other words, when sampling at twice the Nyquist
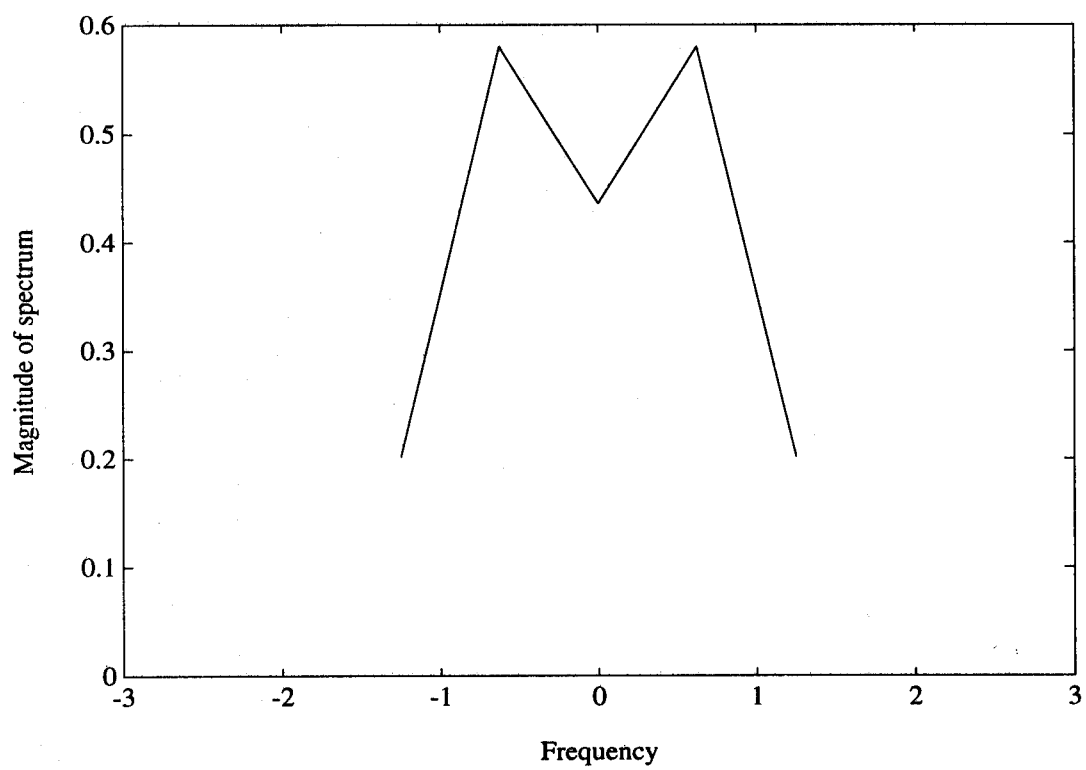
Figure 2.7: Discrete Fourier transform of the signal sampled at 1.25 times the Nyquist rate
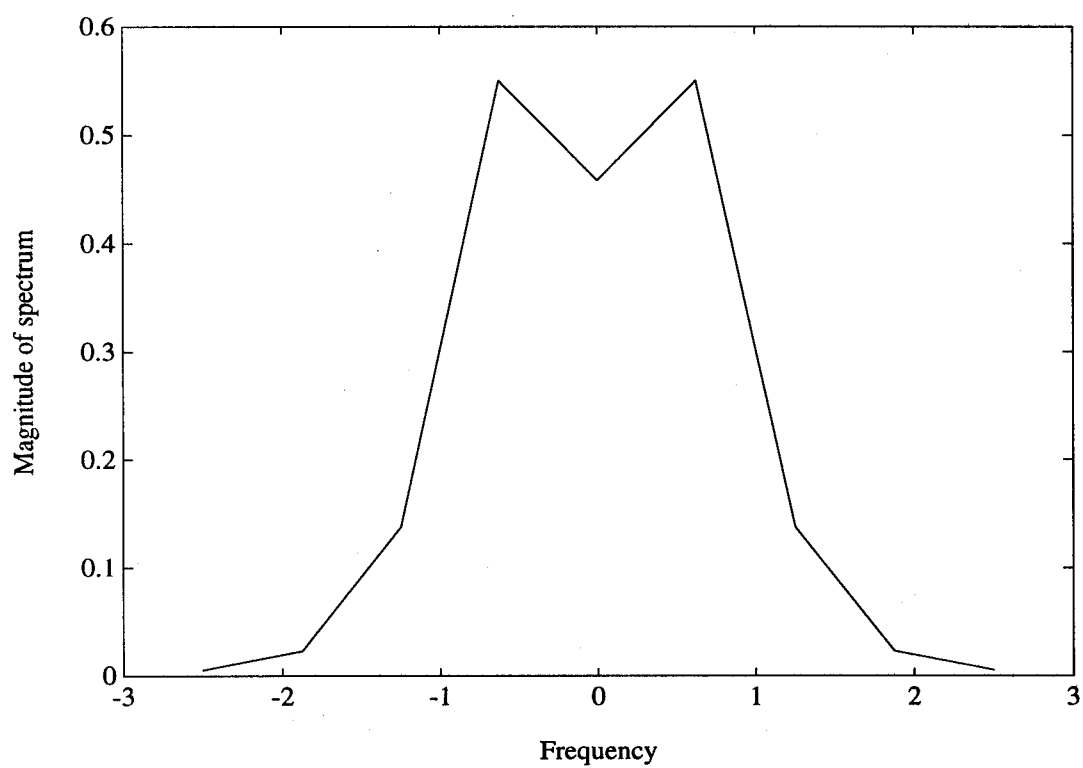
Figure 2.8: Discrete Fourier transform of the signal sampled at 2.5 times the Nyquist rate

47

rate, the discrete ambiguity function is free of aliasing in the region from $-1/(2T_s) + 2B$ to $1/(2T_s) - 2B$ in the Doppler dimension. In the aliasing-free region, we have

$$
\hat{\phi}_{\hat{S}}\left(nT_s, pT_s, \frac{m}{NT_s}, \frac{l}{NT_s}\right) = \frac{1}{NT_s^2} \sum_{l=0}^{N-1} \hat{S}\left(\frac{l}{NT_s}\right) \hat{S}^*\left(\frac{l-(m-q)}{NT_s}\right) \exp\left[j2\pi \frac{l(n-p)}{N}\right]
$$

$$
= \frac{1}{NT_s^2} \sum_{l=0}^{N-1} \tilde{S}\left(\frac{l}{NT_s}\right) \tilde{S}^*\left(\frac{l-(m-q)}{NT_s}\right) \exp\left[j2\pi \frac{l(n-p)}{N}\right]
$$

(2.60)

where $|m-q|/(NT_s) \leq [1/(2T_s) - 2B]$. Since the signal has an essentially limited spectrum, the bounds on the summation in the second line of (2.60) can be extended to infinity. In a manner similar to the one used in deriving (2.52), we have

$$
\sum_{l=-\infty}^{\infty} \tilde{S}\left(\frac{l}{NT_s}\right) \tilde{S}^*\left(\frac{l-(m-q)}{NT_s}\right) \exp\left[j2\pi \frac{l(n-p)}{N}\right]
$$

$$
= \sum_{l=-\infty}^{\infty} \left\{ \int_{-\infty}^{\infty} \tilde{S}(f)\tilde{S}^*\left(f - \frac{m-q}{NT_s}\right) \exp[j2\pi f(nT_s - pT_s)]\delta\left(f - \frac{l}{NT_s}\right) df \right\}
$$

$$
= \int_{-\infty}^{\infty} \tilde{S}(f)\tilde{S}^*\left(f - \frac{m-q}{NT_s}\right) \exp[j2\pi f(nT_s - pT_s)] \left\{ \sum_{l=-\infty}^{\infty} \delta\left(f - \frac{l}{NT_s}\right) \right\} df. \quad (2.61)
$$

Using Poisson's sum formula, we have

$$
\sum_{l=0}^{N-1} \hat{S}\left(\frac{l}{NT_s}\right) \hat{S}^*\left(\frac{l-(m-q)}{NT_s}\right) \exp\left[j2\pi \frac{l(n-p)}{N}\right]
$$

$$
= \int_{-\infty}^{\infty} \tilde{S}(f)\tilde{S}^*\left(f - \frac{m-q}{NT_s}\right) \exp[j2\pi f(nT_s - pT_s)]
$$

$$
\cdot \left\{ NT_s \sum_{l=-\infty}^{\infty} \exp\left(-j2\pi f l NT_s\right) \right\} df
$$

$$
= NT_s \sum_{l=-\infty}^{\infty} \left\{ \int_{-\infty}^{\infty} \tilde{S}(f)\tilde{S}^*\left(f - \frac{m-q}{NT_s}\right) \exp[j2\pi f(nT_s - pT_s - lNT_s)] \right\} df
$$

$$
= NT_s \exp\left(j2\pi \frac{mn-qp}{N}\right) \sum_{l=-\infty}^{\infty} \phi_{\tilde{S}}\left(nT_s - pT_s - lNT_s, \frac{m-q}{NT_s}\right). \quad (2.62)
$$

It follows that

$$
\hat{\theta}_{\hat{S}}\left(nT_s, pT_s, \frac{m}{NT_s}, \frac{q}{NT_s}\right) = \left| \frac{1}{NT_s^2} \sum_{l=0}^{N-1} \hat{S}\left(\frac{l}{NT_s}\right) \hat{S}^*\left(\frac{l-m+q}{NT_s}\right) \exp\left(j2\pi \frac{l(n-p)}{NT_s}\right) \right|^2
$$

$$
= \left| \frac{1}{T_s} \sum_{l=-\infty}^{\infty} \phi_{\tilde{S}}\left(nT_s - pT_s - lNT_s, \frac{m-q}{NT_s}\right) \right|^2. \quad (2.63)
$$

The above relationship indicates that $\hat{\theta}_{\hat{s}}(\cdot)$ consists of a sum of terms, each of which has an extent of $2T = 2N_1 T_s$ and is separated from the others by an integral multiple of NT_s in the τ_H domain. Thus, if (2.46) is used for the region $[0, NT_s]$ in the τ_H domain, N has to be chosen such that $N \geq 2N_1$ to prevent aliasing in the ambiguity function.

Reconstruction of the continuous ambiguity function from the discrete ambiguity function

In the following we consider a procedure for recovering the continuous ambiguity function from the discrete one. The treatment is different from that of [16]. The interpolation formula obtained is simpler than the previous one, but with the drawback that it can only be used to recover the region of the ambiguity function which is free of aliasing. This new result is due to a key observation dealing with the interpolation formulas for time delayed and frequency shifted signals. For the sake of brevity in the present discussion, we place a review on the interpolation formulas for time delayed and frequency shifted signals in Appendix A.

As shown in Appendix A, when the sampling rate is such that $1/T_s > 2(B + |f_{D_H}|)$, the result in (A.6) can be used to obtain

$$
\begin{aligned}
\tilde{s}(t - \tau_H)\exp(j2\pi f_{D_H}t) &= \tilde{s}(t - \tau_H)\exp[j2\pi f_{D_H}(t - \tau_H)]\exp(j2\pi f_{D_H}\tau_H) \\
&= \sum_{l=-\infty}^{\infty} \tilde{s}(lT_s - \tau_H)\exp(j2\pi f_{D_H}lT_s)\frac{\sin\pi(t/T_s - l)}{\pi(t/T_s - l)}.
\end{aligned}
\tag{2.64}
$$

The same procedure can be used to expand $\tilde{s}_r(t)$ when $1/T_s > 2(B + |f_{D_a}|)$. Thus, when the sampling rate is such that $1/T_s > 2(B + |f_{D_H}|)$ and $1/T_s > 2(B + |f_{D_a}|)$, the continuous time-frequency correlation function can be written as

$$
\begin{aligned}
\phi_{\tilde{s}_r\tilde{s}}(\tau_H, f_{D_H}) = \int_{-\infty}^{\infty} &\left[\sum_{k=-\infty}^{\infty} \tilde{s}(kT_s - \tau_a)\exp(j2\pi f_{D_a}kT_s)\frac{\sin\pi(t/T_s - k)}{\pi(t/T_s - k)}\right] \\
&\cdot \left[\sum_{l=-\infty}^{\infty} \tilde{s}(lT_s - \tau_H)\exp(j2\pi f_{D_H}lT_s)\frac{\sin\pi(t/T_s - l)}{\pi(t/T_s - l)}\right]^{*} dt
\end{aligned}
$$

49

$$= \sum_{k=-\infty}^{\infty} \sum_{l=-\infty}^{\infty} \tilde{s}(kT_s - \tau_a)\tilde{s}^*(lT_s - \tau_H) \exp[j2\pi(f_{D_a}kT_s - f_{D_H}lT_s)]$$

$$\cdot \left[\int_{-\infty}^{\infty} \frac{\sin \pi(t/T_s - k)}{\pi(t/T_s - k)} \frac{\sin \pi(t/T_s - l)}{\pi(t/T_s - l)} dt \right]. \qquad (2.65)$$

The integration can be evaluated using Parseval's theorem, as shown below:

$$\int_{-\infty}^{\infty} \frac{\sin \pi(t/T_s - k)}{\pi(t/T_s - k)} \frac{\sin \pi(t/T_s - l)}{\pi(t/T_s - l)} dt$$

$$= \int_{-\infty}^{\infty} \left[T_s \text{rect}(fT_s) \exp(-j2\pi f k T_s) \right] \left[T_s \text{rect}(fT_s) \exp(-j2\pi f l T_s) \right]^* df$$

$$= T_s \frac{\sin[\pi(l - k)]}{\pi(l - k)}$$

$$= T_s \delta_{lk} \qquad (2.66)$$

where δ_{lk} is the Kronecker delta. Thus,

$$\phi_{\tilde{s}_r\tilde{s}}(\tau_H, f_{D_H}) = T_s \sum_{k=-\infty}^{\infty} \tilde{s}(kT_s - \tau_a)\tilde{s}^*(kT_s - \tau_H) \exp[-j2\pi(f_{D_H} - f_{D_a})kT_s], \qquad (2.67)$$

when $1/T_s > 2(B + |f_{D_H}|)$ and $1/T_s > 2(B + |f_{D_a}|)$. At $\tau_H = nT_s$ and $f_{D_H} = m/(NT_s)$, we have

$$\phi_{\tilde{s}_r\tilde{s}}\left(nT_s, \frac{m}{NT_s}\right)$$

$$= T_s \sum_{k=-\infty}^{\infty} \tilde{s}(kT_s - \tau_a)\tilde{s}^*(kT_s - nT_s) \exp\left[-j2\pi\left(\frac{m}{NT_s} - f_{D_a}\right)kT_s\right] \qquad (2.68)$$

provided both $|m/(NT_s)|$ and $|f_{D_a}|$ are less than $[1/(2T_s) - B]$. Comparing with (2.27), we have

$$\phi_{\tilde{s}_r\tilde{s}}\left(nT_s, \frac{m}{NT_s}\right) = T_s \hat{\phi}_{\tilde{s}_r\tilde{s}}\left(nT_s, \frac{m}{NT_s}\right) \qquad (2.69)$$

where both $|m/(NT_s)|$ and $|f_{D_a}|$ are less than $[1/(2T_s) - B]$. This result is consistent with the conclusion about the sampling criteria. On the other hand, we can also use (A.6) to interpolate from one set of reference signal samples to produce references for various τ_H,

$$\tilde{s}(t - \tau_H) \exp(j2\pi f_{D_H}t)$$

$$= \tilde{s}(t - \tau_H) \exp[j2\pi f_{D_H}(t - \tau_H)] \exp(j2\pi f_{D_H}\tau_H)$$

$$= \exp(j2\pi f_{D_H}\tau_H) \sum_{p=-\infty}^{\infty} \tilde{s}(pT_s) \exp(j2\pi f_{D_H}pT_s) \frac{\sin \pi[(t - \tau_H)/T_s - p]}{\pi[(t - \tau_H)/T_s - p]}. \qquad (2.70)$$

50

Thus,

$$\phi_{\tilde{s}_r\tilde{s}}(\tau_H, f_{D_H})$$

$$= \exp(-j2\pi f_{D_H}\tau_H) \int_{-\infty}^{\infty} \left[\sum_{k=-\infty}^{\infty} \tilde{s}(kT_s - \tau_a) \exp(j2\pi f_{D_a}kT_s) \frac{\sin \pi(t/T_s - k)}{\pi(t/T_s - k)} \right]$$

$$\cdot \left[\sum_{p=-\infty}^{\infty} \tilde{s}(pT_s) \exp(j2\pi f_{D_H}pT_s) \frac{\sin \pi[(t - \tau_H)/T_s - p]}{\pi[(t - \tau_H)/T_s - p]} \right]^* dt$$

$$= \exp(-j2\pi f_{D_H}\tau_H) \sum_{k=-\infty}^{\infty} \sum_{p=-\infty}^{\infty} \tilde{s}(kT_s - \tau_a) \tilde{s}^*(pT_s)$$

$$\cdot \exp[j2\pi(f_{D_a}kT_s - f_{D_H}pT_s)] \left[\int_{-\infty}^{\infty} \frac{\sin \pi(t/T_s - k)}{\pi(t/T_s - k)} \frac{\sin \pi[(t - \tau_H)/T_s - p]}{\pi[(t - \tau_H)/T_s - p]} dt \right]. (2.71)$$

The integral can be evaluated by

$$\int_{-\infty}^{\infty} \frac{\sin \pi(t/T_s - k)}{\pi(t/T_s - k)} \frac{\sin \pi[(t - \tau_H)/T_s - p]}{\pi[(t - \tau_H)/T_s - p]} dt$$

$$= \int_{-\infty}^{\infty} [T_s\text{rect}(fT_s) \exp(-j2\pi fkT_s)] [T_s\text{rect}(fT_s) \exp(-j2\pi f[\tau_H + pT_s])]^* df$$

$$= T_s \frac{\sin \pi[\tau_H/T_s - (k - p)]}{\pi[\tau_H/T_s - (k - p)]}. \tag{2.72}$$

It follows that

$$\phi_{\tilde{s}_r\tilde{s}}(\tau_H, f_{D_H}) = T_s \cdot \exp(-j2\pi f_{D_H}\tau_H) \sum_{k=-\infty}^{\infty} \sum_{p=-\infty}^{\infty} \tilde{s}(kT_s - \tau_a) \tilde{s}^*(pT_s)$$

$$\cdot \exp[j2\pi(f_{D_a}kT_s - f_{D_H}pT_s)] \frac{\sin \pi[\tau_H/T_s - (k - p)]}{\pi[\tau_H/T_s - (k - p)]}. \tag{2.73}$$

Letting $n = k - p$ gives

$$\phi_{\tilde{s}_r\tilde{s}}(\tau_H, f_{D_H}) = T_s \cdot \exp(-j2\pi f_{D_H}\tau_H) \sum_{n=-\infty}^{\infty} \sum_{k=-\infty}^{\infty} \tilde{s}(kT_s - \tau_a) \tilde{s}^*[(k - n)T_s]$$

$$\cdot \exp[-j2\pi(f_{D_H} - f_{D_a})kT_s] \exp(j2\pi f_{D_H}nT_s) \frac{\sin \pi(\tau_H/T_s - n)}{\pi(\tau_H/T_s - n)}. \tag{2.74}$$

Then, from (2.68) and (2.74), we arrive at

$$\phi_{\tilde{s}_r\tilde{s}}(\tau_H, f_{D_H}) = e^{(-j2\pi f_{D_H}\tau_H)} \sum_{n=-\infty}^{\infty} \phi_{\tilde{s}_r\tilde{s}}(nT_s, f_{D_H}) e^{(j2\pi f_{D_H}nT_s)} \frac{\sin \pi(\tau_H/T_s - n)}{\pi(\tau_H/T_s - n)} \tag{2.75}$$

where both $|f_{D_H}|$ and $|f_{D_a}|$ are less than $[1/(2T_s) - B]$. Applying (2.69) to the above relationship, we have

$$\phi_{\tilde{s}_r \tilde{s}}\left(\tau_H, \frac{l}{NT_s}\right) = T_s \exp\left(-j2\pi \frac{l}{NT_s}\tau_H\right)$$
$$\cdot \sum_{n=-\infty}^{\infty} \hat{\phi}_{\tilde{s}_r \tilde{s}}\left(nT_s, \frac{l}{NT_s}\right) \exp\left(j2\pi \frac{ln}{NT_s}\right) \frac{\sin \pi(\tau_H/T_s - n)}{\pi(\tau_H/T_s - n)}. \quad (2.76)$$

This result is useful for reconstructing $\phi_{\tilde{s}_r \tilde{s}}(\tau_H, f_{D_H})$ from $\hat{\phi}_{\tilde{s}_r \tilde{s}}[nT_s, l/(NT_s)]$.

Application of (A.14) yields

$$\tilde{S}(f - f_{D_H})\exp(j2\pi f\tau_H) = \tilde{S}(f - f_{D_H})\exp[j2\pi(f - f_{D_H})\tau_H]\exp(j2\pi f_{D_H}\tau_H)$$
$$= \sum_{l=-\infty}^{\infty} \tilde{S}\left(\frac{l}{NT_s} - f_{D_H}\right) \exp\left(-j2\pi \frac{l}{NT_s}\tau_H\right)$$
$$\cdot \exp\left[-j\pi\left(f - \frac{l}{NT_s}\right)T\right] \frac{\sin \pi(fNT_s - l)}{\pi(fNT_s - l)} \quad (2.77)$$

where $0 \le \tau_H \le N_0 T_s$. A similar procedure can be used to expand $\tilde{S}_r(f)$ when $0 \le \tau_a \le N_0 T_s$. Thus, when both τ_H and τ_a are less than $N_0 T_s$, we have

$$\exp[-j2\pi(f_{D_a}\tau_a - f_{D_H}\tau_H)]\phi_{\tilde{S}_r \tilde{S}}(\tau_H, f_{D_H})$$
$$= \int_{-\infty}^{\infty} \left\{ \sum_{m=-\infty}^{\infty} \tilde{S}\left(\frac{m}{NT_s} - f_{D_a}\right) \exp\left(-j2\pi \frac{m}{NT_s}\tau_a\right) \exp\left[-j\pi\left(f - \frac{m}{NT_s}\right)T\right] \right.$$
$$\cdot \frac{\sin \pi(fNT_s - m)}{\pi(fNT_s - m)} \right\} \left\{ \sum_{l=-\infty}^{\infty} \tilde{S}\left(\frac{l}{NT_s} - f_{D_H}\right) \exp\left(-j2\pi \frac{l}{NT_s}\tau_H\right) \right.$$
$$\left. \cdot \exp\left[-j\pi\left(f - \frac{l}{NT_s}\right)T\right] \frac{\sin \pi(fNT_s - l)}{\pi(fNT_s - l)} \right\}^* df$$
$$= \frac{1}{NT_s} \sum_{q=-\infty}^{\infty} \tilde{S}\left(\frac{q}{NT_s} - f_{D_a}\right) \tilde{S}^*\left(\frac{q}{NT_s} - f_{D_H}\right) \exp\left[j2\pi \frac{q}{NT_s}(\tau_H - \tau_a)\right]. \quad (2.78)$$

In particular, when $f_{D_H} = l/(NT_s)$ and l is an integer, we have

$$\phi_{\tilde{S}_r \tilde{S}}\left(\tau_H, \frac{l}{NT_s}\right) = \frac{1}{NT_s} \exp\left[j2\pi\left(f_{D_a}\tau_a - \frac{l}{NT_s}\tau_H\right)\right]$$
$$\cdot \sum_{q=-\infty}^{\infty} \tilde{S}\left(\frac{q}{NT_s} - f_{D_a}\right) \tilde{S}^*\left(\frac{q-l}{NT_s} - f_{D_H}\right) \exp\left[j2\pi \frac{q}{NT_s}(\tau_H - \tau_a)\right] \quad (2.79)$$

where $0 \leq \tau_H, \tau_a \leq N_0 T_s$. On the other hand, one can also use (A.14) to interpolate from one set of reference signal samples to produce references for various f_{D_H}. Thus,

$$\tilde{S}(f - f_{D_H}) \exp(j2\pi f \tau_H)$$

$$= \tilde{S}(f - f_{D_H}) \exp[j2\pi(f - f_{D_H})\tau_H] \exp(j2\pi f_{D_H}\tau_H)$$

$$= \exp(-j2\pi f_{D_H}\tau_H) \sum_{l=-\infty}^{\infty} \tilde{S}\left(\frac{l}{NT_s}\right) \exp\left(-j2\pi \frac{l}{NT_s}\tau_H\right)$$

$$\cdot \exp\left[-j\pi\left(f - f_{D_H} - \frac{l}{NT_s}\right)T\right] \frac{\sin\pi[(f - f_{D_H})NT_s - l]}{\pi[(f - f_{D_H})NT_s - l]}. \tag{2.80}$$

Employing a procedure similar to that used in deriving (2.71) through (2.75), we have

$$\exp[-j2\pi(f_{D_a}\tau_a - f_{D_H}\tau_H)]\phi_{\tilde{S}_r\tilde{S}}(\tau_H, f_{D_H})$$

$$= \int_{-\infty}^{\infty} \left\{ \sum_{m=-\infty}^{\infty} \tilde{S}\left(\frac{m}{NT_s} - f_{D_a}\right) \exp\left(-j2\pi \frac{m}{NT_s}\tau_a\right) \exp\left[-j\pi\left(f - \frac{m}{NT_s}\right)T\right]\right.$$

$$\cdot \frac{\sin\pi(fNT_s - m)}{\pi(fNT_s - m)} \right\} \left\{ \exp(-j2\pi f_{D_H}\tau_H) \sum_{l=-\infty}^{\infty} \tilde{S}\left(\frac{l}{NT_s}\right) \exp\left(-j2\pi \frac{l}{NT_s}\tau_H\right)\right.$$

$$\cdot \exp\left[-j\pi\left(f - f_{D_H} - \frac{l}{NT_s}\right)T\right] \frac{\sin\pi[(f - f_{D_H})NT_s - l]}{\pi[(f - f_{D_H})NT_s - l]} \right\}^* df$$

$$= \frac{1}{NT_s} \exp(j2\pi f_{D_H}\tau_H) \exp(-j\pi f_{D_H}T) \sum_{m=-\infty}^{\infty} \sum_{l=-\infty}^{\infty} \tilde{S}\left(\frac{m}{NT_s} - f_{D_a}\right)$$

$$\cdot \tilde{S}^*\left(\frac{m - l}{NT_s}\right) \exp\left[j2\pi \frac{m}{NT_s}(\tau_H - \tau_a)\right] \exp\left(-j2\pi \frac{l}{NT_s}\tau_H\right)$$

$$\cdot \exp\left(j\pi \frac{l}{NT_s}T\right) \frac{\sin\pi(f_{D_H}NT_s - l)}{\pi(f_{D_H}NT_s - l)}. \tag{2.81}$$

Using (2.79) in (2.81), we arrive at

$$\phi_{\tilde{S}_r\tilde{S}}(\tau_H, f_{D_H}) = \exp(-j\pi f_{D_H}T) \sum_{l=-\infty}^{\infty} \phi_{\tilde{S}_r\tilde{S}}\left(\tau_H, \frac{l}{NT_s}\right) \exp\left(j\pi \frac{l}{NT_s}T\right)$$

$$\cdot \frac{\sin\pi(f_{D_H}NT_s - l)}{\pi(f_{D_H}NT_s - l)} \tag{2.82}$$

where $0 \leq \tau_H, \tau_a \leq N_0 T_s$. Using the fact that $\phi_{\tilde{S}_r\tilde{S}}(\cdot) = \phi_{\tilde{s}_r\tilde{s}}(\cdot)$, and putting (2.76) into (2.82), we have

$$\phi_{\tilde{s}_r\tilde{s}}(\tau_H, f_{D_H}) = T_s \exp(-j\pi f_{D_H}T) \sum_{l=-\infty}^{\infty} \sum_{n=-\infty}^{\infty} \hat{\phi}_{\tilde{s}_r\tilde{s}}\left(nT_s, \frac{l}{NT_s}\right) \exp\left(j\pi \frac{l}{NT_s}T\right)$$

$$\cdot \exp\left[-j2\pi \frac{l}{NT_s}(\tau_H - nT_s)\right] \frac{\sin\pi(\tau_H/T_s - n)}{\pi(\tau_H/T_s - n)} \frac{\sin\pi(f_{D_H}NT_s - l)}{\pi(f_{D_H}NT_s - l)} \quad (2.83)$$

That is, we can use (2.83) to produce the continuous time-frequency correlation function from $\hat{\phi}_{\tilde{s}_r\tilde{s}}(\cdot)$ for the region $0 \le \tau_H \le N_0 T_s$ and $|f_{D_H}| \le [1/(2T_s) - B]$. As a check, at points $(nT_s, l/(NT_s))$ in the $\tau_H - f_{D_H}$ plane, where n and l are integers and $0 \le n < N_0$ and $|l| \le [1/(2T_s) - B]$, the two sides of (2.83) are equal as indicated by (2.69). It should be pointed out that at an integer multiple of T_s in delay or an integer multiple of $1/(NT_s)$ in Doppler, one of the two sinc functions in (2.83) turns into a Kronecker delta. Thus, interpolation along a cut in Doppler or delay using (2.83) involves only one sinc function in this case. This is the same procedure used in interpolating one-dimensional functions. On the other hand, at an integer multiple of T_s in delay or an integer multiple of $1/(NT_s)$ in Doppler, none of the two sinc functions in the interpolation formula given in [16] reduces to a simple Kronecker delta, but one of them changes into a function involving the variable to be interpolated. Therefore, (2.83) is simpler to implement for the region $0 \le \tau_H \le N_0 T_s$ and $|f_{D_H}| \le [1/(2T_s) - B]$.

2.3 Discrete Wigner-Ville Distribution

To enable digital processing of signals based on the Wigner-Ville distribution, various forms of discrete Wigner-Ville distribution have been proposed [13]-[15]. These definitions were conceived so that the discrete versions have the same properties as the continuous one. In this context, aliasing is one of the problems of major concern. In the following, we will examine a few forms of discrete Wigner-Ville distributions. Then, we consider the sampling criteria and recovery of the continuous Wigner-Ville distribution from the discrete one. An interpolation formula which is simpler than the one found in the literature [14] is proposed. This alternative, however, has the drawback that it can only recover that portion of the continuous Wigner-Ville distribution that corresponds to the region in the discrete

Wigner-Ville distribution free from aliasing.

The cross-Wigner-Ville distribution of two continuous signals, $\tilde{s}_1(t)$ and $\tilde{s}_2(t)$, was defined in Chapter 1 as

$$W_{\tilde{s}_1\tilde{s}_2}(t,f) = \int_{-\infty}^{\infty} \tilde{s}_1\left(t + \frac{\tau}{2}\right)\tilde{s}_2^*\left(t - \frac{\tau}{2}\right)\exp(-j2\pi f\tau)d\tau. \qquad (2.84)$$

When $\tilde{s}_1(t) = \tilde{s}_2(t)$, it is called the auto-Wigner-Ville distribution. It was shown that $W_{\tilde{s}_1\tilde{s}_2}(t,f)$ can be written in the forms

$$W_{\tilde{s}_1\tilde{s}_2}(t,f) = 2\int_{-\infty}^{\infty} \tilde{s}_1(t+\tau)\tilde{s}_2^*(t-\tau)\exp(-j4\pi f\tau)d\tau \qquad (2.85)$$

and

$$W_{\tilde{s}_1\tilde{s}_2}(t,f) = 2\int_{-\infty}^{\infty} \tilde{S}_1(f+\nu)\tilde{S}_2^*(f-\nu)\exp(j4\pi\nu t)d\nu. \qquad (2.86)$$

To distinguish whether the Wigner-Ville distribution is given in the time or frequency-domain, we will denote the one that is given in the frequency-domain by $W_{\tilde{S}_1\tilde{S}_2}(\cdot)$. Once again, we will assume that $\tilde{s}_1(t)$ and $\tilde{s}_2(t)$ are both *essentially* limited in duration and spectrum to $[0,T)$ and $(-B,B)$, respectively. It follows that the Wigner-Ville distribution (2.85), or equivalently (2.86), are limited to $(0,T)$ in the time-domain, and $(-B,B)$ in the frequency-domain.

2.3.1 Time-domain Representation

In the following, we will derive the time-domain representation of the discrete Wigner-Ville distribution. As shown in Appendix A, when the sampling rate is greater than the Nyquist rate, relation (A.4) can be used to expand the signal. Thus, we can rewrite (2.85) to obtain

$$W_{\tilde{s}_1\tilde{s}_2}(t,f) = 2\int_{-\infty}^{\infty} \tilde{s}_1(t+\tau)\tilde{s}_2^*(t-\tau)\exp(-j4\pi f\tau)d\tau$$

$$= 2\int_{-\infty}^{\infty}\left\{\sum_{k=-\infty}^{\infty} \tilde{s}_1(kT_s)\frac{\sin\pi[(t+\tau)/T_s - k]}{\pi[(t+\tau)/T_s - k]}\right\}$$

55

$$\cdot \left\{ \sum_{p=-\infty}^{\infty} \tilde{s}_2(pT_s) \frac{\sin \pi[(t-\tau)/T_s - p]}{\pi[(t-\tau)/T_s - p]} \right\}^{*} \exp(-j4\pi f\tau)d\tau$$

$$= 2 \sum_{k=-\infty}^{\infty} \sum_{p=-\infty}^{\infty} \tilde{s}_1(kT_s)\tilde{s}_2^{*}(pT_s)$$

$$\cdot \int_{-\infty}^{\infty} \frac{\sin \pi[(t+\tau)/T_s - k]}{\pi[(t+\tau)/T_s - k]} \frac{\sin \pi[(t-\tau)/T_s - p]}{\pi[(t-\tau)/T_s - p]} \exp(-j4\pi f\tau)d\tau. \qquad (2.87)$$

The integral can be viewed as the Fourier transform of the product of the two sinc functions and it can be evaluated by using the convolution theorem. Hence,

$$\int_{-\infty}^{\infty} \frac{\sin \pi[(t+\tau)/T_s - k]}{\pi[(t+\tau)/T_s - k]} \frac{\sin \pi[(t-\tau)/T_s - p]}{\pi[(t-\tau)/T_s - p]} \exp(-j4\pi f\tau)d\tau$$

$$= T_s^2 \exp[j4\pi f(pT_s - t)] \int_{-\infty}^{\infty} \text{rect}(vT_s)\text{rect}[(2f - v)T_s] \exp[j2\pi v(2t - kT_s - pT_s)]dv$$

$$= T_s^2 \exp[j4\pi f(pT_s - t)] \int_{-1/(2T_s)}^{1/(2T_s)} \text{rect}[(2f - v)T_s] \exp[j2\pi v(2t - kT_s - pT_s)]dv. \qquad (2.88)$$

When $0 \leq 2f < 1/T_s$, the last line of (2.88) can be written as

$$T_s^2 \exp[j4\pi f(pT_s - t)] \int_{-1/(2T_s)}^{1/(2T_s)} \exp[j2\pi v(2t - kT_s - pT_s)]dv$$

$$= T_s^2 \exp[j4\pi f(pT_s - t)] \int_{2f-1/(2T_s)}^{1/(2T_s)} \text{rect}[(2f - v)T_s] \exp[j2\pi v(2t - kT_s - pT_s)]dv$$

$$= T_s^2 \exp[j2\pi f(p - k)T_s] \frac{\sin \pi(1/T_s - 2f)[2t - (k + p)T_s]}{\pi[2t - (k + p)T_s]}. \qquad (2.89)$$

When $-1/T_s \leq 2f < 0$, the last line of (2.88) can be written as

$$T_s^2 \exp[j4\pi f(pT_s - t)] \int_{-1/(2T_s)}^{1/(2T_s)} \exp[j2\pi v(2t - kT_s - pT_s)]dv$$

$$= T_s^2 \exp[j4\pi f(pT_s - t)] \int_{-1/(2T_s)}^{2f+1/(2T_s)} \text{rect}[(2f - v)T_s] \exp[j2\pi v(2t - kT_s - pT_s)]dv$$

$$= T_s^2 \exp[j2\pi f(p - k)T_s] \frac{\sin \pi(1/T_s + 2f)[2t - (k + p)T_s]}{\pi[2t - (k + p)T_s]}. \qquad (2.90)$$

For other values of f, the last line of (2.88) is zero. Thus, we have

$$\int_{-\infty}^{\infty} \frac{\sin \pi[(t+\tau)/T_s - k]}{\pi[(t+\tau)/T_s - k]} \frac{\sin \pi[(t-\tau)/T_s - p]}{\pi[(t-\tau)/T_s - p]} \exp(-j4\pi f\tau)d\tau$$

$$= T_s^2 \exp[j2\pi f(p - k)T_s] \frac{\sin \pi(1/T_s - 2|f|)[2t - (k + p)T_s]}{\pi[2t - (k + p)T_s]} \text{rect}(fT_s). \qquad (2.91)$$

56

Putting (2.91) into (2.87) and letting $n = k + p$, we have

$$W_{\tilde{s}_1 \tilde{s}_2}(t, f) = 2T_s^2 \sum_{n=-\infty}^{\infty} \left\{ \sum_{k=-\infty}^{\infty} \tilde{s}_1(kT_s)\tilde{s}_2^*[(n-k)T_s] \exp[-j2\pi f(2k-n)T_s] \right\}$$
$$\cdot \frac{\sin \pi(2t - nT_s)[1/T_s - 2|f|]}{\pi(2t - nT_s)} \text{rect}(fT_s). \tag{2.92}$$

The term in the braces in (2.92) was defined in [14] as the discrete-time, continuous-frequency Wigner-Ville distribution, which will be denoted as $W_{\hat{t}_{\tilde{s}_1 \tilde{s}_2}}(\cdot)$. That is,

$$W_{\hat{t}_{\tilde{s}_1 \tilde{s}_2}}(nT_s, f) = \sum_{k=-\infty}^{\infty} \tilde{s}_1(kT_s)\tilde{s}_2^*[(n-k)T_s] \exp[-j2\pi f(2k-n)T_s]$$
$$= \exp(j2\pi f nT_s) \sum_{k=-\infty}^{\infty} \tilde{s}_1(kT_s)\tilde{s}_2^*[(n-k)T_s] \exp[-j2\pi(2f)kT_s]. \tag{2.93}$$

In particular, consider the case when f is an integral multiple of $1/(2MT_s)$, where M is an integer and $M \geq T/T_s$. Letting $f = q/(2MT_s)$, we have

$$W_{\hat{t}_{\tilde{s}_1 \tilde{s}_2}}\left(nT_s, \frac{q}{2MT_s}\right) = \exp\left(j\pi\frac{qn}{M}\right) \sum_{k=-\infty}^{\infty} \tilde{s}_1(kT_s)\tilde{s}_2^*[(n-k)T_s] \exp\left(-j2\pi\frac{qk}{M}\right). \tag{2.94}$$

From the above relationship, it is seen that $W_{\hat{t}_{\tilde{s}_1 \tilde{s}_2}}(\cdot)$ can be evaluated at frequencies of integral multiples of $1/(2MT_s)$ via the discrete Fourier transform. The choices of M will be considered further in a later discussion. Thus, we define the discrete Wigner-Ville distribution based on the time samples of the signals [14] as

$$\hat{W}_{\tilde{s}_1 \tilde{s}_2}\left(nT_s, \frac{l}{MT_s}\right) = \sum_{k=-\infty}^{\infty} \tilde{s}_1(kT_s)\tilde{s}_2^*[(n-k)T_s] \exp\left[-j\pi\frac{l(2k-n)}{M}\right]. \tag{2.95}$$

Due to the periodic nature of discrete Fourier transform, we require that the frequency argument $l/(MT_s)$ of $\hat{W}_{\tilde{s}_1 \tilde{s}_2}[nT_s, l/(MT_s)]$ be such that $-1/2 \leq l/M < 1/2$. It is clear that $\hat{W}_{\tilde{s}_1 \tilde{s}_2}[nT_s, l/(MT_s)] = 0$ for $nT_s < 0$ or $nT_s \geq 2T$.

When n in (2.95) is even, say $n = 2p$, we have

$$\hat{W}_{\tilde{s}_1 \tilde{s}_2}\left(2pT_s, \frac{l}{MT_s}\right) = \sum_{k=-\infty}^{\infty} \tilde{s}_1(kT_s)\tilde{s}_2^*[(2p-k)T_s] \exp\left[-j\pi\frac{l(2k-2p)}{M}\right]$$
$$= \sum_{k=-\infty}^{\infty} \tilde{s}_1[(p+k)T_s]\tilde{s}_2^*[(p-k)T_s] \exp\left(-j2\pi\frac{lk}{M}\right). \tag{2.96}$$

The last relationship of (2.96) is defined as the symmetrical form of the discrete Wigner-Ville distribution, which we denote as $\bar{W}_{\tilde{s}_1\tilde{s}_2}(\cdot)$. That is,

$$\bar{W}_{\tilde{s}_1\tilde{s}_2}\left(pT_s, \frac{l}{MT_s}\right) = \sum_{k=-\infty}^{\infty} \tilde{s}_1[(p+k)T_s]\tilde{s}_2^*[(p-k)T_s] \exp\left(-j2\pi\frac{lk}{M}\right) \qquad (2.97)$$

for $-1/2 \leq l/M < 1/2$. Clearly, $\bar{W}_{\tilde{s}_1\tilde{s}_2}[pT_s, l/(MT_s)] = 0$ for $pT_s < 0$ or $pT_s \geq T$. The discrete Wigner-Ville distribution is sometimes defined in the form of (2.97) due to its resemblance to the continuous one. However, it is seen that $\bar{W}_{\tilde{s}_1\tilde{s}_2}(\cdot)$ is a special case of $\hat{W}_{\tilde{s}_1\tilde{s}_2}(\cdot)$ where t is an even integer multiple of T_s. In the following, we will refer to (2.97) as the symmetric form in the time-domain.

2.3.2 Frequency-domain Representation

In this subsection, we will derive the frequency-domain representation of the discrete Wigner-Ville distribution. When M is such that $MT_s \geq T$, we can apply (A.14) with $\tau = 0$ to obtain

$$\tilde{S}_1(f+\nu)$$
$$= \sum_{m=-\infty}^{\infty} \tilde{S}_1\left(\frac{m}{MT_s}\right) \exp\left[-j\pi\left(f+\nu-\frac{m}{MT_s}\right)T\right] \frac{\sin\pi[MT_s(f+\nu)-m]}{\pi[MT_s(f+\nu)-m]}. \qquad (2.98)$$

A similar procedure can be used to expand $\tilde{S}_2(f-\nu)$. Thus,

$$W_{\tilde{s}_1\tilde{s}_2}(t,f)$$
$$= 2\sum_{m=-\infty}^{\infty}\sum_{q=-\infty}^{\infty} \tilde{S}_1\left(\frac{m}{MT_s}\right) \tilde{S}_2^*\left(\frac{q}{MT_s}\right) \exp\left(j\pi\frac{m-q}{MT_s}T\right)$$
$$\cdot \int_{-\infty}^{\infty} \frac{\sin\pi[MT_s(f+\nu)-m]}{\pi[MT_s(f+\nu)-m]} \frac{\sin\pi[MT_s(f-\nu)-q]}{\pi[MT_s(f-\nu)-q]} \exp[j2\pi\nu(2t-T)]d\nu. \qquad (2.99)$$

Viewing the integral term as the Fourier transform of the product of two sinc functions, it can be evaluated by using the convolution theorem,

$$\int_{-\infty}^{\infty} \frac{\sin\pi[MT_s(f+\nu)-m]}{\pi[MT_s(f+\nu)-m]} \frac{\sin\pi[MT_s(f-\nu)-q]}{\pi[MT_s(f-\nu)-q]} \exp[j2\pi\nu(2t-T)]d\nu$$

$$
= \left(\frac{1}{MT_s}\right)^2 \exp\left[j2\pi\frac{m}{MT_s}(2t - T)\right] \exp\left[j2\pi\left(f - \frac{m+q}{NT_s}\right)(2t - T)\right]
$$
$$
\cdot \int_{-\infty}^{\infty} \text{rect}\left(\frac{u}{MT_s}\right) \text{rect}\left(\frac{2t - T - u}{MT_s}\right) \exp\left[-j2\pi\left(2f - \frac{m+q}{NT_s}\right)u\right] du
$$
$$
= \left(\frac{1}{MT_s}\right)^2 \exp\left[j\pi\frac{m-q}{MT_s}(2t - T)\right]
$$
$$
\cdot \frac{\sin\pi[2f - (m+q)/(MT_s)](MT_s - |2t - T|)}{\pi[2f - (m+q)/(MT_s)]}\text{rect}\left(\frac{2t - T}{2MT_s}\right). \tag{2.100}
$$

Putting (2.100) into (2.99) and letting $l = m + q$, we have

$$
W_{\tilde{s}_1\tilde{s}_2}(t, f)
$$
$$
= \frac{2}{(MT_s)^2} \sum_{l=-\infty}^{\infty} \left\{ \sum_{m=-\infty}^{\infty} \tilde{S}_1\left(\frac{m}{MT_s}\right) \tilde{S}_2^*\left(\frac{l-m}{MT_s}\right) \exp\left(j2\pi\frac{2m-l}{MT_s}t\right)\right\}
$$
$$
\cdot \frac{\sin\pi[1 - |2t - T|/(2MT_s)](2MT_sf - l)}{\pi(2MT_sf - l)}\text{rect}\left(\frac{2t - T}{2MT_s}\right). \tag{2.101}
$$

The term in the braces in (2.101) was defined in [14] as the continuous-time, discrete-frequency Wigner-Ville distribution, which we will denote as $W_{\hat{f}_{\tilde{s}_1\tilde{s}_2}}(\cdot)$. That is,

$$
W_{\hat{f}_{\tilde{s}_1\tilde{s}_2}}\left(t, \frac{l}{MT_s}\right) = \sum_{m=-\infty}^{\infty} \tilde{S}_1\left(\frac{m}{MT_s}\right) \tilde{S}_2^*\left(\frac{l-m}{MT_s}\right) \exp\left(j2\pi\frac{2m-l}{MT_s}t\right). \tag{2.102}
$$

However, as seen in Section 2.2, the Fourier transforms that are directly available to the receiver are the ones computed from the discrete-time samples, instead of the Fourier transforms of the continuous signals. In other words, the Fourier transforms available are

$$
\hat{S}_i\left(\frac{m}{MT_s}\right) = T_s \sum_{k=0}^{M-1} \tilde{s}_i(kT_s) \exp\left(-j2\pi\frac{mk}{M}\right), \quad i = 1, 2. \tag{2.103}
$$

At $t = pT_s/2$, where p is an integer, note that $W_{\hat{f}_{\tilde{s}_1\tilde{s}_2}}(\cdot)$ can be expressed as

$$
W_{\hat{f}_{\tilde{s}_1\tilde{s}_2}}\left(\frac{pT_s}{2}, \frac{l}{MT_s}\right)
$$
$$
= \exp\left(-j\pi\frac{lp}{M}\right) \sum_{m=-\infty}^{\infty} \tilde{S}_1\left(\frac{m}{MT_s}\right) \tilde{S}_2^*\left(\frac{l-m}{MT_s}\right) \exp\left(j2\pi\frac{mp}{M}\right). \tag{2.104}
$$

It is seen from the above relationship that $W_{\hat{f}_{\tilde{s}_1\tilde{s}_2}}(\cdot)$ can be evaluated at points of time that are integral multiples of $T_s/2$ via discrete Fourier transform techniques. Thus, we define the

frequency domain representation of the discrete Wigner-Ville distribution as

$$\hat{W}_{\hat{S}_1 \hat{S}_2}\left(nT_s, \frac{l}{MT_s}\right) = \frac{1}{MT_s^2}\sum_{m=0}^{M-1}\hat{S}_1\left(\frac{m}{MT_s}\right)\hat{S}_2^*\left(\frac{l-m}{MT_s}\right)\exp\left[j\pi\frac{(2m-l)n}{M}\right]. \quad (2.105)$$

Due to the periodic nature of the discrete Fourier transform, we require that the arguments nT_s and $l/(MT_s)$ of $\hat{W}_{\hat{s}_1\hat{s}_2}[nT_s, l/(MT_s)]$ be such that $0 \le n < M$ and $-1/2 \le l/M < 1/2$.

When l in (2.105) is even, say $l = 2q$, we have

$$MT_s^2\hat{W}_{\hat{S}_1\hat{S}_2}\left(nT_s, \frac{2q}{MT_s}\right) = \sum_{m=0}^{M-1}\hat{S}_1\left(\frac{m}{MT_s}\right)\hat{S}_2^*\left(\frac{2q-m}{MT_s}\right)\exp\left[j\pi\frac{(2m-2q)n}{M}\right]$$

$$= \sum_{m=0}^{M-1}\hat{S}_1\left(\frac{q+m}{MT_s}\right)\hat{S}_2^*\left(\frac{q-m}{MT_s}\right)\exp\left(j2\pi\frac{mn}{M}\right). \quad (2.106)$$

The last relationship of (2.106) is defined as the symmetrical form frequency-domain representation of the discrete Wigner-Ville distribution, which we will denote as $\bar{W}_{\hat{S}_1\hat{S}_2}(\cdot)$. That is,

$$\bar{W}_{\hat{S}_1\hat{S}_2}\left(nT_s, \frac{q}{MT_s}\right) = \frac{1}{MT_s^2}\sum_{k=0}^{M-1}\hat{S}_1\left(\frac{q+k}{MT_s}\right)\hat{S}_2^*\left(\frac{q-k}{MT_s}\right)\exp\left(j2\pi\frac{kn}{M}\right), \quad (2.107)$$

where $0 \le n < M$ and $-1/2 \le q/M < 1/2$. The frequency-domain discrete Wigner-Ville distribution is sometimes defined in the form of (2.107) due to its resemblance to the continuous one. However, it is seen that $\bar{W}_{\hat{S}_1\hat{S}_2}(\cdot)$ is a special case of $\hat{W}_{\hat{S}_1\hat{S}_2}(\cdot)$ where the frequency is even multiples of $1/(MT_s)$. In the following , we will refer to (2.107) as the symmetric form in the frequency domain.

2.3.3 Relationship between Continuous and Discrete Wigner-Ville Distributions

In the following, we consider the sampling criteria for producing the discrete Wigner-Ville distribution without aliasing. Then, we derive the procedure for reconstructing the continuous Wigner-Ville distribution from the discrete one. The interpolation formula is simpler to the one found in [14] with the drawback that it can only be used to recover that portion of the Wigner-Ville distribution which is free of aliasing.

Sampling criteria

From the time-domain definition of the discrete Wigner-Ville distribution, we have

$$
\hat{W}_{\tilde{s}_1 \tilde{s}_2}\left(nT_s, \frac{l}{MT_s}\right) = \sum_{k=-\infty}^{\infty} \tilde{s}_1(kT_s)\tilde{s}_2^*[(n-k)T_s] \exp\left[-j\pi \frac{l(2k-n)}{M}\right]
$$

$$
= \sum_{k=-\infty}^{\infty} \left\{ \int_{-\infty}^{\infty} \tilde{s}_1(\tau)\tilde{s}_2^*(nT_s - \tau) \exp\left[-j\pi \frac{l(2\tau - nT_s)}{MT_s}\right] \delta(\tau - kT_s)d\tau \right\}
$$

$$
= \int_{-\infty}^{\infty} \tilde{s}_1(\tau)\tilde{s}_2^*(nT_s - \tau) \exp\left[-j\pi \frac{l(2\tau - nT_s)}{MT_s}\right] \left\{ \sum_{k=-\infty}^{\infty} \delta(\tau - kT_s) \right\} dt
$$

$$
= \int_{-\infty}^{\infty} \tilde{s}_1(\tau)\tilde{s}_2^*(nT_s - \tau) \exp\left[-j\pi \frac{l(2\tau - nT_s)}{MT_s}\right] \left\{ \frac{1}{T_s} \sum_{k=-\infty}^{\infty} \exp\left(j2\pi \frac{k\tau}{T_s}\right) \right\} d\tau. \quad (2.108)
$$

The product of the exponential terms in the last relationship of (2.108) can be manipulated in the following manner:

$$
\exp\left[-j\pi \frac{l(2\tau - nT_s)}{MT_s}\right] \exp\left(j2\pi \frac{k\tau}{T_s}\right)
$$

$$
= \exp\left[-j2\pi \frac{(l - kM)(\tau - nT_s/2)}{MT_s}\right] \exp\left(j2\pi \frac{kMnT_s/2}{MT_s}\right)
$$

$$
= (-1)^{kn} \exp\left[-j2\pi \frac{(l - kM)(\tau - nT_s/2)}{MT_s}\right]. \quad (2.109)
$$

Thus,

$$
\hat{W}_{\tilde{s}_1 \tilde{s}_2}\left(nT_s, \frac{l}{MT_s}\right)
$$

$$
= \frac{1}{T_s} \sum_{k=-\infty}^{\infty} (-1)^{kn} \int_{-\infty}^{\infty} \tilde{s}_1(\tau)\tilde{s}_2^*(nT_s - \tau) \exp\left[-j2\pi \frac{(l - kM)(\tau - nT_s/2)}{MT_s}\right] d\tau
$$

$$
= \frac{1}{2T_s} \sum_{k=-\infty}^{\infty} (-1)^{kn} W_{\tilde{s}_1 \tilde{s}_2}\left(\frac{nT_s}{2}, \frac{l - kM}{2MT_s}\right)
$$

$$
= \frac{1}{2T_s} W_{\tilde{s}_1 \tilde{s}_2}\left(\frac{nT_s}{2}, \frac{l}{2MT_s}\right) + \frac{1}{2T_s} \sum_{\substack{k=-\infty \\ k\neq 0}}^{\infty} (-1)^{kn} W_{\tilde{s}_1 \tilde{s}_2}\left(\frac{nT_s}{2}, \frac{l - kM}{2MT_s}\right) \quad (2.110)
$$

Recall that $W_{\tilde{s}_1 \tilde{s}_2}(\cdot)$ has an extent of $2B$ in the frequency-domain. Therefore, to avoid aliasing it is seen from (2.110) that the samples used in calculating $\hat{W}_{\tilde{s}_1 \tilde{s}_2}(\cdot)$ need either to be obtained at a rate higher than twice the Nyquist rate of the signals, or obtained from interpolation [29].

61

Example 2.3

Consider the same example used in the discussion of aliasing with respect to the discrete ambiguity function. In Figures 2.9 through 2.12 we show the effects of aliasing in the discrete auto-Wigner-Ville distribution for the complex envelope

$$\tilde{s}_1(t) = \tilde{s}_2(t) = \sqrt{2B}\frac{\sin 2\pi Bt}{2\pi Bt} = \sqrt{2B}\text{sinc}(2Bt). \tag{2.111}$$

Using the definition given in (2.85), or equivalently (2.86), it is a straightforward analysis to obtain the continuous Wigner-Ville distribution of $\tilde{s}(t)$:

$$W_{\tilde{s}}(t, f) = 2\text{rect}\left(\frac{f}{2B}\right)\frac{(B - |f|)}{B}\text{sinc}\left[4t(B - |f|)\right]. \tag{2.112}$$

The result is plotted in Figure 2.9 for $B = 1$. The discrete Wigner-Ville distribution $\hat{W}_{\tilde{s}}(t, f)$, using a sampling frequency equal to twice the Nyquist rate, is shown in Figure 2.10. Note the periodicity of $\hat{W}_{\tilde{s}}(t, f)$ along the frequency axis and the lack of aliasing. When the sampling rate is dropped to 1.8 and 1.5 times the Nyquist rate, noticeable aliasing occurs, as shown in Figures 2.11 and 2.12. Aliasing becomes more severe as the sampling rate is decreased. □

The discrete Wigner-Ville distribution in the frequency-domain was defined as

$$\hat{W}_{\hat{S}_1\hat{S}_2}\left(nT_s, \frac{l}{MT_s}\right) = \frac{1}{MT_s^2}\sum_{m=0}^{M-1}\hat{S}_1\left(\frac{m}{MT_s}\right)\hat{S}_2^*\left(\frac{l-m}{MT_s}\right)\exp\left[j\pi\frac{(2m-l)n}{M}\right], \tag{2.113}$$

where $0 \leq n < M$ and $-1/2 \leq l/M < 1/2$. Since $\hat{S}_1(\cdot)$, $\hat{S}_2(\cdot)$, and the exponential function are all periodic in frequency with period $1/T_s$, $\hat{W}_{\hat{S}_1\hat{S}_2}(\cdot)$ is also periodic in frequency with period $1/T_s$. Note that the discrete Fourier transforms $\hat{S}_1(\cdot)$ and $\hat{S}_2(\cdot)$ consist of periodic repetitions of $\tilde{S}_1(\cdot)$ and $\tilde{S}_2(\cdot)$, respectively. Since both $\tilde{S}_1(\cdot)$ and $\tilde{S}_2(\cdot)$ are assumed to be limited to $(-B, B)$, $\hat{W}_{\hat{S}_1\hat{S}_2}(\cdot)$ has terms separated from each other by integral multiples of $1/T_s$ in the frequency dimension, and each of these terms has an extent of $2B$ in the frequency dimension. In other words, $\hat{W}_{\hat{S}_1\hat{S}_2}(\cdot)$ is free from aliasing in the region from $-1/(2T_s) + B$ to $1/(2T_s) - B$ in the frequency dimension.
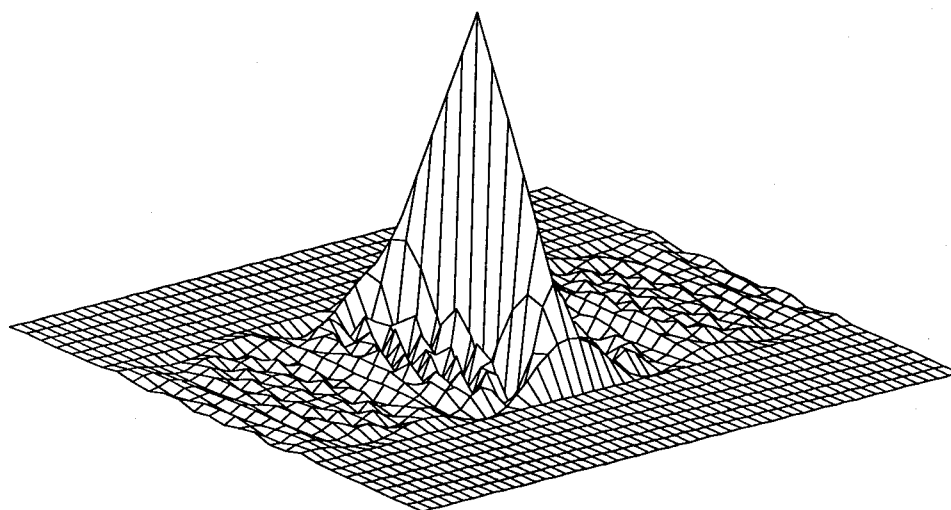
Figure 2.9: Continuous Wigner-Ville distribution
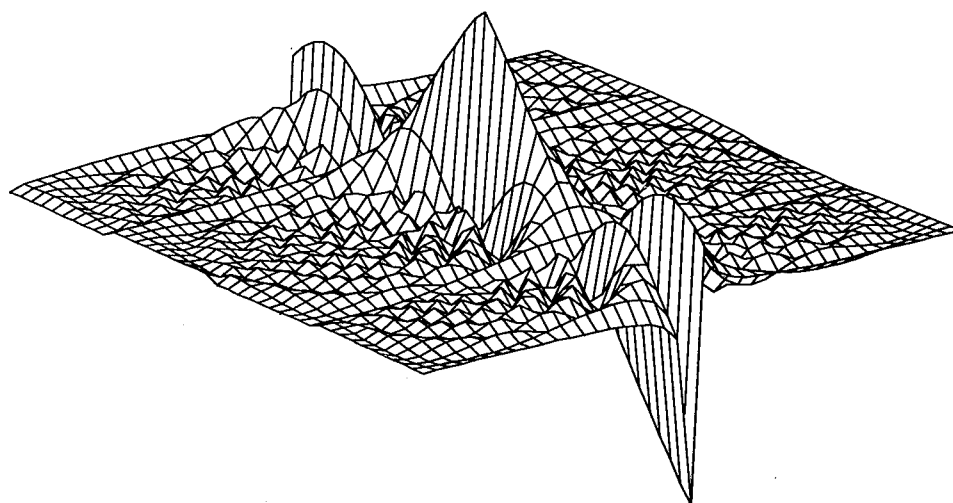
Figure 2.10: Discrete Wigner-Ville distribution of the signal sampled at twice the Nyquist rate
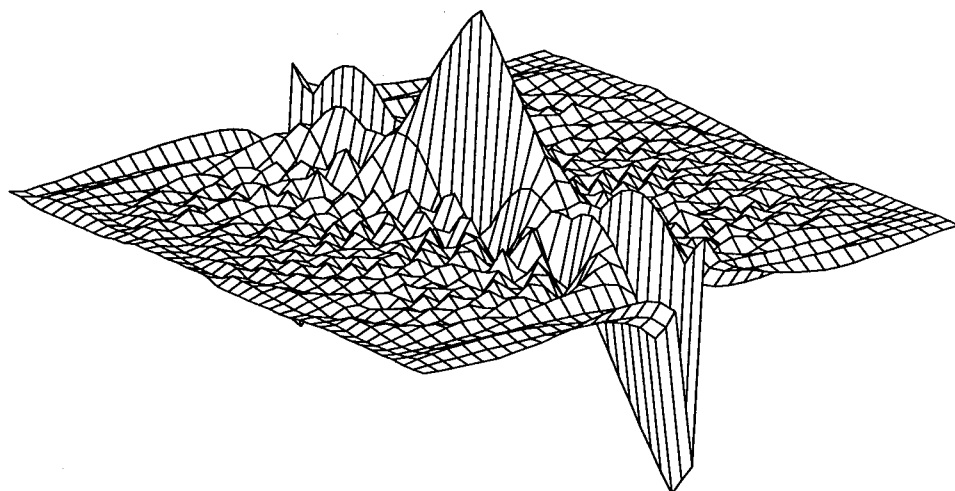
Figure 2.11: Discrete Wigner-Ville distribution of the signal sampling at 1.8 times the Nyquist
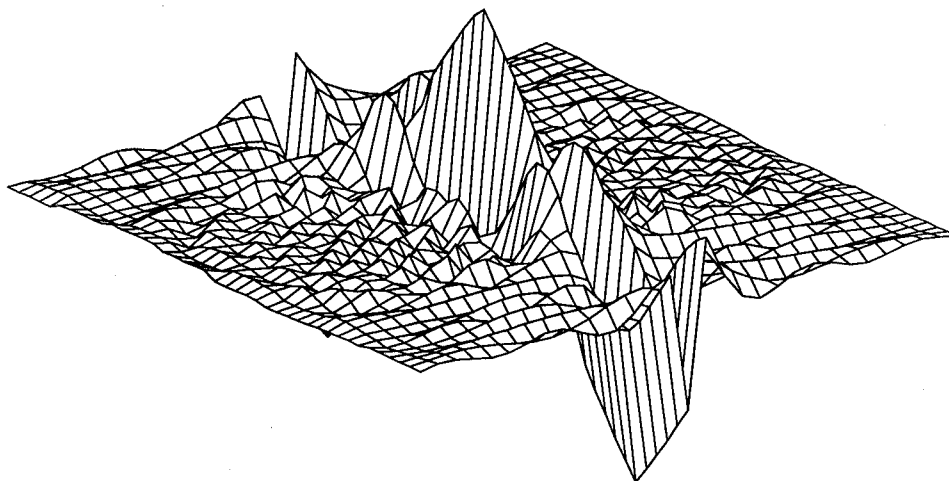
Figure 2.12: Discrete Wigner-Ville distribution of the signal sampling at 1.5 times the Nyquist

In the region where there is essentially no aliasing due to undersampling, we have

$$\sum_{m=0}^{M-1} \hat{S}_1 \left(\frac{m}{MT_s}\right) \hat{S}_2^* \left(\frac{l-m}{MT_s}\right) \exp\left[j\pi \frac{(2m-l)n}{M}\right]$$

$$= \sum_{m=-\infty}^{\infty} \tilde{S}_1 \left(\frac{m}{MT_s}\right) \tilde{S}_2^* \left(\frac{l-m}{MT_s}\right) \exp\left[j\pi \frac{(2m-l)n}{M}\right], \qquad (2.114)$$

where $|l|/(MT_s) < [1/(2T_s) - B]$. Employing the same procedure as that used in deriving (2.109) we have

$$\frac{1}{MT_s^2} \sum_{m=-\infty}^{\infty} \tilde{S}_1 \left(\frac{m}{MT_s}\right) \tilde{S}_2^* \left(\frac{l-m}{MT_s}\right) \exp\left[j\pi \frac{(2m-l)n}{M}\right]$$

$$= \frac{1}{MT_s^2} \sum_{m=-\infty}^{\infty} \left\{ \int_{-\infty}^{\infty} \tilde{S}_1(\nu) \tilde{S}_2^* \left(\frac{l}{MT_s} - \nu\right) \exp\left[j\pi \left(2\nu - \frac{l}{MT_s}\right) nT_s\right] \right\}$$

$$\cdot \delta\left(\nu - \frac{m}{MT_s}\right) d\nu$$

$$= \frac{1}{T_s} \sum_{m=-\infty}^{\infty} (-1)^{ml} \int_{-\infty}^{\infty} \tilde{S}_1(\nu) \tilde{S}_2^* \left(\frac{l}{MT_s} - \nu\right)$$

$$\cdot \exp\left[j2\pi \left(\nu - \frac{l}{2MT_s}\right) (n - mM)T_s\right] d\nu$$

$$= \frac{1}{2T_s} \sum_{m=-\infty}^{\infty} (-1)^{ml} W_{\tilde{s}_1 \tilde{s}_2} \left(\frac{(n-mM)T_s}{2}, \frac{l}{2MT_s}\right). \qquad (2.115)$$

Hence, for $|l|/(MT_s) < [1/(2T_s) - B]$

$$\hat{W}_{\hat{s}_1 \hat{s}_2} \left(nT_s, \frac{l}{MT_s}\right) = \frac{1}{2T_s} \sum_{m=-\infty}^{\infty} (-1)^{ml} W_{\tilde{s}_1 \tilde{s}_2} \left(\frac{(n-mM)T_s}{2}, \frac{l}{2MT_s}\right)$$

$$= \frac{1}{2T_s} W_{\tilde{s}_1 \tilde{s}_2} \left(\frac{nT_s}{2}, \frac{l}{2MT_s}\right)$$

$$+ \frac{1}{2T_s} \sum_{\substack{m=-\infty \\ k \neq 0}}^{\infty} (-1)^{ml} W_{\tilde{s}_1 \tilde{s}_2} \left(\frac{(n-mM)T_s}{2}, \frac{l}{2MT_s}\right). \qquad (2.116)$$

Note that $W_{\tilde{s}_1 \tilde{s}_2}(\cdot)$ has an extent of T in the time-domain. Therefore, to prevent aliasing it is seen from (2.116) that M needs to be chosen such that $M \geq 2T/T_s$. The procedure to recover $W_{\tilde{s}_1 \tilde{s}_2}(\cdot)$ from $\hat{W}_{\tilde{s}_1 \tilde{s}_2}(\cdot)$ is considered next.

Reconstruction of the continuous Wigner-Ville distribution from the discrete Wigner-Ville distribution

Recovery of the continuous Wigner-Ville distribution from the discrete one was considered in [14]. However, the following analysis will show that the interpolation formula can be simplified, but with the drawback that only that portion of the Wigner-Ville distribution that is free from aliasing can be recovered.

When the sampling rate is such that $1/T_s > 2(B + |f|)$, we can utilize (A.6) and have

$$
\tilde{s}_1(t + \tau) \exp(-j2\pi f\tau)
$$

$$
= \exp(j2\pi ft)\tilde{s}_1(t + \tau) \exp[-j2\pi f(t + \tau)]
$$

$$
= \exp(j2\pi ft) \sum_{k=-\infty}^{\infty} \tilde{s}_1(kT_s) \exp(-j2\pi fkT_s) \frac{\sin \pi[(t + \tau)/T_s - k]}{\pi[(t + \tau)/T_s - k]}. \tag{2.117}
$$

A similar procedure can be applied to expand $\tilde{s}_2(t - \tau) \exp(-j2\pi f\tau)$. It follows that

$$
W_{\tilde{s}_1\tilde{s}_2}(t, f) = 2 \sum_{k=-\infty}^{\infty} \sum_{p=-\infty}^{\infty} \tilde{s}_1(kT_s)\tilde{s}_2^*(pT_s) \exp[-j2\pi f(k - p)T_s]
$$

$$
\cdot \int_{-\infty}^{\infty} \frac{\sin \pi[(t + \tau)/T_s - k]}{\pi[(t + \tau)/T_s - k]} \frac{\sin \pi[(t - \tau)/T_s - p]}{\pi[(t - \tau)/T_s - p]} d\tau. \tag{2.118}
$$

Evaluation of the integral can be carried out in a manner similar to that used in deriving (2.72). Thus, we have

$$
W_{\tilde{s}_1\tilde{s}_2}(t, f) = 2T_s \sum_{k=-\infty}^{\infty} \sum_{p=-\infty}^{\infty} \tilde{s}_1(kT_s)\tilde{s}_2^*(pT_s) \exp[-j2\pi f(k - p)T_s]
$$

$$
\cdot \frac{\sin \pi[2t/T_s - (k + p)]}{\pi[2t/T_s - (k + p)]}. \tag{2.119}
$$

Letting $n = k + p$ gives

$$
W_{\tilde{s}_1\tilde{s}_2}(t, f) = 2T_s \sum_{n=-\infty}^{\infty} \sum_{k=-\infty}^{\infty} \tilde{s}_1(kT_s)\tilde{s}_2^*[(n - k)T_s] \exp[-j2\pi f(2k - n)T_s]
$$

$$
\cdot \frac{\sin \pi(2t/T_s - n)}{\pi(2t/T_s - n)}. \tag{2.120}
$$

Thus, for $|f| < 1/(2T_s) - B$, we have

$$
W_{\tilde{s}_1\tilde{s}_2}\left(\frac{nT_s}{2}, f\right) = 2T_s \sum_{k=-\infty}^{\infty} \tilde{s}_1(kT_s)\tilde{s}_2^*[(n - k)T_s] \exp[-j2\pi f(2k - n)T_s] \tag{2.121}
$$

and

$$W_{\tilde{s}_1 \tilde{s}_2} \left(\frac{nT_s}{2}, \frac{l}{2MT_s} \right) = 2T_s \hat{W}_{\tilde{s}_1 \tilde{s}_2} \left(nT_s, \frac{l}{MT_s} \right). \tag{2.122}$$

Substituting (2.121) into (2.120) gives

$$W_{\tilde{s}_1 \tilde{s}_2}(t, f) = \sum_{n=-\infty}^{\infty} W_{\tilde{s}_1 \tilde{s}_2} \left(\frac{nT_s}{2}, f \right) \frac{\sin \pi (2t/T_s - n)}{\pi (2t/T_s - n)}, \tag{2.123}$$

for $|f| < 1/(2T_s) - B$.

When M is such that $MT_s > (T + |t|)$, we can apply (A.14) and have

$$\tilde{S}_1(f + \nu) \exp(j2\pi\nu t)$$

$$= \exp(-j2\pi f t)\tilde{S}_1(f + \nu) \exp[j2\pi(f + \nu)t]$$

$$= \exp(-j2\pi f t) \sum_{m=-\infty}^{\infty} \tilde{S}_1 \left(\frac{m}{MT_s} \right) \exp \left(j2\pi \frac{m}{MT_s} t \right)$$

$$\cdot \exp \left[-j\pi \left(f + \nu - \frac{m}{MT_s} \right) T \right] \frac{\sin \pi [MT_s(f + \nu) - m]}{\pi [MT_s(f + \nu) - m]}. \tag{2.124}$$

A similar procedure can be used to expand $\tilde{S}_2(f - \nu) \exp(j2\pi\nu t)$. Thus,

$$W_{\tilde{s}_1 \tilde{s}_2}(t, f) = 2 \sum_{m=-\infty}^{\infty} \sum_{q=-\infty}^{\infty} \tilde{S}_1 \left(\frac{m}{MT_s} \right) \tilde{S}_2^* \left(\frac{q}{MT_s} \right) \exp \left[j\pi \frac{m - q}{MT_s} (2t + T) \right]$$

$$\cdot \int_{-\infty}^{\infty} \frac{\sin \pi [MT_s(f + \nu) - k]}{\pi [MT_s(f + \nu) - m]} \frac{\sin \pi [MT_s(f - \nu) - q]}{\pi [MT_s(f - \nu) - q]} \exp(-j2\pi\nu T) d\nu. \tag{2.125}$$

The integral can be evaluated in a manner similar to that used in deriving (2.100). Thus, we have

$$W_{\tilde{s}_1 \tilde{s}_2}(t, f) = \frac{2}{MT_s} \sum_{q=-\infty}^{\infty} \sum_{m=-\infty}^{\infty} \tilde{S}_1 \left(\frac{m}{MT_s} \right) \tilde{S}_2^* \left(\frac{q}{MT_s} \right) \exp \left(j2\pi \frac{m - q}{MT_s} t \right)$$

$$\cdot \frac{\sin \pi [2MT_s f - (m + q)][1 - T/(MT_s)]}{\pi [2MT_s f - (m + q)]}. \tag{2.126}$$

Letting $l = m + q$ gives

$$W_{\tilde{s}_1 \tilde{s}_2}(t, f) = \frac{2}{MT_s} \sum_{l=-\infty}^{\infty} \sum_{m=-\infty}^{\infty} \tilde{S}_1 \left(\frac{m}{MT_s} \right) \tilde{S}_2^* \left(\frac{l - m}{MT_s} \right) \exp \left(j2\pi \frac{2m - l}{MT_s} t \right)$$

$$\cdot \frac{\sin \pi (2MT_s f - l)[1 - T/(2MT_s)]}{\pi (2MT_s f - l)}. \tag{2.127}$$

At $f = l/(2MT_s)$,

$$W_{\tilde{S}_1 \tilde{S}_2}\left(t, \frac{l}{2MT_s}\right)$$
$$= \frac{2[1 - T/(2MT_s)]}{MT_s} \sum_{m=-\infty}^{\infty} \tilde{S}_1\left(\frac{m}{MT_s}\right) \tilde{S}_2^*\left(\frac{l-m}{MT_s}\right) \exp\left[j2\pi \frac{(2m-l)t}{MT_s}\right]. \quad (2.128)$$

Then,

$$W_{\tilde{S}_1 \tilde{S}_2}\left(\frac{nT_s}{2}, \frac{l}{2MT_s}\right)$$
$$= \frac{2[1 - T/(2MT_s)]}{MT_s} \sum_{m=-\infty}^{\infty} \tilde{S}_1\left(\frac{m}{MT_s}\right) \tilde{S}_2^*\left(\frac{l-m}{MT_s}\right) \exp\left[j\pi \frac{(2m-l)n}{MT_s}\right] \quad (2.129)$$

where $|nT_s| < MT_s - T$. Substituting (2.129) into (2.127) yields

$$W_{\tilde{S}_1 \tilde{S}_2}\left(\frac{nT_s}{2}, f\right) = \frac{1}{1 - T/(2MT_s)} \sum_{l=-\infty}^{\infty} W_{\tilde{S}_1 \tilde{S}_2}\left(\frac{nT_s}{2}, \frac{l}{2MT_s}\right)$$
$$\cdot \frac{\sin \pi(2MT_s f - l)[1 - T/(2MT_s)]}{\pi(2MT_s f - l)} \quad (2.130)$$

where $|nT_s| < MT_s - T$.

Using the fact that $W_{\tilde{S}_1 \tilde{S}_2}(\cdot) = W_{\tilde{s}_1 \tilde{s}_2}(\cdot)$ and putting (2.130) into (2.123), we have

$$W_{\tilde{s}_1 \tilde{s}_2}(t, f) = \frac{1}{1 - T/(2MT_s)} \sum_{n=-\infty}^{\infty} \sum_{l=-\infty}^{\infty} W_{\tilde{s}_1 \tilde{s}_2}\left(\frac{nT_s}{2}, \frac{l}{2MT_s}\right)$$
$$\cdot \frac{\sin \pi(2MT_s f - l)[1 - T/(2MT_s)]}{\pi(2MT_s f - l)} \frac{\sin \pi(2t/T_s - n)}{\pi(2t/T_s - n)}. \quad (2.131)$$

Thus, substituting (2.122) into the above relationship, the continuous Wigner-Ville distribution can be reconstructed from $\hat{W}_{\tilde{s}_1 \tilde{s}_2}(\cdot)$ for the region $|f| < [1/(2T_s) - B]$ and $|t| < (MT_s - T)$. Specifically, for $|f| < [1/(2T_s) - B]$ and $|t| < (MT_s - T)$,

$$W_{\tilde{s}_1 \tilde{s}_2}(t, f) = \frac{2T_s}{1 - T/(2MT_s)} \sum_{n=-\infty}^{\infty} \sum_{l=0}^{\infty} \hat{W}_{\tilde{s}_1 \tilde{s}_2}\left(nT_s, \frac{l}{MT_s}\right)$$
$$\cdot \frac{\sin \pi(2MT_s f - l)[1 - T/(2MT_s)]}{\pi(2MT_s f - l)} \frac{\sin \pi(2t/T_s - n)}{\pi(2t/T_s - n)}. \quad (2.132)$$

Note that at points $(nT_s, l/(MT_s))$ in the time-frequency plane, where n and l are integers and $|t| < (MT_s - T)$ and $|f| < [1/(2T_s) - B]$, (2.132) reduces to (2.122) as expected. It

should be pointed out that at an integer multiple of T_s in time or an integer multiple of $1/(MT_s)$ in frequency, one of the two sinc functions in (2.132) turns into a Kronecker delta. Thus, interpolation for a cut in frequency or in time using (2.132) involves only one sinc function in this case. This is the same procedure used in interpolating any one-dimensional function. On the other hand, at an integer multiple of T_s in time or an integer multiple of $1/(MT_s)$ in frequency, none of the two sinc functions in the interpolation formula given in [14] reduces to a simple Kronecker delta, but one of them changes into a function involving the variable to be interpolated. Therefore, (2.132) is simpler to implement for the region $|t| < (MT_s - T)$ and $|f| < [1/(2T_s) - B]$.

2.4   Discussion

In this chapter we have derived the discrete ambiguity function and the discrete Wigner-Ville distribution in both the time- and frequency-domains. Relationships between the discrete ambiguity function and the continuous one, and between the discrete Wigner-Ville distribution and its continuous counterpart were examined. Sampling criteria were also analyzed. It was concluded that the discrete-time signal samples used in generating both time-frequency distributions have to be obtained at twice the Nyquist rate to prevent aliasing. When this sampling criteria cannot be satisfied due to hardware limitations, interpolation of missing signal samples is needed. In generating the frequency-domain representation of both time-frequency distributions the sampling rate has to be twice the Nyquist rate and the sampling process has to be twice as long as the signal's duration. Procedures to recover the continuous time-frequency distributions from their discrete counterparts were given. These procedures are simpler than the ones previously derived. They can be used as long as the sampling rate is greater than the Nyquist rate and the observation interval is longer than the signal's duration. The restriction is that they can only be used to recover those portions of the time-frequency distributions which are free from aliasing.

Chapter 3

Discrete Time-Frequency Distribution Based Radar Receivers

Radar detection and estimation procedures using either continuous or discrete observations in the presence of additive white Gaussian noise were developed in the previous chapters. The conventional optimal receiver consists of a matched filter/correlator followed by a square law device. For this type of receiver, the ambiguity function is employed to assess the ability of the transmitted waveform to satisfy the requirements for detection, measurement accuracy, resolution, ambiguity, and clutter rejection [30]-[32].

In recent years researchers [6]-[10] have shown that a receiver based on the Wigner-Ville distribution presents an alternative to the conventional receiver. This alternative not only retains the optimality but also possesses other merits. For example, the receiver based on the Wigner-Ville distribution will enable the estimation of unknowns when the problem is not completely specified. In addition, noise suppression using time-variant filtering in such receivers when the signal waveshape is unknown is more effective [9]. However, research efforts devoted to this subject thus far have been restricted to the continuous case, and the form proposed for the Wigner-Ville distribution based receiver computes the test statistic in a point by point manner in the hypothesized delay-Doppler plane.

In this chapter we consider a variety of alternatives to realize the optimum discrete

receiver. First, we consider how to use the discrete Wigner-Ville distribution to realize the optimum discrete receiver. The derivation demonstrates the potential for aliasing. It is shown that aliasing can be circumvented with a proper sampling rate depending on the form of the discrete Wigner-Ville distribution on which the receiver is based. It is also shown that instead of generating the test statistic point by point in the hypothesized delay-Doppler plane as derived for the continuous case in the literature, a more efficient estimation procedure for these types of receivers is possible. In Section 3.2, we consider another approach for implementing the receiver based on the discrete time-frequency correlation function. This method has a computational advantage over the one based on the discrete Wigner-Ville distribution.

3.1 Discrete Wigner-Ville Distribution Based Receiver

In this section we derive the procedure for implementation of the optimum receiver based on the discrete Wigner-Ville distribution. The signals considered will be assumed to be *essentially* limited both in duration and frequency to $[0, T)$ and $(-B, B)$, respectively. Also, the sampling rate will be assumed to be at least twice the Nyquist rate.

3.1.1 Time-domain Realization

As described in Chapter 1, the optimality of the continuous Wigner-Ville distribution based receiver is established via Moyal's formula. It states that the magnitude-square of the inner product of two signals, say $\tilde{s}_1(t)$ and $\tilde{s}_2(t)$, is equivalent to the inner product of the Wigner-Ville distributions of $\tilde{s}_1(t)$ and $\tilde{s}_2(t)$. That is,

$$\left| \int_{-\infty}^{\infty} \tilde{s}_1(t)\tilde{s}_2^*(t)dt \right|^2 = \int_{-\infty}^{\infty}\int_{-\infty}^{\infty} W_{\tilde{s}_1}(t,f)W_{\tilde{s}_2}^*(t,f)dtdf. \tag{3.1}$$

It is obvious that when $\tilde{s}_1(t) = \tilde{r}(t)$ and $\tilde{s}_2(t) = \tilde{s}(t - \tau_H)\exp(j2\pi f_{D_H}t)$, the left-hand side

73

of (3.1) is the test statistic used by the optimum radar receiver as shown in Chapter 1. For different values of τ_H and f_{D_H} in the reference signal, the receiver calculates the left-hand side of (3.1) and compares the result with a threshold to perform detection. If a target is declared present at (τ_H, f_{D_H}), the corresponding values of τ_H and f_{D_H} are used as the estimates of the actual delay and Doppler. However, the right-hand side of (3.1) indicates that the above procedure can be equivalently implemented by matched filtering the Wigner-Ville distributions of the received signal and the reference signal. Thus, the optimality of the receiver based on the continuous Wigner-Ville distribution is established.

Since optimality of the receiver based on the continuous Wigner-Ville distribution is established through Moyal's formula, it is reasonable to believe that receivers based on the discrete Wigner-Ville distribution can be analyzed in a parallel manner showing that the test statistic can be equivalently calculated by matched filtering two discrete Wigner-Ville distributions. However, because of aliasing, the discrete versions the Moyal's formula in the time-domain and the frequency-domain, as derived in [13], are not as useful in the realization of the optimal receiver based on the discrete Wigner-Ville distributions. The time-domain discrete Moyal's formula derived in [13] is phrased in terms of the symmetric form discrete Wigner-Ville distribution, which was defined in (2.97). Here, we rederive the results given in [13] to show how the aliasing problem arises and how it can be circumvented.

Receiver based on the symmetrical form discrete Wigner-Ville distribution

Denote the sampling interval by T_s and let $N = T/T_s$. For convenience, we assume that N is an even number. This assumption does not affect the generality of the results. Using the symmetric form of the Wigner-Ville distribution as defined in (2.97), the inner product of $\bar{W}_{\tilde{s}_1}$ and $\bar{W}_{\tilde{s}_2}$ can be expanded as

$$\sum_{k=0}^{N-1} \sum_{l=-N/2}^{N/2-1} \bar{W}_{\tilde{s}_1}\left(kT_s, \frac{l}{NT_s}\right) \bar{W}_{\tilde{s}_2}^*\left(kT_s, \frac{l}{NT_s}\right)$$

$$= \sum_{k=-\infty}^{\infty} \sum_{l=-N/2}^{N/2-1} \bar{W}_{\tilde{s}_1}\left(kT_s, \frac{l}{NT_s}\right) \bar{W}_{\tilde{s}_2}^*\left(kT_s, \frac{l}{NT_s}\right)$$

$$= \sum_{k=-\infty}^{\infty} \sum_{l=-N/2}^{N/2-1} \left\{ \sum_{p=-\infty}^{\infty} \tilde{s}_1[(k+p)T_s]\tilde{s}_1^*[(k-p)T_s]\exp\left(-j2\pi\frac{lp}{N}\right) \right\}$$

$$\cdot \left\{ \sum_{n=-\infty}^{\infty} \tilde{s}_2[(k+n)T_s]\tilde{s}_2^*[(k-n)T_s]\exp\left(-j2\pi\frac{ln}{N}\right) \right\}^*$$

$$= \sum_{k=-\infty}^{\infty} \sum_{p=-\infty}^{\infty} \sum_{n=-\infty}^{\infty} \tilde{s}_1[(k+p)T_s]\tilde{s}_1^*[(k-p)T_s]\tilde{s}_2^*[(k+n)T_s]\tilde{s}_2[(k-n)T_s]$$

$$\cdot \left\{ \sum_{l=-N/2}^{N/2-1} \exp\left[j2\pi\frac{l(n-p)}{N}\right] \right\}. \tag{3.2}$$

The summation of the exponential term in the last line of (3.2) can be evaluated by using Poisson's sum formula, and we have

$$\sum_{l=-N/2}^{N/2-1} \exp\left[j2\pi\frac{l(n-p)}{N}\right] = N\delta_{np} \tag{3.3}$$

where δ_{np} is the Kronecker delta. Thus, after summing over n, (3.2) can be written as

$$\sum_{k=0}^{N-1} \sum_{l=-N/2}^{N/2-1} \bar{W}_{\tilde{s}_1}\left(kT_s, \frac{l}{NT_s}\right) \bar{W}_{\tilde{s}_2}^*\left(kT_s, \frac{l}{NT_s}\right)$$

$$= N \sum_{k=-\infty}^{\infty} \sum_{p=-\infty}^{\infty} \sum_{n=-\infty}^{\infty} \left\{ \tilde{s}_1[(k+p)T_s]\tilde{s}_2^*[(k+p)T_s] \right\} \left\{ \tilde{s}_1[(k-p)T_s]\tilde{s}_2^*[(k-p)T_s] \right\}^* \tag{3.4}$$

Letting $k' = k - p$ in the summation on the right-hand side of (3.4), we have

$$\sum_{k=0}^{N-1} \sum_{l=-N/2}^{N/2-1} \bar{W}_{\tilde{s}_1}\left(kT_s, \frac{l}{NT_s}\right) \bar{W}_{\tilde{s}_2}^*\left(kT_s, \frac{l}{NT_s}\right)$$

$$= N \sum_{k'=-\infty}^{\infty} \sum_{p=-\infty}^{\infty} \left\{ \tilde{s}_1[(k'+2p)T_s]\tilde{s}_2^*[(k'+2p)T_s] \right\} \left\{ \tilde{s}_1(k'T_s)\tilde{s}_2^*(k'T_s) \right\}^*. \tag{3.5}$$

Summing the even and odd terms with respect to k' separately, i.e., summing over $k' = 2n$ and $k' = 2n + 1$ separately, and letting $m = n + p$, we have

$$\sum_{k=0}^{N-1} \sum_{l=-N/2}^{N/2-1} \bar{W}_{\tilde{s}_1}\left(kT_s, \frac{l}{NT_s}\right) \bar{W}_{\tilde{s}_2}^*\left(kT_s, \frac{l}{NT_s}\right)$$

$$= N \sum_{m=-\infty}^{\infty} \sum_{n=-\infty}^{\infty} \left\{ \tilde{s}_1(2mT_s)\tilde{s}_2^*(2mT_s) \right\} \left\{ \tilde{s}_1(2nT_s)\tilde{s}_2^*(2nT_s) \right\}^*$$

$$+ N \sum_{m=-\infty}^{\infty} \sum_{n=-\infty}^{\infty} \left\{ \tilde{s}_1[(2m+1)T_s]\tilde{s}_2^*[(2m+1)T_s] \right\} \left\{ \tilde{s}_1[(2n+1)T_s]\tilde{s}_2^*[(2n+1)T_s] \right\}^* \tag{3.6}$$

Note that the first term on the right-hand side of (3.6) is a summation of the products of those even-indexed samples of $\tilde{s}_1(t)$ and $\tilde{s}_2(t)$, and the second term involves odd-indexed samples. Therefore, it is equal to summing the products of all samples of $\tilde{s}_1(t)$ and $\tilde{s}_2(t)$ and then subtracting those products of odd and even-indexed samples. Consequently, we have

$$
\begin{aligned}
\sum_{k=0}^{N-1} \sum_{l=-N/2}^{N/2-1} & \bar{W}_{\tilde{s}_1}\left(kT_s, \frac{l}{NT_s}\right) \bar{W}_{\tilde{s}_2}^*\left(kT_s, \frac{l}{NT_s}\right) \\
&= \frac{N}{2} \sum_{m=-\infty}^{\infty} \sum_{n=-\infty}^{\infty} \{\tilde{s}_1(mT_s)\tilde{s}_2^*(mT_s)\} \{\tilde{s}_1(nT_s)\tilde{s}_2^*(nT_s)\}^* \\
&\quad + \frac{N}{2} \sum_{m=-\infty}^{\infty} \sum_{n=-\infty}^{\infty} (-1)^{m+n} \{\tilde{s}_1(mT_s)\tilde{s}_2^*(mT_s)\} \{\tilde{s}_1(nT_s)\tilde{s}_2^*(nT_s)\}^*.
\end{aligned} \tag{3.7}
$$

Substituting $\exp(-j\pi m)$ for $(-1)^m$ and $\exp(-j\pi n)$ for $(-1)^n$, we rewrite (3.7) as

$$
\begin{aligned}
\sum_{k=0}^{N-1} \sum_{l=-N/2}^{N/2-1} & \bar{W}_{\tilde{s}_1}\left(kT_s, \frac{l}{NT_s}\right) \bar{W}_{\tilde{s}_2}^*\left(kT_s, \frac{l}{NT_s}\right) \\
&= \frac{N}{2} |\langle \tilde{s}_1, \tilde{s}_2 \rangle|^2 + \frac{N}{2} \sum_{m=-\infty}^{\infty} \sum_{n=-\infty}^{\infty} \{\tilde{s}_1(mT_s) [\exp(-jm\pi)\tilde{s}_2^*(mT_s)]\} \\
&\quad \cdot \{\tilde{s}_1(nT_s) [\exp(-jn\pi)\tilde{s}_2^*(nT_s)]\}^*
\end{aligned} \tag{3.8}
$$

where $\langle \cdot \rangle$ denotes the inner product.

Letting $\tilde{s}_{2_f}(mT_s)$ denote the frequency shifted sequence $\exp(j\pi m)\tilde{s}_2(mT_s)$, we write

$$
\sum_{k=0}^{N-1} \sum_{l=-N/2}^{N/2-1} \bar{W}_{\tilde{s}_1}\left(kT_s, \frac{l}{NT_s}\right) \bar{W}_{\tilde{s}_2}^*\left(kT_s, \frac{l}{NT_s}\right) = \frac{N}{2} |\langle \tilde{s}_1, \tilde{s}_2 \rangle|^2 + \frac{N}{2} \left|\langle \tilde{s}_1, \tilde{s}_{2_f} \rangle\right|^2. \tag{3.9}
$$

Let $\tilde{s}_1 = \tilde{r}$ and $\tilde{s}_2 = \tilde{s}_H$. Then, the first term on the right-hand side of (3.9) is the test statistic for optimum detection and estimation as specified by (2.21) of Chapter 2. In the absence of the noise, the test statistic is maximized by a reference signal matched to the target return. On the other hand, because of a shift in frequency by one half of the sampling frequency, the reference signal maximizing the test statistic will not necessarily maximize the second term on the right-hand side of (3.9). Thus, the reference signal giving rise to the maximum of the right-hand side of (3.9) is not necessarily the one most accurately matched to the target return. It follows that matched filtering between $\bar{W}_{\tilde{r}}$ and $\bar{W}_{\tilde{s}_H}$ is not always optimum. In the following, we will establish the condition under which the second term on

76

the right-hand side of (3.9) reduces to zero and consequently matched filtering $\bar{W}_{\tilde{r}}$ and $\bar{W}_{\tilde{s}_H}$ is equivalent to calculating $|\tilde{s}_H^\dagger \tilde{r}|^2$.

First, we briefly mention a useful property of the inner product of two vectors of signal samples. Denote the vector of discrete-time samples of $\tilde{s}_i(t)$ by $\tilde{s}_i$, $i = 1, 2$, and denote the vector of discrete-frequency samples of $\tilde{S}_i(f)$ by $\tilde{S}_i$, $i = 1, 2$. As shown by (A.17), when the sampling rate is at least the Nyquist rate and the sampling lasts longer than the signal duration, we have

$$\langle \tilde{S}_1, \tilde{S}_2 \rangle = N T_s^2 \langle \tilde{s}_1, \tilde{s}_2 \rangle. \tag{3.10}$$

Using (3.10), we can rewrite the second term on the right-hand side of (3.9) to obtain

$$\sum_{k=0}^{N-1} \sum_{l=-N/2}^{N/2-1} \bar{W}_{\tilde{s}_1}\left(kT_s, \frac{l}{NT_s}\right) \bar{W}_{\tilde{s}_2}^*\left(kT_s, \frac{l}{NT_s}\right) = \frac{N}{2}\left|\langle \tilde{s}_1, \tilde{s}_2 \rangle\right|^2 + \frac{1}{2NT_s^4}\left|\langle \tilde{S}_1, \tilde{S}_{2_f} \rangle\right|^2 \tag{3.11}$$

where $\tilde{S}_{2_f}$ denotes the vector of discrete-frequency samples of $\tilde{s}_{2_f}$. It is clear that $\langle \tilde{S}_1, \tilde{S}_{2_f} \rangle$ reduces to zero when $\tilde{S}_1$ and $\tilde{S}_{2_f}$ do not overlap each other. In particular, denoting the frequency shifted reference samples by $\tilde{s}_{H_f}$ and denoting the vector of its discrete-frequency samples by $\tilde{S}_{H_f}$, we have

$$\sum_{k=0}^{N-1} \sum_{l=-N/2}^{N/2-1} \bar{W}_{\tilde{r}}\left(kT_s, \frac{l}{NT_s}\right) \bar{W}_{\tilde{s}_H}^*\left(kT_s, \frac{l}{NT_s}\right) = \frac{N}{2}\left|\langle \tilde{r}, \tilde{s}_H \rangle\right|^2 + \frac{1}{2NT_s^4}\left|\langle \tilde{R}, \tilde{S}_{H_f} \rangle\right|^2. \tag{3.12}$$

For the second term on the right-hand side of (3.12) to reduce to zero in the absence of noise, it is required that the spectra of $\tilde{R}$ and $\tilde{S}_{H_f}$ be non-overlapping. Consequently, $[1/(2T_s) + f_{D_H}] - f_{D_a}$ is required to be greater than $2B$, or equivalently, $1/(2T_s) \geq 2B - (f_{D_H} - f_{D_a})$. Since $(f_{D_H} - f_{D_a})$ can range from $-2B$ to $2B$, it follows that $1/(2T_s) \geq 4B$ is needed. In other words, in the absence of noise,

$$\sum_{k=0}^{N-1} \sum_{l=-N/2}^{N/2-1} \bar{W}_{\tilde{r}}\left(kT_s, \frac{l}{NT_s}\right) \bar{W}_{\tilde{s}_H}^*\left(kT_s, \frac{l}{NT_s}\right) = \frac{N}{2}\left|\langle \tilde{r}, \tilde{s}_H \rangle\right|^2 \tag{3.13}$$

when the sampling rate is greater than four times the Nyquist rate of the transmitted signal.

The foregoing analysis shows that matched filtering $\bar{W}_{\tilde{r}}$ and $\bar{W}_{\tilde{s}_H}$ is equivalent to the processing of $|\langle \tilde{r}, \tilde{s}_H \rangle|^2$ when the sampling rate is greater than four times the Nyquist rate

of the transmitted signal. Furthermore, according to (2.58) of Chapter 2, a sampling rate of at least twice the Nyquist rate of the transmitted signal ensures that the processing of $|\langle \tilde{r}, \tilde{s}_H \rangle|^2$ is free from aliasing in its ambiguity function. Thus, with a sampling rate higher than four times the Nyquist rate of the signal, the receiver based on the Wigner-Ville distribution is not only optimal, but also the test statistic it produces is free from aliasing in the ambiguity function. The requirement on the sampling rate nonetheless imposes a severe burden on implementation of the receiver. In the following, we consider the possibility of a less stringent alternative.

From (2.110) of Chapter 2, it can be seen that $\bar{W}_{\tilde{s}}(\cdot)$ consists of repetitions of $W_{\tilde{s}}(\cdot)$ displaced in frequency by $1/(2T_s)$. Sampling at a rate higher than twice the signal Nyquist rate only introduces zeros in the frequency dimension between the adjacent replicas of $W_{\tilde{s}}(\cdot)$ in the discrete Wigner-Ville distribution. Assume that $1/T_s = 4B$ and $N = T/T_s$. When sampling is done at four times the signal Nyquist rate, there are N zeros in the frequency domain between adjacent replicas. Thus, augmenting N zeros in the frequency domain between replicas of $W_{\tilde{s}}(\cdot)$ in $\bar{W}_{\tilde{s}}(\cdot)$ that was obtained by sampling the signal at twice the Nyquist rate has the same effect as obtaining $\bar{W}_{\tilde{s}}(\cdot)$ by sampling the signal at four times the Nyquist rate. Let $\check{W}_{\tilde{s}}(\cdot)$ denote the result of appending zeros to $\bar{W}_{\tilde{s}}(\cdot)$ which is obtained by sampling the signal at twice the Nyquist rate. The difference between $\check{W}_{\tilde{s}}(\cdot)$ and $\bar{W}_{\tilde{s}}(\cdot)$ which is obtained by sampling the signal at four times the Nyquist rate is that the former has a time increment twice as large as the latter. Next, it will be shown that using $\check{W}_{\tilde{s}}(\cdot)$ instead of $\bar{W}_{\tilde{s}}(\cdot)$ which is obtained by sampling the signal at four times the Nyquist rate still results in the optimum receiver regardless of the aforementioned difference.

Let $T_s' = T_s/2$. For simplicity, we use $\bar{W}_{\tilde{s}}[kT_s', l/(2NT_s')]$ to denote the discrete Wigner-Ville distribution obtained from signals that have been sampled at four times the Nyquist rate, i.e., with $1/T_s' = 8B$. For $-N/2 \leq l \leq N/2 - 1$, it follows that

$$\check{W}_{\tilde{s}}\left(kT_s, \frac{l}{NT_s}\right) = \bar{W}_{\tilde{s}}\left(kT_s, \frac{l}{NT_s}\right) = \bar{W}_{\tilde{s}}\left(2kT_s', \frac{l}{2NT_s'}\right). \tag{3.14}$$

For $-N \leq l \leq -N/2 + 1$ and $N/2 \leq l \leq N-1$,

$$\check{W}_{\tilde{s}}\left(kT_s, \frac{l}{NT_s}\right) = \bar{W}_{\tilde{s}}\left(2kT_s', \frac{l}{2NT_s'}\right) = 0. \tag{3.15}$$

Then we have

$$\sum_{k=0}^{N-1} \sum_{l=-N}^{N-1} \check{W}_{\tilde{s}_1}\left(kT_s, \frac{l}{NT_s}\right) \check{W}_{\tilde{s}_2}^*\left(kT_s, \frac{l}{NT_s}\right)$$

$$= \sum_{k=-\infty}^{\infty} \sum_{l=-N}^{N-1} \bar{W}_{\tilde{s}_1}\left(2kT_s', \frac{l}{2NT_s'}\right) \bar{W}_{\tilde{s}_2}^*\left(2kT_s', \frac{l}{2NT_s'}\right)$$

$$= \sum_{k=-\infty}^{\infty} \sum_{l=-N}^{N-1} \left\{ \sum_{p=-\infty}^{\infty} \tilde{s}_1[(2k+p)T_s']\tilde{s}_1^*[(2k-p)T_s'] \exp\left(-j2\pi\frac{lp}{2N}\right) \right\}$$

$$\cdot \left\{ \sum_{n=-\infty}^{\infty} \tilde{s}_2[(2k+n)T_s']\tilde{s}_2^*[(2k-n)T_s'] \exp\left(-j2\pi\frac{ln}{2N}\right) \right\}^*$$

$$= 2N \sum_{k=-\infty}^{\infty} \sum_{p=-\infty}^{\infty} \tilde{s}_1[(2k+p)T_s']\tilde{s}_1^*[(2k-p)T_s']\tilde{s}_2^*[(2k+p)T_s']\tilde{s}_2[(2k-p)T_s']. \tag{3.16}$$

Letting $k' = 2k - p$ in the last step of (3.16), we have

$$\sum_{k=0}^{N-1} \sum_{l=-N}^{N-1} \check{W}_{\tilde{s}_1}\left(kT_s, \frac{l}{NT_s}\right) \check{W}_{\tilde{s}_2}^*\left(kT_s, \frac{l}{NT_s}\right)$$

$$= 2N \sum_{k'=-\infty}^{\infty} \sum_{p=-\infty}^{\infty} \left\{ \tilde{s}_1[(2k'+2p)T_s']\tilde{s}_2^*[(2k'+2p)T_s'] \right\} \left\{ \tilde{s}_1(2k'T_s')\tilde{s}_2^*(2k'T_s') \right\}^*$$

$$= 2N \sum_{k'=-\infty}^{\infty} \sum_{p=-\infty}^{\infty} \left\{ \tilde{s}_1[(k'+p)T_s]\tilde{s}_2^*[(k'+p)T_s] \right\} \left\{ \tilde{s}_1(k'T_s)\tilde{s}_2^*(k'T_s) \right\}^*$$

$$= 2N \left| \langle \tilde{\mathbf{s}}_1, \tilde{\mathbf{s}}_2 \rangle \right|^2. \tag{3.17}$$

Thus, $\check{W}_{\tilde{s}}(\cdot)$, instead of $\bar{W}_{\tilde{s}}(\cdot)$ which is obtained by sampling the signal at four times the Nyquist rate, can be used to implement the optimal receiver. However, unlike (2.21) of Chapter 2, which is useful in calculating the test statistic for various Doppler values at a fixed delay with one discrete Fourier transform calculation of the products $\{\tilde{r}(kT_s)\tilde{s}^*(kT_s - nT_s)\}$, the receiver implemented using (3.17) only produces a test statistic at one point in the delay-Doppler plane specified by the hypothesized delay and Doppler of the reference signal. Therefore, (3.17) needs to be further modified in order to make it more useful.

Recall that $\tilde{s}_H(t)$ is a time delayed and frequency shifted version of $\tilde{s}(t)$. Let $\tilde{s}_H(t) = \tilde{s}(t - pT_s) \exp[j2\pi qt/(NT_s)]$, where p, q are integers. The relationship between $\bar{W}_{\tilde{s}_H}(\cdot)$ and $\bar{W}_{\tilde{s}}(\cdot)$ is given by

$$
\begin{aligned}
\bar{W}_{\tilde{s}_H}\left(nT_s, \frac{l}{NT_s}\right) &= \sum_{k=-\infty}^{\infty} \tilde{s}_H[(n + k)T_s]\tilde{s}_H^*[(n - k)T_s] \exp\left(-j2\pi\frac{lk}{N}\right) \\
&= \sum_{k=-\infty}^{\infty} \tilde{s}[(n + k - p)T_s]\tilde{s}^*[(n - k - p)T_s] \exp\left[-j2\pi\frac{(l - 2q)k}{N}\right] \\
&= \bar{W}_{\tilde{s}}\left[(n - p)T_s, \frac{l - 2q}{NT_s}\right].
\end{aligned}
\tag{3.18}
$$

The above relationship indicates that $\bar{W}_{\tilde{s}_H}(\cdot)$ can be obtained by shifting $\bar{W}_{\tilde{s}}(\cdot)$ in the time and/or frequency dimensions. It follows that $\check{W}_{\tilde{s}_H}(\cdot)$ can be obtained by shifting $\bar{W}_{\tilde{s}}(\cdot)$ in the time and/or frequency dimensions and appending the result with zeros. Thus, from (3.17), we have

$$
\begin{aligned}
|\langle\tilde{r}, \tilde{s}_H\rangle|^2 &= \frac{1}{2N} \sum_{k=0}^{N-1} \sum_{l=-N}^{N-1} \check{W}_{\tilde{r}}\left(kT_s, \frac{l}{NT_s}\right) \check{W}_{\tilde{s}_H}^*\left(kT_s, \frac{l}{NT_s}\right) \\
&= \frac{1}{2N} \sum_{k=0}^{N-1} \sum_{l=-N}^{N-1} \check{W}_{\tilde{r}}\left(kT_s, \frac{l}{NT_s}\right) \check{W}_{\tilde{s}}^*\left[(k - p)T_s, \frac{l - 2q}{NT_s}\right].
\end{aligned}
\tag{3.19}
$$

The above result shows that the test statistic can be generated by correlating $\check{W}_{\tilde{r}}(\cdot)$ and $\check{W}_{\tilde{s}}(\cdot)$. By fixing the shift in one argument and convolving with the other one, a cut in the test statistic of either delay or Doppler can be produced.

Receiver based on the general form discrete Wigner-Ville distribution

As mentioned at the beginning of this subsection, the time-domain discrete Moyal's formula was originally derived in terms of the symmetrical form discrete Wigner-Ville distribution. It was found that there is an aliasing problem to be dealt with in matched filtering two symmetrical form discrete Wigner-Ville distributions. In the following, we examine the possibility of realizing the receiver based on $\hat{W}_{\tilde{s}}(\cdot)$ by deriving the discrete Moyal's formula

80

in terms of $\hat{W}_{\tilde{s}}(\cdot)$. To distinguish this case from the one where the symmetrical form is considered, we refer $\hat{W}_{\tilde{s}}(\cdot)$ as the general form.

Consider the following.

$$\sum_{k=0}^{2N-1} \sum_{l=-N/2}^{N/2-1} \hat{W}_{\tilde{s}_1}\left(kT_s, \frac{l}{NT_s}\right) \hat{W}_{\tilde{s}_2}^*\left(kT_s, \frac{l}{NT_s}\right)$$

$$= \sum_{k=-\infty}^{\infty} \sum_{l=-N/2}^{N/2-1} \left\{ \sum_{p=-\infty}^{\infty} \tilde{s}_1(pT_s)\tilde{s}_1^*[(k-p)T_s] \exp\left[-j\pi \frac{l(2p-k)}{N}\right] \right\}$$

$$\cdot \left\{ \sum_{q=-\infty}^{\infty} \tilde{s}_2(qT_s)\tilde{s}_2^*[(k-q)T_s] \exp\left[-j\pi \frac{l(2q-k)}{N}\right] \right\}^*$$

$$= N \sum_{k=-\infty}^{\infty} \sum_{p=-\infty}^{\infty} \tilde{s}_1(pT_s)\tilde{s}_1^*[(k-p)T_s]\tilde{s}_2^*(pT_s)\tilde{s}_2[(k-p)T_s]$$

$$= N \left|\langle \tilde{\boldsymbol{s}}_1, \tilde{\boldsymbol{s}}_2 \rangle\right|^2 \tag{3.20}$$

From (3.20), it follows that a receiver implemented such that it performs matched filtering between $\hat{W}_{\tilde{r}}(\cdot)$ and $\hat{W}_{\tilde{s}_H}(\cdot)$ produces the test statistic as required for optimum detection and estimation. Sampling at twice the Nyquist rate is needed for this receiver to prevent aliasing in the ambiguity function of the test statistic. However, a receiver of the form of (3.20) is only capable of producing the statistic at one point in the delay-Doppler plane. Again, assume that $\tilde{s}_H(t) = \tilde{s}(t - pT_s) \exp[j2\pi qt/(NT_s)]$, p, q are integers. It follows that

$$\hat{W}_{\tilde{s}_H}\left(kT_s, \frac{l}{NT_s}\right) = \sum_{n=-\infty}^{\infty} \tilde{s}_H(nT_s)\tilde{s}_H^*[(k-n)T_s] \exp\left[-j\pi \frac{l(2n-k)}{N}\right]$$

$$= \sum_{n=-\infty}^{\infty} \tilde{s}[(n-p)T_s]\tilde{s}^*[(k-n-p)T_s] \exp\left[-j\pi \frac{(l-2q)(2n-k)}{N}\right]$$

$$= \sum_{n=-\infty}^{\infty} \tilde{s}(nT_s)\tilde{s}^*[(k-2p-n)T_s] \exp\left[-j\pi \frac{(l-2q)(2n-k+2p)}{N}\right]$$

$$= \hat{W}_{\tilde{s}}\left[(k-2p)T_s, \frac{l-2q}{NT_s}\right]. \tag{3.21}$$

The above relationship indicates that $\hat{W}_{\tilde{s}_H}(\cdot)$ can be obtained by shifting $\hat{W}_{\tilde{s}_H}(\cdot)$ in the time and/or frequency domains. Thus, applying the above result to (3.20), we have

$$\left|\langle \tilde{\boldsymbol{r}}, \tilde{\boldsymbol{s}}_H \rangle\right|^2 = \frac{1}{N} \sum_{k=0}^{2N-1} \sum_{l=-N/2}^{N/2-1} \hat{W}_{\tilde{r}}\left(kT_s, \frac{l}{NT_s}\right) \hat{W}_{\tilde{s}_H}^*\left(kT_s, \frac{l}{NT_s}\right)$$

81

$$= \frac{1}{N} \sum_{k=0}^{2N-1} \sum_{l=-N/2}^{N/2-1} \hat{W}_{\tilde{r}} \left(kT_s, \frac{l}{NT_s} \right) \hat{W}_{\tilde{s}}^* \left[(k-2p)T_s, \frac{l-2q}{NT_s} \right]. \qquad (3.22)$$

Therefore, the test statistic along a cut in either delay or Doppler in the delay-Doppler plane can be produced by convolving $\hat{W}_{\tilde{r}}(\cdot)$ and $\hat{W}_{\tilde{s}}(\cdot)$. Next, we give an example to illustrate the effect of sampling rate on the discrete Moyal's formula.

Example 3.1

In this example we examine the effect of sampling rate on the discrete Moyal's formula by way of convolving $\bar{W}_{\tilde{s}}(\cdot)$ with itself and convolving $\hat{W}_{\tilde{s}}(\cdot)$ with itself under different sampling rates. This is the same as the computation of the test statistic using (3.19) and (3.22) when there is no noise such that $\tilde{r} = \tilde{s}$. In other words, the result is the calculation of the discrete ambiguity function of $\tilde{s}$ based on (3.19) and (3.22). The signal complex envelope is assumed to be

$$\tilde{s}(t) = \sqrt{2B} \frac{\sin 2\pi Bt}{2\pi Bt} = \sqrt{2B} \text{sinc}(2Bt). \qquad (3.23)$$

This is the same waveform used in the previous chapter in demonstrating the aliasing effects in the discrete ambiguity function and the discrete Wigner-Ville distribution. The one-sided bandwidth of this signal is assumed to be $B = 1$Hz. The Nyquist rate is 2Hz. The sampling process is assumed to take place in the time interval from -0.8sec to 0.8sec. For comparison, Figure 3.1 is plotted for $\hat{\theta}_{\tilde{s}}(\cdot)$ with a sampling rate of twice the Nyquist rate. With the same sampling rate, Figure 3.2 is plotted for the convolution of $\bar{W}_{\tilde{s}}(\cdot)$ with itself. The aliasing effect is clearly shown in Figure 3.2. In Figure 3.3, the result of raising the sampling rate to four times the Nyquist rate for the convolution of $\bar{W}_{\tilde{s}}(\cdot)$ with itself is plotted. In Figure 3.4, we show the result of convolving $\check{W}_{\tilde{s}}(\cdot)$ with itself . Finally, the result of convolving $\hat{W}_{\tilde{s}}(\cdot)$ with itself with twice the Nyquist sampling rate is shown in Figure 3.5. Note the lack of aliasing. $\square$

In the analysis, thus far, we have shown that the test statistic for optimum detection and estimation is $|\langle \tilde{r}, \tilde{s}_H \rangle|^2$. The optimum receiver is conventionally built as a direct-form
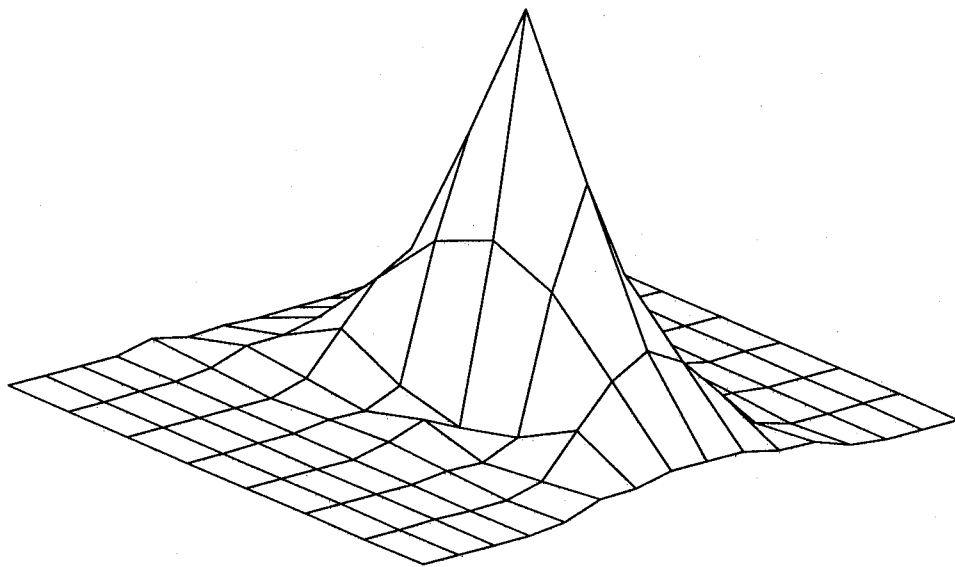
Figure 3.1: Test statistic generated from the conventional matched filter based receiver with twice the Nyquist rate sampling
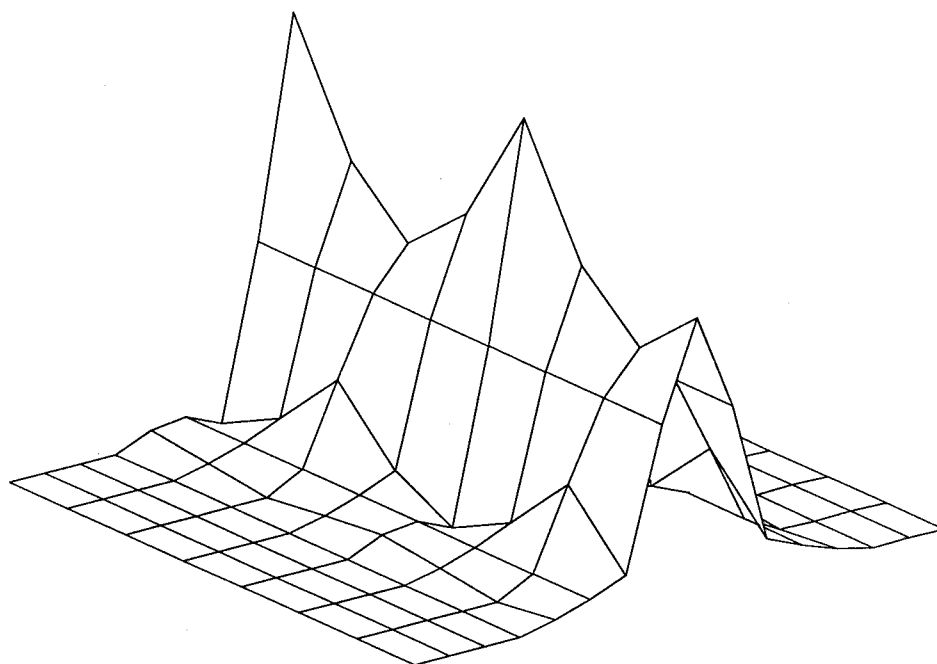
Figure 3.2: Test statistic generated from the receiver based on the symmetrical form discrete Wigner-Ville distribution with twice the Nyquist rate sampling
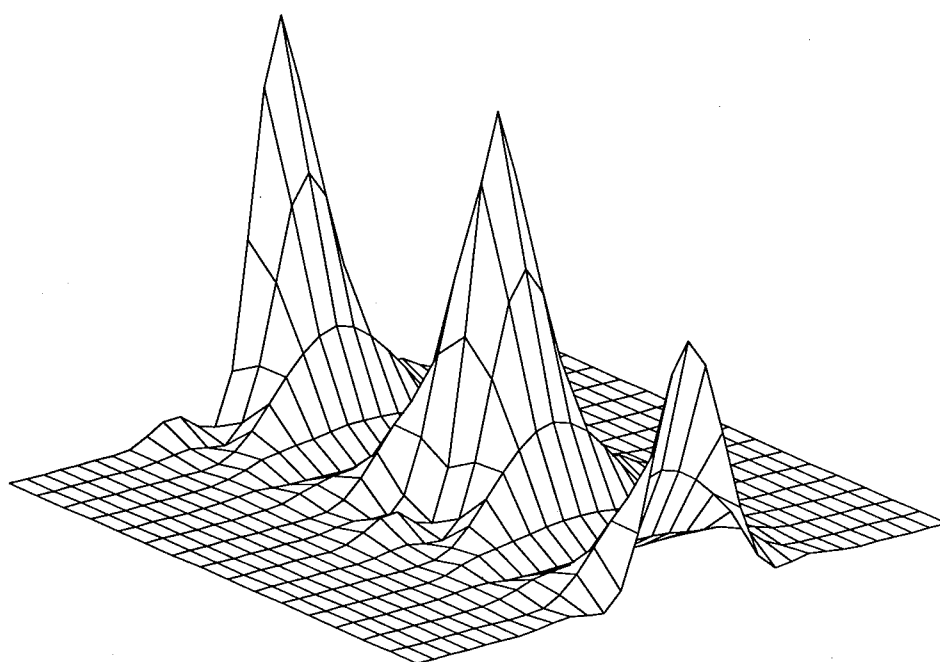
Figure 3.3: Test statistic generated from the receiver based on the symmetrical form discrete Wigner-Ville distribution with four times the Nyquist rate sampling
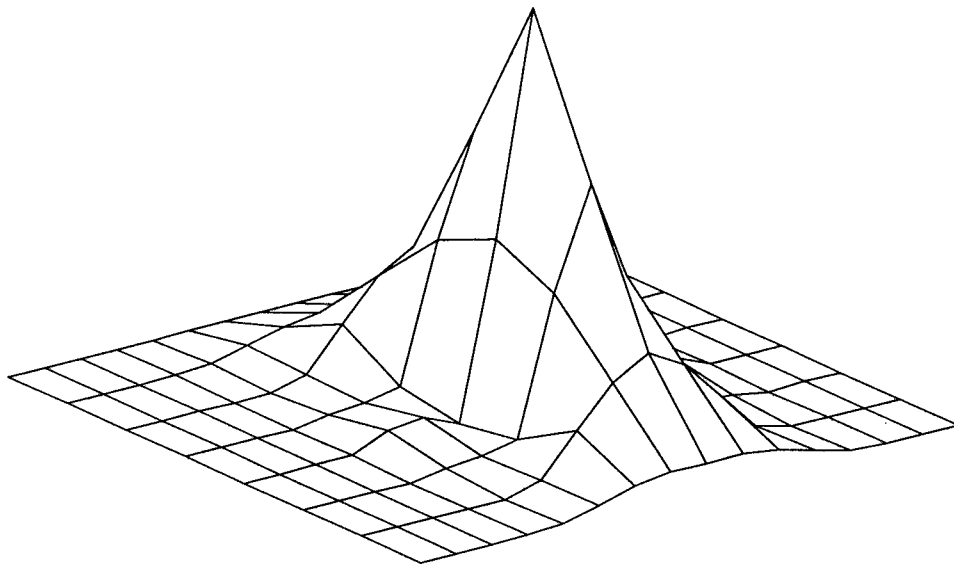
Figure 3.4: Test statistic generated from the receiver based on the symmetrical form discrete Wigner-Ville distribution with twice the Nyquist rate sampling and zero padding
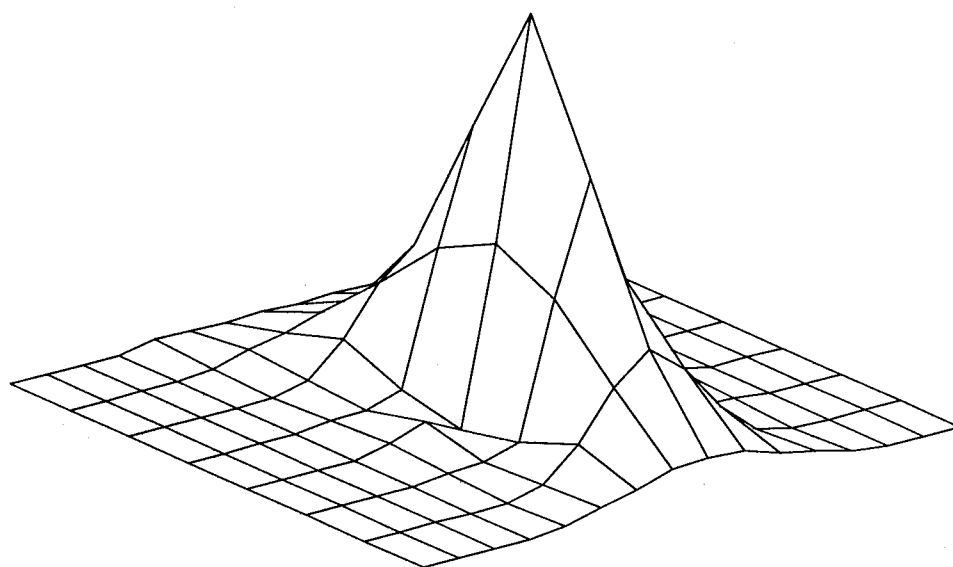
Figure 3.5: Test statistic generated from the receiver based on the general form discrete Wigner-Ville distribution with twice the Nyquist rate sampling

realization of the test statistic such that it consists of a matched filter/correlator and square-law devices. The sampling rate should be greater than twice the Nyquist rate of the signal to avoid aliasing in the ambiguity function associated with the test statistic. The analysis has also shown that the conventional receiver can be equivalently built such that it either correlates $\check{W}_{\tilde{r}}(\cdot)$ with $\check{W}_{\tilde{s}}(\cdot)$ or $\hat{W}_{\tilde{r}}(\cdot)$ with $\hat{W}_{\tilde{s}}(\cdot)$. The two functions $\check{W}_{\tilde{r}}(\cdot)$ and $\check{W}_{\tilde{s}}(\cdot)$ are obtained by zero padding $\bar{W}_{\tilde{r}}(\cdot)$ and $\bar{W}_{\tilde{s}}(\cdot)$ which are obtained with a sampling rate of twice the Nyquist rate of the signal. Sampling at twice the Nyquist rate is needed if $\hat{W}_{\tilde{r}}(\cdot)$ and $\hat{W}_{\tilde{s}}(\cdot)$ are used. Comparing (3.19) and (3.22) it is seen that the use of $\hat{W}_{\tilde{s}}(\cdot)$ or $\check{W}_{\tilde{s}}(\cdot)$ does not affect the basic structure of the receiver. The test statistic on a cut along either delay or Doppler in the delay-Doppler plane can be produced by convolving $\check{W}_{\tilde{r}}(\cdot)$ and $\check{W}_{\tilde{s}}(\cdot)$, or convolving $\hat{W}_{\tilde{r}}(\cdot)$ and $\hat{W}_{\tilde{s}}(\cdot)$, over the time or frequency arguments. A receiver based on either $\hat{W}_{\tilde{s}}(\cdot)$ or $\check{W}_{\tilde{s}}(\cdot)$ can be built in the form depicted in Figure 3.6.

3.1.2 Frequency-Domain Realization

In this section we consider the frequency-domain implementation of the discrete Wigner-Ville distribution based receiver. This receiver needs to compute the test statistic, as given by (2.37), i.e., the magnitude square of the inner product of the discrete Fourier transforms of the received signal and the reference signal. Similar to the previous discussion on the time-domain implementation of the discrete Wigner-Ville distribution based receiver, the optimality of the frequency-domain implemented receiver can be established through Moyal's formula. However, when it was first derived in [13], the discrete Moyal's formula in the frequency-domain was phrased in terms of the symmetric form discrete Wigner-Ville distribution as defined in (2.107). This form of the discrete Moyal's formula is not useful because of aliasing. Next, we rederive the results given in [13] to show how this problem arises and how it can be circumvented. Since the procedure is similar to the previous discussion, only key results will be given. A detailed derivation is placed in Appendix B.
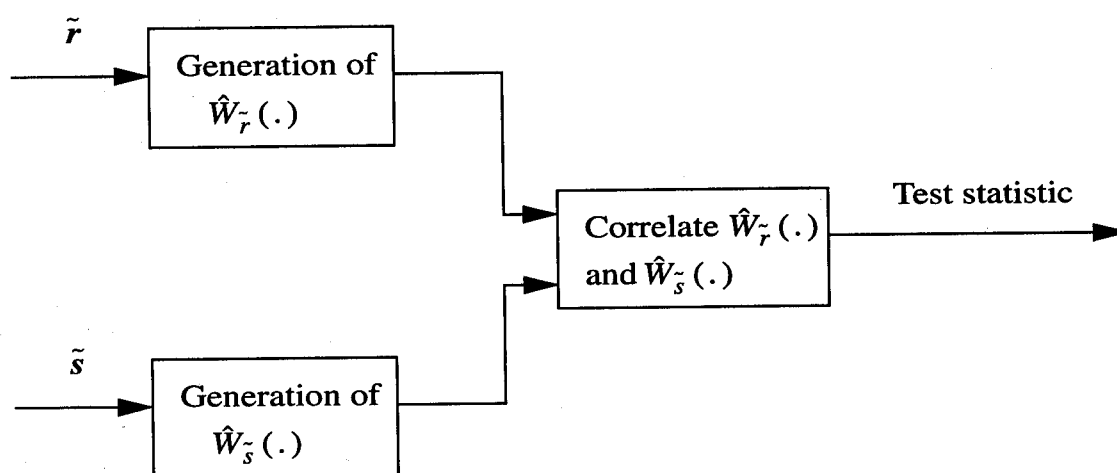
Figure 3.6: Discrete Wigner-Ville distribution based receiver in time-domain

Receiver based on the symmetrical form discrete Wigner-Ville distribution

Substituting the definition of the symmetric form of the Wigner-Ville distribution as defined in (2.107) and using (3.10), Moyal's formula in this case is given by

$$\sum_{k=0}^{N-1} \sum_{l=-N/2}^{N/2-1} \bar{W}_{\hat{S}_1}\left(kT_s, \frac{l}{NT_s}\right) \bar{W}_{\hat{S}_2}^*\left(kT_s, \frac{l}{NT_s}\right) = \frac{1}{2NT_s^4}\left|\langle\hat{\boldsymbol{S}}_1, \hat{\boldsymbol{S}}_2\rangle\right|^2 + \frac{N}{2}\left|\langle\tilde{\boldsymbol{s}}_1, \tilde{\boldsymbol{s}}_{2_t}\rangle\right|^2 \quad (3.24)$$

where $\tilde{\boldsymbol{s}}_{2_t}$ denotes the time shifted signal samples, whose continuous counterpart has a Fourier transform $\exp(-j\pi f NT_s)\tilde{S}_2(f)$. From (3.24), it is seen that the second term on the right-hand side of (3.24) is the aliasing term which reduces to zero when $\tilde{\boldsymbol{s}}_1$ and $\tilde{\boldsymbol{s}}_{2_t}$ are non-overlapping in time.

Denoting the discrete symmetric form auto-Wigner-Ville distributions of $\{\hat{R}[m/(NT_s)]\}$ and $\{\hat{S}_H[m/(NT_s)]\}$ by $\bar{W}_{\hat{R}}(\cdot)$ and $\bar{W}_{\hat{S}_H}(\cdot)$, respectively, we have

$$\sum_{k=0}^{N-1} \sum_{l=-N/2}^{N/2-1} \bar{W}_{\hat{R}}\left(kT_s, \frac{l}{NT_s}\right) \bar{W}_{\hat{S}_H}^*\left(kT_s, \frac{l}{NT_s}\right) = \frac{1}{2NT_s^4}\left|\langle\hat{\boldsymbol{R}}, \hat{\boldsymbol{S}}_H\rangle\right|^2 + \frac{N}{2}\left|\langle\tilde{\boldsymbol{r}}, \tilde{\boldsymbol{s}}_{H_t}\rangle\right|^2 \quad (3.25)$$

where $\tilde{\boldsymbol{s}}_{H_t}$ denotes the time shifted reference samples. The first term on the right-hand side of (3.25) is the test statistic for optimum detection and estimation as specified by (2.37) of Chapter 2. In the absence of noise, the test statistic is maximized by a reference signal that is matched to the target return. On the other hand, because of a mismatch in delay by amount of time $NT_s/2$, the reference signal maximizing the test statistic will not necessarily maximize the second term on the right-hand side of (3.25). Thus, the reference signal giving rise to the maximum of the right-hand side of (3.25) is not necessarily the one most accurately matched to the target return. It follows that matched filtering between $\bar{W}_{\hat{R}}$ and $\bar{W}_{\tilde{S}_H}$ is not always optimum. In the following, we will establish the condition under which the second term on the right-hand side of (3.25) reduces to zero such that matched filtering between $\bar{W}_{\hat{R}}$ and $\bar{W}_{\hat{R}_H}$ is equivalent to calculating (2.37).

For the second term on the right-hand side of (3.25) to reduce to zero in the absence of noise, it is needed that $(NT_s/2 + \tau_H) - \tau_a$ be greater than T, or equivalently, $NT_s/2 \geq$

$T - (\tau_H - \tau_a)$, so that $\tilde{r}(t)$ and $\tilde{s}_{H_t}(t)$ are non-overlapping in time. Since the effective range of $(\tau_H - \tau_a)$ is $[-T, T]$, it is required that $NT_s/2 \geq 2T$, or equivalently, $N \geq 4T/T_s$. Thus, in the absence of noise,

$$\sum_{k=0}^{N-1} \sum_{l=-N/2}^{N/2-1} \bar{W}_{\hat{R}}\left(kT_s, \frac{l}{NT_s}\right) \bar{W}_{\hat{S}_H}^*\left(kT_s, \frac{l}{NT_s}\right) = \frac{1}{2NT_s^4} \left|\langle \hat{R}, \hat{S}_H \rangle\right|^2 \qquad (3.26)$$

when $N \geq 4T/T_s$. The above analysis shows that matched filtering between $\bar{W}_{\hat{R}}(\cdot)$ and $\bar{W}_{\hat{S}_H}(\cdot)$ is equal to the processing of $|\langle \hat{R}, \hat{S}_H \rangle|^2$ when $N \geq 4T/T_s$. As discussed immediately after (2.58) and shown in (2.63) of Chapter 2, when $1/T_s \geq 4B$ and $N \geq 2T/T_s$, $|\langle \hat{R}, \hat{S}_H \rangle|^2$ is free from aliasing with respect to the corresponding ambiguity function. Thus, the optimality of the receiver based on $\bar{W}_{\hat{S}}(\cdot)$ is achievable with $NT_s \geq 4T$ and a sampling rate higher than twice the Nyquist rate of the transmitted signal. The requirement on N can also be satisfied with a less stringent alternative which is indicated by the following observation.

From (2.115) of Chapter 2, it is seen that $\bar{W}_{\hat{S}}(\cdot)$ consists of replicas of $W_{\tilde{S}}(\cdot)$ displaced in time by $NT_s/2$. Any N such that $NT_s \geq 2T$ only introduces zeros in the time dimension between adjacent replicas of $W_{\tilde{S}}(\cdot)$ in the discrete Wigner-Ville distribution. Assume that $1/T_s = 4B$. When $NT_s = 4T$, there are N zeros between adjacent replicas of $W_{\tilde{S}}(\cdot)$ in the time dimension. Augmenting N zeros in the time dimension to each of the replicas of $W_{\tilde{S}}(\cdot)$ in $\bar{W}_{\hat{S}}(\cdot)$ that was obtained with $N = 2T/T_s$ has the same effect as obtaining $\bar{W}_{\hat{S}}(\cdot)$ with $N = 4T/T_s$. Denote by $\check{W}_{\hat{S}}(\cdot)$ the result of appending zeros in the time dimension to $\bar{W}_{\hat{S}}(\cdot)$ which was obtained with $N = 2T/T_s$. The difference between $\check{W}_{\hat{S}}(\cdot)$ and $\bar{W}_{\hat{S}}(\cdot)$ obtained with extending the sampling process to $N = 4T/T_s$ is that the former has a frequency increment twice as large as the latter. Let $N' = 4T/T_s = 2N$. For simplicity, we use $\bar{W}_{\hat{S}}[kT_s, l/(N'T_s)]$ to denote the discrete Wigner-Ville distribution obtained with $N = 4T/T_s$. Then, for $0 \leq k \leq (N-1)$,

$$\check{W}_{\hat{S}}\left(kT_s, \frac{l}{NT_s}\right) = \bar{W}_{\hat{S}}\left(kT_s, \frac{l}{NT_s}\right) = \bar{W}_{\hat{S}}\left(kT_s, \frac{2l}{N'T_s}\right). \qquad (3.27)$$

For $N \leq k \leq (2N - 1)$,

$$\check{W}_{\hat{S}}\left(kT_s, \frac{l}{NT_s}\right) = \hat{W}_{\hat{S}}\left(kT_s, \frac{2l}{N'T_s}\right) = 0 \tag{3.28}$$

because of zeros in the time dimension between adjacent replicas of $W_{\tilde{S}}(\cdot)$. Furthermore, employing a similar procedure to that used in deriving (3.16), we can show that

$$\sum_{k=0}^{2N-1} \sum_{l=-N/2}^{N/2-1} \check{W}_{\hat{S}_1}\left(kT_s, \frac{l}{NT_s}\right) \check{W}_{\hat{S}_2}^*\left(kT_s, \frac{l}{NT_s}\right) = \frac{1}{2NT_s^4}\left|\langle \hat{\boldsymbol{S}}_1, \hat{\boldsymbol{S}}_2 \rangle\right|^2. \tag{3.29}$$

That is, instead of using $\bar{W}_{\hat{S}}(\cdot)$ which is obtained with $N = 4T/T_s$ in order to generate the optimal test statistic, one can use $\check{W}_{\hat{S}}(\cdot)$ which is obtained with $N = 2T/T_s$.

However, the receiver that does matched filtering between $\check{W}_{\hat{R}}(\cdot)$ and $\check{W}_{\hat{S}_H}(\cdot)$, as indicated by (3.29) can only produce the test statistic at one point in the delay-Doppler plane. Recall that $\tilde{s}_H(t)$ is a time and frequency shifted version of $\tilde{s}(t)$. The Fourier transforms of these two signals are related by $\hat{S}_H[l/(NT_s)] = \hat{S}[(l-q)/(NT_s)]\exp[-j2\pi(l-q)pT_s/(NT_s)]$, where p and q are integers. Then,

$$\begin{aligned}
\bar{W}_{\hat{S}_H}\left(nT_s, \frac{l}{NT_s}\right) &= \frac{1}{NT_s^2} \sum_{m=-N/2}^{N/2-1} \hat{S}_H\left(\frac{l+m}{NT_s}\right) \hat{S}_H^*\left(\frac{l-m}{NT_s}\right) \exp\left(j2\pi\frac{mn}{N}\right) \\
&= \frac{1}{NT_s^2} \sum_{m=-N/2}^{N/2-1} \hat{S}\left(\frac{l+m-q}{NT_s}\right) \hat{S}^*\left(\frac{l-m-q}{NT_s}\right) \exp\left[j\pi\frac{m(n-2p)}{N}\right] \\
&= \bar{W}_{\hat{S}}\left[(n-2p)T_s, \frac{l-q}{NT_s}\right].
\end{aligned} \tag{3.30}$$

The above relationship indicates that $\bar{W}_{\hat{S}_H}(\cdot)$ can be obtained by shifting $\bar{W}_{\hat{S}}(\cdot)$ in the time and/or frequency dimensions. It follows that $\check{W}_{\hat{S}_H}(\cdot)$ can be obtained by shifting $\bar{W}_{\hat{S}}(\cdot)$ in the time and/or frequency dimensions as required and appending the result with zeros. Thus, from (3.29), we have

$$\begin{aligned}
\left|\langle \hat{\boldsymbol{R}}, \hat{\boldsymbol{S}}_H \rangle\right|^2 &= 2NT_s^4 \sum_{k=0}^{2N-1} \sum_{l=N/2}^{N/2-1} \check{W}_{\hat{R}}\left(kT_s, \frac{l}{NT_s}\right) \check{W}_{\hat{S}_H}^*\left(kT_s, \frac{l}{NT_s}\right) \\
&= 2NT_s^4 \sum_{k=0}^{2N-1} \sum_{l=-N/2}^{N/2-1} \check{W}_{\hat{R}}\left(kT_s, \frac{l}{NT_s}\right) \check{W}_{\hat{S}}^*\left[(k-2p)T_s, \frac{l-q}{NT_s}\right].
\end{aligned} \tag{3.31}$$

92

The above result shows that the test statistic can be generated by correlating $\breve{W}_{\hat{R}}(\cdot)$ and $\breve{W}_{\hat{S}}(\cdot)$. By fixing the shift in one argument and convolving the other one, the test statistic along a cut in delay or Doppler can be produced.

Receiver based on the general form discrete Wigner-Ville distribution

As mentioned at the beginning of this subsection, the frequency-domain discrete Moyal's formula was originally derived in terms of the symmetrical form discrete Wigner-Ville distribution. It was found that an aliasing problem exists when matched filtering two symmetrical form discrete Wigner-Ville distributions. In the following, we examine the possibility of realizing the receiver based on the discrete Moyal's formula in terms of $\hat{W}_{\hat{S}}(\cdot)$. To distinguish this case from the one where the symmetrical form is considered, we refer to $\hat{W}_{\hat{S}}(\cdot)$ as the general form.

As shown in Appendix B that the discrete Moyal's formula in terms of $\hat{W}_{\hat{S}}(\cdot)$ is given by

$$\sum_{k=0}^{N-1} \sum_{l=-N/2}^{N/2-1} \hat{W}_{\hat{S}_1}\left(kT_s, \frac{l}{NT_s}\right) \hat{W}_{\hat{S}_2}^*\left(kT_s, \frac{l}{NT_s}\right) = \frac{1}{NT_s^4} \left|\langle \hat{S}_1, \hat{S}_2 \rangle\right|^2, \qquad (3.32)$$

where $1/T_s \geq 4B$. That is, when $1/T_s \geq 4B$, matched filtering $\hat{W}_{\hat{R}}(\cdot)$ and $\hat{W}_{\hat{S}_H}(\cdot)$ is equivalent to the processing of $|\langle \hat{R}, \hat{S}_H \rangle|^2$ as used in optimal detection and estimation. From (2.115), it is seen that the processing of $|\langle \hat{R}, \hat{S}_H \rangle|^2$ requires that $1/T_s \geq 4B$ and $N \geq 2T/T_s$ to prevent aliasing in the associated ambiguity function in the test statistic. Thus, the receiver based on $\hat{W}_{\hat{S}}(\cdot)$ is optimal when $1/T_s \geq 4B$ and $N \geq 2T/T_s$. Generating the test statistic along a cut in delay or Doppler with the above receiver can be achieved in a manner similar to that of the previous case. Again, letting $\hat{S}_H[m/(NT_s)] = \tilde{S}[(m-q)/(NT_s)] \exp[-j2\pi(m-q)pT_s/(NT_s)]$, we have

$$\hat{W}_{\hat{S}_H}\left(nT_s, \frac{l}{NT_s}\right) = \frac{1}{NT_s^2} \sum_{m=-N/2}^{N/2-1} \hat{S}_H\left(\frac{m}{NT_s}\right) \hat{S}_H^*\left(\frac{l-m}{NT_s}\right) \exp\left[j\pi \frac{(2m-l)n}{N}\right]$$

$$= \frac{1}{NT_s^2} \sum_{m=-N/2}^{N/2-1} \hat{S}\left(\frac{m-q}{NT_s}\right) \hat{S}^*\left(\frac{l-m-q}{NT_s}\right) \exp\left[j\pi \frac{(2m-l)(n-2p)}{N}\right]$$

$$= \frac{1}{NT_s^2} \sum_{m=-N/2-q}^{N/2-1-q} \hat{S}\left(\frac{m}{NT_s}\right) \hat{S}^*\left(\frac{l-2q-m}{NT_s}\right) \exp\left[j\pi \frac{(2m-l+2q)(n-2p)}{N}\right]. \quad (3.33)$$

Since $\hat{S}(\cdot)$ and $\exp(j2\pi k/N)$ are periodic,

$$\hat{W}_{\hat{S}_H}\left(nT_s, \frac{l}{NT_s}\right)$$

$$= \frac{1}{NT_s^2} \sum_{m=-N/2}^{N/2-1} \hat{S}\left(\frac{m}{NT_s}\right) \hat{S}^*\left(\frac{l-2q-m}{NT_s}\right) \exp\left[j\pi \frac{(2m-l+2q)(n-2p)}{N}\right]$$

$$= \hat{W}_{\hat{S}}\left[(n-2p)T_s, \frac{l-2q}{NT_s}\right]. \quad (3.34)$$

Thus, we have

$$\left|\langle \hat{\boldsymbol{R}}, \hat{\boldsymbol{S}}_H \rangle\right|^2 = NT_s^4 \sum_{k=0}^{N-1} \sum_{l=-N/2}^{N/2-1} \hat{W}_{\hat{R}}\left(kT_s, \frac{l}{NT_s}\right) \hat{W}_{\hat{S}_H}^*\left(kT_s, \frac{l}{NT_s}\right)$$

$$= NT_s^4 \sum_{k=0}^{N-1} \sum_{l=-N/2}^{N/2-1} \hat{W}_{\hat{R}}\left(kT_s, \frac{l}{NT_s}\right) \hat{W}_{\hat{S}}^*\left[(k-2p)T_s, \frac{l-2q}{NT_s}\right]. \quad (3.35)$$

From (3.35) it is seen that the test statistic along a cut in delay or Doppler can be obtained by fixing the shift in one argument of $\hat{W}_{\hat{S}}(\cdot)$ and convolving $\hat{W}_{\hat{R}}(\cdot)$ and $\hat{W}_{\hat{S}}(\cdot)$ over the other argument.

In summary, we have shown that $\left|\langle \hat{\boldsymbol{R}}, \hat{\boldsymbol{S}}_H \rangle\right|^2$ is the optimum test statistic for Gaussian target detection. The optimum receiver is conventionally built as a direct-form realization of the test statistic such that it consists of a matched filter/correlator and square-law device. The sampling rate should be greater than twice the Nyquist rate of the signal, and the sampling process should be extended twice as long as the duration of the signal in order to avoid aliasing in the ambiguity function associated with the test statistic. The analysis has also shown that an equivalent receiver can be built that correlates either $\check{W}_{\hat{R}}(\cdot)$ with $\check{W}_{\hat{S}}(\cdot)$ or $\hat{W}_{\hat{R}}(\cdot)$ with $\hat{W}_{\hat{S}}(\cdot)$. The two functions $\check{W}_{\hat{R}}(\cdot)$ and $\check{W}_{\hat{S}}(\cdot)$ are obtained by zero padding $\bar{W}_{\hat{R}}(\cdot)$ and $\bar{W}_{\hat{S}}(\cdot)$ which are obtained with sampling at least twice the Nyquist rate and extending

the sampling process to twice as long as the duration of the signal. The test statistic along a cut in delay or Doppler in the delay-Doppler plane can be produced by convolving over the time or frequency arguments, respectively, either $\check{W}_{\hat{R}}(\cdot)$ with $\check{W}_{\hat{S}}(\cdot)$ or $\hat{W}_{\hat{R}}(\cdot)$ with $\hat{W}_{\hat{S}}(\cdot)$. A receiver based on either $\hat{W}_{\hat{S}}(\cdot)$ or $\check{W}_{\hat{S}}(\cdot)$ can be built in the form depicted in Figure 3.7. From the discussion right after (2.58) it can be seen that receivers based on $\hat{W}_{\hat{S}}(\cdot)$ or $\check{W}_{\hat{S}}(\cdot)$ are more suitable when sampling at twice the Nyquist rate is physically unattainable. This is due to the fact that augmenting zeros to the discrete Fourier transform of the signal is equivalent to raising the sampling rate when the discrete-time samples are originally obtained at a rate higher than the Nyquist rate.

3.2 Discrete Time-Frequency Correlation Function Based Receiver

Instead of implementing the receiver based on the continuous Wigner-Ville distribution, the realization can also be based on the continuous time-frequency correlation function of the signal, as reported in [11]. The resulting receiver is computationally more tractable for detecting and estimating linear frequency modulated signals. Nevertheless, the estimation procedure is still based on the concept that was developed in implementing the receiver based on the Wigner-Ville distribution. This procedure estimates the unknown parameters in a point by point manner in the $\tau_H - f_{D_H}$ plane.

In this section, we extend the results obtained in the previous section and derive a receiver based on the discrete time-frequency correlation function. Instead of generating the test statistic point by point in the hypothesized delay-Doppler plane, it is also shown that a more efficient estimation procedure for these types of receivers is possible.
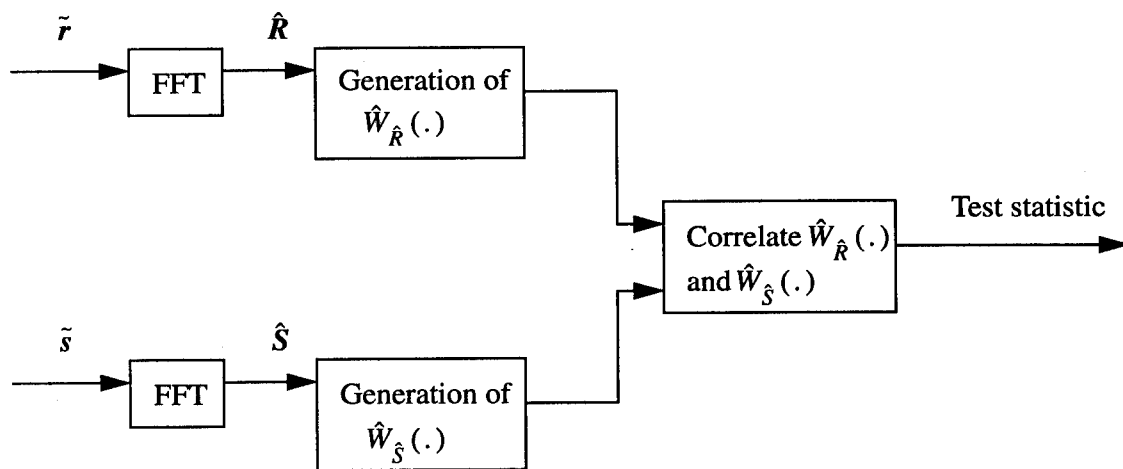
3.2.1 Time-domain Realization

Figure 3.7: Discrete Wigner-Ville distribution based receiver in frequency domain

To derive a receiver based on the discrete time-frequency correlation function, we first derive another relationship between the discrete Wigner-Ville distribution and the time-frequency correlation function. Using the definition of $\bar{W}_{\tilde{s}_1}(\cdot)$, the inverse discrete Fourier transform over its frequency argument is given by

$$
\sum_{l=-N/2}^{N/2-1} \bar{W}_{\tilde{s}_1}\left(kT_s, \frac{l}{NT_s}\right) \exp\left(j2\pi\frac{lp}{N}\right)
$$

$$
= \sum_{l=-N/2}^{N/2-1} \left\{ \sum_{n=-\infty}^{\infty} \tilde{s}_1[(k+n)T_s]\tilde{s}_1^*[(k-n)T_s] \exp\left(-j2\pi\frac{ln}{N}\right) \right\} \exp\left(j2\pi\frac{lp}{N}\right)
$$

$$
= \sum_{n=-\infty}^{\infty} \tilde{s}_1[(k+n)T_s]\tilde{s}_1^*[(k-n)T_s] \sum_{l=-N/2+1}^{N/2} \exp\left[j2\pi\frac{l(p-n)}{N}\right]
$$

$$
= N\tilde{s}_1[(k+p)T_s]\tilde{s}_1^*[(k-p)T_s]. \tag{3.36}
$$

It follows that

$$
\sum_{k=0}^{N-1} \left\{ \sum_{l=-N/2}^{N/2-1} \bar{W}_{\tilde{s}_1}\left(kT_s, \frac{l}{NT_s}\right) \exp\left(j2\pi\frac{lp}{N}\right) \right\} \exp\left(-j2\pi\frac{mk}{N}\right)
$$

$$
= N \sum_{k=0}^{N-1} \tilde{s}_1[(k+p)T_s]\tilde{s}_1^*[(k-p)T_s] \exp\left(-j2\pi\frac{mk}{N}\right)
$$

$$
= N \sum_{k=-\infty}^{\infty} \tilde{s}_1[(k+p)T_s]\tilde{s}_1^*[(k-p)T_s] \exp\left(-j2\pi\frac{mk}{N}\right)
$$

$$
= N \exp\left(j2\pi\frac{mp}{N}\right) \bar{\phi}_{\tilde{s}_1}\left(pT_s, \frac{m}{NT_s}\right). \tag{3.37}
$$

The above equation indicates that $\bar{W}_{\tilde{s}_1}(\cdot)$ and $\bar{\phi}_{\tilde{s}_1}(\cdot)$ form a two dimensional discrete Fourier transform pair. Using relationship (3.37), we have

$$
\sum_{k=-N/2}^{N/2-1} \sum_{l=-N/2}^{N/2-1} \bar{\phi}_{\tilde{s}_1}\left(kT_s, \frac{l}{NT_s}\right) \bar{\phi}_{\tilde{s}_2}^*\left(kT_s, \frac{l}{NT_s}\right)
$$

$$
= \sum_{k=-N/2}^{N/2-1} \sum_{l=-N/2}^{N/2-1} \left\{ \frac{1}{N} \exp\left(-j2\pi\frac{lk}{N}\right) \right.
$$

$$
\cdot \sum_{n=0}^{N-1} \sum_{m=-N/2}^{N/2-1} \bar{W}_{\tilde{s}_1}\left(nT_s, \frac{m}{NT_s}\right) \exp\left(-j2\pi\frac{ln}{N}\right) \exp\left(j2\pi\frac{mk}{N}\right) \right\}
$$

$$
\cdot \left\{ \frac{1}{N} \exp\left(-j2\pi\frac{lk}{N}\right) \sum_{p=0}^{N-1} \sum_{q=-N/2}^{N/2-1} \bar{W}_{\tilde{s}_2}\left(pT_s, \frac{q}{NT_s}\right) \exp\left(-j2\pi\frac{lp}{N}\right) \exp\left(j2\pi\frac{qk}{N}\right) \right\}^*
$$

97

$$= \frac{1}{N^2} \sum_{k=-N/2+1}^{N/2} \sum_{l=-N/2+1}^{N/2} \sum_{n=0}^{N-1} \sum_{m=-N/2+1}^{N/2} \sum_{p=0}^{N-1} \sum_{q=-N/2+1}^{N/2} \bar{W}_{\tilde{s}_1} \left(nT_s, \frac{m}{NT_s} \right)$$

$$\cdot \bar{W}_{\tilde{s}_2}^* \left(pT_s, \frac{q}{NT_s} \right) \exp \left(j2\pi \frac{l(p-n)}{N} \right) \exp \left(j2\pi \frac{(m-q)k}{N} \right)$$

$$= \sum_{n=0}^{N-1} \sum_{m=-N/2+1}^{N/2} \bar{W}_{\tilde{s}_1} \left(nT_s, \frac{m}{NT_s} \right) \bar{W}_{\tilde{s}_2}^* \left(nT_s, \frac{m}{NT_s} \right). \tag{3.38}$$

Letting $\tilde{r}(t) = \tilde{s}_1(t)$ and $\tilde{s}_H(t) = \tilde{s}_2(t)$, the above relationship shows that matched filtering $\bar{\phi}_{\tilde{r}}(\cdot)$ with $\bar{\phi}_{\tilde{s}_H}(\cdot)$ is equivalent to matched filtering $\bar{W}_{\tilde{r}}(\cdot)$ with $\bar{W}_{\tilde{s}_H}(\cdot)$. From (3.13) it is seen that matched filtering $\bar{W}_{\tilde{r}}(\cdot)$ with $\bar{W}_{\tilde{s}_H}(\cdot)$ can be used to generate the test statistic for optimum detection and estimation when $1/T_s \geq 8B$. Thus, (3.38) indicates that the optimum receiver can also be realized in a manner such that it computes the inner product of the time-frequency correlation functions of the received signal and the reference signal with signal sampling done at four times the Nyquist rate. However, a sampling rate of four times the Nyquist rate is a rather stringent requirement. In the following, we derive another alternative.

As seen from (2.54) of Chapter 2, that $\hat{\phi}_{\tilde{s}}(\cdot)$ consists of replicas of $\phi_{\tilde{s}}(\cdot)$ in the frequency dimension displaced by $1/T_s$. Sampling at a rate higher than twice the signal's Nyquist rate only brings in zeros in the frequency dimension between adjacent replicas. Let $1/T_s = 4B$ and $N = T/T_s$. Sampling at four times the Nyquist rate brings in N zeros in the frequency dimension. Therefore, inserting N zeros in the frequency dimension between the adjacent replicas of $\phi_{\tilde{s}}(\cdot)$ in $\hat{\phi}_{\tilde{s}}(\cdot)$ which was obtained by sampling the signal at twice the Nyquist rate, has the same effect as producing the correlation function by using discrete-time samples obtained at four times the Nyquist rate. The only difference is that the time-frequency correlation function of four times the Nyquist rate has an increment in the delay-domain that is one half of that in the correlation function obtained at the lower sampling rate but with zero padding. Let $T_s' = 8B$. From (3.37) it is clear that

$$\sum_{k=0}^{2N-1} \sum_{l=-N}^{N-1} \bar{W}_{\tilde{s}_1} \left(kT_s', \frac{l}{2NT_s'} \right) \exp \left(-j2\pi \frac{mk}{2N} \right) \exp \left(j2\pi \frac{lp}{2N} \right)$$

$$= 2N \exp\left(j2\pi \frac{mp}{2N}\right) \bar{\phi}_{\tilde{s}_1}\left(pT'_s, \frac{m}{2NT'_s}\right). \tag{3.39}$$

By definition, $\bar{\phi}_{\tilde{s}_1}(pT'_s, m/(2NT'_s)) = \hat{\phi}_{\tilde{s}_1}(2pT'_s, m/(2NT'_s))$. Denote the resulting correlation function after padding zeros to $\hat{\phi}_{\tilde{s}}(\cdot)$ which was obtained by sampling the signal at twice the Nyquist rate by $\check{\phi}_{\tilde{s}}(\cdot)$. Then, $\check{\phi}_{\tilde{s}}(pT_s, m/(NT_s)) = \hat{\phi}_{\tilde{s}}(2pT'_s, m/(2NT'_s))$. It follows that

$$\sum_{k=-N}^{N-1}\sum_{l=-N}^{N-1} \check{\phi}_{\tilde{s}_1}\left(kT_s, \frac{l}{NT_s}\right) \check{\phi}^*_{\tilde{s}_2}\left(kT_s, \frac{l}{NT_s}\right)$$

$$= \sum_{k=-N}^{N-1}\sum_{l=-N}^{N-1} \left\{ \frac{1}{2N} \exp\left(-j2\pi \frac{lk}{2N}\right) \right.$$

$$\left. \cdot \sum_{n=0}^{2N-1}\sum_{m=-N}^{N-1} \bar{W}_{\tilde{s}_1}\left(nT'_s, \frac{m}{2NT'_s}\right) \exp\left(-j2\pi \frac{ln}{2N}\right) \exp\left(j2\pi \frac{mk}{2N}\right) \right\}$$

$$\cdot \left\{ \frac{1}{2N} \exp\left(-j2\pi \frac{lk}{2N}\right) \sum_{p=0}^{2N-1}\sum_{q=-N}^{N-1} \bar{W}_{\tilde{s}_2}\left(pT'_s, \frac{q}{2NT'_s}\right) \right.$$

$$\left. \cdot \exp\left(-j2\pi \frac{lp}{2N}\right) \exp\left(j2\pi \frac{qk}{2N}\right) \right\}^*$$

$$= \frac{1}{4N^2} \sum_{k=-N}^{N-1}\sum_{l=-N}^{N-1}\sum_{n=0}^{2N-1}\sum_{m=-N}^{N-1}\sum_{p=0}^{2N-1}\sum_{q=-N}^{N-1} \bar{W}_{\tilde{s}_1}\left(nT'_s, \frac{m}{2NT'_s}\right)$$

$$\cdot \bar{W}^*_{\tilde{s}_2}\left(pT'_s, \frac{q}{2NT'_s}\right) \exp\left[j2\pi \frac{l(p-n)}{2N}\right] \exp\left[j2\pi \frac{(m-q)k}{2N}\right]$$

$$= \sum_{n=0}^{2N-1}\sum_{m=-N}^{N-1} \bar{W}_{\tilde{s}_1}\left(nT'_s, \frac{m}{2NT'_s}\right) \bar{W}^*_{\tilde{s}_2}\left(nT'_s, \frac{m}{2NT'_s}\right). \tag{3.40}$$

The above relationship shows that the inner product between $\check{\phi}_{\tilde{r}}(\cdot)$ and $\check{\phi}_{\tilde{s}_H}(\cdot)$ is equal to the inner product between $\bar{W}_{\tilde{r}}(\cdot)$ and $\bar{W}_{\tilde{s}_H}(\cdot)$ which were obtained by sampling the signal at four times the Nyquist rate. Therefore, it is seen from (3.13) that the receiver can also be realized based on $\check{\phi}_{\tilde{s}}(\cdot)$.

However, a receiver of the form of the first line of (3.40) is capable of producing the test statistic at only one point in the delay-Doppler plane. Recall that the hypothesized target return is a time delayed and frequency shifted version of the transmitted signal. Assume that $\tilde{s}_H(t) = \tilde{s}(t - pT_s) \exp[j2\pi qt/(NT_s)]$, p, q are integers. It follows that

$$\hat{\phi}_{\tilde{s}_H}\left(nT_s, \frac{l}{NT_s}\right) = \sum_{k=-\infty}^{\infty} \tilde{s}_H(kT_s)\tilde{s}^*_H[(k-n)T_s] \exp\left(-j2\pi \frac{lk}{N}\right)$$

$$= \sum_{k=-\infty}^{\infty} \tilde{s}[(k-p)T_s]\tilde{s}^*[(k-p-n)T_s] \exp\left[-j2\pi\frac{lk-qn}{N}\right]$$

$$= \hat{\phi}_{\tilde{s}}\left(nT_s, \frac{l}{NT_s}\right) \exp\left(-j2\pi\frac{lp-qn}{N}\right). \tag{3.41}$$

The above relationship indicates that $\hat{\phi}_{\tilde{s}_H}(\cdot)$ can be obtained by shifting the frequency of $\hat{\phi}_{\tilde{s}}(\cdot)$. It follows that $\check{\phi}_{\tilde{s}_H}(\cdot)$ can be obtained by shifting the frequency of $\check{\phi}_{\tilde{s}_H}(\cdot)$ and appending the result with zeros. Thus, using (3.13), (3.40) and (3.41), we have

$$|\langle \tilde{r}, \tilde{s}_H \rangle|^2 = \frac{1}{N} \sum_{n=-N}^{N-1} \sum_{l=-N}^{N-1} \check{\phi}_{\tilde{r}}\left(nT_s, \frac{l}{NT_s}\right) \check{\phi}_{\tilde{s}_H}^*\left(nT_s, \frac{l}{NT_s}\right)$$

$$= \frac{1}{N} \sum_{n=-N}^{N-1} \sum_{l=-N}^{N-1} \check{\phi}_{\tilde{r}}\left(nT_s, \frac{l}{NT_s}\right) \check{\phi}_{\tilde{s}}^*\left(nT_s, \frac{l}{NT_s}\right) \exp\left[j2\pi\frac{lp}{2N}\right] \exp\left[-j2\pi\frac{qn}{2N}\right]. \tag{3.42}$$

The above relationship indicates that a test statistic along a cut in either delay or Doppler can be obtained by calculating the discrete Fourier transform of the product of $\check{\phi}_{\tilde{r}}(\cdot)$ and $\check{\phi}_{\tilde{s}}^*(\cdot)$ over the delay or Doppler arguments, respectively. Figure 3.8 gives the block diagram of the receiver of the form of (3.42). Next, we compare the computational complexity of the receiver specified by (3.42) with that of the receivers based on the discrete Wigner-Ville distribution.

It is clear from the definitions of the discrete Wigner-Ville distribution and the time-frequency correlation function that the generation of these two distributions require the same amount of computations. Then, the complexities of the two types of receivers lie in whether to compute the discrete Fourier transform of the product of two time-frequency correlation functions or to compute the convolution of two Wigner-Ville distributions. Since convolution is more efficiently carried out by applying the convolution theorem and using fast Fourier transform algorithms for a large number of samples [28], it is evident that the receiver specified by (3.42) is more desirable because it requires fewer discrete Fourier transforms. For example, to generate the test statistic along a cut in Doppler at a given delay the number of multiplications, which is the dominant factor in computational complexity, that is required by the receiver of (3.42) consists of two $(2N)^2$ complex number multiplications
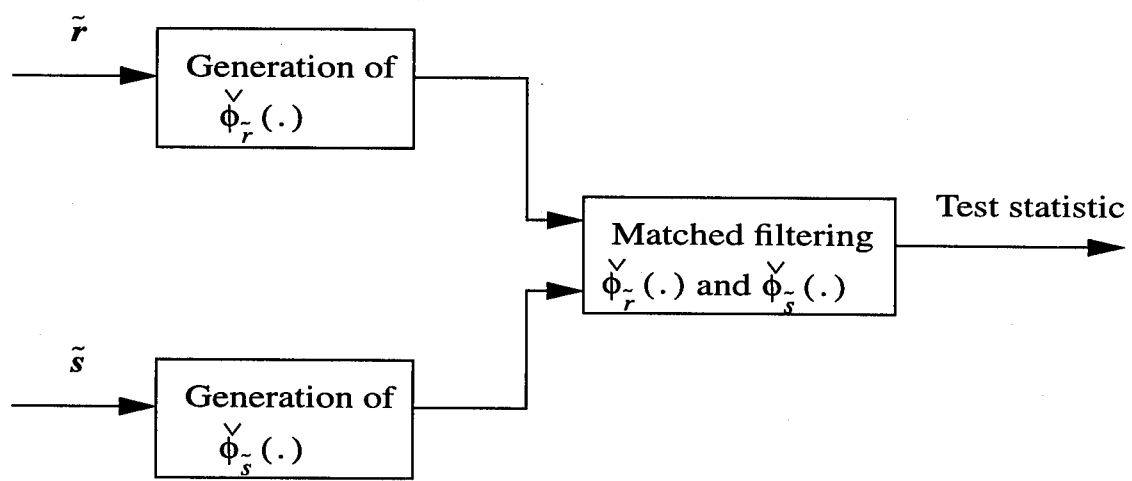
Figure 3.8: Discrete time-frequency correlation function based receiver in time domain

forming the product $\{\check{\phi}_{\tilde{r}}(nT_s, l/(NT_s))\check{\phi}_{\tilde{s}}^*(nT_s, l/(NT_s)) \exp[j2\pi lp/(2N)]\}$ and of one $2N$-point discrete Fourier transform. On the other hand, the receiver specified by (3.22) requires $2N$ $2N$-point discrete Fourier transforms, one $(2N)^2$ complex number multiplication, and one $2N$-point discrete Fourier transform. Assume that the discrete Fourier transforms are carried out using a radix-2 fast Fourier transform algorithm. As shown in the literature [34], $(N/2)\log_2 N$ multiplications are required in an N point radix-2 fast Fourier transform. Therefore, the receiver (3.42) requires $2N^2 \log_2(N/2)$ less multiplications than the receiver of (3.22). Similar conclusions can be drawn when we compare (3.42) with (3.19), or when we compare the numbers of calculations needed to generate the test statistic along a cut in delay.

3.2.2 Frequency-Domain Realization

In a manner similar to that used in the time-domain realization, we can also realize the optimum receiver based on the discrete time-frequency correlation function in the frequency-domain. Since the procedures are similar, we give only the key results here and put the detailed derivation in Appendix B.

Recall that the realization of the discrete time-frequency correlation function based receiver follows from the observation of the Fourier transform relationship between $\bar{W}_{\tilde{s}_1}(\cdot)$ and $\check{\phi}_{\tilde{s}_1}(\cdot)$. Therefore, we first derive the relationship between $\bar{W}_{\hat{S}_1}(\cdot)$ and $\check{\phi}_{\hat{S}_1}(\cdot)$:

$$\sum_{l=-N/2}^{N/2-1} \left\{ \sum_{k=0}^{N-1} \bar{W}_{\hat{S}_1}\left(kT_s, \frac{l}{NT_s}\right) \exp\left(-j2\pi\frac{mk}{N}\right) \right\} \exp\left(j2\pi\frac{ln}{N}\right)$$
$$= N \exp\left(-j2\pi\frac{mn}{N}\right) \check{\phi}_{\hat{S}_1}\left(nT_s, \frac{m}{NT_s}\right). \tag{3.43}$$

Using the above result we can demonstrate that

$$\sum_{k=-N/2}^{N/2-1} \sum_{l=-N/2}^{N/2-1} \check{\phi}_{\hat{S}_1}\left(kT_s, \frac{l}{NT_s}\right) \check{\phi}_{\hat{S}_2}^*\left(kT_s, \frac{l}{NT_s}\right)$$

$$= \sum_{n=0}^{N-1} \sum_{m=-N/2}^{N/2-1} \bar{W}_{\hat{S}_1} \left(nT_s, \frac{m}{NT_s} \right) \bar{W}_{\hat{S}_2}^* \left(nT_s, \frac{m}{NT_s} \right). \tag{3.44}$$

For the same reason as in the previous discussions, we conclude that the optimum receiver can be implemented in such a manner that it computes the inner product $\bar{\phi}_{\hat{R}}(\cdot)$ and $\bar{\phi}_{\hat{S}_H}(\cdot)$ with $N \geq 4T/T_s$ and $1/T_s = 4B$. Also, it appears to be possible to find an alternative to reduce the requirement on the number of samples as suggested by the substitution of $\check{W}_{\hat{S}}(\cdot)$ for $\bar{W}_{\hat{S}}(\cdot)$.

It is seen from (2.62) of Chapter 2 that $\hat{\phi}_{\tilde{S}}(\cdot)$ consists of replicas of $\phi_{\tilde{S}}(\cdot)$ in the time dimension displaced by NT_s. Sampling the signal for longer than twice the signal's duration only brings in zeros between adjacent replicas. Let $1/T_s = 4B$ and $N = 2T/T_s$. Sampling for four times the signal's duration brings in N zeros. Therefore, inserting N zeros in the time dimension between the adjacent replicas of $\phi_{\tilde{S}}(\cdot)$ in $\bar{\phi}_{\tilde{S}}(\cdot)$ which was originally obtained by sampling the signal for twice the duration of the signal has the same effect as producing the correlation function by sampling for four times the duration. Let $N' = 4T/T_s = 2N$. From (3.43)

$$\sum_{k=0}^{N'-1} \sum_{l=-N'/2}^{N'/2-1} \bar{W}_{\hat{S}_1}' \left(kT_s, \frac{l}{N'T_s} \right) \exp \left(-j2\pi \frac{mk}{N'} \right) \exp \left(j2\pi \frac{ln}{N'} \right)$$
$$= N' \exp \left(-j2\pi \frac{mn}{N'} \right) \bar{\phi}_{\hat{S}_1}' \left(nT_s, \frac{m}{N'T_s} \right). \tag{3.45}$$

By definition, $\bar{\phi}_{\hat{S}_1} (nT_s, q/(N'T_s)) = \hat{\phi}_{\hat{S}_1} (nT_s, 2q/(N'T_s))$. Denote the resulting correlation function after padding zeros in the time dimension to $\hat{\phi}_{\hat{S}_1}(\cdot)$ by $\check{\phi}_{\hat{S}_1}(\cdot)$. Hence, we have $\check{\phi}_{\hat{S}_1} (nT_s, q/(NT_s)) = \hat{\phi}_{\hat{S}_1} (nT_s, 2q/(N'T_s))$. Thus,

$$\sum_{k=-N}^{N-1} \sum_{l=-N/2}^{N/2-1} \check{\phi}_{\hat{S}_1} \left(kT_s, \frac{l}{NT_s} \right) \check{\phi}_{\hat{S}_2}^* \left(kT_s, \frac{l}{NT_s} \right)$$
$$= \sum_{k=-N}^{N-1} \sum_{l=-N}^{N-1} \check{\phi}_{\hat{S}_1}' \left(kT_s, \frac{l}{NT_s} \right) \check{\phi}_{\hat{S}_2}'^* \left(kT_s, \frac{l}{NT_s} \right)$$
$$= \sum_{k=-N}^{N-1} \sum_{l=-N}^{N-1} \left\{ \frac{1}{N'} \sum_{n=0}^{N'-1} \sum_{m=-N'/2}^{N'/2-1} \bar{W}_{\hat{S}_1}' \left(nT_s, \frac{m}{N'T_s} \right) \exp \left(-j2\pi \frac{ln}{N'} \right) \exp \left(j2\pi \frac{mk}{N'} \right) \right\}$$

$$\cdot \left\{ \frac{1}{N'} \sum_{p=0}^{N'-1} \sum_{q=-N'/2}^{N'/2-1} \bar{W}'_{\hat{S}_2} \left(pT_s, \frac{q}{N'T_s} \right) \exp \left(-j2\pi \frac{lp}{N'} \right) \exp \left(j2\pi \frac{qk}{N'} \right) \right\}^*$$

$$= \sum_{n=0}^{2N-1} \sum_{m=-N'}^{N'-1} \bar{W}'_{\hat{S}_1} \left(nT_s, \frac{m}{N'T_s} \right) \bar{W}'^*_{\hat{S}_2} \left(nT_s, \frac{m}{N'T_s} \right)$$

$$= \sum_{n=0}^{2N-1} \sum_{m=-N}^{N-1} \bar{W}_{\hat{S}_1} \left(nT_s, \frac{m}{N'T_s} \right) \bar{W}^*_{\hat{S}_2} \left(nT_s, \frac{m}{N'T_s} \right). \qquad (3.46)$$

The last step in (3.46) indicates that the optimum receiver can also be realized by utilizing $\check{\phi}_{\hat{S}}(\cdot)$.

To generate the test statistic along a cut in delay, we consider the following. Letting $\hat{S}_H[k/(NT_s)] = \hat{S}[(k-q)/(NT_s)] \exp[-j2\pi(k-q)pT_s/(NT_s)]$, we have

$$\hat{\phi}_{\hat{S}_H} \left(nT_s, \frac{l}{NT_s} \right) = \frac{1}{NT_s^2} \sum_{k=0}^{N-1} \hat{S}_H \left(\frac{k}{NT_s} \right) \hat{S}_H^* \left(\frac{k-l}{NT_s} \right) \exp \left[j2\pi \frac{(k-l)n}{N} \right]$$

$$= \frac{1}{NT_s^2} \sum_{k=0}^{N-1} \hat{S} \left(\frac{k-q}{NT_s} \right) \hat{S}^* \left(\frac{k-l-q}{NT_s} \right) \exp \left[j2\pi \frac{(k-l)n - lp}{N} \right]$$

$$= \frac{1}{NT_s^2} \sum_{k=0}^{N-1} \hat{S} \left(\frac{k-q}{NT_s} \right) \hat{S}^* \left(\frac{k-l-q}{NT_s} \right) \exp \left[j2\pi \frac{(k-l-q)n}{N} \right]$$

$$\cdot \exp \left(j2\pi \frac{qn - lp}{N} \right)$$

$$= \hat{\phi}_{\hat{S}} \left(nT_s, \frac{l}{NT_s} \right) \exp \left(-j2\pi \frac{lp}{N} \right) \exp \left(j2\pi \frac{qn}{N} \right). \qquad (3.47)$$

The above relationship indicates that $\hat{\phi}_{\hat{S}_H}(\cdot)$ can be obtained by shifting the phase of $\hat{\phi}_{\hat{S}}(\cdot)$. It follows that $\check{\phi}_{\hat{S}_H}(\cdot)$ can be obtained by shifting the phase of $\hat{\phi}_{\hat{S}}(\cdot)$ and appending zeros in the time dimension to the result. Thus, together with (3.26), the test statistic can be obtained by

$$\left| \langle \hat{\boldsymbol{R}}, \hat{\boldsymbol{S}}_H \rangle \right|^2 = 4NT_s^4 \sum_{n=-N}^{N-1} \sum_{l=-N/2}^{N/2-1} \check{\phi}_{\hat{R}} \left(nT_s, \frac{l}{NT_s} \right) \check{\phi}^*_{\hat{S}_H} \left(nT_s, \frac{l}{NT_s} \right)$$

$$= 4NT_s^4 \sum_{n=-N}^{N-1} \sum_{l=-N/2}^{N/2-1} \check{\phi}_{\hat{R}} \left(nT_s, \frac{l}{NT_s} \right) \check{\phi}^*_{\hat{S}} \left(nT_s, \frac{l}{NT_s} \right) \exp \left(j2\pi \frac{lp}{N} \right) \exp \left(-j2\pi \frac{qn}{2N} \right)$$

$$\qquad (3.48)$$

A block diagram of the receiver of the form (3.48) is given in Figure 3.9. It is clear that the
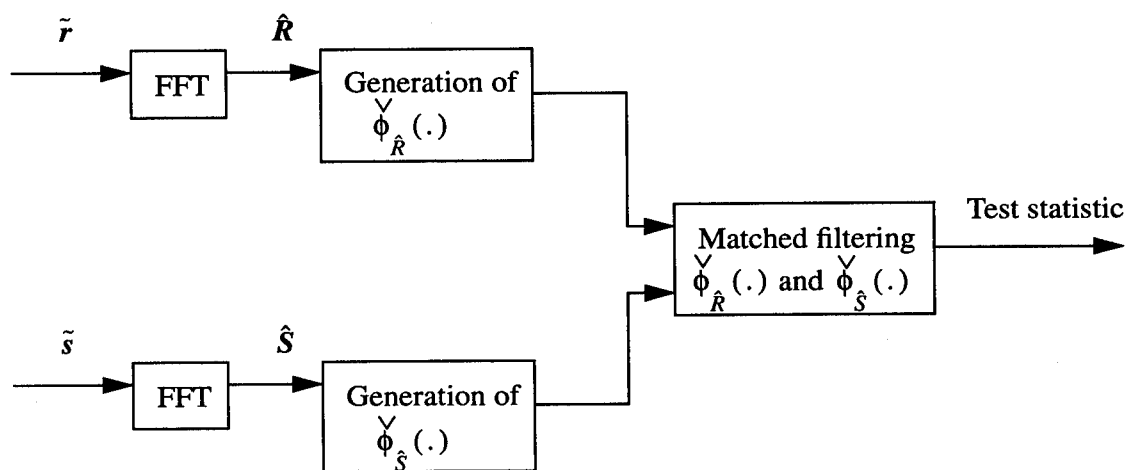
Figure 3.9: Discrete time-frequency correlation function based receiver in frequency-domain

105

receiver specified by (3.48) has a computational advantage over those of (3.31) and (3.35) for the same reason as discussed at the end of the last subsection. The frequency-domain implementation of the time-frequency correlation function based receiver has the advantage over the time-domain implementation when sampling at twice the Nyquist rate is beyond the capability of hardware.

3.3 Application of the Discrete Time-Frequency Distribution Based Receiver

In the preceding analysis, we derived the criteria under which a radar receiver based either on the discrete Wigner-Ville distribution or on the discrete time-frequency correlation function is equivalent to the conventional discrete-time radar receiver, which performs matched filtering/correlation and envelope detection. As mentioned earlier, previous literature on this subject has been restricted to the continuous case.

One of the major advantages of performing radar reception based on time-frequency distributions is that it transfers the detection and estimation procedure into a time-frequency space, where feature selection and time-variant filtering are easier [25]. This is most useful in situations where uncertainty exists with regard to the complex envelope of the desired target return. Only when the target is a nonmaneuvering slowly fluctuating point target is its return a time delayed and Doppler shifted version of the transmitted signal attenuated in amplitude. If the receiver has knowledge of the exact form of the transmitted signal, it can readily generate the optimum test statistic by matched filtering/correlation and envelope detection without the need to resort to a time-frequency distribution based method. In practice, however, there are situations where the receiver does not have exact knowledge of the transmitted signal. Also, the acceleration of a maneuvering target creates uncertainty in the received target return.

106

The problem where the transmitted signal is unknown to the receiver arises in several radar and sonar applications. For example, receivers that take advantage of transmitters which are not colocated are rarely equipped with the exact knowledge of the transmitted signal. In such cases, detection is commonly carried out in the form of energy detection. Methods to improve this approach are of interest.

When the target is maneuvering and has high acceleration, the target return model given in Chapter 1 has to be modified. The result is that the Doppler shift in the target return is a linear function of time instead of a constant [32],[16]. A Doppler shift which is a linear function of time results in a linear frequency modulated signal (*lfm*). As a consequence, an estimate of the modulation is needed for the purpose of choosing a suitable reference signal for coherent detection. If estimation of the modulation is based on maximum likelihood estimation, a third dimension is added to two-dimensional estimation procedures for the delay and Doppler shift. Methods to reduce this increased burden are of interest.

Although it has been shown that the various forms of the receiver discussed in this work are all optimal in the Neyman-Pearson sense for a nonmaneuvering slowly fluctuating point target in an additive white Gaussian noise environment, complete knowledge of the transmitted signal is assumed. As discussed in the last two paragraphs, there are situations where uncertainty exists with regard to the received target return. In the following, we use two instructive examples to illustrate that time-frequency distribution based receivers are more versatile in dealing with the aforementioned problems because of their ability to extract information about the received signal.

Signal Localization in Time-frequency Space

When the transmitted signal is unknown to the receiver, matched filtering/correlation is infeasible, and energy detection is commonly employed to determine whether a target return

is present. The Wigner-Ville distribution is a very useful tool in this case due to its ability to preserve the energy concentration of a signal [9],[10]. While the spectrum of the target return may sweep across the entire receiver bandwidth during the observation interval because of acceleration or frequency modulation, note that the instantaneous bandwidth of the target return is usually much narrower than the total receiver bandwidth. On the other hand, white noise has a flat power spectrum throughout the receiver bandwidth. Therefore, an energy concentration in the time-frequency plane will reveal the presence of a useful signal. This property is illustrated with the following two signals.

The first signal to be considered is a linearly frequency modulated signal. During the observation interval $t = [0, 8)$, assume that a signal of the form

$$\tilde{s}_1(t) = \exp\left[-j2\pi f_m(t-4)^2\right], \quad f_m = 1/16 \tag{3.49}$$

is received by a receiver which samples the signal at a sampling rate of $1/T_s = 1/8$, producing 64 samples. For reference, the discrete Wigner-Ville distribution of $\tilde{s}_1(t)$ is given in Figure 3.10. Note that the large amplitude portion of $\hat{W}_{\tilde{s}_1}(\cdot)$ concentrates in one area forming a ridge. The power spectral density of the corrupting additive white Gaussian noise is assumed to be unity so that the signal-to-noise ratio is 0dB. The discrete Wigner-Ville distribution of the corrupted signal is given in Figure 3.11. It is seen from Figure 3.11 that the ridge caused by the signal is still discernible despite presence of noise.

The second signal to be considered is a train of linearly frequency modulated Gaussian pulses. During the observation interval $t = [0, 64)$, suppose that the receiver received a signal of the form

$$\tilde{s}_2(t) = \frac{1}{2}\sum_{k=0}^{3}\exp\left[(1+j2f_m)\pi\frac{-(t-3-kT_p)^2}{16}\right], \quad f_m = 1/2, \quad T_p = 16. \tag{3.50}$$

The sampling rate is assumed to be $1/T_s = 1$ resulting in 64 samples. $\hat{W}_{\tilde{s}_2}(\cdot)$ is plotted in Figure 3.12. Note that the large amplitude portion of $\hat{W}_{\tilde{s}_2}(\cdot)$ provides information of the signal's repetition period. The power spectral density of the noise is assumed to be $1/(\sqrt{2}T_p)$
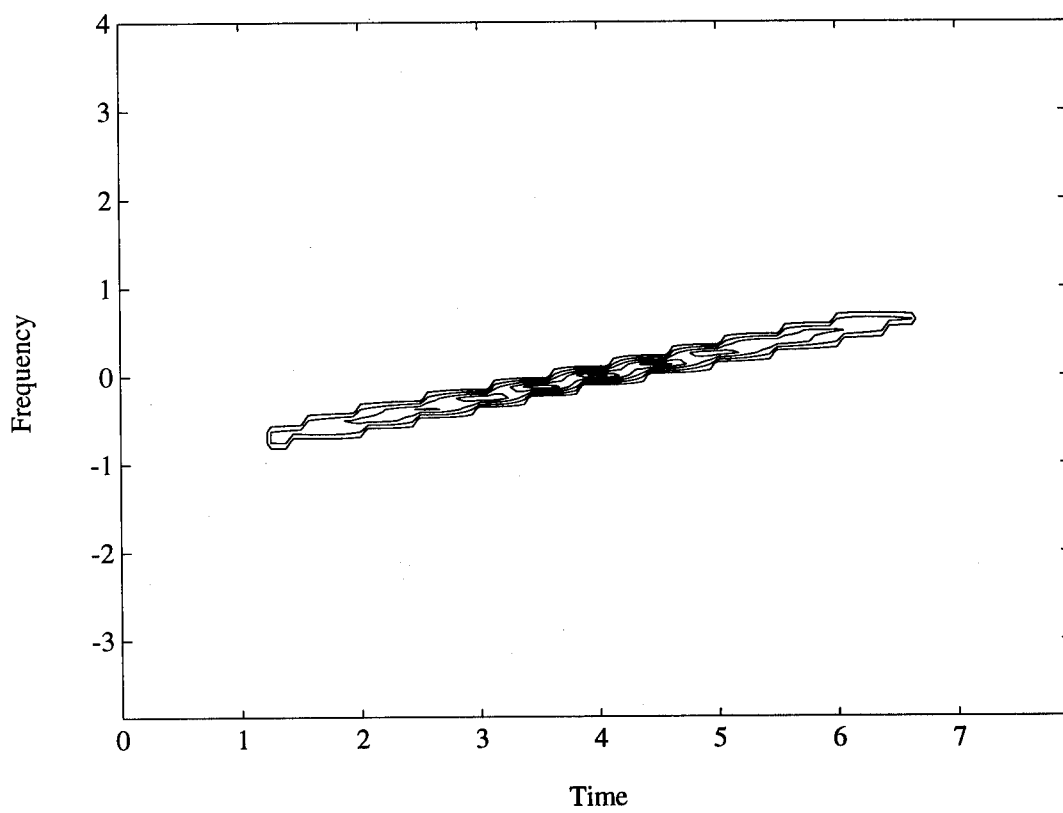
108

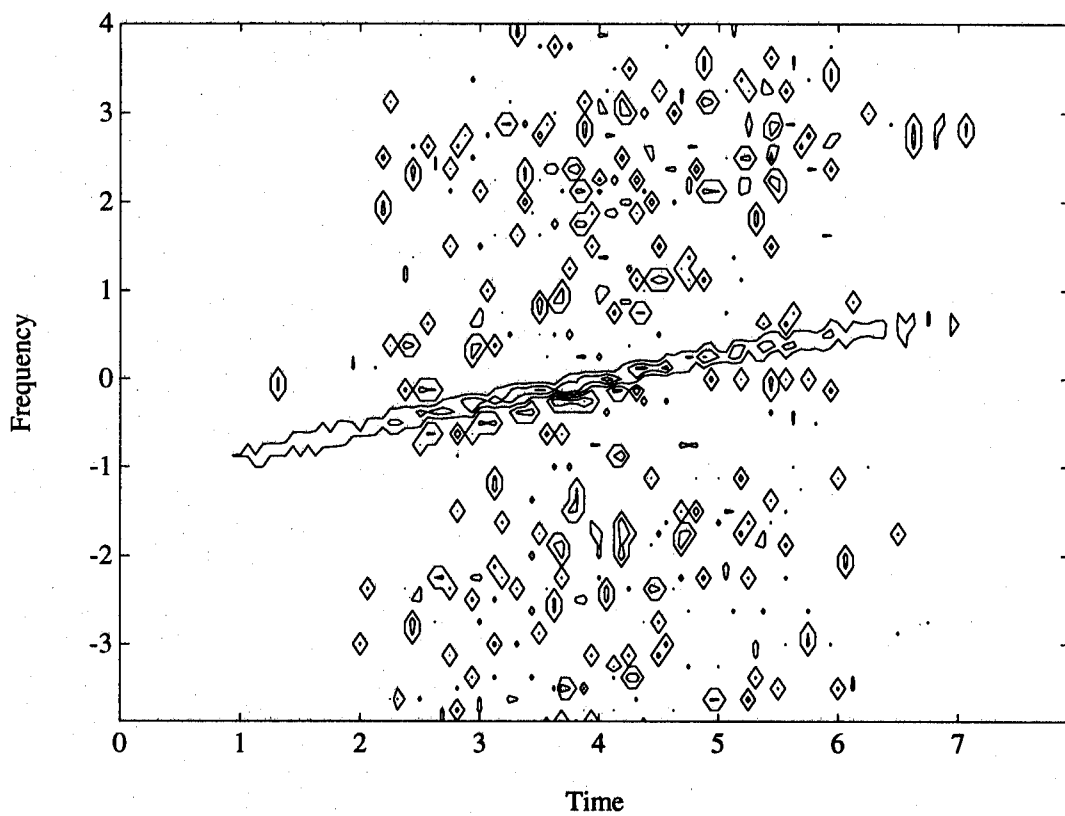Figure 3.10: Discrete Wigner-Ville distribution of a *lfm* signal

Figure 3.11: Discrete Wigner-Ville distribution of a *lfm* signal embedded in 0dB noise
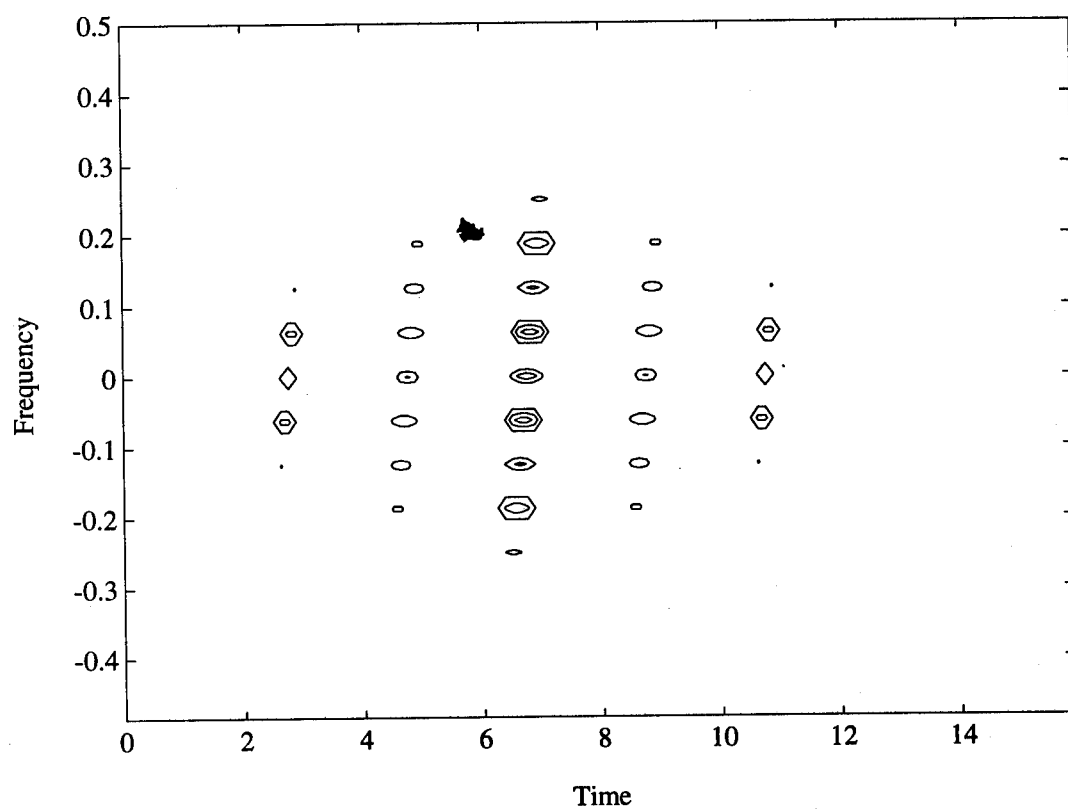
110

Figure 3.12: Discrete Wigner-Ville distribution of a train of four *lfm* Gaussian pulses

so that the one-pulse signal-to-noise ratio is 0dB. The discrete Wigner-Ville distribution of the corrupted signal is given in Figure 3.13. It is seen from Figure 3.13 that the repetitive ridges are still observable despite presence of the noise.

From the two cases considered above, it is seen that the Wigner-Ville distribution preserves the energy concentration of a signal and contains its characteristics. Consequently, Wigner-Ville distribution of the received signal provides useful information about the target return when the knowledge of the transmitted signal is lacking. This acquired information about the signal may enable one to choose a proper reference signal. Moreover, this information helps to eliminate unwanted noise. Therefore, a Wigner-Ville distribution based receiver is rather useful when the transmitted signal is unknown such that matched filtering is infeasible. To implement such a process digitally, criteria for the discrete Wigner-Ville distribution based receiver to be alias-free were established in this work.

Estimation of the Instantaneous Frequency of the Target Return

As mentioned earlier, the nonmaneuvering slowly fluctuating point target model may not always be suitable; there are occasions where the target is maneuvering and its acceleration cannot be ignored. Acceleration in the target return has the same effect as frequency modulating the target return. The problem of how to estimate this modulating factor as well as estimate other parameters in an *lfm* signal has been drawing considerable research efforts. One recent paper [33] proposed a simple algorithm based on the discrete ambiguity function. It is shown that the estimated variance of this suboptimal algorithm is about 7 percent higher than the Cramer-Rao bound at high signal-to-noise ratios, and about 60 percent higher than the bound at a signal-to-noise ratio of 0dB. This algorithm relies on finding the maximum of the ambiguity function along a cut in frequency. However, the reason that the maximum of the ambiguity function along a cut in frequency provides information about
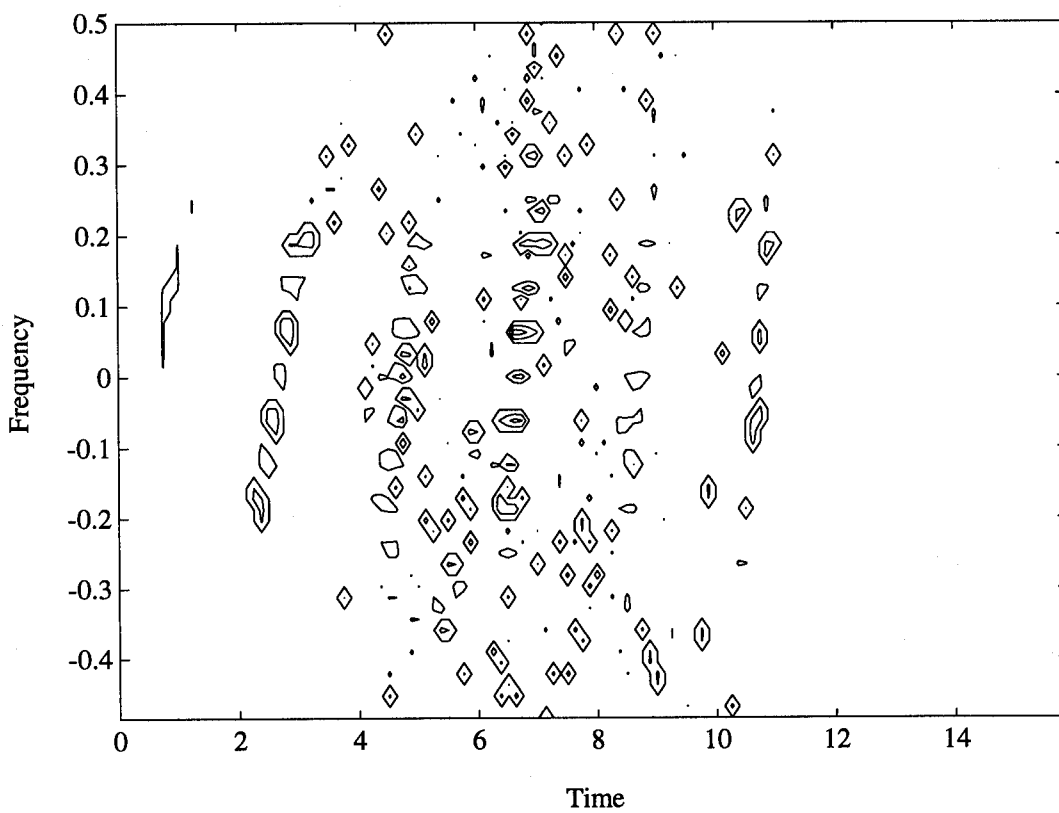
Figure 3.13: Discrete Wigner-Ville distribution of a train of four *lfm* Gaussian pulses embedded in 0dB noise

the modulating factor was shown only for an *lfm* signal of constant amplitude by deriving the ambiguity function of this signal. In the following, we demonstrate that this result can be extended to a broader class of signals.

Let $\tilde{s}_3(t)$ be a nonnegative low-pass signal which has finite energy. For example, $\tilde{s}_3(t)$ may be a monotone Gaussian pulse or a train of rectangular pulses. The continuous ambiguity function of $\tilde{s}_3(t)$ is given by

$$\theta_{\tilde{s}_3}(\tau, f_D) = \left| \int_{-\infty}^{\infty} \tilde{s}_3(t) \tilde{s}_3^*(t - \tau) \exp(-j2\pi f_D t) dt \right|^2 . \tag{3.51}$$

Using the Schwartz inequality, we have

$$\left| \int_{-\infty}^{\infty} \tilde{s}_3(t) \tilde{s}_3^*(t - \tau) \exp(-j2\pi f_D t) dt \right| \leq \int_{-\infty}^{\infty} \left| \tilde{s}_3(t) \tilde{s}_3^*(t - \tau) \right| dt. \tag{3.52}$$

Since $\tilde{s}_3(t)$ is real and nonnegative,

$$\begin{aligned} \int_{-\infty}^{\infty} \left| \tilde{s}_3(t) \tilde{s}_3^*(t - \tau) \right| dt &= \int_{-\infty}^{\infty} \tilde{s}_3(t) \tilde{s}_3(t - \tau) dt \\ &= \left| \int_{-\infty}^{\infty} \tilde{s}_3(t) \tilde{s}_3(t - \tau) dt \right| \\ &= \left\| \int_{-\infty}^{\infty} \tilde{s}_3(t) \tilde{s}_3(t - \tau) \exp(-j2\pi f_D t) dt \right\|_{f_D = 0} . \end{aligned} \tag{3.53}$$

Thus, we conclude that

$$\theta_{\tilde{s}_3}(\tau, f_D) \leq \theta_{\tilde{s}_3}(\tau, 0) \tag{3.54}$$

when $\tilde{s}_3(t)$ is a nonnegative low-pass signal which has finite energy. Relationship (3.54) indicates that the ambiguity function of a nonnegative low-pass signal of finite energy has the highest peak of the ambiguity function at $f_D = 0$ along any cut in Doppler.

Let $\tilde{s}_4(t) = \tilde{s}_3(t) \exp(j2\pi\alpha t^2)$. Then the time-frequency correlation function of $\tilde{s}_4(t)$ is given by

$$\phi_{\tilde{s}_4}(\tau, f_D) = \int_{-\infty}^{\infty} \tilde{s}_4(t) \tilde{s}_4^*(t - \tau) \exp(-j2\pi f_D t). \tag{3.55}$$

Using the relationship between $\tilde{s}_4(t)$ and $\tilde{s}_3(t)$, we have

$$\begin{aligned} \phi_{\tilde{s}_4}(\tau, f_D) &= \exp(-j2\pi\alpha\tau^2) \int_{-\infty}^{\infty} \tilde{s}_3(t) \tilde{s}_3^*(t - \tau) \exp\left[-j2\pi(f_D - 2\alpha\tau)t \right] \\ &= \exp(-j2\pi\alpha\tau^2) \phi_{\tilde{s}_3}(\tau, f_D - 2\alpha\tau) . \end{aligned} \tag{3.56}$$

It follows that

$$\theta_{\tilde{s}_4}(\tau, f_D) = \theta_{\tilde{s}_3}(\tau, f_D - 2\alpha\tau).$$ (3.57)

The above relationship indicates that the ridge in $\theta_{\tilde{s}_3}(\cdot)$ along $f_D = 0$ is shifted in frequency in $\theta_{\tilde{s}_4}(\cdot)$.

Recall that the sampling criteria under which the continuous and discrete ambiguity functions are equal were derived in Chapter 2. Therefore, similar relationships as (3.54) and (3.57) can be obtained for the discrete case when those criteria are satisfied. With the following example, we illustrate the relationship between the discrete time-frequency correlation function of a monotone signal $\tilde{s}_3(t)$ and that of its linear frequency modulated version $\tilde{s}_4(t)$. Let $\tilde{s}_3(t)$ be given by

$$\tilde{s}_3(t) = \frac{1}{2} \exp\left[\frac{-\pi(t-4)^2}{16}\right].$$ (3.58)

Assume that $\tilde{s}_3(t)$ and $\tilde{s}_4(t)$ are sampled from $t = 0$ to $t = 8$ with a sampling rate of $1/T_s = 2$. Figure 3.14 depicts $\hat{\theta}_{\tilde{s}_3}(\cdot)$. Assume $\alpha = 0.025$. Figure 3.15 depicts $\hat{\theta}_{\tilde{s}_4}(\cdot)$. The shift of the peak can be seen by comparing Figures 3.14 and 3.15.

From the foregoing discussion it is seen that the maximum of the ambiguity function of a linearly frequency modulated nonnegative signal provides information about the frequency modulation factor. Thus, the algorithm proposed in [33] can be applied not only to an *lfm* signal of constant amplitude but can also be applied to any linearly frequency modulated nonnegative signals.

In this subsection we discussed application of the ambiguity function to estimation of a signal's instantaneous frequency. It was shown that the estimation procedure proposed in [33] can be extended to a broad class of signals. With this estimation, the reference time-frequency correlation function of a time-frequency correlation function based receiver can be properly chosen for optimum detection and estimation of the delay and Doppler in the target return. However, due to the fact that the estimation procedure in [33] is simple but suboptimal, the result may be unsatisfactory such that iterations using different reference
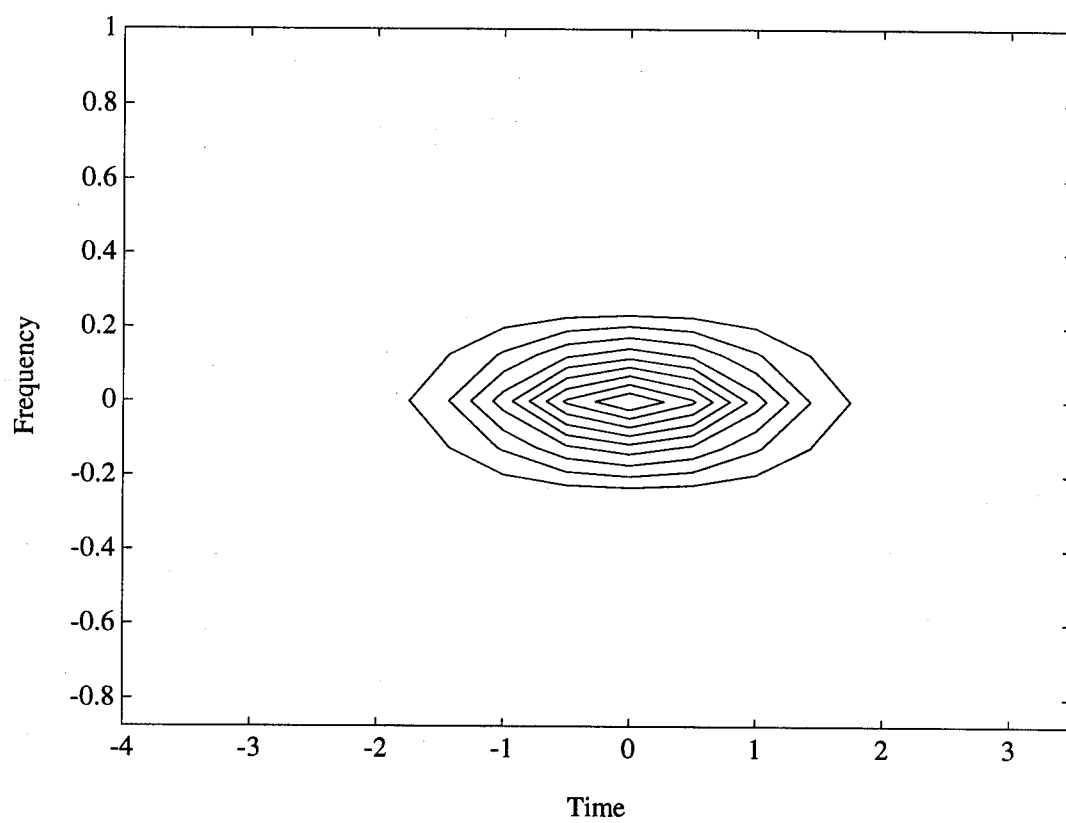
Figure 3.14: Discrete time-frequency correlation function of a monotone Gaussian pulse
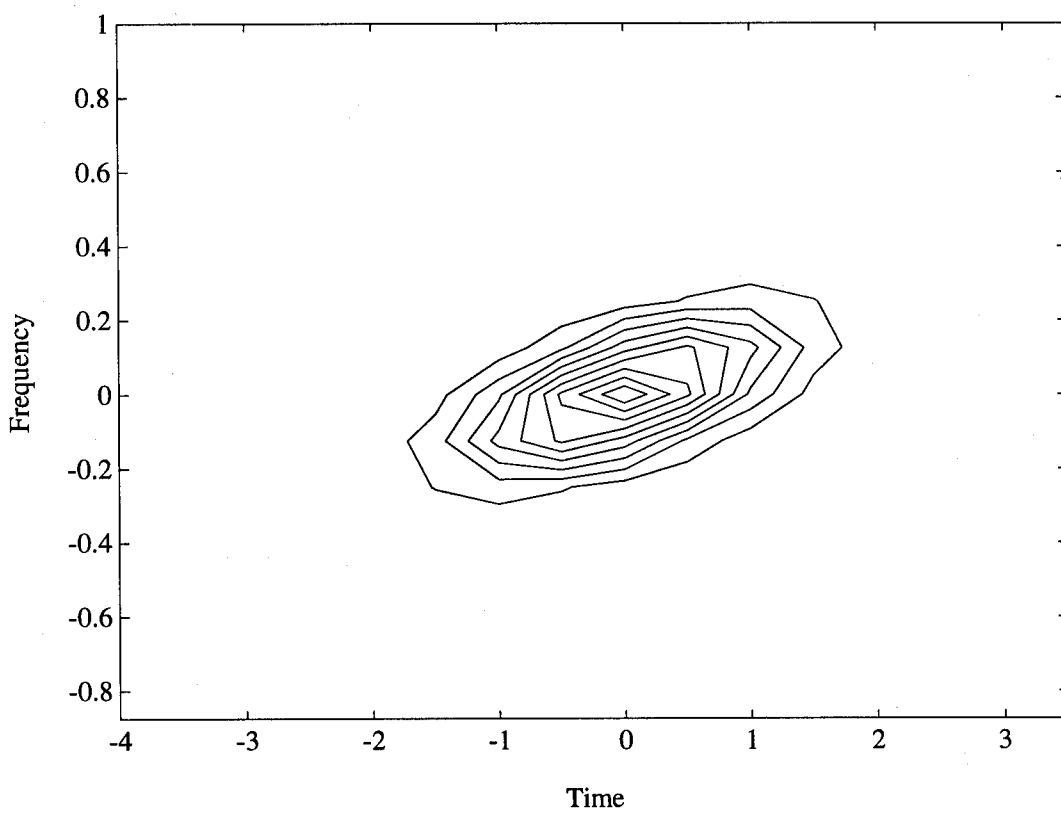
Figure 3.15: Discrete time-frequency correlation function of a *lfm* Gaussian pulse

time-frequency correlation functions are needed. Nonetheless, the maximum of the ambiguity function of the received signal may still prove to be a good indicator of the instantaneous frequency of the signal so that an exhaustive search is not needed.

3.4 Discussion

In this chapter we derived criteria for realizing the optimum discrete radar receiver based on both the discrete Wigner-Ville distribution and the discrete time-frequency correlation function. It was shown that correlating the discrete Wigner-Ville distributions of the received samples with the reference can be used to generate the test statistic for optimum detection and estimation in a Gaussian noise environment provided the aforementioned criteria are satisfied. Matched filtering the discrete time-frequency correlation functions of the received samples and the reference can also be used to generate the test statistic. Schemes to lower the requirement on the sampling rate and to reduce the requirement on the duration of the sampling process were also derived. Application of alternative forms of the radar receiver was illustrated with two examples. It was shown that a Wigner-Ville distribution based receiver is more versatile than the conventional one in dealing with problems where the transmitted signal is unknown. It was also shown that a time-frequency correlation function based receiver is useful in dealing with a maneuvering target or a linearly frequency modulated nonnegative signal.

Chapter 4

Quantization Effects in Time-Frequency Distribution Based Radar Receivers

As derived in Chapter 2, the optimum discrete receiver computes the statistic

$$\Lambda\left(nT_s, \frac{m}{NT_s}\right) = \left|\sum_{k=0}^{N-1} \tilde{r}(kT_s)\tilde{s}^*(kT_s - nT_s)\exp\left(-j2\pi\frac{mk}{N}\right)\right|^2. \tag{4.1}$$

It was shown that there are various equivalent structures to implement the receiver. Conventionally, the receiver is either a direct form realization of (4.1), or it can be a frequency-domain equivalent as shown in (2.37) of Chapter 2. In the previous discussion it was also shown that (4.1) can be realized by correlating the discrete Wigner-Ville distribution of the received signal and that of the reference, as given in (3.19), (3.22), (3.31), and (3.35) of Chapter 3. Another approach to realize (4.1) is by matched filtering the discrete time-frequency correlation function of the received signal and that of the reference as shown in (3.42) and (3.46) of Chapter 3. Advantages of each form were discussed in Chapter 3.

In practice, discrete receivers are implemented with digital devices of finite register length. Consequently, signal samples need to be quantized and computations are based on finite precision arithmetic. Effects of signal quantization and finite precision arithmetic can be viewed as additional noise introduced in the system. It is important to examine the effects

of this noise on the performance of the receivers developed thus far. This chapter is devoted to the study of quantization effects in these receivers, i.e., effects of rounding of the signal samples and performing finite precision arithmetic in these receivers. The analysis is based on a statistical approach with the measure of error being the ratio of the second moment of the quantization error in the receiver output to the second moment of the receiver output without quantization error. The use of statistical methods in problems where processes are unknown or too complex for a deterministic representation is a well established method [34]. In the literature the aforementioned ratio is simply called the noise-to-signal ratio, which will also be used in the following analysis. Analytical results on the output noise-to-signal ratio are first obtained and then verified by computer simulations.

In most radar applications, both the computational speed and hardware complexity are of great concern. Fast Fourier transform algorithm and fixed-point arithmetic are usually employed to fulfill these requirements. Therefore, we will assume that fast Fourier transform algorithm with fixed-point arithmetic is used in realizing the receiver whenever it is required to perform discrete Fourier transform. In the first section of this chapter we will review the results given in the literature on the quantization effects in fast Fourier transform computation. Specifically, we will consider a radix-2 decimation-in-time fast Fourier transform algorithm which uses fixed-point rounding arithmetic. Attention will be paid to the effects of coefficient quantization. In the previous work, the distinction between the two cases when the coefficients are generated as a part of the fast Fourier transform computation, i.e., in-place computation, or are obtained from a look-up table was recognized [34] but not analyzed accordingly. The quantization effects of both methods of generating the coefficients will be examined. The treatment given in Section 4.1 will follow closely the one given in [34]. Then, in Section 4.2 we consider the quantization effects in the receivers of the forms (4.1), (3.22) and (3.42). Similar procedures can be applied to the analysis of other receivers.

4.1 Quantization Effects in Fast Fourier Transform Computation

In this section, we consider quantization effects resulting from finite precision arithmetic. Specifically, we determine the mean-square value of quantization errors that are produced when summation and multiplication are carried out. Also, we examine the manner in which these errors propagate in successive summations and/or multiplications. Then, we analyze quantization effects while computing fast Fourier transform with a radix-2 decimation-in-time algorithm.

4.1.1 Effects of Finite-Precision Arithmetic

In this work, the number system is assumed to be a $(b+1)$-bit sign-magnitude fixed-point binary number system, with 1 sign bit and b fractional bits to represent the fraction part. With this number system, it is necessary that the input be appropriately scaled before it can be represented. This is usually achieved by using the full-scale amplitude of the analog-to-digital converter as the normalizing factor. There are occasions when an input falls outside of the range of the converter even when attenuation of the input is used. This results in truncation. For example, digitization of a sequence of Gaussian distributed random numbers may require truncations of some of the numbers. However, the number of times truncation is needed is negligible when the variance of the random numbers is much smaller than the range of the A/D converter. In the following analysis, we will assume that the variance of the noise in the received signal is much smaller than the full-scale amplitude of the A/D converter so that the error due to truncation at the input of the converter is negligible.

Since the smallest increment that can be represented in the number system under consideration here is 2^{-b}, the input must be quantized when more than $(b+1)$ bits are needed

for an exact representation. Assume that this is accomplished by rounding the number to the nearest representable number, and rounding up when the number is at the midpoint between two quantization levels. Then, the output of the quantizer for an input sequence of real numbers $\{s(k)\}, k = 1, \cdots, N$ can be written in the form

$$Q\{s(k)\} = s(k) + e(k) \tag{4.2}$$

where $Q\{\cdot\}$ denotes the quantization operation, and $e(k)$ denotes the quantization error,

$$-\frac{2^{-b}}{2} < e(k) \leq \frac{2^{-b}}{2}. \tag{4.3}$$

It is commonly assumed [34] that

1. The error sequence $\{e(k)\}$ is a sample sequence of a stationary random process.

2. The error sequence is uncorrelated with the input signal sequence $\{s(k)\}$.

3. The elements of the error sequence are uncorrelated, i.e., the error is a white-noise process.

4. The elements of the error sequence are uniformly distributed over the range of quantization error, i.e., they are uniformly distributed over -2^{-b-1} to 2^{-b-1}.

The validity of these assumptions has been examined extensively in the literature, for example in [35]-[37] and the references listed therein. It was shown that for most waveforms of practical interest and large register lengths the above assumptions give a reasonable model of the quantization error. Considering the availability of 12 and 16 bit analog-to-digital converters of reasonable sampling rates for radar application, the above assumptions are suitable for analyses for radar systems [38]. With these assumptions the first and second moments of the quantization noise are

$$E\{e(k)\} = 0, \tag{4.4}$$

and

$$E\{e(k)e(l)\} = \begin{cases} \frac{2^{-2b}}{12} & k = l \\ 0 & k \neq l. \end{cases} \tag{4.5}$$

The foregoing discussion characterizes the errors in representing analog inputs using the prescribed numerical system. Next, we consider the effects of quantization on the results of two basic types of arithmetic operations, i.e., addition and multiplication.

Since it was assumed that there are b bits to represent the magnitude of a number, the magnitude of the result of an addition can not exceed $1 - 2^{-b}$. Otherwise, an error is introduced. However, with proper scaling of the numbers to be added, this type of error can be avoided. For example, the two numbers can be divided by two before addition. On the other hand, multiplication does introduce roundoff errors. Since we are interested in operations involving complex numbers in later analysis, we consider the quantization error while forming the product of two complex numbers $\tilde{s}_1$ and $\tilde{s}_2$. Denote the real and imaginary parts of the two numbers by s_{i_R} and $s_{i_I}, i = 1, 2$, respectively. In the multiplication of two complex numbers four real multiplications are involved. Therefore, there are four roundoff errors corresponding to rounding of each of the four real products. The rounded product of $\tilde{s}_1 \tilde{s}_2$ can be written as

$$\begin{aligned} Q\{s_{1R}s_{2R}\} - Q\{s_{1I}s_{2I}\} &+ jQ\{s_{1R}s_{2I}\} + jQ\{s_{1I}s_{2R}\} \\ &= (s_{1R}s_{2R} + e_1) - (s_{1I}s_{2I} + e_2) + j(s_{1R}s_{2I} + e_3) + j(s_{1I}s_{2R} + e_4) \\ &= \tilde{s}_1\tilde{s}_2 + e_1 - e_2 + je_3 + je_4 \end{aligned} \tag{4.6}$$

where $e_i, i = 1, \cdots, 4$, denote errors due to the roundoff of the four real products. Assume that $e_i, i = 1, \cdots, 4$, have the following properties:

1. The errors $e_i, i = 1, \cdots, 4$, are uniformly distributed random variables over the range -2^{-b-1} to 2^{-b-1}. Therefore, each error e_i has mean zero and variance $2^{-2b}/12$.

2. The errors are mutually uncorrelated.

123

3. All the errors are uncorrelated with the input and consequently the output.

Denote the error resulting from rounding the complex product $\tilde{s}_1\tilde{s}_2$ by $\tilde{e}_P$, which is a complex number. Since it was assumed that e_is are uncorrelated and have zero means, it is easy to see that the mean square magnitude of e_P is

$$\mathrm{E}\left\{|\tilde{e}_P|^2\right\} = 4 \cdot \frac{2^{-2b}}{12} = \frac{2^{-2b}}{3}. \tag{4.7}$$

The above result indicates that an error of variance of $2^{-2b}/3$ is introduced after every fixed-point multiplication of two complex numbers. In some problems of interest this large error variance can be avoided by carrying out the computation in a different manner. For example, consider the calculation of the product of a complex number and its complex conjugate to obtain the squared magnitude. The squared magnitude of a complex number can also be obtained by summing the squares of its real and imaginary parts. Calculation in this manner reduces the error variance to one-half of the value given in (4.7). This can be seen by letting $\tilde{s}_2 = \tilde{s}_1^*$ and dropping the imaginary parts in (4.6). In what follows we examine the manner in which the quantization errors accumulate in summation and multiplication.

Recall that it was assumed that the quantization errors are mutually uncorrelated, and they are uncorrelated with the inputs. It follows that the error component in the result of an addition has a variance that equals the sum of the variances of the error components of the two numbers being added. This is not the case in multiplication. Denote the two rounded complex numbers to be multiplied by $\tilde{s}_{i_Q}, i = 1, 2$, and the accumulated errors in the real and imaginary parts of these two inputs, which were introduced prior to the multiplication, by e_{i_R} and $e_{i_I}, i = 1, 2$, respectively. That is, if $\tilde{s}_1$ and $\tilde{s}_2$ denote the exact results of infinite-precision operations, we have

$$\tilde{s}_{i_Q} = \tilde{s}_i + \left(e_{i_R} + je_{i_I}\right), \ i = 1, 2. \tag{4.8}$$

The product of the rounded numbers can be written as

$$\tilde{s}_{1_Q}\tilde{s}_{2_Q} = \left(s_{1_R} + e_{1_R}\right)\left(s_{2_R} + e_{2_R}\right) + j\left(s_{1_R} + e_{1R}\right)\left(s_{2_I} + e_{2_I}\right)$$

124

$$+j\left(s_{1_I}+e_{1_I}\right)\left(s_{2_R}+e_{2_R}\right)-\left(s_{1_I}+e_{1_I}\right)\left(s_{2_I}+e_{2_I}\right)$$

$$= s_{1_R}s_{2_R}-s_{1_I}s_{2_I}+js_{1_R}s_{2_I}+js_{1_I}s_{2_R}+e_{1_R}s_{2_R}+e_{2_R}s_{1_R}$$

$$-e_{1_I}s_{2_I}-e_{2_I}s_{1_I}+je_{1_R}s_{2_I}+je_{2_I}s_{1_R}+je_{1_I}s_{2_R}+je_{2_R}s_{1_I}$$

$$+e_{1_R}e_{2_R}-e_{1_I}e_{2_I}+je_{1_R}e_{2_I}+je_{1_I}e_{2_R}. \tag{4.9}$$

Then, the mean-square magnitude of the error is given by

$$\sigma_M^2 = \mathrm{E}\,|[e_{1_R}s_{2_R}+e_{2_R}s_{1_R}-e_{1_I}s_{2_I}-e_{2_I}s_{1_I}+e_{1_R}e_{2_R}-e_{1_I}e_{2_I}]$$

$$+j\,[e_{1_R}s_{2_I}+e_{2_I}s_{1_R}+e_{1_I}s_{2_R}+e_{2_R}s_{1_I}+e_{1_R}e_{2_I}+e_{1_I}e_{2_R}]|^2$$

$$= \mathrm{E}\Big\{[e_{1_R}s_{2_R}+e_{2_R}s_{1_R}-e_{1_I}s_{2_I}-e_{2_I}s_{1_I}+e_{1_R}e_{2_R}-e_{1_I}e_{2_I}]^2$$

$$+[e_{1_R}s_{2_I}+e_{2_I}s_{1_R}+e_{1_I}s_{2_R}+e_{2_R}s_{1_I}+e_{1_R}e_{2_I}+e_{1_I}e_{2_R}]^2\Big\}. \tag{4.10}$$

As before, assume that the errors are uncorrelated with each other, they are uncorrelated with the input or output, and they all have zero means. It follows that

$$\sigma_M^2 = \mathrm{E}\Big\{[e_{1_R}s_{2_R}]^2+[e_{2_R}s_{1_R}]^2+[e_{1_I}s_{2_I}]^2+[e_{2_I}s_{1_I}]^2+[e_{1_R}s_{2_I}]^2+[e_{2_I}s_{1_R}]^2$$

$$+[e_{1_I}s_{2_R}]^2+[e_{2_R}s_{1_I}]^2+[e_{1_R}e_{2_R}]^2+[e_{1_I}e_{2_I}]^2+[e_{1_R}e_{2_I}]^2+[e_{1_I}e_{2_R}]^2\Big\}. \tag{4.11}$$

Assume that e_{1_R} and e_{1_I} have equal variances denoted by $\sigma_{e_1}^2/2$,. Similarly, let $\sigma_{e_2}^2/2$ denote the variance of e_{2_R} and e_{2_I}. In many applications, the complex numbers $\tilde{s}_i, i=1,2$, are modeled as random variables with their real and imaginary parts assumed to be mutually uncorrelated and all with zero means. Assume that s_{1_R} and s_{1_I} have equal variances that are denoted by $\sigma_{s_1}^2/2$. Similarly, let $\sigma_{s_2}^2/2$ denote the variances of s_{2_R} and s_{2_I}. In this case, Equation (4.11) reduces to

$$\sigma_M^2 = \sigma_{s_1}^2\sigma_{e_2}^2+\sigma_{s_2}^2\sigma_{e_1}^2+\sigma_{e_1}^2\sigma_{e_2}^2$$

$$\cong \sigma_{s_1}^2\sigma_{e_2}^2+\sigma_{s_2}^2\sigma_{e_1}^2 \tag{4.12}$$

where it is assumed that $\sigma_{s_i}^2 \gg \sigma_{e_i}^2$. By letting $\tilde{s}_{2_Q}=\tilde{s}_{1_Q}^*$ in (4.9), we can analyze the manner in which error accumulates in the calculation of the squared magnitude of a complex

125

number. When $\tilde{s}_{2Q} = \tilde{s}_{1Q}^*$ is substituted in (4.9), it is seen that the imaginary part does not contribute towards error. The derivation of the error variance is similar to the derivations (4.10) to (4.12). The result shows that the output error has a variance equal to $\sigma_{s_1}^2 \sigma_{e_1}^2$.

There are occasions in which one of the two numbers being multiplied is modeled as deterministic and the other one is modeled as random. This situation usually arises in the analyses of quantization effects in a digital system. In this case, the coefficients are modeled as deterministic, but the errors resulting from coefficient quantization are substituted with random variables. Let us consider multiplication of $\tilde{s}_1$ and $\tilde{s}_2$ where $\tilde{s}_1$ is deterministic and $\tilde{s}_2$ is random. From (4.11) we have,

$$
\begin{aligned}
\sigma_M^2 &= |\tilde{s}_1|^2 \sigma_{e_2}^2 + \sigma_{s_2}^2 \sigma_{e_1}^2 + \sigma_{e_1}^2 \sigma_{e_2}^2 \\
&\cong |\tilde{s}_1|^2 \sigma_{e_2}^2 + \sigma_{s_2}^2 \sigma_{e_1}^2
\end{aligned}
\tag{4.13}
$$

where again we have assumed that $\sigma_{s_2}^2$ and $|\tilde{s}_1|^2$ are much greater than $\sigma_{e_i}^2$.

Finally, we consider the problem of dividing a number by 2. In this case error occurs when the least significant bit of the number is discarded. When the number is positive and its least significant bit b_l is one, the error introduced is $-2^{-b}/2$. When the number is negative and b_l is one, the error introduced is $2^{-b}/2$. No error is introduced when the least significant bit of the number is zero. Assume that b_l is equally likely to be zero or one. The mean-square error σ_D^2 in this case is given by

$$
\begin{aligned}
\sigma_D^2 &= \text{Prob(the number is positive, } b_l \text{ is one)} \left(-\frac{2^{-b}}{2} \right)^2 \\
&\quad + \text{Prob(the number is negative, } b_l \text{ is one)} \left(\frac{2^{-b}}{2} \right)^2 \\
&= \text{Prob(the number is positive)} \cdot \frac{1}{2} \cdot \left(-\frac{2^{-b}}{2} \right)^2 \\
&\quad + \text{Prob(the number is negative)} \cdot \frac{1}{2} \cdot \left(\frac{2^{-b}}{2} \right)^2 \\
&= \frac{2^{-2b}}{8}.
\end{aligned}
\tag{4.14}
$$

126

This result can readily be applied to the scaling of a rounded complex number by 1/2, which involves scaling both the real and imaginary parts of the number by 1/2. Assuming the errors from scaling the real and imaginary parts to be uncorrelated, the resulting error in the scaled complex number has a variance of $2^{-2b}/4$.

## 4.1.2 Quantization Effects in Fast Fourier Transform Computation

In this subsection, we apply the results developed in the last subsection to determine the effects of quantization on fast Fourier transform computation. This topic has been treated thoroughly in the literature, for example in [34]. However, the distinction between whether the coefficients are generated from in-place computation or are obtained from a look-up table was only acknowledged [34] but not analyzed in detail. This issue will be clarified in the following.

Consider a sequence of N input signal samples, where N is an integer power of 2. All standard radix-2 decimation-in-time fast Fourier transform algorithms have the following common features. The Fourier transform is computed in $\nu = \log_2 N$ stages. At each stage a new array of N numbers is obtained from the previous array by linearly combining its elements taken two at a time. The resulting array at the νth stage contains the desired discrete Fourier transform. Figure 4.1 depicts the flow graph of an 8-point radix-2 decimation-in-time fast Fourier transform algorithm. Denote the complex numbers resulting from the mth stage of computation as $\hat{S}_m(k)$, where $k = 0, \cdots, N-1$ and $m = 1, \cdots, \nu$. Further, let $\hat{S}_0(k)$ be the input, i.e., $\hat{S}_0(k) = \tilde{s}(kT_s)$. Thus, $\hat{S}_{m-1}(k)$ can be viewed as the input array and $\hat{S}_m(k)$ as the output array for the mth stage of computation. The basic numerical computation performed repeatedly, which is often called a butterfly, can be written as

$$\hat{S}_m(p) = \hat{S}_{m-1}(p) + \Omega_N^r \hat{S}_{m-1}(q)$$
$$\hat{S}_m(q) = \hat{S}_{m-1}(p) - \Omega_N^r \hat{S}_{m-1}(q)$$

$$(4.15)$$
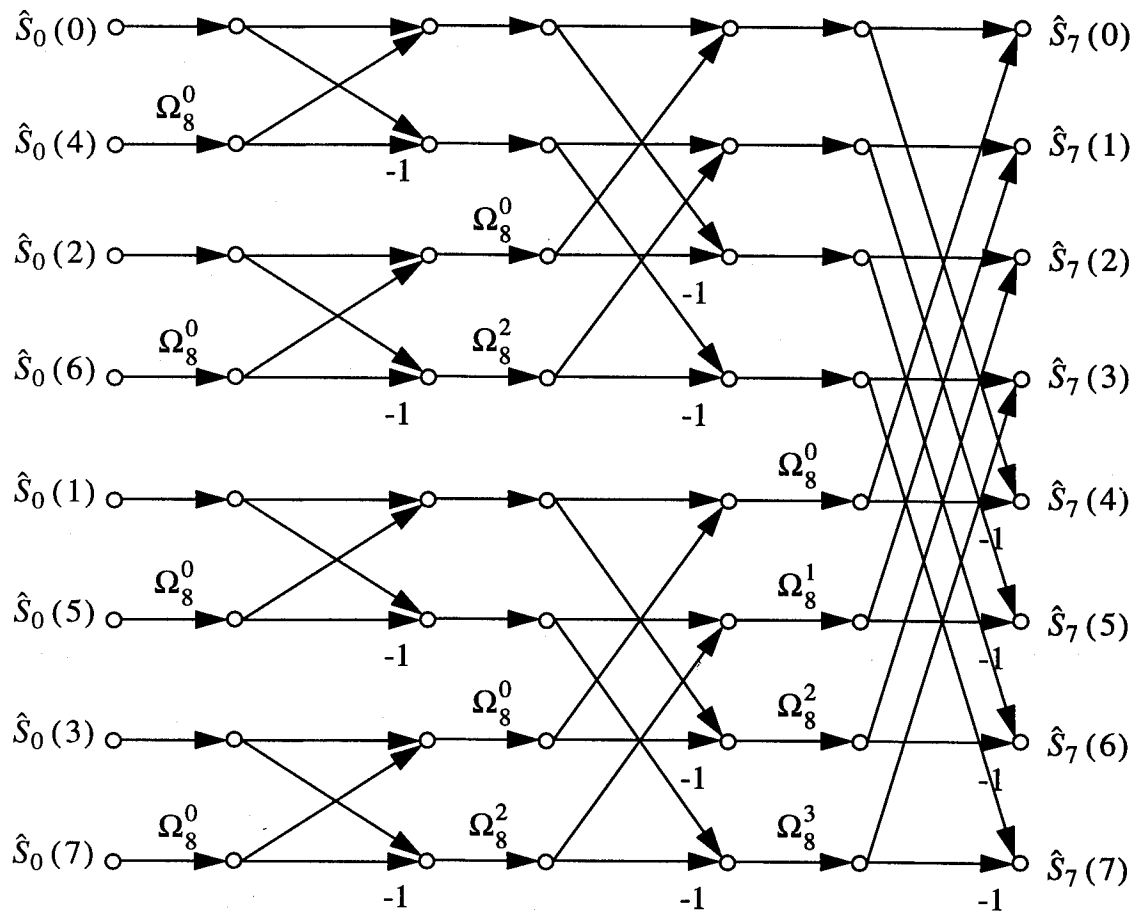
(a) An 8-point radix-2 decimation-in-time fast Fourier transform
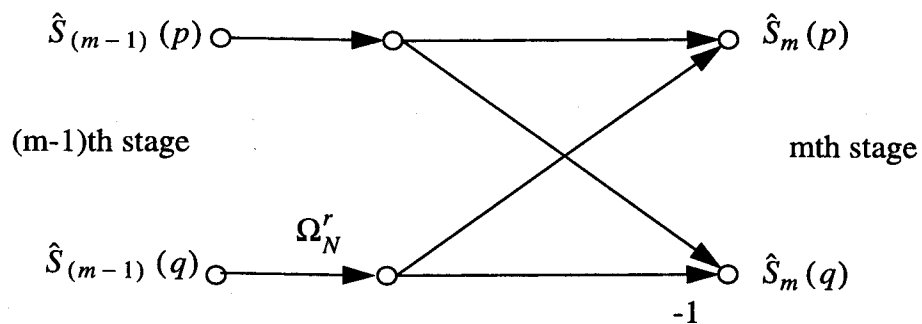
(b) A butterfly computation

Figure 4.1: Flow graph of a radix-2 decimation-in-time fast Fourier transform algorithm

128

where r is an integer and $\Omega_N^r = \exp(-j2\pi r/N)$ is the exponential coefficient. The butterfly computation is also illustrated in Figure 4.1. At each stage, $N/2$ separate butterfly computations are carried out to produce the next array. In the following, we assume that the signal samples to be processed are white, in the sense that all $2N$ real components associated with the N complex samples are mutually uncorrelated random variables. Furthermore, they are assumed to have zero means and equal variances. It should be pointed out that the assumptions about the input are made to facilitate the analysis, but as will be shown in later computer simulations that the results obtained hold for a broad class of signals [34].

Since we require that the result of any addition can not exceed $1 - 2^{-b}$, we insert a scaling factor of $1/2$ at the input of each stage to prevent overflow in the butterfly calculation of (4.15). Thus, the butterfly computation in (4.15) is modified as

$$\hat{S}_m(p) = \hat{S}_{m-1}(p)/2 + \Omega_N^r \hat{S}_{m-1}(q)/2$$
$$\hat{S}_m(q) = \hat{S}_{m-1}(p)/2 - \Omega_N^r \hat{S}_{m-1}(q)/2$$

$$(4.16)$$

From (4.16), it is seen that

$$\left| \hat{S}_m(p) \right| \leq \frac{1}{2} \left\{ \left| \hat{S}_{m-1}(p) \right| + \left| \hat{S}_{m-1}(q) \right| \right\}. \tag{4.17}$$

By letting $m = 1$ the above relationship gives the requirement on the magnitude of the input samples to prevent overflow. For simplicity, we require that both the real and imaginary parts of the initial input be restricted to the interval $-1/\sqrt{2}$ and $1/\sqrt{2}$. Clearly, this is a sufficient but not necessary condition to ensure $|\hat{S}_0(k)|$, and consequently $|\hat{S}_m(k)|, m = 1, \cdots, \nu$, to be less than or equal to one. Assume that the real and imaginary parts of the initial inputs are uniformly distributed over $[-1/\sqrt{2}, 1/\sqrt{2}]$. Then the mean-square magnitude of the input is $1/3$. As mentioned before, the assumptions about the input are made to facilitate the analysis, but they are not restrictive and the results obtained hold for a broad class of signals.

With the assumptions about the input samples, the mean-square magnitude of the sam-

ples at the mth stage can be obtained with the following observation:

$$
\begin{aligned}
E\left[\left|\hat{S}_m(p)\right|^2\right] &= E\left[\left|\frac{\hat{S}_{m-1}(p)}{2} + \frac{\hat{S}_{m-1}(q)}{2}\Omega_N^r\right|^2\right] \\
&= \frac{1}{4}\left\{E\left[\left|\hat{S}_{m-1}(p)\right|^2\right] + |\Omega_N^r|^2 E\left[\left|\hat{S}_{m-1}(p)\right|^2\right]\right\} \\
&= \frac{1}{2}E\left[\left|\hat{S}_{m-1}(p)\right|^2\right].
\end{aligned}
\tag{4.18}
$$

It follows that

$$
E\left[\left|\hat{S}_m(p)\right|^2\right] = \frac{1}{2^m}E\left[\left|\hat{S}_0(p)\right|^2\right] = \frac{1}{3\cdot 2^m}.
\tag{4.19}
$$

The average squared magnitude of the output can be obtained from (4.19) by setting $m = \nu$ so that

$$
E\left[\left|\hat{S}_\nu(k)\right|^2\right] = \frac{1}{3\cdot 2^\nu} = \frac{1}{3N}.
\tag{4.20}
$$

Next, we determine the variance of the quantization error in the fast Fourier transform calculation. Note that if the coefficients Ω_N^r can be expressed exactly, the only two sources of roundoff errors in the butterfly computations are the scaling of the numbers by $1/2$ and the quantization of the products of $\hat{S}_m(q)$ and Ω_N^r. In the following, we will first assume that the coefficients can be represented exactly, and then consider the case when they are quantized.

As derived earlier, the scaling of a rounded complex number by $1/2$ introduces an error whose variance is $2^{-2b}/4$. It was also shown that the error due to quantization of the product of two complex numbers has a variance of $2^{-2b}/3$. Recall that the errors from performing finite precision arithmetic were assumed to be uncorrelated with the input. Thus, the calculation of $\hat{S}_m(p)/2$ results in an error of variance $2^{-2b}/4$ and the calculation of $\Omega_N^r \hat{S}_m(q)/2$ results in an error of variance $2^{-2b}(1/4 + 1/3) = 7\cdot 2^{-2b}/12$. It follows that there is an error of variance $2^{-2b}(1/4 + 7/12) = 5\cdot 2^{-2b}/6$ introduced after each butterfly calculation. To find out the error in the output of a fast Fourier transform calculation, we need to consider how many butterfly calculations are involved in producing the final result. It is noted that for the general case with $N = 2^\nu$, each output node of the transform connects to

$2^{(\nu-m-1)}$ butterflies that originate at the mth stage. An inspection of Figure 4.1 verifies this observation. Then, at the kth output node, $k = 0, \ldots, (N-1)$, the mean-square magnitude of the noise is

$$
\begin{aligned}
\mathrm{E}[|e(k)|^2] &= \sum_{m=0}^{\nu-1} 2^{(\nu-m-1)} \frac{5 \cdot 2^{-2b}}{6} \left(\frac{1}{2}\right)^{2(\nu-m-1)} \\
&= \frac{5 \cdot 2^{-2b}}{3N} \sum_{m=0}^{\nu-1} \left(\frac{1}{2}\right)^{-m} \\
&= \frac{5 \cdot 2^{-2b}}{3} \left(1 - \frac{1}{N}\right).
\end{aligned}
\tag{4.21}
$$

For large N, we have

$$
\mathrm{E}[|e(k)|^2] \cong \frac{5 \cdot 2^{-2b}}{3}.
\tag{4.22}
$$

This result is the same as given in [39]. In the remainder of this work we will assume the case of large N. Thus, from (4.20) and (4.22), the output noise-to-signal ratio for the case of white input and when scaling is carried out at each step is given by

$$
\frac{\mathrm{E}[|e(k)|^2]}{\mathrm{E}\left[|\hat{S}_\nu(k)|^2\right]} = 5N \cdot 2^{-2b}.
\tag{4.23}
$$

From the above result it is seen that the output noise-to-signal ratio degrades as N increases. Also, the relationship between output noise-to-signal ratio with input sample power can be deduced as follows. Since discrete Fourier transform is a linear operation, scaling of the input samples results in a scaling of the output by the same amount. It follows that reducing the input sample power reduces the output power. On the other hand, since the output quantization noise does not depend on the input signal level, changing the input sample power does not affect the output quantization noise power. Therefore, lowering of the input level degrades the output noise-to-signal ratio. In other words, it is imperative that we maintain the level of the input signal samples as high as possible to ensure that the output noise-to-signal ratio is acceptable.

Next, we consider the situation when the coefficients used in the fast Fourier transform computation are quantized. One of the approaches that has been found to be useful in the

literature in determining the effects of coefficient quantization is to introduce random jitter [39] in the coefficients and determine the output noise-to-signal ratio due to this noise. Denote the exact coefficients by Ω_N^r, and the quantized ones by $\hat{\Omega}_N^r, r = 0, \cdots, \nu - 1$, respectively. That is,

$$\hat{\Omega}_N^r = Q\left\{\Omega_N^r\right\} = \Omega_N^r + \epsilon_r \tag{4.24}$$

where ϵ_r is a complex number whose real and imaginary parts are the quantization errors of the real and imaginary parts of Ω_N^r, respectively. Using the random jitter method, we do not express ϵ_r exactly to analyze the effect of coefficient quantization. Instead, we substitute them with complex random variables whose real and imaginary parts are uncorrelated. Although this method does not predict with great accuracy the error variance in a fast Fourier transform algorithm due to coefficient quantization, it is helpful in providing a rough estimate of the error variance [39]. It should be pointed out that the effect of coefficient quantization also depends on how the coefficients are obtained. All the required values can be stored in a table, or they can be computed as needed. The first alternative has the advantage of speed but requires extra storage. On the other hand, calculation of the coefficients as needed saves storage but is less time efficient than a look-up table. Furthermore, if the coefficients are obtained through calculation, the errors accumulate. In the previous work the distinction between whether the coefficients are obtained from in-place computation or from storage was recognized [34] but not analyzed in detail. In the analysis given in [39] the variances of the coefficient quantization errors were treated as constants. Therefore, the results can only be used to predict the coefficient quantization effect for the case when coefficients are obtained from a look-up table. In the following analysis we distinguish between these two cases and treat them separately.

Coefficients from a look-up table

When the coefficients are obtained from a look-up table, the effect of finite-precision representation can be analyzed in the following manner [39]. Using the random jitter method, we assume that in the required coefficient there is a jittering noise whose real and imaginary parts are uncorrelated and are uniformly distributed over -2^{-b-1} to 2^{-b-1} such that its magnitude has a variance of $2^{-2b}/6$. The output of a butterfly computation at the $(m+1)$th stage with jittered coefficient can be written as

$$
\begin{aligned}
\hat{S}_{m+1}(p) &= \frac{\hat{S}_m(p)}{2} + \hat{\Omega}_N^r \frac{\hat{S}_m(q)}{2} \\
&= \frac{\hat{S}_m(p)}{2} + (\Omega_N^r + \epsilon_r) \frac{\hat{S}_m(q)}{2} \\
&= \frac{\hat{S}_m(p)}{2} + \Omega_N^r \frac{\hat{S}_m(q)}{2} + \epsilon_r \frac{\hat{S}_m(q)}{2}.
\end{aligned}
\tag{4.25}
$$

Assuming that ϵ_r is independent of $\hat{S}_m(k)$, $k = 0, \ldots, N-1$, the mean-square magnitude of the error contained in the output of a butterfly at the $(m+1)$th stage due to coefficient quantization is given by

$$
\begin{aligned}
\sigma_{c_{m+1}}^2 &= \frac{1}{4} \mathrm{E}\left[\left|\hat{S}_m(q)\right|^2\right] \mathrm{E}[|\epsilon_r|^2] \\
&= \frac{1}{4} \frac{2^{-2b}}{6} \mathrm{E}\left[\left|\hat{S}_m(q)\right|^2\right] \\
&= \frac{1}{4} \frac{2^{-2b}}{6} \frac{1}{3 \cdot 2^m}
\end{aligned}
\tag{4.26}
$$

where (4.19) has been used. In a manner similar to the one used in deriving (4.21), the mean-square magnitude of the noise at the kth output node can be obtained by

$$
\begin{aligned}
\sigma_c^2(k) &= \sum_{m=0}^{\nu-1} 2^{(\nu-m-1)} \cdot \sigma_{c_{m+1}}^2 \cdot \left(\frac{1}{2}\right)^{2(\nu-m-1)} \\
&= \frac{2^{-2b}}{72} \sum_{m=0}^{\nu-1} \frac{1}{2^{(\nu-1)}} \\
&= \frac{\nu \cdot 2^{-2b}}{36N}.
\end{aligned}
\tag{4.27}
$$

It follows that the output noise-to-signal ratio is

$$
\frac{\sigma_c^2(k)}{\mathrm{E}\left[\left|\hat{S}_\nu(k)\right|^2\right]} = \frac{\nu \cdot 2^{-2b}}{12}.
\tag{4.28}
$$

133

Although we would not expect (4.28) to predict the error performance with great accuracy, it still provides us a good estimate. The key result of (4.28) is that the noise-to-signal ratio increases very mildly with N, being proportional to $\nu = \log_2 N$.

Coefficients from in-place calculation

The analysis of the effect of coefficient quantization is more involved when the coefficients are obtained from in-place computation. When the coefficients are to be computed at each butterfly, it is generally most efficient to use a recursion formula, such that the required coefficients are all powers of a complex number of the form $\Omega_N^{r_m}, m = 1, \cdots, \nu$, where r_m depends on the algorithm and the stage. In the following, we consider the algorithm given in [34], which closely follows the form originally given by Cooley et al. In this algorithm, there are 2^m coefficients generated at the mth stage. At each stage, there are $N/2$ butterflies. If $2^m < N/2$, the coefficients are used $(N/2)/2^m$ times at that stage. The lth coefficient at the mth stage is given by

$$\Omega_N^{r_m(l-1)} = \prod_{i=1}^{l-1} \Omega_N^{r_m}. \tag{4.29}$$

The first iteration of (4.29) yields unity. In fact, the coefficients used in the butterflies of the first two stages are $1, -1, j$, and $-j$. Since the multiplication of unity can be performed without error, the butterflies whose coefficients are unity do not contribute towards output noise. The second and later iterations of (4.29) involve the multiplication of the quantity $\Omega_N^{r_m}$ and result in quantization error. In the second iteration of (4.29), we have

$$Q\left[\hat{\Omega}_N^{r_m(l-1)}\Big|_{l=2}\right] = Q\left[\hat{\Omega}_N^{r_m}\right] = \Omega_N^{r_m} + \epsilon_{r_m} \tag{4.30}$$

where ϵ_{r_m} denotes the corresponding quantization error. As before, we substitute ϵ_{r_m} with a jitter noise whose real and imaginary parts are uniformly distributed over the range -2^{-b-1} to 2^{-b-1}. Thus, the mean-square magnitude of the error in the second iteration of (4.29) is

$2^{-2b}/6$. The rest of the iteration of (4.29) can be described by

$$\hat{\Omega}_N^{rm(l-1)} = Q\left[\cdots Q\left[\hat{\Omega}_N^{rm}\left[Q\left(\hat{\Omega}_N^{rm}\cdot\hat{\Omega}_N^{rm}\right)\right]\right]\cdots\right], \qquad (4.31)$$

where $l \geq 3$. The coefficient in the third iteration of (4.29) at the mth stage, $m \geq 3$, is obtained by multiplying $\hat{\Omega}_N^{rm}$ to itself and then quantizing the result. That is,

$$\begin{aligned}
\hat{\Omega}_N^{rm(l-1)}\Big|_{l=3} &= Q\left[\hat{\Omega}_N^{rm}\hat{\Omega}_N^{rm}\right]\\
&= \hat{\Omega}_N^{rm}\hat{\Omega}_N^{rm} + e_P(1)\\
&= \Omega_N^{2rm} + 2\Omega_N^{rm}\epsilon_{r_m} + \epsilon_{r_m}^2 + e_P(1) \qquad (4.32)
\end{aligned}$$

where $e_P(1)$ is the quantization error in representing the complex product $\hat{\Omega}_N^{rm}\hat{\Omega}_N^{rm}$. Again, assume that $e_P(1)$ is zero mean, is uncorrelated with the input, is uncorrelated with ϵ_{r_m} and has a variance $2^{-2b}/3$. Denote the resulting error by $e_c(3)$ and its mean-square magnitude by σ_3^2. It follows that

$$e_c(3) = 2\Omega_N^{rm}\epsilon_{r_m} + \epsilon_{r_m}^2 + e_P(1) \qquad (4.33)$$

and

$$\begin{aligned}
\sigma_3^2 &= E\left[\left|2\Omega_N^{rm}\epsilon_{r_m} + \epsilon_{r_m}^2 + e_P(1)\right|^2\right]\\
&= 4E[|\epsilon_{r_m}|^2] + E[|e_P(1)|^2] + E[|\epsilon_{r_m}^2|^2]\\
&\cong 2^{-2b} \qquad (4.34)
\end{aligned}$$

where the assumption that ϵ_{r_m} and $e_P(1)$ are uncorrelated was used. Also, the fourth moment of ϵ_{r_m} was assumed to be negligible.

It is straightforward to generalize the above result. The error due to coefficient quantization in the lth iteration, $l \geq 4$, can be expressed as

$$e_c(l) = e_c(l-1)\left(\Omega_N^{rm} + \epsilon_{r_m}\right) + \Omega_N^{rm(l-1)}\epsilon_{r_m} + e_P(l-2), \qquad (4.35)$$

where $e_P(l)$ is the error due to quantization of the product $\hat{\Omega}_N^{rm}Q[(\hat{\Omega}_N^{rm})^l]$, and it is assumed to have a variance $2^{-2b}/3$. When $l \geq 5$, we have

$$e_c(l) = \left[e_c(l-2)\left(\Omega_N^{rm} + \epsilon_{r_m}\right) + \Omega_N^{rm(l-2)}\epsilon_{r_m} + e_p(l-3)\right]\left(\Omega_N^{rm} + \epsilon_{r_m}\right)$$

135

$$+\Omega_N^{r_m(l-1)}\epsilon_{r_m} + e_P(l-2)$$

$$= e_c(l-2)\Omega_N^{2r_m} + 2\Omega_N^{r_m(l-1)}\epsilon_{r_m} + e_P(l-3)\Omega_N^{r_m} + e_P(l-2)$$

$$+\{\text{higher order terms of noise}\}. \tag{4.36}$$

From the recursive relationships, we conclude that for $l \geq 4$,

$$e_c(l) = e_c(3)\Omega_N^{r_m(l-3)} + (l-3)\Omega_N^{r_m(l-1)}\epsilon_{r_m} + \sum_{i=2}^{l-2} e_P(i)\Omega_N^{r_m(l-i-2)}$$

$$+\{\text{higher order terms of noise}\}. \tag{4.37}$$

Substituting for $e_c(3)$ given by (4.33), we have

$$e_c(l) = \left(2\Omega_N^{r_m}\epsilon_{r_m} + \epsilon_{r_m}^2 + e_P(1)\right)\Omega_N^{r_m(l-3)} + (l-3)\Omega_N^{r_m(l-1)}\epsilon_{r_m}$$

$$+\sum_{i=2}^{l-2} e_P(i)\Omega_N^{r_m(l-i-2)} + \{\text{higher order terms of noise}\}$$

$$= (l-1)\Omega_N^{r_m(l-1)}\epsilon_{r_m} + \sum_{i=1}^{l-2} e_P(i)\Omega_N^{r_m(l-i-2)} + \{\text{higher order terms of noise}\} \tag{4.38}$$

Thus, the mean-squared magnitude of the resulting error is given by

$$\mathrm{E}\left[|e_c(l)|^2\right]$$

$$= \mathrm{E}\left[\left|(l-1)\Omega_N^{r_m(l-1)}\epsilon_{r_m} + \sum_{i=1}^{l-2} e_P(i)\Omega_N^{r_m(l-i-2)} + \{\text{higher order terms of noise}\}\right|^2\right]$$

$$= (l-1)^2\frac{2^{-2b}}{6} + \sum_{i=1}^{l-2}\frac{2^{-2b}}{3} + \mathrm{E}\left|\{\text{higher order terms of noise}\}\right|^2$$

$$\cong \left(l^2 - 3\right)\frac{2^{-2b}}{6} \tag{4.39}$$

where it is assumed that the third and higher order moments of the noise can be ignored. Using (4.39) we can determine the mean square magnitude of noise due to coefficient quantization for any butterfly at the $(m+1)$th stage. Following the same approach as used in deriving (4.26), we have

$$\sigma^2_{c_{m+1}}(l) = \frac{1}{4}\mathrm{E}\left[|\hat{S}_m(q)|^2\right]\mathrm{E}\left[|e_c(l)|^2\right]$$

$$= \frac{1}{4}\frac{(l^2-3)2^{-2b}}{6}\frac{1}{3\cdot 2^m}. \tag{4.40}$$

136

Next, we examine the mean square magnitude of noise in the output.

From (4.40) it is seen that different butterflies have different mean square magnitudes of noise due to their dependence on l and m. Since each output of the fast Fourier transform connects to different sets of butterflies, each output contains different mean square magnitudes of noise that is due to coefficient quantization. It is difficult to determine the mean square noise according to which butterflies have been used to generate a specific output. In the following analysis for the noise in the output, we use (4.40) to compute an average. Denoting the average of the mean square noise at the $(m+1)$th stage by $\bar{\sigma}^2_{c_{m+1}}$, we write

$$
\begin{aligned}
\bar{\sigma}^2_{c_{m+1}} &= \frac{1}{N/2} \cdot \sum_{l=2}^{2^m} \left(\frac{N/2}{2^m}\right) \left[\frac{1}{4} \frac{(l^2-3)2^{-2b}}{6} \frac{1}{3 \cdot 2^m}\right] \\
&= \frac{2^{-2b}}{72} \cdot \frac{1}{2^{2m}} \left[\frac{1}{6}\left(2 \cdot 2^{3m} + 3 \cdot 2^{2m} + 2^m\right) - 1 - 3\left(2^m - 1\right)\right] \\
&= \frac{2^{-2b}}{432} \left[2 \cdot 2^m + 3 - 17 \cdot \left(\frac{1}{2}\right)^m + 12 \cdot \left(\frac{1}{4}\right)^m\right].
\end{aligned}
\tag{4.41}
$$

Thus, $\bar{\sigma}^2_{c_{m+1}}$ is used as the mean square error of coefficient quantization that occurs at any butterfly in the $(m+1)$th stage. In a manner similar to the derivation of (4.21), the output mean square noise due to coefficient quantization is approximately

$$
\begin{aligned}
\sigma^2_c &= \sum_{m=2}^{\nu-1} 2^{(\nu-m-1)} \cdot \bar{\sigma}^2_{c_{m+1}} \cdot \left(\frac{1}{2}\right)^{2(\nu-m-1)} \\
&= \sum_{m=2}^{\nu-1} \left(\frac{1}{2}\right)^{(\nu-m-1)} \cdot \frac{2^{-2b}}{432} \left[2 \cdot 2^m + 3 - 17 \cdot \left(\frac{1}{2}\right)^m + 12 \cdot \left(\frac{1}{4}\right)^m\right] \\
&= \frac{2^{-2b}}{216N} \sum_{m=2}^{\nu-1} \left[2 \cdot 2^{2m} + 3 \cdot 2^m - 17 + 12\left(\frac{1}{2}\right)^m\right].
\end{aligned}
\tag{4.42}
$$

Using the identity

$$
\sum_{m=2}^{\nu-1} r^m = \frac{r^\nu - r^2}{r - 1}
\tag{4.43}
$$

and assuming N is much greater than unity, we have

$$
\sigma^2_c \cong \frac{2^{-2b}}{324}N.
\tag{4.44}
$$

Since the output has variance $1/(3N)$, the noise-to-signal ratio in the case where coefficients are obtained from in-place calculation with finite-precision is roughly

$$\frac{\sigma_c^2}{\mathrm{E}|\hat{S}_\nu(k)|^2} = \frac{2^{-2b}}{108} N^2. \tag{4.45}$$

Comparing the results given in (4.28) and (4.45), it is obvious that the effect of coefficient quantization depends on how they are generated. The alternative of in-place calculation has the advantage of hardware simplicity, but it introduces a much greater amount of quantization error. In particular, (4.45) indicates that the noise-to-signal ratio is roughly proportional to N^2. It has been pointed out [34] that to reduce the problem of accumulation of errors when the coefficients are obtained from in-place computation, it is generally necessary to reset the values at prescribed points. However, to reset the coefficients, the values have to be stored. It becomes a tradeoff between noise-to-signal ratio performance and hardware complexity. Nevertheless, storing the coefficients in a table is preferable when high accuracy is important. In the following, we assume that the coefficients are stored in hardware, and therefore, the effects of coefficient quantization are negligible.

4.2 Quantization Effects in Radar Receivers

This section is devoted to the analysis of quantization effects in radar receivers. The receivers considered are the conventional matched filter based receiver as given by (4.1), the discrete Wigner-Ville distribution based receiver as given by (3.22) of Chapter 3, and the discrete time-frequency correlation function based receiver as given by (3.42) of Chapter 3. Specifically, we will evaluate the effect of quantization error on the test statistic along a cut in Doppler using the aforementioned receivers. All of these receivers are implemented in the time-domain; however, the analysis can be extended to their equivalents in the frequency-domain and other types of receivers derived in previous chapters with minor modifications. Furthermore, since the operation of the conventional receiver can be viewed as calculation of the cross-ambiguity function of the received and the reference signals, the result obtained in this section can be applied to the analysis of the effect of quantization error on the discrete

ambiguity function. In the following discussion, the effects of quantization error on the discrete Wigner-Ville distribution and the time-frequency correlation function can also be observed.

In the analysis, we assume that the sampling rate is $1/T_s = 4B$, the number of samples obtained is $N = T/T_s$, where $N = 2^\nu$ and ν is an integer. Also, we assume that the number system is a $(b + 1)$-bit sign-magnitude fixed-point binary number system, with 1 bit representing the sign and b bits representing the magnitude of the number. The fast Fourier transform is assumed to be of radix-2 decimation-in-time form and a scale factor of $1/2$ is inserted before each butterfly computation to prevent overflow. The input sequences $\{\tilde{r}(kT_s)\}$ and $\{\tilde{s}(kT_s)\}$ are assumed to be uncorrelated and each is assumed to be white such that the real and imaginary parts of the two sequences ($4N$ real samples) are uncorrelated. Furthermore, each real sample is assumed to be uniformly distributed over $-1/\sqrt{2}$ to $1/\sqrt{2}$. It follows that each complex sample of the input sequences has power equal to $1/3$. Again, the assumptions about the input are made to facilitate the analysis, but they are not restrictive and the results obtained hold for a broad class of signals.

4.2.1 Conventional Matched Filter Based Receiver

In this subsection, we evaluate the effect of quantization error on the test statistic along a cut in Doppler as calculated by a conventional matched filter receiver. There are two sources of quantization error in a discrete receiver. One source is the analog-to-digital conversion of the signals. The other quantization error source is finite precision arithmetic. Note that operations such as shifts and rotations of the reference signal sample sequence do not result in quantization errors. The arithmetic performed in the conventional receiver can be implemented with the following three-step algorithm.

Step 1. Cross multiply the received and reference samples to obtain $\{\tilde{r}(kT_s)\tilde{s}^*(kT_s - nT_s)\}$, $k = 1, 2, \ldots, N$.

Step 2. Compute the N-point fast Fourier transform of $\{\tilde{r}(kT_s)\tilde{s}^*(kT_s - nT_s)\}$, resulting in $\hat{\phi}_{\tilde{r}\tilde{s}}[nT_s, m/(NT_s)]$, $m = 1, 2, \ldots, N$.

Step 3. Take magnitude-square of the result of Step 2, yielding $\Lambda[nT_s, m/(NT_s)]$, $m = 1, 2, \ldots, N$.

A block diagram describing the computations in this algorithm is shown in Figure 4.2.

To obtain an analytical expression for the output noise-to-signal ratio of the receiver in terms of wordlength b and sample sequence length N, the signal and noise powers will be derived at different points of the block diagram. As depicted in Figure 4.2, μ_i^2 denotes the signal power and σ_i^2 denotes the noise power, $i = 1, 2, 3$. Furthermore, $e_{\tilde{r}}$ and $e_{\tilde{s}}$ denote the initial quantization errors due to analog to digital conversion of the received samples and the reference samples, respectively. As before, the following assumptions will be adopted.

1. $e_{\tilde{r}}$ and $e_{\tilde{s}}$ are uncorrelated with each other and the inputs, and their real and imaginary parts are uniformly distributed over $-2^{-b}/2$ to $2^{-b}/2$.

2. The roundoff noise due to each real multiplication is uniformly distributed over $-2^{-b}/2$ to $2^{-b}/2$ with variance $2^{-2b}/12$.

3. All noises due to each real multiplication are mutually uncorrelated.

4. All noises are uncorrelated with the input, and consequently, they are also uncorrelated with the result of the computation.

With the previous assumptions about the probability distributions of the signal samples, the signal power after Step 1 is given by

$$\mu_1^2 = \mathrm{E}\left[|\tilde{r}(kT_s)\tilde{s}^*(kT_s - nT_s)|^2\right] = \mathrm{E}\left[|\tilde{r}(kT_s)|^2\right]\mathrm{E}\left[|\tilde{s}^*(kT_s - nT_s)|^2\right] = \frac{1}{3} \cdot \frac{1}{3} = \frac{1}{9}. \quad (4.46)$$

The signal power after Step 2 can be seen from (4.20), which indicates that the output power of the N-point fast Fourier transform algorithm considered here is $1/N$ times the input power.

140
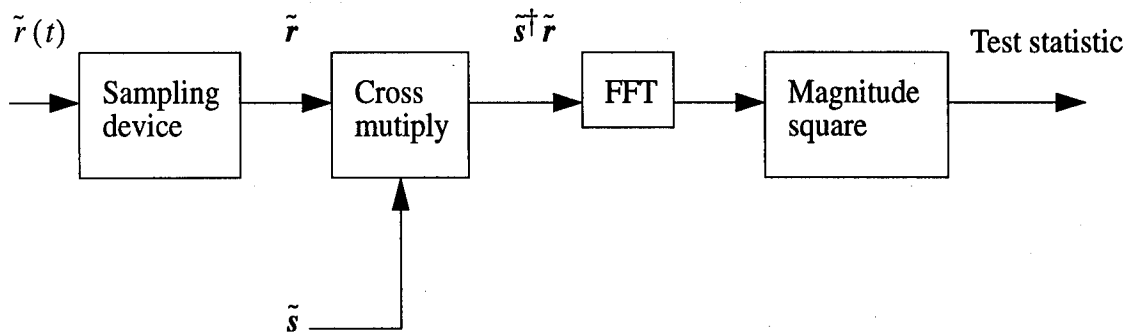
(a) Computational flow graph
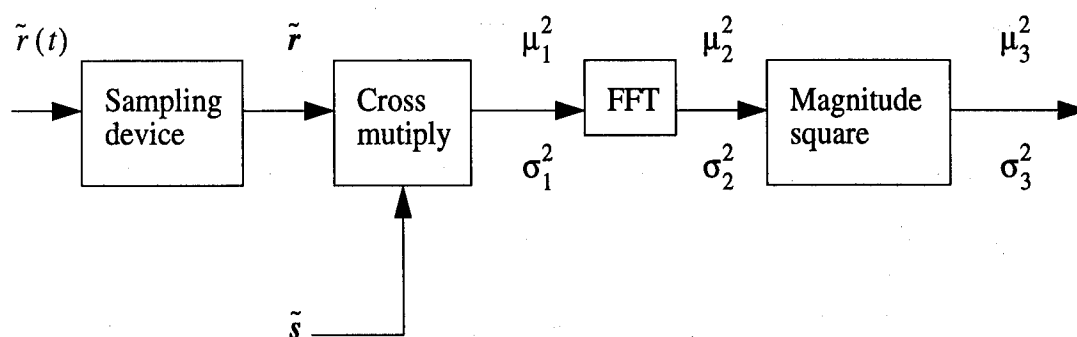
(b) Signal and noise power propagation

Figure 4.2: Computational flow graph of the conventional discrete matched filter based receiver

141

Hence, $\mu_2^2 = 1/(9N)$. To obtain the signal power after Step 3, we need to calculate the second moment of $\hat{\theta}_{\tilde{r}\tilde{s}}[nT_s, m/(NT_s)]$. One method to carry out this calculation is to make further assumptions about the joint probability distribution of samples of $\hat{\theta}_{\tilde{r}\tilde{s}}[nT_s, m/(NT_s)]$. However, it is difficult to find a distribution that suitably describes $\hat{\theta}_{\tilde{r}\tilde{s}}(\cdot)$ for arbitrary signals.

Another approach to calculate the output signal power is to directly utilize the properties of the discrete ambiguity function. Since it was assumed that $1/T_s = 4B$ and $N = T/T_s$, there are $2N$ points in delay direction and N points in the Doppler direction in one repetition of the discrete ambiguity function. Averaging the magnitude square of the discrete ambiguity function over one repetition, we have

$$\frac{1}{2N \cdot N} \sum_n \sum_m \left| \sum_k \tilde{r}(kT_s)\tilde{s}^*(kT_s - nT_s) \exp\left(-j2\pi\frac{mk}{N}\right) \right|^4$$

$$= \frac{1}{2N^2} \sum_n \sum_m \left[\sum_k \sum_l \tilde{r}(kT_s)\tilde{s}^*(kT_s - nT_s)\tilde{r}^*(lT_s)\tilde{s}(lT_s - nT_s) \exp\left(j2\pi\frac{m(l-k)}{N}\right) \right]^2$$

$$= \frac{1}{2N^2} \sum_n \sum_m \sum_k \sum_l \sum_p \sum_q \tilde{r}(kT_s)\tilde{r}^*(lT_s)\tilde{r}(pT_s)\tilde{r}^*(qT_s)\tilde{s}^*(kT_s - nT_s)\tilde{s}(lT_s - nT_s)$$

$$\cdot \tilde{s}^*(pT_s - nT_s)\tilde{s}(qT_s - nT_s) \exp\left[j2\pi\frac{m(l-k+q-p)}{N}\right]. \tag{4.47}$$

Note that the above summations are performed over one repetition of the discrete ambiguity function. Summing the exponential term over m by the Poisson's sum formula, we have

$$\frac{1}{2N^2} \sum_n \sum_m \left| \sum_k \tilde{r}(kT_s)\tilde{s}^*(kT_s - nT_s) \exp\left(-j2\pi\frac{mk}{N}\right) \right|^4$$

$$= \frac{1}{2N} \sum_n \sum_k \sum_l \sum_p \tilde{r}(kT_s)\tilde{r}^*(lT_s)\tilde{r}(pT_s)\tilde{r}^*[(k+p-l)T_s]\tilde{s}^*(kT_s - nT_s)$$

$$\cdot \tilde{s}(lT_s - nT_s)\tilde{s}^*(pT_s - nT_s)\tilde{s}[(k+p-l-n)T_s]. \tag{4.48}$$

Letting $m' = p - l$ in (4.48), we have

$$\frac{1}{2N^2} \sum_n \sum_{m'} \left| \sum_k \tilde{r}(kT_s)\tilde{s}^*(kT_s - nT_s) \exp\left(-j2\pi\frac{m'k}{N}\right) \right|^4$$

$$= \frac{1}{2N} \sum_n \sum_k \sum_l \sum_{m'} \tilde{r}(kT_s)\tilde{r}^*(lT_s)\tilde{r}[(l+m')T_s]\tilde{r}^*[(k+m')T_s]\tilde{s}^*(kT_s - nT_s)$$

$$\cdot \tilde{s}(lT_s - nT_s)\tilde{s}^*[(l+m'-n)T_s]\tilde{s}[(k+m'-n)T_s]$$

$$= \frac{1}{2N} \sum_n \sum_{m'} \left| \sum_k \tilde{r}(kT_s)\tilde{r}^*[(k+m')T_s]\tilde{s}^*(kT_s - nT_s)\tilde{s}[(k+m'-n)T_s] \right|^2. \tag{4.49}$$

Applying the Cauchy-Schwarz inequality

$$\frac{1}{2N^2} \sum_n \sum_m \left| \sum_k \tilde{r}(kT_s)\tilde{s}^*(kT_s - nT_s) \exp\left(-j2\pi \frac{mk}{N}\right) \right|^4$$

$$= \frac{1}{2N} \sum_n \sum_{m'} \left| \sum_k \tilde{r}(kT_s)\tilde{r}^*[(k+m')T_s]\tilde{s}^*(kT_s - nT_s)\tilde{s}[(k+m'-n)T_s] \right|^2$$

$$\leq \frac{1}{2N} \sum_n \sum_{m'} \left[\sum_k |\tilde{r}(kT_s)\tilde{s}[(k+m'-n)T_s]|^2 \right] \left[\sum_l |\tilde{r}[(l+m')T_s]\tilde{s}(lT_s - nT_s)|^2 \right]$$

$$= \frac{1}{2N} \sum_n \sum_{m'} \left[\sum_k |\tilde{r}(kT_s)\tilde{s}[(k+m'-n)T_s]|^2 \right] \left[\sum_l |\tilde{r}(lT_s)\tilde{s}[(l-m'-n)T_s]|^2 \right]. \quad (4.50)$$

Let

$$\varphi(n) \triangleq \sum_k |\tilde{r}(kT_s)\tilde{s}[(k-n)T_s]|^2. \quad (4.51)$$

Then,

$$\frac{1}{2N^2} \sum_n \sum_m \left| \sum_k \tilde{r}(kT_s)\tilde{s}^*(kT_s - nT_s) \exp\left(-j2\pi \frac{mk}{N}\right) \right|^4$$

$$\leq \frac{1}{2N} \sum_n \sum_{m'} \left[\sum_k |\tilde{r}(kT_s)\tilde{s}[(k+m'-n)T_s]|^2 \right] \left[\sum_l |\tilde{r}(lT_s)\tilde{s}[(l-m'-n)T_s]|^2 \right]$$

$$= \frac{1}{2N} \sum_n \sum_{m'} \varphi(n-m')\varphi(n+m'). \quad (4.52)$$

Employing manipulation similar to those used in deriving (3.2) through (3.7) of Chapter 3, we have

$$\sum_n \sum_{m'} \varphi(n-m')\varphi(n+m')$$

$$= \sum_k \sum_l \varphi(2k)\varphi(2l) + \sum_k \sum_l \varphi(2k+1)\varphi(2l+1)$$

$$= \frac{1}{2} \sum_k \sum_l \varphi(k)\varphi(l) + \frac{1}{2} \sum_k \sum_l (-1)^{k+l}\varphi(k)\varphi(l)$$

$$= \frac{1}{2} \sum_k \sum_l \varphi(k)\varphi(l) + \frac{1}{2} \left[\sum_k (-1)^k \varphi(k) \right] \left[\sum_l (-1)^l \varphi(l) \right]. \quad (4.53)$$

However,

$$\sum_k (-1)^k \varphi(k) = \sum_k (-1)^k \left[\sum_p |\tilde{r}(pT_s)\tilde{s}[(p-k)T_s]|^2 \right]. \quad (4.54)$$

Substituting $\exp(j\pi k)$ for $(-1)^k$, we obtain

$$\sum_k (-1)^k \varphi(k) = \sum_k \sum_p \exp(j\pi k) |\tilde{r}(pT_s)\tilde{s}[(p-k)T_s]|^2$$
$$= \sum_p |\tilde{r}(pT_s)|^2 \sum_k \exp(j\pi k) |\tilde{s}[(p-k)T_s]|^2 . \qquad (4.55)$$

Letting $k' = p - k$ on the right-hand side of (4.55), we have

$$\sum_k (-1)^k \varphi(k) = \sum_p |\tilde{r}(pT_s)|^2 \sum_{k'} \exp[j\pi(p-k')] |\tilde{s}(k'T_s)|^2$$
$$= \sum_p \exp(j\pi p) |\tilde{r}(pT_s)|^2 \sum_{k'} \exp(-j\pi k') |\tilde{s}(k'T_s)|^2 . \qquad (4.56)$$

The term $\sum_{k'} |\tilde{s}(k'T_s)|^2 \exp(-j\pi k')$ is the discrete Fourier transform of $\{|\tilde{s}(k'T_s)|^2\}$ evaluated at frequency $1/(2T_s) = 2B$ and the result can be readily obtained from the following observation. Since the Fourier transform of $|\tilde{s}(t)|^2$ is the convolution of that of $\tilde{s}(t)$ with itself, it has an extent from $-2B$ to $2B$ and is zero outside. It follows that the term $\sum_{k'} |\tilde{s}(k'T_s)|^2 \exp(-j\pi k')$ reduces to zero. Consequently, we have

$$\frac{1}{2N^2} \sum_n \sum_m \left| \sum_k \tilde{r}(kT_s)\tilde{s}^*(kT_s - nT_s) \exp\left(-j2\pi \frac{mk}{N}\right) \right|^4$$
$$\leq \frac{1}{4N} \sum_k \sum_l \varphi(k)\varphi(l)$$
$$= \frac{1}{4N} \left[\sum_k \sum_p |\tilde{r}(pT_s)\tilde{s}[(p-k)T_s]|^2 \right]^2$$
$$= \frac{1}{4N} \left[\sum_p |\tilde{r}(pT_s)|^2 \sum_k |\tilde{s}(kT_s)|^2 \right]^2$$
$$= \frac{N^3}{4} \left[\frac{1}{N} \sum_p |\tilde{r}(pT_s)|^2 \cdot \frac{1}{N} \sum_k |\tilde{s}(kT_s)|^2 \right]^2 . \qquad (4.57)$$

From the derivation of (4.50), it is seen that the equality in the above relationship holds if, and only if,

$$\tilde{r}(kT_s)\tilde{s}[(k+m-n)T_s] = C\tilde{r}[(k+m)T_s]\tilde{s}[(k-n)T_s] \qquad (4.58)$$

for all k, n, m and some complex constant C. It should be pointed out that relationship (4.57) is obtained under the assumption that the sampling rate is higher than twice the

144

signal Nyquist rate. Also, a generalized version of (4.57) for a continuous signal can be found in [17].

Assume that the number of samples is large enough such that

$$\frac{1}{N} \sum_p |\tilde{r}(pT_s)|^2 \cong \mathrm{E}[|\tilde{r}(pT_s)|^2] = \frac{1}{3} \tag{4.59}$$

and

$$\frac{1}{N} \sum_k |\tilde{s}(kT_s)|^2 \cong \mathrm{E}[|\tilde{s}(kT_s)|^2] = \frac{1}{3}. \tag{4.60}$$

Thus, from (4.57) we have

$$\frac{1}{2N^2} \sum_n \sum_m \left| \sum_k \tilde{r}(kT_s)\tilde{s}^*(kT_s - nT_s) \exp\left(-j2\pi\frac{mk}{N}\right) \right|^4 \leq \frac{N^3}{4} \cdot \frac{1}{81} = \frac{N^3}{324}. \tag{4.61}$$

or equivalently,

$$\frac{1}{2N^2} \sum_n \sum_m \left| \frac{1}{N} \sum_k \tilde{r}(kT_s)\tilde{s}^*(kT_s - nT_s) \exp\left(-j2\pi\frac{mk}{N}\right) \right|^4 \leq \frac{1}{324N}. \tag{4.62}$$

The left-hand side of (4.62) gives the mean-square value of the receiver since the fast Fourier transform algorithm assumed for the receiver inserts a scaling factor 1/2 at each butterfly, and the output of the fast Fourier transform is $1/N$ times the discrete Fourier transform written inside the magnitude sign in (4.61). Therefore, $\mu_3^2 \leq 1/(324N)$.

It is also possible to obtain a lower bound for μ_3^2. Since the magnitude square of a quantity is non-negative, we have

$$\sum_n \sum_m \left[\left| \hat{\phi}_{\tilde{r}\tilde{s}}\left(nT_s, \frac{m}{NT_s}\right) \right|^2 - \frac{1}{2N^2} \sum_k \sum_l \left| \hat{\phi}_{\tilde{r}\tilde{s}}\left(kT_s, \frac{l}{NT_s}\right) \right|^2 \right]^2 \geq 0. \tag{4.63}$$

It follows that

$$\sum_n \sum_m \left| \hat{\phi}_{\tilde{r}\tilde{s}}\left(nT_s, \frac{m}{NT_s}\right) \right|^4 \geq \frac{1}{2N^2} \left[\sum_k \sum_l \left| \hat{\phi}_{\tilde{r}\tilde{s}}\left(kT_s, \frac{l}{NT_s}\right) \right|^2 \right]^2, \tag{4.64}$$

or, equivalently,

$$\frac{1}{2N^2} \sum_n \sum_m \left| \hat{\phi}_{\tilde{r}\tilde{s}}\left(nT_s, \frac{m}{NT_s}\right) \right|^4 \geq \left[\frac{1}{2N^2} \sum_k \sum_l \left| \hat{\phi}_{\tilde{r}\tilde{s}}\left(kT_s, \frac{l}{NT_s}\right) \right|^2 \right]^2. \tag{4.65}$$

However,

$$\sum_k \sum_l \left| \hat{\phi}_{\tilde{r}\tilde{s}} \left(kT_s, \frac{l}{NT_s} \right) \right|^2$$

$$= \sum_k \sum_l \sum_p \sum_q \tilde{r}(pT_s) \tilde{r}^*(qT_s) \tilde{s}^*(pT_s - kT_s) \tilde{s}(qT_s - kT_s) \exp\left[-j2\pi \frac{l(p-q)}{N} \right]$$

$$= N \sum_p |\tilde{r}(pT_s)|^2 \sum_k |\tilde{s}(kT_s)|^2 . \tag{4.66}$$

Thus, applying (4.66) to (4.65), we have

$$\frac{1}{2N^2} \sum_n \sum_m \left| \hat{\phi}_{\tilde{r}\tilde{s}} \left(nT_s, \frac{m}{NT_s} \right) \right|^4 \geq \frac{1}{4N^2} \left[\sum_p |\tilde{r}(pT_s)|^2 \sum_k |\tilde{s}(kT_s)|^2 \right]^2 . \tag{4.67}$$

Using the assumption (4.59), we have

$$\frac{1}{2N^2} \sum_n \sum_m \left| \hat{\phi}_{\tilde{r}\tilde{s}} \left(nT_s, \frac{m}{NT_s} \right) \right|^4 \geq \frac{N^2}{324}, \tag{4.68}$$

or equivalently,

$$\frac{1}{2N^2} \sum_n \sum_m \left| \frac{1}{N} \hat{\phi}_{\tilde{r}\tilde{s}} \left(nT_s, \frac{m}{NT_s} \right) \right|^4 \geq \frac{1}{324N^2}. \tag{4.69}$$

For the same reason as explained in the paragraph following (4.62), we have $\mu_3^2 \geq 1/(324N^2)$. Thus, we arrive at the conclusion

$$\frac{1}{324N^2} \leq \mu_3^2 = \frac{1}{2N^2} \sum_n \sum_m \left| \frac{1}{N} \sum_k \tilde{r}(kT_s) \tilde{s}^*(kT_s - nT_s) \exp\left(-j2\pi \frac{mk}{N} \right) \right|^4 \leq \frac{1}{324N} \tag{4.70}$$

when the sampling rate is higher than twice the Nyquist rate and relationship (4.59) can be satisfied. As an illustration, we compare the bounds obtained in (4.70) and the mean-square value of the discrete ambiguity function of two signals in the following example.

Example 4.1

In this example we calculate and plot the mean-square value of the ambiguity function of two signals, assuming the number of samples obtained are $8, 16, \ldots, 256$ for each signal. Since the validity of (4.70) does not depend on the specific form of the signals $\{\tilde{r}(kT_s)\}$ and $\{\tilde{s}(kT_s)\}$, we arbitrarily assume that the received samples are noise-free so that $\tilde{r}(kT_s) = \tilde{s}(kT_s)$.

The first set of signal samples are sequences of random complex numbers. The real and imaginary parts of the random numbers are uncorrelated and each of them is uniformly distributed over $(-1/\sqrt{2}, 1/\sqrt{2})$. The discrete ambiguity function is calculated for each sequence, and the magnitude square of each point of the obtained ambiguity function is summed and then averaged to obtain the mean-square value of the discrete ambiguity function of that sequence. The number of samples for each sequence is $N = 8, 16, \ldots, 256$. Figure 4.3 depicts the bounds as given by (4.70) and the actual mean-square values. It is seen from Figure 4.3 that the mean-square magnitude of the discrete ambiguity function is roughly proportional to $1/N^2$.

The second set of samples are sequences of samples obtained from sampling the signal

$$\tilde{s}(t) = \frac{1}{\sqrt{2}} \text{rect}\left(\frac{t - 0.4}{0.8}\right) \exp\left(j\frac{\pi}{2}t^2\right). \tag{4.71}$$

The sampling process is performed in the time interval from 0 to 1.6. The sampling rates are $8/1.6$, $16/1.6, \cdots, 256/1.6$ to obtain sequences of $N = 8, 16, \ldots, 256$ samples. Figure 4.4 shows both the bounds given in (4.70) and the actual mean-square values. It can be seen from Figure 4.4 that the mean-square magnitude of the discrete ambiguity function is within the bounds, being roughly proportional to $1/N$, even though the signal does not quite satisfy (4.59). $\square$

The propagation and accumulation of the quantization noise power is analyzed in the following. After Step 1 of the computational algorithm, the noise power can be obtained using the result (4.12), which gives

$$\sigma_1^2 = \text{E}[|\tilde{r}(kT_s)|^2]\text{E}[|e_{\tilde{s}}|^2] + \text{E}[|\tilde{s}(kT_s)|^2]\text{E}[|e_{\tilde{r}}|^2]$$
$$\cong \frac{1}{3}\left(\frac{2^{-2b}}{6} + \frac{2^{-2b}}{6}\right) = \frac{2^{-2b}}{9} \tag{4.72}$$

where it was assumed that $1/3 \gg 2^{-2b}/12$. After Step 2, the power of the noise is $1/N$ times the noise power from the previous step plus the noise power generated by the fast Fourier
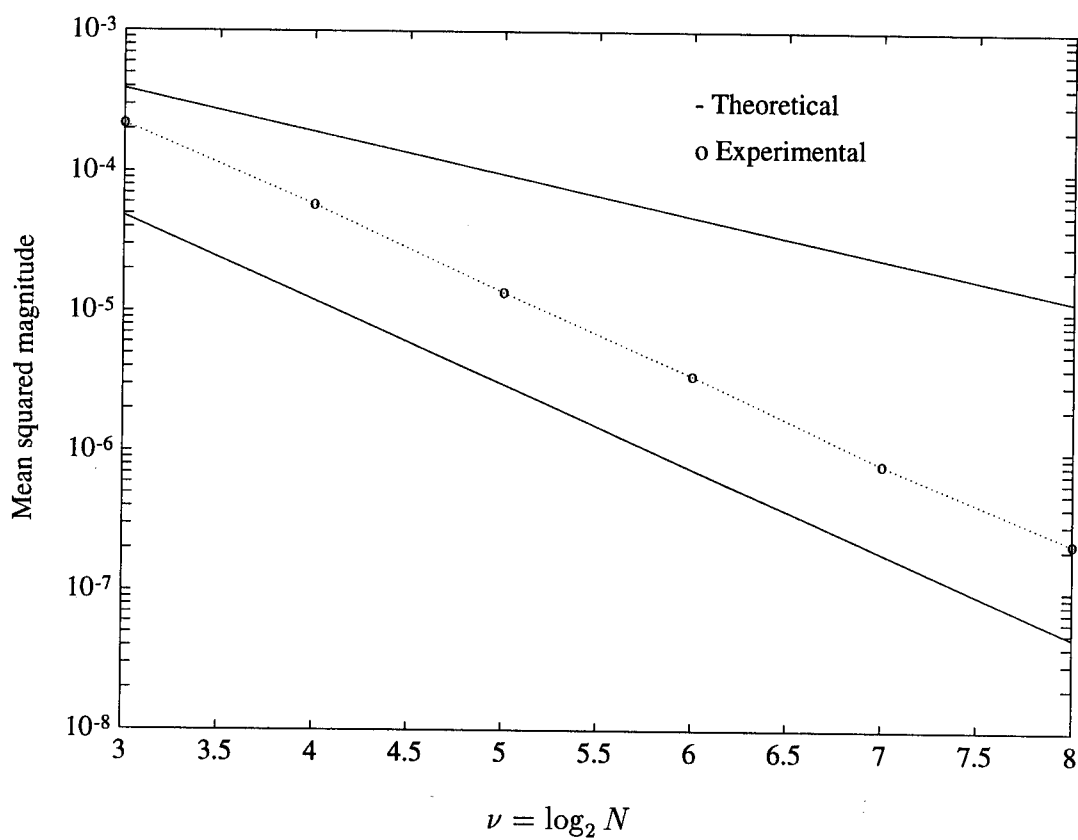
Figure 4.3: Mean-square magnitude of the discrete ambiguity function of a random sequence
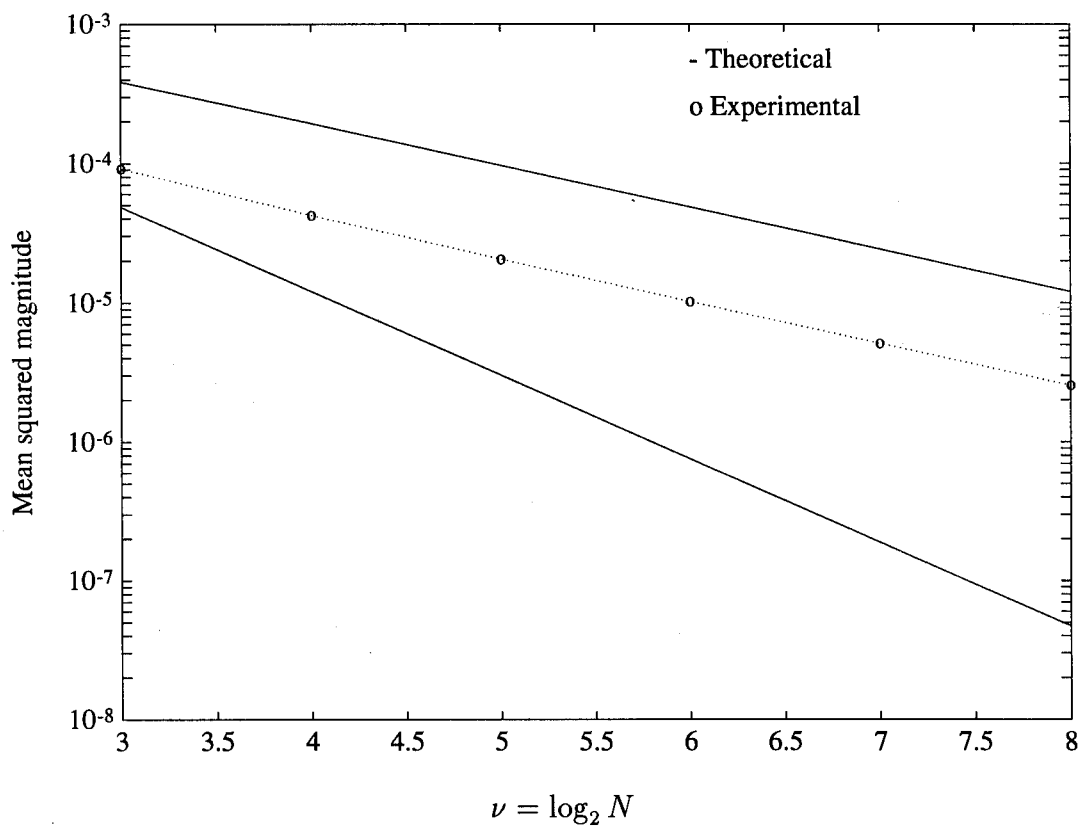
Figure 4.4: Mean-square magnitude of the discrete ambiguity function of a *lfm* rectangular pulse

transform, which according to (4.22) is $2^{-2b} \cdot 5/3$. Thus,

$$\sigma_2^2 = \frac{\sigma_1^2}{N} + 2^{-2b} \cdot \frac{5}{3} = \frac{2^{-2b}}{9N} + 2^{-2b} \cdot \frac{5}{3}. \tag{4.73}$$

The noise after Step 3 consists of two parts; one is from the calculation of magnitude-square of a complex number, and the other is from the noise of the previous step. To calculate the magnitude-square of a complex number, two real multiplications are performed, and the noise generated has power $2^{-2b}/6$. The error caused from the input noise has power $\mu_2^2 \sigma_2^2$ as indicated by the discussion following (4.12). Thus,

$$\sigma_3^2 = \frac{2^{-2b}}{6} + \frac{2^{-2b}}{9N} \left(\frac{5}{3} + \frac{1}{9N} \right). \tag{4.74}$$

From the foregoing derivations, the output noise-to-signal ratio is given by

$$2^{-2b} \left(54N^2 + \frac{5N}{12} + 4 \right) \le \frac{\sigma_3^2}{\mu_3^2} \le 2^{-2b} \left(54N + \frac{5}{12} + \frac{4}{N} \right). \tag{4.75}$$

The above relationship indicates that the output noise-to-signal ratio is at best proportional to N, with the worst case as being proportional to N^2. It is important to point out that the output signal power is linearly proportional to the input signal power as can be seen from the derivation of μ_3^2. Thus, the output noise-to-signal ratio degrades as the input signal power decreases. It should also be noted that the derivation of (4.75) assumes the quantization errors are uncorrelated.

4.2.2 General Form Discrete Wigner-Ville Distribution Based Receiver

In this subsection, we evaluate the effect of quantization error on the test statistic along a cut in Doppler as calculated by the discrete Wigner-Ville distribution based receiver (3.22). The receiver (3.22) performs convolution between the discrete Wigner-Ville distributions of the received samples and of the reference samples. Due to computation speed requirements,

this convolution is assumed to be based on the convolution theorem. Hence, there are multiple fast Fourier transforms to be encountered in the receiver. Recall from the previous section, where we examined the quantization effects in the fast Fourier transform computation, that it is important to raise the signal power at the input of the transform as high as possible to achieve a low ratio of the output quantization error power to the output signal power. Therefore, we insert scaling factors between cascading fast Fourier transforms in the receiver to raise the signal power and to maintain a low output noise to signal ratio. The placement and the magnitude of these scaling factors are chosen in the manner such that no overflow will result. The arithmetic performed in the receiver (3.22) can be described by the following 10-step algorithm.

Step 1. Cross multiply the received samples to form the sequence $\{\tilde{r}(kT_s)\tilde{r}^*(nT_s - kT_s)\}$.

Step 2. Perform N-point fast Fourier transform of the sequence obtained from Step 1. Let $m/(NT_s), -N/2 \leq m \leq N/2 - 1$ denote the frequency arguments of the resulting sequence.

Step 3. Multiply $\exp(j\pi mn/N)$ to the sequence resulted from Step 2 to obtain the auto-Wigner-Ville distribution of the received samples.

Step 4. Perform $2N$-point fast Fourier transform over the frequency arguments of the result of Step 3. Denote the transform domain by u.

Step 5. Multiply a constant N to the sequence resulted from Step 4.

Step 6. Perform $2N$-point fast Fourier transform over the frequency arguments of the reference Wigner-Ville distribution.

Step 7. Multiply a constant N to the sequence resulted from Step 6.

Step 8. Cross multiply over the arguments of u the resulting sequences from Step 5 and Step 7.

Step 9. Perform $2N$-point inverse fast Fourier transform over u of the sequence resulted from Step 8.

Step 10. Sum over the time arguments of the result of Step 9.

A block diagram describing the computation in this algorithm is shown in Figure 4.5. It should be pointed out that the above algorithm assumes that the reference Wigner-Ville distribution is readily available and calculation in real time is not needed. Only minor modifications to the following analysis is needed if this assumption is not satisfied.

In a manner similar to the derivation of the previous subsection, it can be shown that the signal power $\mu_1^2 = 1/9$ after Step 1, and $\mu_2^2 = 1/(9N)$ after Step 2. Since the magnitude of $\exp(j\pi mn/N)$ is unity, the signal power after Step 3 is $\mu_3^2 = 1/(9N)$. Whether it is possible to place a scaling factor at this point and how much it may be can be determined by examining the greatest magnitude of the sequence after Step 3. Using the Cauchy-Schwarz inequality the upper bound on the magnitude of the sequence resulted from Step 3 is given by

$$\left| \frac{1}{N} \sum_k \tilde{r}(kT_s)\tilde{r}^*(nT_s - kT_s) \exp\left[-j\pi \frac{m(2k-n)}{N}\right] \right| \leq \frac{1}{N} \sum_k |\tilde{r}(kT_s)|^2 \qquad (4.76)$$

where the factor $1/N$ inside the magnitude sign on the left-hand side is included to reflect the fact that the fast Fourier transform algorithm under consideration here introduces a scaling factor of $1/2$ at every butterfly. Applying the assumption (4.59) to the right-hand side of (4.76), the upper bound on the magnitude of the sequence resulted from Step 3 is $1/3$. On one hand, it is seen that a scaling factor of 3 can be placed after Step 3 without causing overflow; on the other hand, this scaling may not be significant enough to justify the additional hardware complexity. Therefore, we choose to omit scaling at this point. The signal power after Step 4 is $1/(2N)$ times μ_3^2, i.e., $\mu_4^2 = 1/(18N^2)$. Note that the sequence resulted from Step 4 is given by

$$\frac{1}{2N} \sum_m \left[\frac{1}{N} \hat{W}_{\tilde{r}} \left(nT_s, \frac{m}{NT_s} \right) \right] \exp\left(j2\pi \frac{mu}{2N} \right)$$
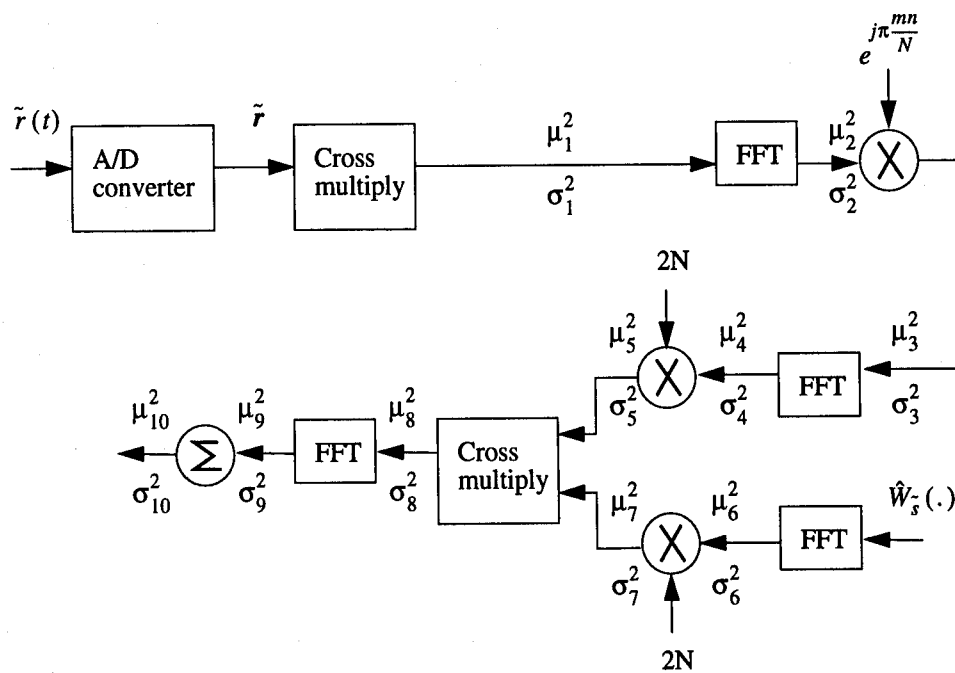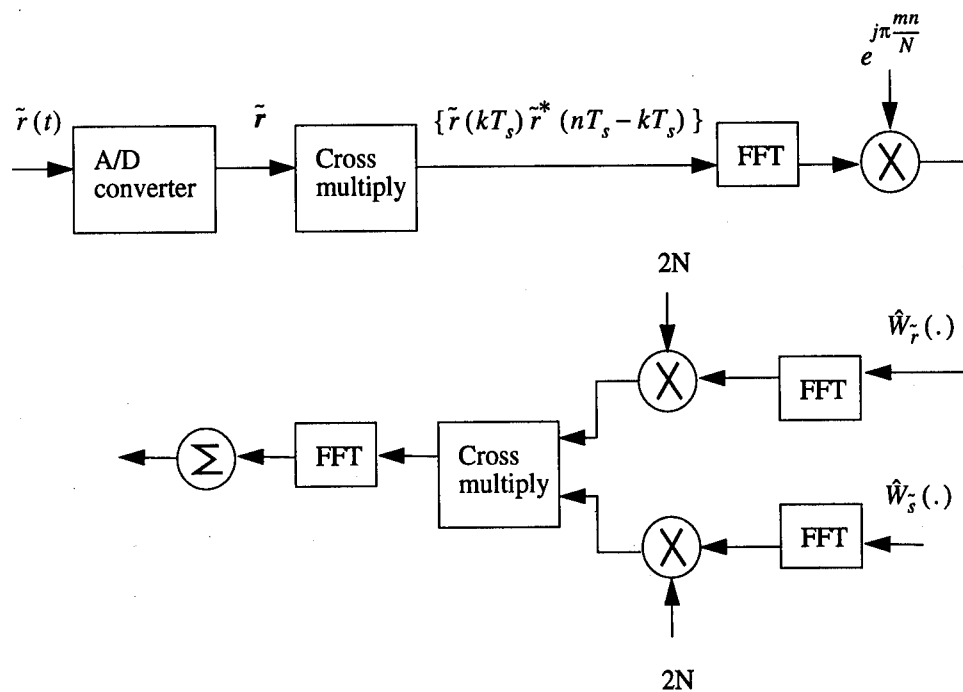
152

(a) Computational flow graph

(b) Signal and noise power propagation

Figure 4.5: Computational flow graph of the general form discrete Wigner-Ville distribution based receiver

153

$$= \frac{1}{2N} \sum_m \left\{ \frac{1}{N} \sum_k \tilde{r}(kT_s)\tilde{r}^*(nT_s - kT_s) \exp\left[-j\pi\frac{m(2k-n)}{N}\right] \right\} \exp\left(j2\pi\frac{mu}{2N}\right)$$

$$= \begin{cases} N^{-1} \cdot \tilde{r}[(n+u)/2]\tilde{r}^*[(n-u)/2], & (n+u) \text{ is even} \\ 0, & (n+u) \text{ is odd} \end{cases} \qquad (4.77)$$

where the factors $1/(2N)$ and $1/N$ are included since the fast Fourier transforms employ a scaling factor of $1/2$ at each butterfly, and the Poisson's sum formula was used to obtain the third line of the above relationships. Hence, we have

$$\left| \frac{1}{2N} \sum_m \hat{W}_{\tilde{r}}\left(nT_s, \frac{m}{NT_s}\right) \exp\left(j2\pi\frac{mu}{2N}\right) \right| \leq \frac{1}{N} |\tilde{r}[(n+u)/2]\tilde{r}^*[(n-u)/2]| \leq \frac{1}{N}. \qquad (4.78)$$

The above result indicates that the maximum magnitude of the output of Step 4 is $1/N$. Therefore, it is possible to introduce a scaling factor N after Step 4 to raise the signal power without causing overflow. Since this scaling is significant for large N, we introduce this scaling at Step 5. Thus, $\mu_5^2 = N^2\mu_4^2 = 1/18$. From Figure 4.5, it is clear $\mu_6^2 = \mu_4^2$ and $\mu_7^2 = \mu_5^2 = 1/18$. Assuming the output of Step 5 and Step 7 are uncorrelated, the signal power after Step 8 is $\mu_8^2 = \mu_5^2 \cdot \mu_7^2 = 1/324$. The signal power after Step 9 is $\mu_9^2 = \mu_8^2/(2N) = 1/(648N)$. There are two approaches to derive the output signal power. First, the output signal can be assumed to be a sum of $2N$ uncorrelated random variables from the output of Step 9. The mean square magnitude of these random variables is $2/(81N)$. Note that in this summation scaling is needed to prevent overflow. The scaling can be carried out in a manner similar to that used in the fast Fourier transform computation by introducing a scaling factor of $1/2$ to each pair of summations. Figure 4.6 depicts the special case of $N = 3$. With the same reasoning as used in the radix-2 fast Fourier transform discussion, summation of $2N$ numbers introduces a factor of $1/(2N)$ to the output power. Thus, we have $\mu_{10}^2 = \mu_9^2/(2N) = 1/(1296N^2)$. Another method of obtaining an estimate of the output signal power is to apply the result (4.70) to the relationship (3.22) of Chapter 3. Recall that (4.70) describes the mean square magnitude of the output of the conventional receiver. The output of the conventional receiver considered is a scaled version of the left-hand side of (3.22) due to the scaling at each butterfly of the fast Fourier transform. In fact, after
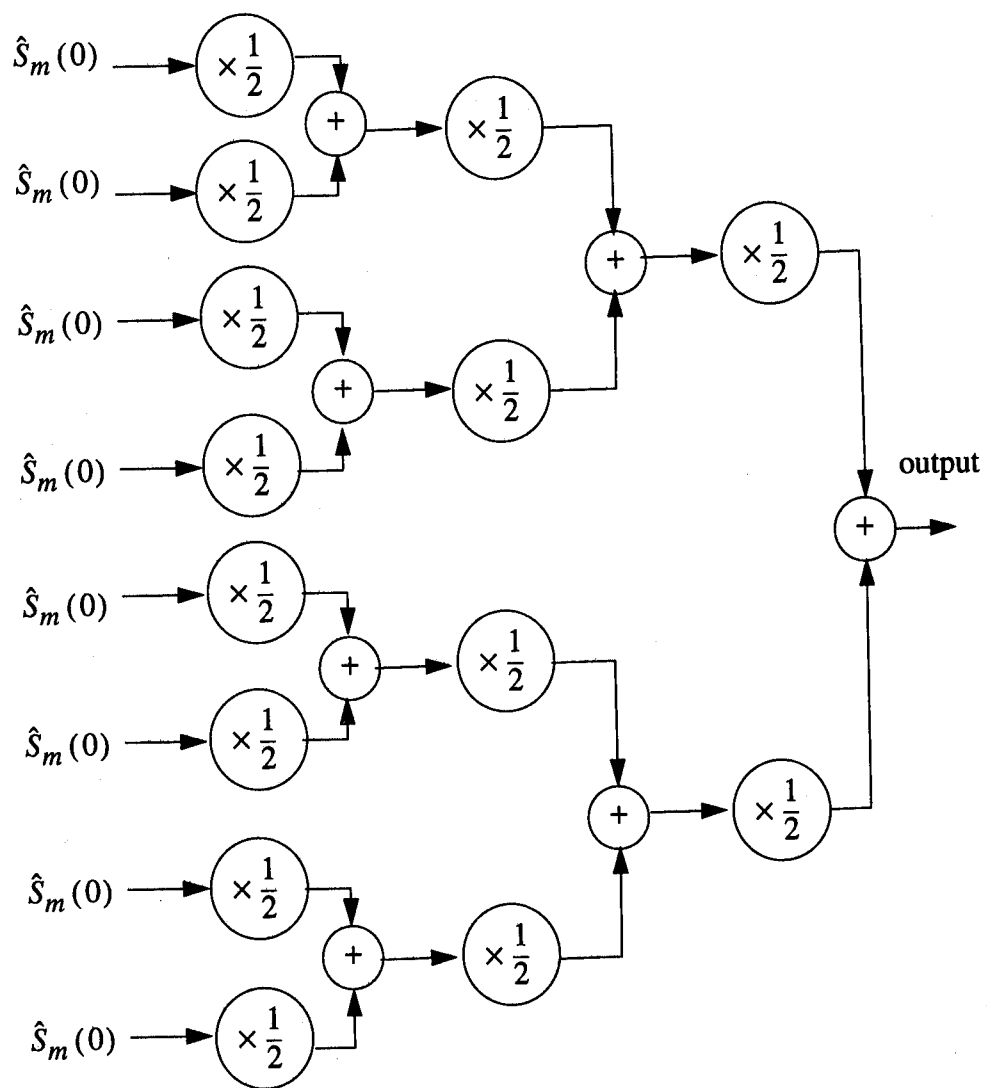
Figure 4.6: Summation with scaling factor included

155

taking the magnitude square, the output of the receiver analyzed in the previous subsection is $1/N^2$ times the left-hand side of (3.22). Hence, the mean square magnitude of the left-hand side of (3.22) is N^4 times (4.70). The Wigner-Ville distribution based receiver can be analyzed in a similar manner. If no scaling were introduced in the fast Fourier transforms, the convolution of two Wigner-Ville distributions performed in Steps 4, 6, 8, and 9 would be twice the direct form convolution given in the right-hand side of (3.22). However, while the multiplication by N in Steps 5 and 7 cancels out the scaling in the two N-point fast Fourier transforms in producing the Wigner-Ville distributions, the two $2N$-point forward fast Fourier transforms and the final summation of $2N$ numbers introduce a total scaling of $(2N)^{-3}$ to the output. Finally, considering the factor $1/N$ on the right-hand side of (3.22), we conclude that the output of the Wigner-Ville distribution based receiver as specified in this subsection is $2 \cdot 1/(8N^3) \cdot N = 1/(4N^2)$ times the right-hand side of (3.22). With the foregoing observation, we conclude that the mean-square magnitude of the output signal of the Wigner-Ville distribution based receiver is $N^4 \cdot (4N^2)^{-2}$ times (4.70) and is in the interval $[1/(5184N^2), 1/(5184N)]$. It is seen that the previous result using the assumption that the outputs of Step 9 are uncorrelated random variables is in this interval for $N \geq 4$. In the following analysis we will use $\mu_{10}^2 = 1/(1296N^2)$ as the estimate of the output signal power.

Next, we consider the quantization error. As before, the initial quantization error due to analog-to digital conversion of the received samples is assumed to have power $\sigma_{\tilde{r}}^2 = 2^{-2b}/6$. It will also be assumed that the finite register length storage of the factors $\exp(j\pi mn/N)$ used in Step 3 and the reference Wigner-Ville distribution used in Step 6 introduces errors with power $2^{-2b}/6$. Using the results (4.7) and (4.12), the noise power after Step 1 is

$$\sigma_1^2 = 2^{-2b}\left(\frac{1}{3} + \frac{1}{3} \cdot \frac{1}{6} + \frac{1}{3} \cdot \frac{1}{6}\right) = 2^{-2b} \cdot \frac{4}{9}. \tag{4.79}$$

After Step 2, the noise consists of two parts: one from the previous step and the other from the computation of the fast Fourier transform.

$$\sigma_2^2 = 2^{-2b} \cdot \frac{5}{3} + \frac{\sigma_1^2}{N} = 2^{-2b} \cdot \left(\frac{5}{3} + \frac{4}{9N}\right). \tag{4.80}$$

Using the result (4.7) and (4.13), the noise power after Step 3 is

$$\sigma_3^2 = 2^{-2b} \left(\frac{1}{3} + \frac{5}{3} + \frac{4}{9N} + \frac{1}{9N} \cdot \frac{1}{6} \right) = 2^{-2b} \cdot \left(2 + \frac{25}{9N} \right). \tag{4.81}$$

As in (4.80), the noise power after Step 4 is

$$\sigma_4^2 = 2^{-2b} \cdot \frac{5}{3} + \frac{\sigma_3^2}{2N} = 2^{-2b} \cdot \left(\frac{5}{3} + \frac{1}{N} + \frac{25}{18N^2} \right). \tag{4.82}$$

It is clear that the noise power $\sigma_5^2 = N^2 \sigma_4^2$ after Step 5. Assume that the power of quantization error resulting from storing the reference Wigner-Ville distribution is $2^{-2b}/6$. After Step 6, the noise power is

$$\sigma_6^2 = 2^{-2b} \cdot \left(\frac{5}{3} + \frac{1}{6} \cdot \frac{1}{2N} \right). \tag{4.83}$$

Clearly, $\sigma_7^2 = N^2 \sigma_6^2$. Using (4.7) and (4.12), the noise power after Step 8 is

$$\sigma_8^2 = \frac{2^{-2b}}{3} + \mu_7^2 \cdot \sigma_5^2 + \mu_5^2 \cdot \sigma_7^2 = 2^{-2b} \cdot \left(\frac{5N^2}{27} + \frac{13N}{216} + \frac{133}{324} \right). \tag{4.84}$$

After Step 9, the noise power is

$$\sigma_9^2 = 2^{-2b} \cdot \frac{5}{3} + \frac{\sigma_8^2}{2N} = 2^{-2b} \cdot \left(\frac{5N}{54} + \frac{733}{432} + \frac{133}{648N} \right). \tag{4.85}$$

The noise at the output consists of two parts; one is from the noise output at Step 9 and the other is from the scaling of 1/2 in the summations in Step 10. After the scaling in the summations, the power of the noise originated from Step 9 is $1/(2N)$ of its input power, i.e., $\sigma_9^2/(2N)$. To obtain the noise power from the scaling by 1/2 in the summations, we note that the error power of dividing a complex number by 1/2 is $2^{-2b}/4$ as indicated in the paragraph following (4.14). Then, with the assumption of uncorrelated noises, the noise power from adding two samples is $2(2^{-2b}/4)$. With the same procedure as used in deriving (4.21) for the noise output of a radix-2 fast Fourier transform, we can calculate the noise power generated from the scaling in Step 10 by

$$\sigma_d^2 = \sum_{m=0}^{\nu'-1} 2^{(\nu'-m-1)} \cdot \frac{2^{-2b}}{2} \cdot \left(\frac{1}{2} \right)^{2(\nu'-m-1)}$$
$$\cong 2^{-2b} \tag{4.86}$$

157

where $\nu' = \log_2(2N)$ and it is assumed that $2N \gg 1$. With the assumption of uncorrelated noise, we have

$$\sigma_{10}^2 = \frac{\sigma_9^2}{2N} + \sigma_d^2 = 2^{-2b} \cdot \left(\frac{113}{108} + \frac{733}{864N} + \frac{133}{1296N^2} \right). \tag{4.87}$$

Thus, the output noise-to-signal ratio is

$$\frac{\sigma_{10}^2}{\mu_{10}^2} = 2^{-2b} \cdot \left(1356N^2 + \frac{2199}{2}N + 133 \right). \tag{4.88}$$

The above relationship indicates that the output noise-to-signal ratio is approximately proportional to N^2. It is important to point out that the output signal power is linearly proportional to the input signal power as can be seen from the derivation of μ_{10}^2. Thus, the output noise-to-signal ratio degrades as the input signal power decreases. It is also seen that the scaling by N at Step 5 and Step 7 is important. The noise-to-signal ratio would be worse without those scalings.

4.2.3 Discrete Time-Frequency Correlation Function Based Receiver

In this subsection, we evaluate the effects of quantization error on the test statistic along a cut in Doppler using the discrete time-frequency correlation function based receiver (3.42). In this receiver, there are multiple fast Fourier transforms to be performed. Recall that it is important to raise the signal power at the input of a fast Fourier transform as high as possible to achieve a low ratio of the output quantization error power to the output signal power. Therefore, we insert scaling factors between cascading fast Fourier transforms in the receiver to raise the signal power and to maintain a low output noise-to-signal ratio. The placement and the magnitude of these scaling factors are chosen in the manner such that no overflow will result. The arithmetic performed by the receiver (3.42) of Chapter 3 can be described by the following 7-step algorithm.

Step 1. Cross multiply the received samples to form a sequence $\{\tilde{r}(kT_s)\tilde{r}^*(kT_s - nT_s)\}$.

Step 2. Perform N-point fast Fourier transform of the sequence from Step 1, to obtain the time-frequency auto-correlation function of the received samples.

Step 3. Multiply the reference time-frequency correlation function $\hat{\phi}_{\tilde{s}}[nT_s, m/(NT_s)]$ by $\exp[j2\pi mp/(2N)]$.

Step 4. Cross multiply the result of Step 2 and Step 3.

Step 5. Sum over the frequency arguments of the sequence resulting from Step 4.

Step 6. Multiply the sequence resulting from Step 5 by $2N$.

Step 7. Perform $2N$-point fast Fourier transform over the time arguments of the sequence resulting from Step 6.

A block diagram describing the computations in this algorithm is given in Figure 4.7. The above algorithm assumes that the reference time-frequency correlation function is readily available and calculation in real time is not required. However, only minor modifications of the following analysis are needed if this assumption is not satisfied.

The signal power $\mu_1^2 = 1/9$ after step 1, and $\mu_2^2 = 1/(9N)$ after Step 2. To examine whether it is possible to introduce scaling after Step 2 without causing overflow, we need to know the upper bound of the magnitude of the output of Step 2. Using the Cauchy-Schwarz inequality, we have the greatest magnitude of the output from Step 2

$$\left| \frac{1}{N} \sum_k \tilde{r}(kT_s)\tilde{r}^*(kT_s - nT_s) \exp\left[-j2\pi\frac{mk}{N}\right] \right| \le \frac{1}{N^2} \sum_k |\tilde{r}(kT_s)|^2 \qquad (4.89)$$

where the factor $1/N$ is included to reflect the fact that the fast Fourier transform introduces a scaling factor of $1/2$ at every butterfly. By the assumption (4.59) it is seen that the maximum magnitude of the output of Step 2 is $1/3$. Therefore, we can raise the signal power by introducing a scaling factor of 3 without causing overflow. On the other hand, this amount of scaling may not be significant enough to justify the additional hardware
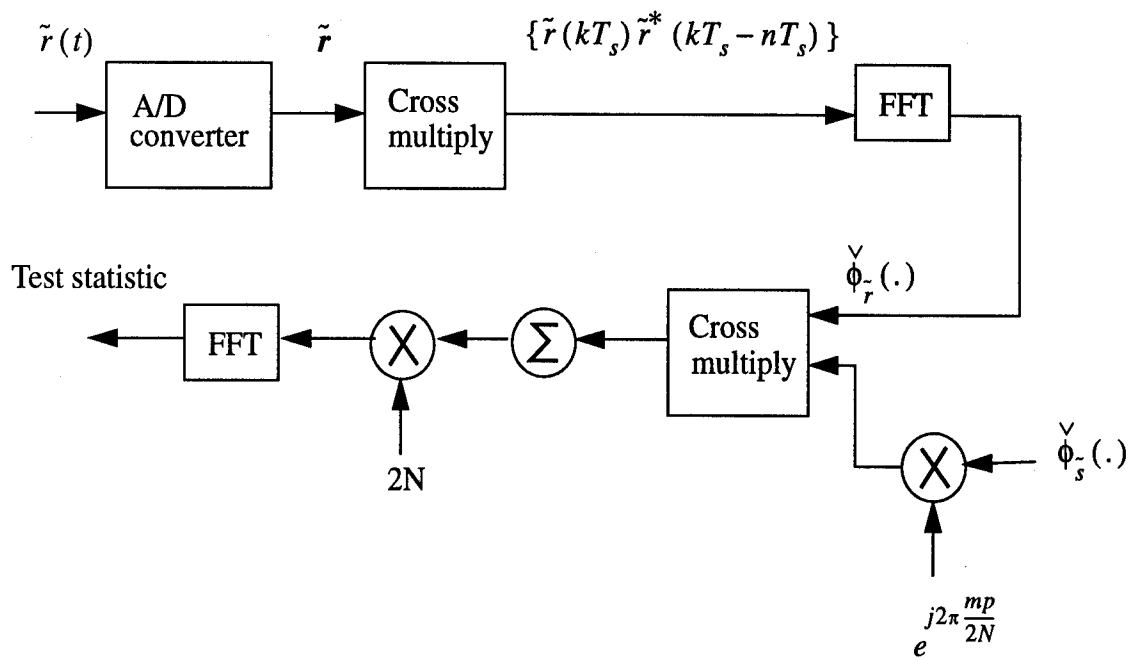
(a) Computational flow graph
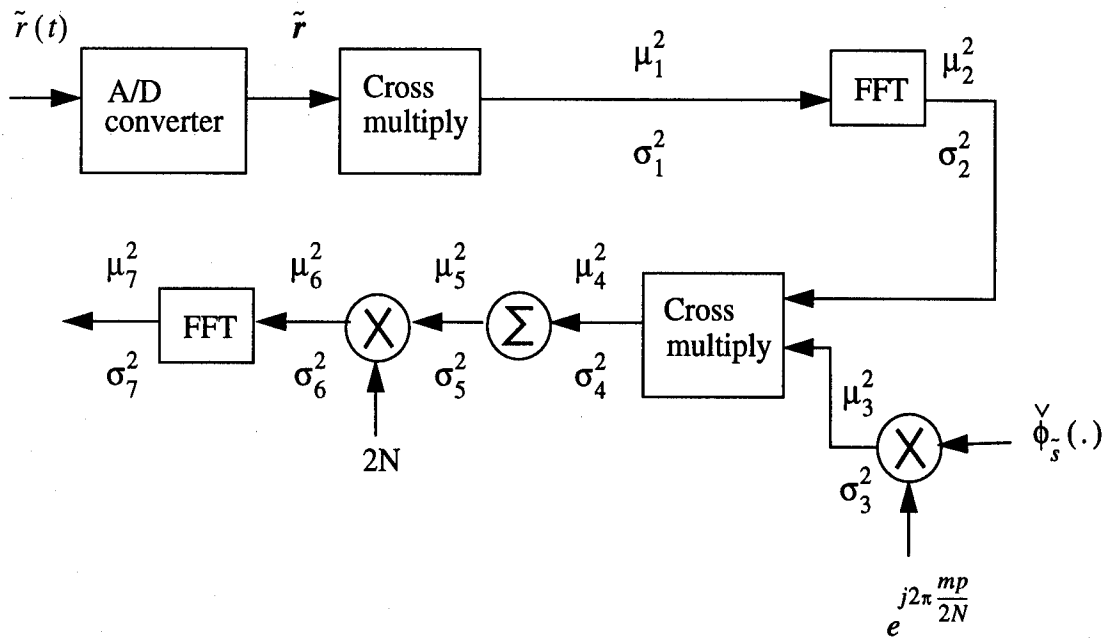
(b) Signal and noise power propagation

Figure 4.7: Computational flow graph of the discrete time-frequency correlation function based receiver

160

complexity. Therefore, we choose to omit scaling at this point. The output signal power of Step 3 is the same as the input, which is $1/(9N)$, since the magnitude of $\exp[j2\pi mp/N]$ is unity. Since the power of the reference time-frequency correlation function is the same as μ_2^2, the signal power after Step 4 is $\mu_4^2 = \mu_2^2 \cdot \mu_3^2 = 1/(81N^2)$. The summation in Step 5 is calculated in the same manner as that used in Step 10 of the previous subsection to prevent overflow. The output signal power after Step 5 is $1/(2N)$ times the input as a result of the scaling factor of $1/2$ at each summation pair. Therefore, $\mu_5^2 = 1/(162N^3)$. The greatest magnitude after Step 5 can be obtained by using the Cauchy-Schwarz inequality

$$\left| \frac{1}{2N} \sum_m \check{\phi}_{\tilde{r}}\left(nT_s, \frac{m}{NT_s}\right) \check{\phi}_{\tilde{s}}^*\left(nT_s, \frac{m}{NT_s}\right) \exp\left[j2\pi\frac{mp}{2N}\right] \right|^2$$

$$\leq \left\{ \frac{1}{2N} \sum_m \left| \check{\phi}_{\tilde{r}}\left(nT_s, \frac{m}{NT_s}\right) \right|^2 \right\} \left\{ \frac{1}{2N} \sum_l \left| \check{\phi}_{\tilde{s}}\left(nT_s, \frac{l}{NT_s}\right) \right|^2 \right\} \qquad (4.90)$$

where the factor $1/(2N)$ is included on the left-hand to reflect the fact that the summations are performed with a scaling factor of $1/2$ added. Consider the term in the first pair of braces on the right-hand side of (4.90)

$$\frac{1}{2N} \sum_m \left| \check{\phi}_{\tilde{r}}\left(nT_s, \frac{m}{NT_s}\right) \right|^2$$

$$= \frac{1}{2N} \sum_m \left| \frac{1}{N} \sum_k \tilde{r}(kT_s)\tilde{r}^*(kT_s - nT_s) \exp\left(-j2\pi\frac{mk}{N}\right) \right|^2$$

$$= \frac{1}{2N^3} \sum_m \sum_k \sum_p \tilde{r}(kT_s)\tilde{r}^*(kT_s - nT_s)\tilde{r}^*(pT_s)\tilde{r}(pT_s - nT_s) \exp\left[-j2\pi\frac{m(k-p)}{N}\right]$$

$$= \frac{1}{2N^2} \sum_k |\tilde{r}(kT_s)|^2 |\tilde{r}(kT_s - nT_s)|^2 \qquad (4.91)$$

where the factor $1/N$ has been included to reflect the fact that $1/2$ is included in each butterfly of the fast Fourier transform. By the previous assumption, $|\tilde{r}(kT_s)| \leq 1$, for all k; therefore $|\tilde{r}(kT_s)|^2 \leq 1$, for all k. It follows that

$$\frac{1}{2N} \sum_m \left| \check{\phi}_{\tilde{r}}\left(nT_s, \frac{m}{NT_s}\right) \right|^2 = \frac{1}{2N^2} \sum_k |\tilde{r}(kT_s)|^2 |\tilde{r}(kT_s - nT_s)|^2 \leq \frac{1}{2N}. \qquad (4.92)$$

The same conclusion can be drawn about the term in the second pair of braces of the right-hand side of (4.90). Therefore, the greatest magnitude of the output after Step 5 is given

161

by

$$\left| \frac{1}{2N} \sum_m \check{\phi}_{\tilde{r}}\left(nT_s, \frac{m}{NT_s}\right) \check{\phi}_{\tilde{s}}^*\left(nT_s, \frac{m}{NT_s}\right) \exp\left[j2\pi\frac{mp}{2N}\right] \right| \leq \frac{1}{2N}. \qquad (4.93)$$

With (4.93), it is clear that we may multiply a factor of $2N$ to the output of Step 5 to raise the signal power without causing overflow. Then, we have $\mu_6^2 = 4N^2\mu_5^2 = 2/(81N)$. The fast Fourier transform in Step 7 is a $2N$-point transform. Thus, Step 7 reduces the output signal power to $1/(2N)$ times the input, and $\mu_7^2 = 1/(81N^2)$. On the other hand, we can also apply the result (4.70) to the relationship (3.42) to obtain an estimate of the output signal power by taking into account the scaling involved. The scaling involved in the conventional receiver was analyzed in the previous subsection. The scaling in the time-frequency correlation function based receiver can be examined in an analogous manner to that given for Step 10 of the previous subsection. The result shows that the output signal power is in the interval $[1/(648N^2), 1/(648N)]$. Since $1/(81N^2)$ is in the interval $[1/(648N^2), 1/(648N)]$ for $N \geq 8$, we will use $\mu_7 = 1/(81N^2)$ as the estimate of the output signal power in the following analysis.

Next, we consider the quantization error. As before, the initial quantization error due to analog-to-digital conversion of the received samples is assumed to have power $\sigma_{\tilde{r}}^2 = 2^{-2b}/6$. It will also be assumed that the finite register length storage of the reference correlation function and the coefficients $\exp(j2\pi mp/N)$ used in Step 3 introduces errors of power $2^{-2b}/6$. Using the results (4.7) and (4.12), the noise power after Step 1 is

$$\sigma_1^2 = 2^{-2b} \cdot \left(\frac{1}{3} + \frac{1}{3}\cdot\frac{1}{6} + \frac{1}{3}\cdot\frac{1}{6}\right) = 2^{-2b}\cdot\frac{4}{9}. \qquad (4.94)$$

After Step 2, the noise consists of two parts; one from the previous step and the other from the computation of the fast Fourier transform.

$$\sigma_2^2 = 2^{-2b} \cdot \frac{5}{3} + \frac{\sigma_1^2}{N} = 2^{-2b} \cdot \left(\frac{5}{3} + \frac{4}{9N}\right). \qquad (4.95)$$

Using (4.7) and (4.13), the noise power after Step 3 is

$$\sigma_3^2 = \left|\exp(j2\pi\frac{mp}{N})\right| \cdot \frac{2^{-2b}}{6} + \frac{1}{9N}\cdot\frac{2^{-2b}}{6} + \frac{2^{-2b}}{3} = 2^{-2b} \cdot \left(\frac{1}{2} + \frac{1}{54N}\right) \qquad (4.96)$$

162

where $1/(9N)$ is the power of the reference sequence. Using (4.7) and (4.12), the noise power after Step 4 is

$$\sigma_4^2 = \frac{2^{-2b}}{3} + \mu_2^2 \cdot \sigma_3^2 + \frac{1}{9N} \cdot \sigma_2^2 = 2^{-2b} \cdot \left(\frac{1}{3} + \frac{13}{54N} + \frac{25}{486N^2} \right). \tag{4.97}$$

The noise power after Step 5 can be obtained in a similar manner as that in deriving σ_{10}^2 in the previous subsection:

$$\sigma_5^2 = \frac{\sigma_4^2}{2N} + 2^{-2b} = 2^{-2b} \cdot \left(1 + \frac{1}{6N} + \frac{13}{108N^2} + \frac{50}{972N^3} \right). \tag{4.98}$$

The multiplication by $2N$ in Step 6 increases the noise power to $\sigma_6^2 = 4N^2 \sigma_5^2$. The output noise is given by

$$\sigma_7^2 = 2^{-2b} \cdot \frac{5}{3} + \frac{\sigma_6^2}{2N} = 2^{-2b} \cdot \left(2N + 2 + \frac{13}{54N} + \frac{50}{486N^2} \right). \tag{4.99}$$

Thus, the output noise-to-signal ratio is

$$\frac{\sigma_7^2}{\mu_7^2} = 2^{-2b} \cdot \left(162N^3 + 162N^2 + \frac{39}{2}N + \frac{25}{3} \right). \tag{4.100}$$

The above relationship indicates that the output noise-to-signal ratio is proportional to N^3. It is important to point out that the output signal power is linearly proportional to the input signal power as can be seen from the derivation of μ_7^2. Thus, the output noise-to-signal ratio degrades as the input signal power decreases. It can also be seen that the scaling by $2N$ at Step 6 is important. Without the scaling the output noise-to-signal ratio would be worse.

4.3   Simulation Results

To verify the theoretical results (4.75), (4.88), and (4.100), we perform computer simulations using two types of inputs for each of the receivers considered. The first type of input is sequences of random complex numbers. The second type of input is sequences of samples obtained from sampling a *lfm* signal. The simulations are performed on a *SUN Sparc* workstation using the software package *MATLAB*. Due to limitations on computation speed, the

input sequences are confined to $N = 8$ to $N = 256$, and $1024/N$ runs are carried out for each N, e.g., 128 runs are carried out for $N = 8$. In each run for a particular N, the input sequence of length N is first generated and then the test statistic in the forms of (4.1), (3.22), and (3.42) are computed. The computation of the test statistic is performed both in double precision floating-point arithmetic and in fixed-point arithmetic. The results obtained in double precision floating-point arithmetic are considered to be accurate and are used to determine the experimental output signal power. The wordlength used in the fixed-point arithmetic is $b = 16$ bits plus one sign bit. The magnitude squared difference between the fixed-point and floating-point results are used to determine the experimental quantization error power. The experimental noise-to-signal ratio is then averaged over all runs for that particular N.

In the generation of the input sequences, the noise in the received samples is assumed to be Gaussian distributed with zero mean and variance $1/6$. For simplicity, we also assume that the delay and Doppler in the target return are zero. It should be emphasized that the assumption about the noise is not vital in the analyses since we are only concerned with the effects of quantization and finite-precision arithmetic and not the noise performance of the receiver.

Random Number Sequence

In the first set of experiments, we used as reference a sequence of uncorrelated random complex numbers whose real and imaginary parts are uniformly distributed over $(-1/\sqrt{2}, 1/\sqrt{2})$. The above sequence plus the Gaussian noise samples sequence with the sum truncated to the interval $(-1/\sqrt{2}, 1/\sqrt{2})$ is used as the received samples. The procedure of obtaining the experimental noise-to-signal ratio as described in the beginning of this section is then carried out for the conventional matched filter based receiver. The result shown in Figure

4.8 is obtained by averaging the noise-to-signal ratios of every cut in Doppler of the test statistic. In other words, the result is obtained as an average over the entire domain of the test statistic. The result confirms the theoretical prediction. The result shown in Figure 4.9 is obtained from the cut of the statistic at the hypothesized delay $\tau_H = 0$. It is clear that the noise-to-signal ratio is much lower than the average and is lower than the theoretical prediction. However, the noise-to-signal ratio still increases roughly proportional to N^2, but a little milder, as predicted. Due to limitations on computation speed, we will only simulate over the cut of the test statistic at $\tau_H = 0$, but not generate every cut of the statistic and obtain the average in the following experiments. The experimental and theoretical noise-to-signal ratios are plotted in Figure 4.10 and Figure 4.11 for the receivers (3.22) and (3.42), respectively. The simulated noise-to-signal ratios increase with the number of samples a little milder than the theoretical predictions. The discrepancy can be explained from the following observations. First, the simulations were performed over the cut of the test statistic where the peak of the ambiguity function occurs. On this cut of the test statistic, it appears that the signal has higher power than predicted, i.e., the signal samples have higher variance than the average. Secondly, the theoretical output noise-to-signal ratios were derived based on the assumptions about the properties of the signal samples and quantization errors. Especially, the quantization errors were assumed to be uncorrelated from sample to sample. However, it appears that the quantization errors are mildly correlated in the simulations. Nonetheless, in such cases the theoretical results still provide good guidelines to the output noise-to-signal ratios.

Linear *fm* rectangular pulse

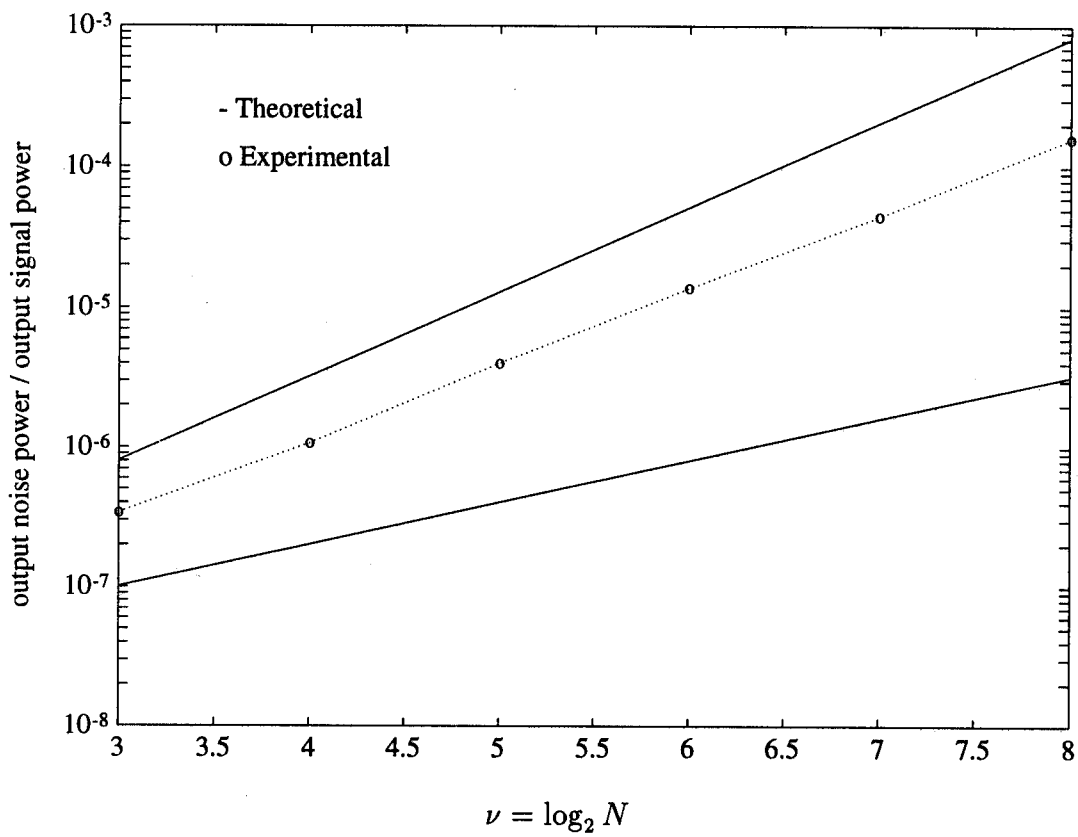In the second set of experiments, we used as reference a sequence of samples obtained

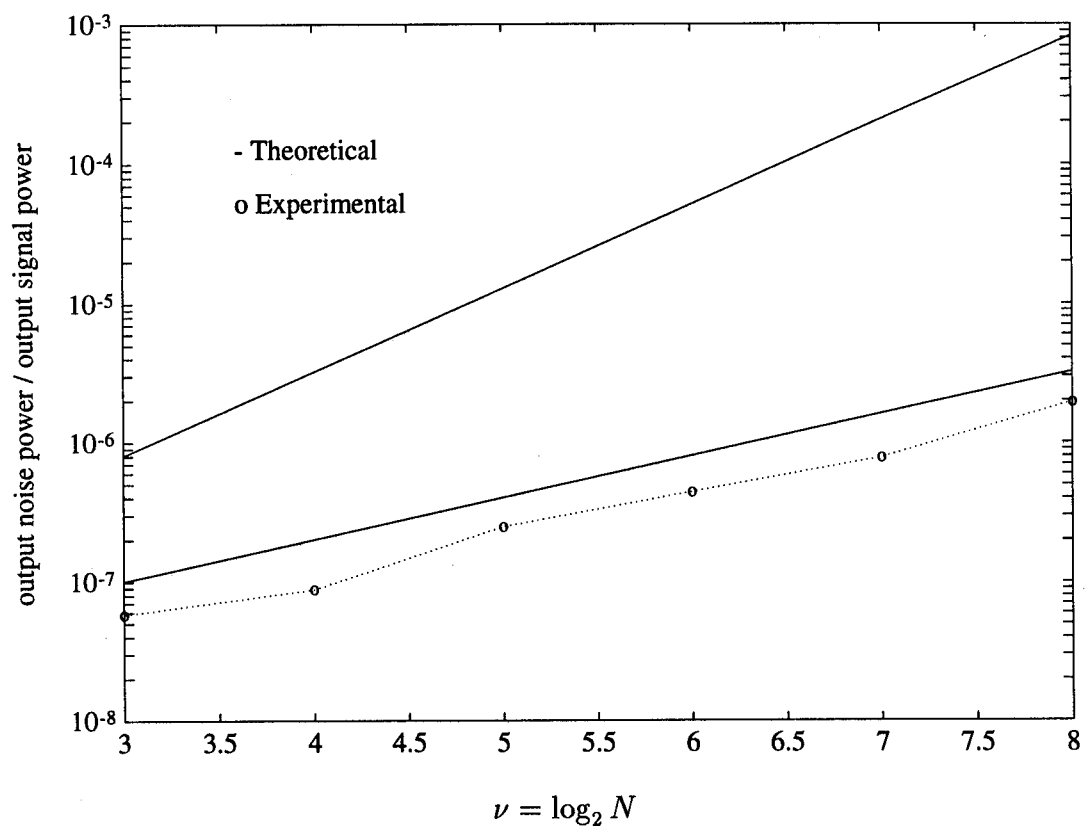Figure 4.8: Noise-to-signal ratio of the conventional matched filter based receiver

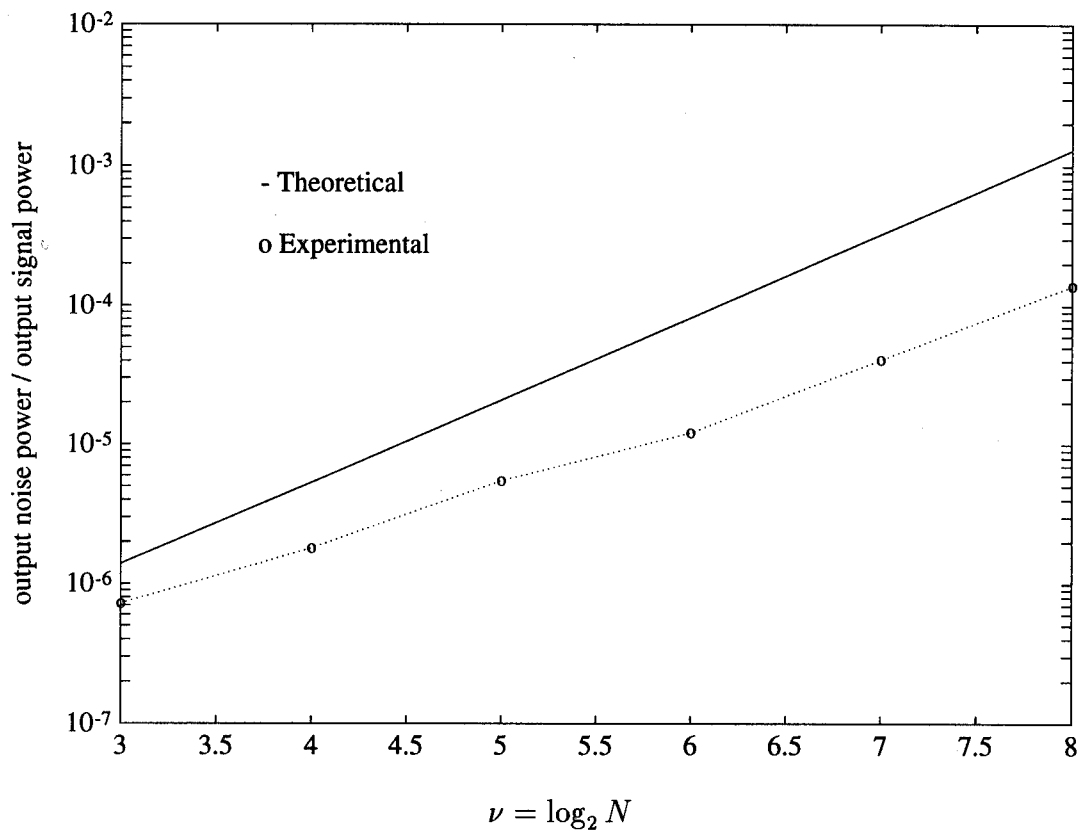Figure 4.9: Noise-to-signal ratio of the conventional matched filter based receiver

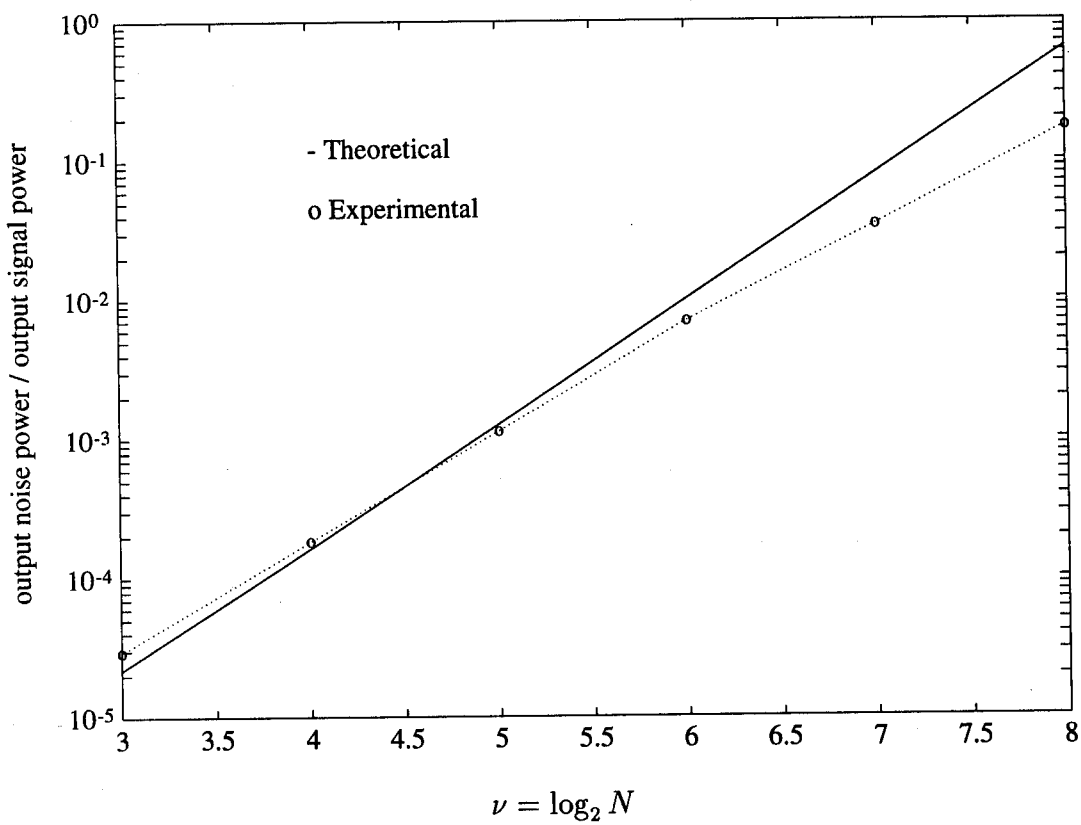Figure 4.10: Noise-to-signal ratio of the general form Wigner-Vile distribution based receiver

Figure 4.11: Noise-to-signal ratio of the time-frequency correlation function based receiver

169

from sampling the signal

$$\tilde{s}(t) = \frac{1}{\sqrt{2}}\text{rect}\left(\frac{t - 0.8}{0.6}\right)\exp\left(j\frac{\pi}{2}t^2\right). \tag{4.101}$$

The sampling is done in the interval $[0, 1.6)$. The sampling rates $1/T_s$ are $2^3/1.6, 2^4/1.6,$ $\cdots, 2^8/1.6$. The same sequence plus the noise with the sum truncated to the interval $(-1/\sqrt{2}, 1/\sqrt{2})$ is used as the received samples. The experimental and theoretical noise-to-signal ratios are plotted in Figures 4.12 to 4.14 for the receivers (4.1), (3.22), and (3.42), respectively. In each receiver, the simulated noise-to-signal ratios increase with the number of samples a little milder than the theoretical predictions. The reason for the discrepancy should be the same as that for the previous case using random complex numbers as inputs.

4.4   Discussion

In this chapter, we dealt with the quantization error in the conventional matched filter based receiver, the general form Wigner-Ville distribution based receiver, and the time-frequency correlation function based receiver, as given by (4.1), (3.22), and (3.42), respectively.

In Section 4.1, we reviewed the derivation of the mean-square magnitude of the output quantization error in calculating radix-2 decimation-in-time fast Fourier transforms. Special attention was paid to whether the coefficients in the fast Fourier transform algorithm are from a look-up table or from in-place calculation in the transform algorithm. This distinction is only recognized in the literature, but not analyzed accordingly. It is shown that the result on noise-to-signal ratio due to coefficient quantization found in the literature is for the case where the coefficients are from a look-up table. For the case where the coefficients are obtained from in-place calculation, it is shown analytically in this work that the effect of quantization error is much worse.
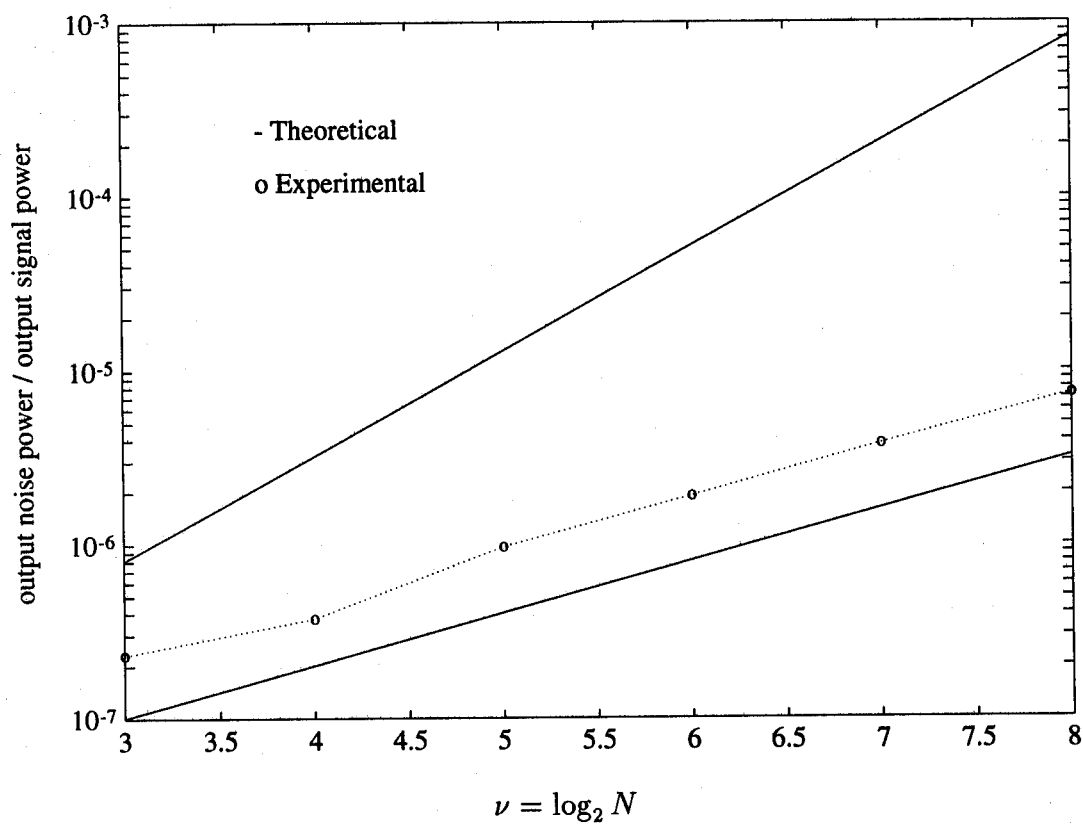
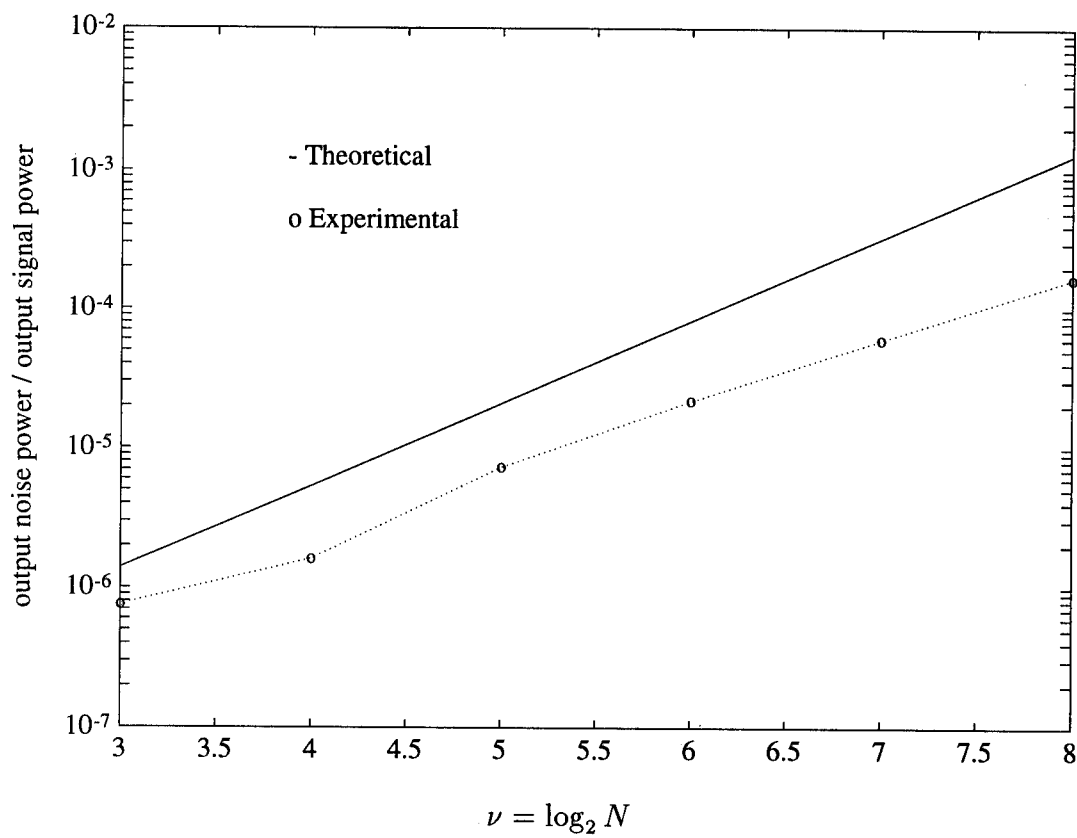Figure 4.12: Noise-to-signal ratio of the conventional matched filter based receiver

Figure 4.13: Noise-to-signal ratio of the general form Wigner-Ville distribution based receiver
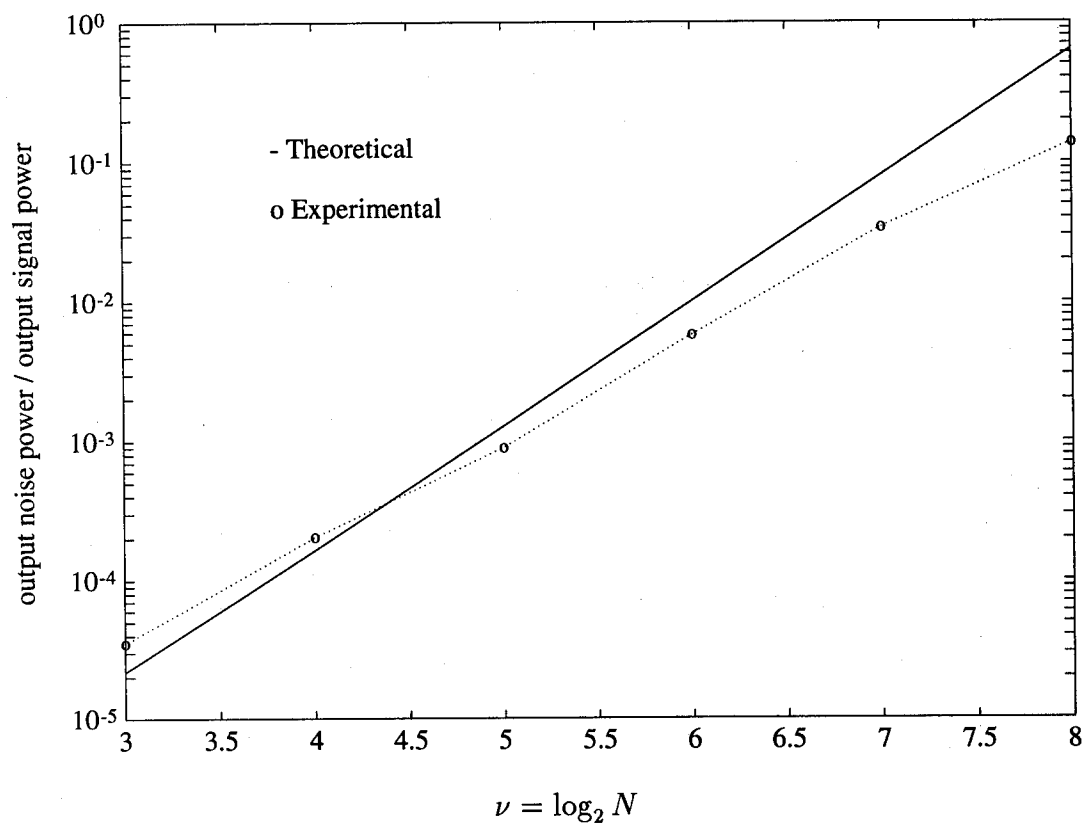
Figure 4.14: Noise-to-signal ratio of the time-frequency correlation function based receiver

In Section 4.2, we examined the effects of quantization error on the receivers. The ratios of the output quantization noise power to the output signal power were obtained. In order to obtain these results we also derived the upper and lower bounds of the mean-square magnitude of the discrete ambiguity function. The output noise-to-signal ratios were then verified by computer simulations using two types of input. It was shown that using a random number sequence as input, the simulated noise-to-signal ratio averaged over the entire domain of the test statistic is consistent with the theoretical prediction for the conventional receiver case. Due to computational limitations, the rest of the simulations were performed over one cut of the test statistic. In such cases the noise-to-signal ratios increase with the number of samples more moderately than predicted. The discrepancy can be explained from the following observations. First, the simulations were performed over the cut of the test statistic where the peak of the ambiguity function occurs. On this cut of the test statistic, it appears that the signal has higher power than predicted, i.e., the signal samples have higher variance than the average. Secondly, the theoretical output noise-to-signal ratios were derived based on the assumptions about the properties of the signal samples and quantization errors. Especially, the quantization errors were assumed to be uncorrelated from sample to sample. However, it appears that the quantization errors are mildly correlated in the simulations. Nonetheless, in such cases the theoretical results still provide good guidelines to the output noise-to-signal ratios. Finally, in the attempt to raise the signal power so as to improve the output noise-to-signal ratio, we introduced multiplication factors in the calculation of the test statistic. The amount of these factors and their positions were chosen in such a way that no overflow would occur.

Chapter 5

Conclusions

In this work, we studied issues related to the application of time-frequency distributions in radar detection and parameter estimation problems. The analysis was from a receiver structure standpoint.

To facilitate digital signal processing, we studied various forms of the discrete ambiguity function and the discrete Wigner-Ville distribution in both the time-domain and the frequency-domain. Connection between the discrete ambiguity function and the optimal radar receiver was established. The relationships between the discrete ambiguity function and the discrete Wigner-Ville distribution and their continuous counterparts were also examined. Sampling criteria to avoid aliasing were analyzed. It was concluded that the discrete-time samples used in generating either time-frequency distribution have to be obtained at twice the Nyquist rate to prevent aliasing. This sampling criteria can be satisfied through physically sampling the signal at twice the Nyquist rate or via interpolation. In generating the frequency-domain representation of either time-frequency distribution, the sampling rate has to be twice the Nyquist rate and the sampling process has to last twice as long as the signal duration. New procedures to recover the continuous time-frequency distributions from their discrete counterparts were given. The procedures are simpler than the ones previously derived. They can be used as long as the sampling rate is greater than the Nyquist rate and

the observation interval is longer than the signal duration. The restriction is that they can be used to recover only those portions of the time-frequency distributions that are alias-free.

Using the analysis of the discrete Wigner-Ville distribution and the discrete ambiguity function, we derived the criteria for the realization of the optimum discrete radar receiver based on the discrete Wigner-Ville distribution and on the discrete time-frequency correlation function. It was shown that correlation of the discrete Wigner-Ville distributions of the received samples with the reference Wigner-Ville distribution can be used to generate the test statistic for optimum detection and estimation for a Gaussian noise environment if the prescribed sampling criteria are satisfied. Matched filtering the discrete time-frequency correlation functions of the received samples with the reference time-frequency correlation function can also generate the test statistic. Schemes to reduce the requirement on the sampling rate and to reduce the requirement on the duration of the sampling process were also devised. The applications of the radar receivers in the alternative form were illustrated by means of two examples. It was shown that the Wigner-Ville distribution based receiver is useful when the transmitted signal is unknown such that matched filtering is not feasible. In this case, the Wigner-Ville distribution of the received signal can be used to extract information about the transmitted signal. It was also shown that a time-frequency correlation function based receiver is useful for estimating the instantaneous frequency of the target return for a broad class of transmitted signals.

Finally, we considered the quantization error in digital implementation of the conventional matched filter based receiver, the Wigner-Ville distribution based receiver, and the time-frequency correlation function based receiver. The derivation of the mean-square magnitude of the output quantization error present during calculation of the radix-2 decimation in time fast Fourier transform was reviewed. Special attention was paid to whether the coefficients in the transform are from look-up table or from in-place calculation in the transform algorithm. The results on coefficient quantization found in the literature are for the case where the

coefficients are from a look-up table. For the case where the coefficients are obtained from in-place calculation the effect of quantization error is much more severe. This result was only recognized previously, but not analyzed accordingly. We derived the output quantization noise to signal ratio for each receiver. In the process we also derived the upper and lower bounds of the mean-square magnitude of the discrete ambiguity function. In an attempt to raise the signal power so as to improve the output noise-to-signal ratio, multiplication factors were introduced in the calculation of the test statistic. These factors were chosen and placed at positions such that no overflow would occur.

The output noise-to-signal ratios were verified by computer simulations using two types of input. It was shown that using a random number sequence as input, the simulated noise-to-signal ratio, averaged over the entire domain of the test statistic, is consistent with the theoretical prediction for the case of a conventional matched filter based receiver. Due to computational limitations, the rest of the simulations were performed over one cut of the test statistic. In these cases the noise-to-signal ratios increase more moderately with the number of samples than predicted. Nonetheless, in such cases the theoretical results still provide useful guidelines to the output noise-to-signal ratios.

Appendix A

Some Useful Properties of Discrete-Time and Discrete-Frequency Signals

In the following we discuss a few properties of signals that can be assumed to be *essentially* limited in both time and frequency. First, we consider the reconstruction of the continuous signals from their samples in the time and frequency domains. We then consider the relationships between inner products of continuous signals and discrete signals.

A.1   Time-domain interpolation

Assume that a complex signal $\tilde{g}(t)$, with its Fourier transform $\tilde{G}(f)$, is essentially duration and frequency limited to $[0, T)$ and $(-B, B)$, respectively. It follows that

$$\tilde{G}(f) = \begin{cases} T_s \sum_{k=-\infty}^{\infty} \tilde{g}(kT_s) \exp(-j2\pi f k T_s), & \text{for } |f| < \frac{1}{2T_s} \\ 0, & \text{otherwise} \end{cases} \tag{A.1}$$

where $1/T_s \geq 2B$. The infinite summation in the above relation is used with the understanding that zeros can be appended to the finite sample sequence. Also, instead of requiring $|f| \leq B$, we have allowed $1/(2T_s)$ to be the bound since the spectral components of $\tilde{g}(t)$ are essentially limited to $(-B, B)$ and approximately zero outside. Let $\tilde{g}_{f_D}(t)$ be a fre-

quency shifted version of $\tilde{g}(t)$, such that $\tilde{g}_{f_D}(t) = \tilde{g}(t)\exp(j2\pi f_D t)$ and its Fourier transform $\tilde{G}_{f_D}(f) = \tilde{G}(f - f_D)$. Since

$$\tilde{G}(f - f_D) = T_s \sum_{k=-\infty}^{\infty} \tilde{g}(kT_s)\exp[-j2\pi(f - f_D)kT_s], \quad \text{for } |f - f_D| < \frac{1}{2T_s} \quad (A.2)$$

and $\tilde{G}(f - f_D) = 0$, otherwise, we have

$$\tilde{G}_{f_D}(f) = \begin{cases} T_s \sum_{k=-\infty}^{\infty} \tilde{g}(kT_s)\exp[-j2\pi(f - f_D)kT_s], & \text{for } |f - f_D| < \frac{1}{2T_s} \\ 0, & \text{otherwise.} \end{cases} \quad (A.3)$$

Taking the inverse Fourier transform of both sides of the above relation, we have the expected result, namely,

$$\tilde{g}_{f_D}(t) = \exp(j2\pi f_D t)\left[\sum_{k=-\infty}^{\infty} \tilde{g}(kT_s)\frac{\sin\pi(t/T_s - k)}{\pi(t/T_s - k)}\right]. \quad (A.4)$$

However, if $1/T_s > 2(B + |f_D|)$, or equivalently $|f_D| < (1/T_s - 2B)/2$, can be assured, we can rewrite (A.3) as

$$\tilde{G}_{f_D}(f) = \begin{cases} T_s \sum_{k=-\infty}^{\infty} \tilde{g}(kT_s)\exp[-j2\pi(f - f_D)kT_s], & \text{for } |f| < \frac{1}{2T_s} \\ 0, & \text{otherwise.} \end{cases} \quad (A.5)$$

Taking the inverse Fourier transform of both sides of the above relation, we find that samples of $\tilde{g}_{f_D}(t)$ can be used directly and

$$\tilde{g}_{f_D}(t) = \sum_{k=-\infty}^{\infty} \tilde{g}(kT_s)\exp(j2\pi f_D kT_s)\frac{\sin\pi(t/T_s - k)}{\pi(t/T_s - k)}. \quad (A.6)$$

A.2 Frequency-domain interpolation

Next, let $\tilde{h}(t)$ be a train of periodic repetitions of $\tilde{g}(t)$ with period $T_p \geq T$, i.e.,

$$\tilde{h}(t) = \sum_{k=-\infty}^{\infty} \tilde{g}(t - kT_p). \quad (A.7)$$

It follows that $\tilde{h}(t)$ can be expanded in a Fourier series, which in this case reads

$$\tilde{h}(t) = \frac{1}{T_p}\sum_{l=-\infty}^{\infty} \tilde{G}\left(\frac{l}{T_p}\right)\exp\left(j2\pi\frac{l}{T_p}t\right). \quad (A.8)$$

179

We can then write

$$\tilde{g}(t) = \begin{cases} \frac{1}{T_p} \sum_{l=-\infty}^{\infty} \tilde{G}\left(\frac{l}{T_p}\right) \exp\left(j2\pi\frac{l}{T_p}t\right), & \text{for } |t - T/2| < T_p/2 \\ 0, & \text{otherwise.} \end{cases} \tag{A.9}$$

In (A.9) note that we have allowed $|t - T/2| < T_p/2$, instead of imposing the more stringent condition $|t - T/2| < T/2$, since $\tilde{g}(t)$ is limited to the time interval $(0, T)$ and zero outside. Let $\tilde{g}_\tau(t)$, with its Fourier transform $\tilde{G}_\tau(f)$, be a time shifted version of $\tilde{g}(t)$, such that $\tilde{g}_\tau(t) = \tilde{g}(t - \tau)$. Since

$$\tilde{g}(t - \tau) = \frac{1}{T_p} \sum_{l=-\infty}^{\infty} \tilde{G}\left(\frac{l}{T_p}\right) \exp\left[j2\pi\frac{l}{T_p}(t - \tau)\right], \quad \text{for } \left|t - \tau - \frac{T}{2}\right| < \frac{T_p}{2} \tag{A.10}$$

and $\tilde{g}(t - \tau) = 0$, otherwise, we have

$$\tilde{g}_\tau(t) = \begin{cases} \frac{1}{T_p} \sum_{l=-\infty}^{\infty} \tilde{G}\left(\frac{l}{T_p}\right) \exp\left[j2\pi\frac{l}{T_p}(t - \tau)\right], & \text{for } |t - \tau - T/2| < T_p/2 \\ 0, & \text{otherwise.} \end{cases} \tag{A.11}$$

Taking the Fourier transform of both sides of the above relation, we have the expected result, namely,

$$\tilde{G}_\tau(f) = \exp(-j2\pi f\tau)\left\{ \sum_{l=-\infty}^{\infty} \tilde{G}\left(\frac{l}{T_p}\right) \exp\left[-j\pi\left(f - \frac{l}{T_p}\right)T\right] \frac{\sin\pi(fT_p - l)}{\pi(fT_p - l)} \right\}. \tag{A.12}$$

However, if $T_p > (T + |\tau|)$, or equivalently $|\tau| < (T_p - T)$, can be assured, we can rewrite (A.11) as

$$\tilde{g}(t - \tau) = \begin{cases} \frac{1}{T_p} \sum_{l=-\infty}^{\infty} \tilde{G}\left(\frac{l}{T_p}\right) \exp\left[j2\pi\frac{l}{T_p}(t - \tau)\right], & \text{for } |t - T/2| < T_p/2 \\ 0, & \text{otherwise.} \end{cases} \tag{A.13}$$

Taking the Fourier transform of both sides of the above relation, we find that samples of $\tilde{G}_\tau(f)$ can be used directly and

$$\begin{aligned} \tilde{G}_\tau(f) &= \sum_{l=-\infty}^{\infty} \left[\tilde{G}\left(\frac{l}{T_p}\right) \exp\left(-j2\pi\frac{l}{T_p}\tau\right)\right] \exp\left[-j\pi\left(f - \frac{l}{T_p}\right)T\right] \\ &\quad \cdot \frac{\sin\pi(fT_p - l)}{\pi(fT_p - l)}. \end{aligned} \tag{A.14}$$

180

A.3 Inner Product

In the following we discuss the properties of the inner product of two vectors of signal samples. Assume that the two signals $g_1(t)$ and $g_2(t)$ are both *essentially* limited in time to $[0, T)$ and in frequency to $(-B, B)$. Also, assume that N samples are obtained for each signal. Denote the vectors formed by the samples of $g_1(t)$ and $g_2(t)$ by $\tilde{g}_1$ and $\tilde{g}_2$, respectively.

When $1/T_s \geq 2B$, the inner product of $\tilde{g}_1$ and $\tilde{g}_2$ is equal to $1/T_s$ times the inner product of $\tilde{g}_1(t)$ and $\tilde{g}_2(t)$. This can be shown by using the interpolation formula:

$$
\begin{aligned}
&\int_{-\infty}^{\infty} \tilde{g}_1(t)\tilde{g}_2^*(t)dt \\
&= \int_{-\infty}^{\infty} \left\{ \sum_{k=-\infty}^{\infty} \tilde{g}_1(kT_s)\frac{\sin \pi(t/T_s - k)}{\pi(t/T_s - k)} \right\} \left\{ \sum_{n=-\infty}^{\infty} \tilde{g}_2^*(nT_s)\frac{\sin \pi(t/T_s - n)}{\pi(t/T_s - n)} \right\} dt \\
&= \sum_{k=-\infty}^{\infty} \sum_{n=-\infty}^{\infty} \tilde{g}_1(kT_s)\tilde{g}_2^*(nT_s) \int_{-\infty}^{\infty} \frac{\sin \pi(t/T_s - k)}{\pi(t/T_s - k)}\frac{\sin \pi(t/T_s - n)}{\pi(t/T_s - n)}dt \\
&= T_s \sum_{k=-\infty}^{\infty} \tilde{g}_1(kT_s)\tilde{g}_2^*(kT_s)
\end{aligned}
\tag{A.15}
$$

where the last step follows from the orthogonality of the two sinc functions.

Denote the Fourier transforms of $g_1(t)$ and $g_2(t)$ by $G_1(t)$ and $G_2(t)$, respectively. Also, denote the discrete Fourier transforms of $\tilde{g}_1$ and $\tilde{g}_2$ by $\hat{G}_1$ and $\hat{G}_2$, respectively. Using a similar procedure, it can be shown that the inner product of $\tilde{G}_1$ and $\tilde{G}_2$ is equal to NT_s times that of $\tilde{G}_1(f)$ and $\tilde{G}_2(f)$, when $N \geq T/T_s$. Specifically,

$$
\begin{aligned}
&\int_{-\infty}^{\infty} \tilde{G}_1(f)\tilde{G}_2^*(f)df \\
&= \int_{-\infty}^{\infty} \left\{ \sum_{k=-\infty}^{\infty} \tilde{G}_1\left(\frac{k}{NT_s}\right) \frac{\sin \pi(fNT_s - k)}{\pi(fNT_s - k)} \right\} \\
&\quad \cdot \left\{ \sum_{l=-\infty}^{\infty} \tilde{G}_2^*\left(\frac{l}{NT_s}\right) \frac{\sin \pi(fNT_s - l)}{\pi(fNT_s - l)} \right\} dt \\
&= \sum_{k=-\infty}^{\infty} \sum_{l=-\infty}^{\infty} \tilde{G}_1\left(\frac{k}{NT_s}\right) \tilde{G}_2^*\left(\frac{l}{NT_s}\right) \int_{-\infty}^{\infty} \frac{\sin \pi(fNT_s - k)}{\pi(fNT_s - k)}\frac{\sin \pi(fNT_s - l)}{\pi(fNT_s - l)}dt \\
&= \frac{1}{NT_s} \sum_{k=-\infty}^{\infty} \tilde{G}_1\left(\frac{k}{NT_s}\right) \tilde{G}_2^*\left(\frac{k}{NT_s}\right).
\end{aligned}
\tag{A.16}
$$

From the generalized Parseval's theorem, it is known that the inner product of $\tilde{g}_1(t)$ and $\tilde{g}_2(t)$ is equal to that of $\tilde{G}_1(f)$ and $\tilde{G}_2(f)$, $i,j = 1,2$. Therefore, for signals that are essentially limited in duration and frequency, we have

$$\langle \tilde{G}_1, \tilde{G}_2 \rangle = NT_s^2 \langle \tilde{g}_1, \tilde{g}_2 \rangle. \tag{A.17}$$

Note that the left-hand side of (A.17) is phrased in terms of samples of the continuous Fourier transforms $\tilde{G}_i$, $i = 1,2$. There are situations where it is the discrete Fourier transforms that are of interest. For such cases, it may be possible to express (A.17) in terms of discrete Fourier transforms. Denote the discrete Fourier transform of $\tilde{g}_i$ by $\hat{G}_i$, $i = 1,2$, where

$$\hat{G}_i \left(\frac{l}{NT_s} \right) = T_s \sum_{k=0}^{N-1} \tilde{g}_i(kT_s) \exp \left(-j2\pi \frac{lk}{N} \right), \quad i = 1,2. \tag{A.18}$$

As indicated by (A.1), when the sampling rate is higher than the Nyquist rate, we have

$$\hat{G} \left(\frac{l}{NT_s} \right) = \tilde{G} \left(\frac{l}{NT_s} \right), \tag{A.19}$$

for $-1/2 \le l/N < 1/2$. Thus, the left-hand side of (A.17) can be written in terms of the discrete Fourier transforms of the signals instead of their continuous Fourier transforms, i.e.,

$$\langle \hat{G}_1, \hat{G}_2 \rangle = NT_s^2 \langle \tilde{g}_1, \tilde{g}_2 \rangle. \tag{A.20}$$

Appendix B

Frequency-domain Realization of the Discrete Time-Frequency Distribution Based Receivers

In the following we give the detailed derivation for the implementation of the time-frequency distribution based receivers in the frequency-domain.

B.1 Discrete Wigner-Ville distribution based receiver

B.1.1 Receiver based on the symmetrical form discrete Wigner-Ville distribution

Moyal's formula in the frequency-domain in terms of the symmetric form of the Wigner-Ville distribution, as defined in (2.107), is obtained by

$$
N^2 T_s^4 \sum_{k=0}^{N-1} \sum_{l=-N/2}^{N/2-1} \bar{W}_{\hat{S}_1}\left(kT_s, \frac{l}{NT_s}\right) \bar{W}_{\hat{S}_2}^*\left(kT_s, \frac{l}{NT_s}\right)
$$

$$
= \sum_{k=0}^{N-1} \sum_{l=-N/2}^{N/2-1} \left\{ \sum_{p=-N/2}^{N/2-1} \hat{S}_1\left(\frac{l+p}{NT_s}\right) \hat{S}_1^*\left(\frac{l-p}{NT_s}\right) \exp\left(j2\pi\frac{pk}{N}\right) \right\}
$$

$$
\cdot \left\{ \sum_{q=-N/2}^{N/2-1} \hat{S}_2\left(\frac{l+q}{NT_s}\right) \hat{S}_2^*\left(\frac{l-q}{NT_s}\right) \exp\left(j2\pi\frac{qk}{N}\right) \right\}^*
$$

$$
= N \sum_{l=-N/2}^{N/2-1} \sum_{p=-N/2}^{N/2-1} \hat{S}_1\left(\frac{l+p}{NT_s}\right) \hat{S}_1^*\left(\frac{l-p}{NT_s}\right) \hat{S}_2^*\left(\frac{l+p}{NT_s}\right) \hat{S}_2\left(\frac{l-p}{NT_s}\right) \tag{B.1}
$$

where Poisson's sum formula was used. When the sampling rate is at least twice the signal Nyquist rate, we have

$$\sum_{l=-N/2}^{N/2-1} \sum_{p=-N/2}^{N/2-1} \hat{S}_1\left(\frac{l+p}{NT_s}\right) \hat{S}_1^*\left(\frac{l-p}{NT_s}\right) \hat{S}_2^*\left(\frac{l+p}{NT_s}\right) \hat{S}_2\left(\frac{l-p}{NT_s}\right)$$

$$= \sum_{l=-N/2}^{N/2-1} \sum_{p=-N/2}^{N/2-1} \tilde{S}_1\left(\frac{l+p}{NT_s}\right) \tilde{S}_1^*\left(\frac{l-p}{NT_s}\right) \tilde{S}_2^*\left(\frac{l+p}{NT_s}\right) \tilde{S}_2\left(\frac{l-p}{NT_s}\right)$$

$$= \sum_{l=-\infty}^{\infty} \sum_{p=-\infty}^{\infty} \tilde{S}_1\left(\frac{l+p}{NT_s}\right) \tilde{S}_1^*\left(\frac{l-p}{NT_s}\right) \tilde{S}_2^*\left(\frac{l+p}{NT_s}\right) \tilde{S}_2\left(\frac{l-p}{NT_s}\right). \tag{B.2}$$

Following a similar manipulation as that used in deriving (3.6) and (3.7), we have

$$N^2 T_s^4 \sum_{k=0}^{N-1} \sum_{l=-N/2}^{N/2-1} \bar{W}_{\hat{S}_1}\left(kT_s, \frac{l}{NT_s}\right) \bar{W}_{\hat{S}_2}^*\left(kT_s, \frac{l}{NT_s}\right)$$

$$= N \sum_{m=-\infty}^{\infty} \sum_{n=-\infty}^{\infty} \left\{\tilde{S}_1\left(\frac{2m}{NT_s}\right) \tilde{S}_2^*\left(\frac{2m}{NT_s}\right)\right\} \left\{\tilde{S}_1\left(\frac{2n}{NT_s}\right) \tilde{S}_2^*\left(\frac{2n}{NT_s}\right)\right\}^*$$

$$+ N \sum_{m=-\infty}^{\infty} \sum_{n=-\infty}^{\infty} \left\{\tilde{S}_1\left(\frac{2m+1}{NT_s}\right) \tilde{S}_2^*\left(\frac{2m+1}{NT_s}\right)\right\} \left\{\tilde{S}_1\left(\frac{2n+1}{NT_s}\right) \tilde{S}_2^*\left(\frac{2n+1}{NT_s}\right)\right\}^*$$

$$= \frac{N}{2} \sum_{m=-\infty}^{\infty} \sum_{n=-\infty}^{\infty} \left\{\tilde{S}_1\left(\frac{m}{NT_s}\right) \tilde{S}_2^*\left(\frac{m}{NT_s}\right)\right\} \left\{\tilde{S}_1\left(\frac{n}{NT_s}\right) \tilde{S}_2^*\left(\frac{n}{NT_s}\right)\right\}^*$$

$$+ \frac{N}{2} \sum_{m=-\infty}^{\infty} \sum_{n=-\infty}^{\infty} (-1)^{m+n} \left\{\tilde{S}_1\left(\frac{m}{NT_s}\right) \tilde{S}_2^*\left(\frac{m}{NT_s}\right)\right\} \left\{\tilde{S}_1\left(\frac{n}{NT_s}\right) \tilde{S}_2^*\left(\frac{n}{NT_s}\right)\right\}^*. \tag{B.3}$$

Following the same approach as that used in deriving (3.8), we arrive at

$$N^2 T_s^4 \sum_{k=0}^{N-1} \sum_{l=-N/2}^{N/2-1} \bar{W}_{\hat{S}_1}\left(kT_s, \frac{l}{NT_s}\right) \bar{W}_{\hat{S}_2}^*\left(kT_s, \frac{l}{NT_s}\right)$$

$$= \frac{N}{2} \left|\langle \hat{\boldsymbol{S}}_1, \hat{\boldsymbol{S}}_2 \rangle\right|^2 + \frac{N}{2} \sum_{m=-\infty}^{\infty} \sum_{n=-\infty}^{\infty} \left\{\tilde{S}_1\left(\frac{m}{NT_s}\right) \left[\exp(jm\pi)\tilde{S}_2^*\left(\frac{m}{NT_s}\right)\right]\right\}$$

$$\cdot \left\{\tilde{S}_1\left(\frac{n}{NT_s}\right) \left[\exp(jn\pi)\tilde{S}_2^*\left(\frac{n}{NT_s}\right)\right]\right\}^*, \tag{B.4}$$

where (A.20) has been used. Denoting $\exp(j\pi f NT_s)\tilde{S}_2(f)$ by $\tilde{S}_{2_t}(f)$, we can rewrite (B.4) to obtain

$$\sum_{k=0}^{N-1} \sum_{l=-N/2}^{N/2-1} \bar{W}_{\hat{S}_1}\left(kT_s, \frac{l}{NT_s}\right) \bar{W}_{\hat{S}_2}^*\left(kT_s, \frac{l}{NT_s}\right)$$

$$= \frac{1}{2NT_s^4} \left|\langle \hat{\boldsymbol{S}}_1, \hat{\boldsymbol{S}}_2 \rangle\right|^2 + \frac{1}{2NT_s^4} \left|\langle \hat{\boldsymbol{S}}_1, \tilde{\boldsymbol{S}}_{2_t} \rangle\right|^2. \tag{B.5}$$

184

Then using (3.10) to rewrite the second term on the right-hand side of (B.5), we have

$$\sum_{k=0}^{N-1} \sum_{l=-N/2}^{N/2-1} \bar{W}_{\hat{S}_1}\left(kT_s, \frac{l}{NT_s}\right) \bar{W}_{\hat{S}_2}^*\left(kT_s, \frac{l}{NT_s}\right) = \frac{1}{2NT_s^4}\left|\langle \hat{S}_1, \hat{S}_2\rangle\right|^2 + \frac{N}{2}\left|\langle \tilde{s}_1, \tilde{s}_{2_t}\rangle\right|^2 \quad \text{(B.6)}$$

where $\tilde{s}_{2_t}$ denotes the time shifted signal samples, whose discrete Fourier transform is $\tilde{S}_{2_t}$. From (B.6) it is seen that the second term on the right-hand side of (B.6) reduces to zero when $\tilde{s}_1$ and $\tilde{s}_{2_t}$ are non-overlapping in time.

Denote with $\check{W}_{\hat{S}}(\cdot)$ the result of appending zeros in the frequency dimension to $\bar{W}_{\hat{S}}(\cdot)$ which was obtained with $N = 2T/T_s$. Let $N' = 4T/T_s = 2N$. For simplicity, let $\bar{W}_{\hat{S}}[kT_s, l/(N'T_s)]$ denote the symmetric form discrete Wigner-Ville distribution $\bar{W}_{\hat{S}}(\cdot)$ that was obtained with $N' = 4T/T_s$. With a similar procedure used in deriving (3.16) and (3.17), we have

$$4N^2T_s^4 \sum_{k=0}^{2N-1} \sum_{l=-N/2}^{N/2-1} \check{W}_{\hat{S}_1}\left(kT_s, \frac{l}{NT_s}\right) \check{W}_{\hat{S}_2}^*\left(kT_s, \frac{l}{NT_s}\right)$$

$$= 4N^2T_s^4 \sum_{k=0}^{2N-1} \sum_{l=-N/2}^{N/2-1} \bar{W}_{\hat{S}_1}\left(kT_s, \frac{2l}{N'T_s}\right) \bar{W}_{\hat{S}_2}^*\left(kT_s, \frac{2l}{N'T_s}\right)$$

$$= \sum_{k=0}^{2N-1} \sum_{l=-N/2}^{N/2-1} \left\{ \sum_{p=-N/2}^{N/2-1} \hat{S}_1\left(\frac{2l+p}{N'T_s}\right) \hat{S}_1^*\left(\frac{2l-p}{N'T_s}\right) \exp\left(-j2\pi\frac{pk}{N'}\right) \right\}$$

$$\cdot \left\{ \sum_{q=-N/2}^{N/2-1} \hat{S}_2\left(\frac{2l+q}{N'T_s}\right) \hat{S}_2^*\left(\frac{2l-q}{N'T_s}\right) \exp\left(-j2\pi\frac{qk}{N'}\right) \right\}^*$$

$$= 2N \sum_{l=-N/2}^{N/2-1} \sum_{p=-N/2}^{N/2-1} \hat{S}_1\left(\frac{2l+p}{N'T_s}\right) \hat{S}_1^*\left(\frac{2l-p}{N'T_s}\right) \hat{S}_2^*\left(\frac{2l+p}{N'T_s}\right) \hat{S}_2\left(\frac{2l-p}{N'T_s}\right)$$

$$= 2N \left|\langle \hat{S}_1, \hat{S}_2\rangle\right|^2. \quad \text{(B.7)}$$

Thus, the optimal statistic can be obtained by using $\check{W}_{\hat{S}}(\cdot)$ with $N = 2T/T_s$ and zero-padding instead of $\bar{W}_{\hat{S}}(\cdot)$ with $N = 4T/T_s$.

B.1.2 Receiver based on the general form discrete Wigner-Ville distribution

To develop a receiver based on $\hat{W}_{\hat{S}}(\cdot)$, we have

$$N^2 T_s^4 \sum_{k=0}^{N-1} \sum_{l=-N/2}^{N/2-1} \hat{W}_{\hat{S}_1}\left(kT_s, \frac{l}{NT_s}\right) \hat{W}_{\hat{S}_2}^*\left(kT_s, \frac{l}{NT_s}\right)$$

$$= \sum_{k=0}^{N-1} \sum_{l=-N/2}^{N/2-1} \left\{ \sum_{p=-N/2}^{N/2-1} \hat{S}_1\left(\frac{p}{NT_s}\right) \hat{S}_1^*\left(\frac{l-p}{NT_s}\right) \exp\left[j\pi\frac{(2p-l)k}{N}\right] \right\}$$

$$\cdot \left\{ \sum_{q=-N/2}^{N/2-1} \hat{S}_2\left(\frac{q}{NT_s}\right) \hat{S}_2^*\left(\frac{l-q}{NT_s}\right) \exp\left[j\pi\frac{(2q-l)k}{N}\right] \right\}^*$$

$$= \sum_{l=-N/2}^{N/2-1} \sum_{p=-N/2}^{N/2-1} \sum_{q=-N/2}^{N/2-1} \hat{S}_1\left(\frac{p}{NT_s}\right) \hat{S}_1^*\left(\frac{l-p}{NT_s}\right) \hat{S}_2^*\left(\frac{q}{NT_s}\right) \hat{S}_2\left(\frac{l-q}{NT_s}\right)$$

$$\cdot \sum_{k=0}^{N-1} \exp\left[j2\pi\frac{(p-q)k}{N}\right]$$

$$= N \sum_{l=-N/2}^{N/2-1} \sum_{p=-N/2}^{N/2-1} \hat{S}_1\left(\frac{p}{NT_s}\right) \hat{S}_1^*\left(\frac{l-p}{NT_s}\right) \hat{S}_2^*\left(\frac{p}{NT_s}\right) \hat{S}_2\left(\frac{l-p}{NT_s}\right)$$

$$= \frac{1}{NT_s^4} \left|\langle \hat{\boldsymbol{S}}_1, \hat{\boldsymbol{S}}_2 \rangle\right|^2 . \tag{B.8}$$

The above relationship shows that, when $1/T_s \geq 4B$, matched filtering $\hat{W}_{\hat{R}}(\cdot)$ with $\hat{W}_{\hat{S}_H}(\cdot)$ is equivalent to the processing of $|\langle \hat{\boldsymbol{R}}, \hat{\boldsymbol{S}}_H \rangle|^2$ as used in optimal detection and estimation.

B.2 Discrete Time-Frequency Correlation Function Based Receiver

The realization of a discrete time-frequency correlation function based receiver can be analyzed in a manner similar to that used in the time-domain analysis. First we derive the relationship between $\bar{W}_{\hat{S}_1}(\cdot)$ and $\bar{\phi}_{\hat{S}_1}(\cdot)$.

$$\sum_{k=0}^{N-1} \bar{W}_{\hat{S}_1}\left(kT_s, \frac{l}{NT_s}\right) \exp\left(-j2\pi\frac{mk}{N}\right)$$

$$= \frac{1}{NT_s^2} \sum_{k=0}^{N-1} \left\{ \sum_{p=-N/2}^{N/2-1} \hat{S}_1\left(\frac{l+p}{NT_s}\right) \hat{S}_1^*\left(\frac{l-p}{NT_s}\right) \exp\left(j2\pi\frac{pk}{N}\right) \right\} \exp\left(-j2\pi\frac{mk}{N}\right)$$

$$= \frac{1}{T_s^2} \hat{S}_1\left(\frac{l+m}{NT_s}\right) \hat{S}_1^*\left(\frac{l-m}{NT_s}\right) \tag{B.9}$$

where $-N/2 \leq m \leq N/2 - 1$. Hence,

$$\sum_{l=-N/2}^{N/2-1} \left\{ \sum_{k=0}^{N-1} \bar{W}_{\hat{S}_1}\left(kT_s, \frac{l}{NT_s}\right) \exp\left(-j2\pi\frac{mk}{N}\right) \right\} \exp\left(j2\pi\frac{ln}{N}\right)$$

$$= N \exp\left(-j2\pi\frac{mn}{N}\right) \bar{\phi}_{\hat{S}_1}\left(nT_s, \frac{m}{NT_s}\right). \tag{B.10}$$

It follows that

$$\sum_{k=-N/2}^{N/2-1} \sum_{l=-N/2}^{N/2-1} \bar{\phi}_{\hat{S}_1}\left(kT_s, \frac{l}{NT_s}\right) \bar{\phi}_{\hat{S}_2}^*\left(kT_s, \frac{l}{NT_s}\right)$$

$$= \sum_{k=-N/2}^{N/2-1} \sum_{l=-N/2}^{N/2-1} \left\{ \frac{1}{N} \sum_{n=0}^{N-1} \sum_{m=-N/2}^{N/2-1} \bar{W}_{\hat{S}_1}\left(nT_s, \frac{m}{NT_s}\right) \exp\left(-j2\pi\frac{ln}{N}\right) \right.$$

$$\left. \cdot \exp\left(j2\pi\frac{mk}{N}\right) \right\} \left\{ \frac{1}{N} \sum_{p=0}^{N-1} \sum_{q=-N/2}^{N/2-1} \bar{W}_{\hat{S}_2}\left(pT_s, \frac{q}{NT_s}\right) \exp\left(-j2\pi\frac{lp}{N}\right) \right.$$

$$\left. \cdot \exp\left(j2\pi\frac{qk}{N}\right) \right\}^*$$

$$= \sum_{n=0}^{N-1} \sum_{m=-N/2}^{N/2-1} \bar{W}_{\hat{S}_1}\left(nT_s, \frac{m}{NT_s}\right) \bar{W}_{\hat{S}_2}^*\left(nT_s, \frac{m}{NT_s}\right). \tag{B.11}$$

For the same reason as in the discussion on the time-domain realization, we conclude that the optimum receiver can be implemented in such a manner that it computes the inner product of $\bar{\phi}_{\hat{R}}(\cdot)$ with $\bar{\phi}_{\hat{S}_H}(\cdot)$ for $N \geq 4T/T_s$ and $1/T_s = 4B$.

Bibliography

[1] L. Cohen, "Time-Frequency Distributions - A Review," *Proc. IEEE*, vol. 77, no. 7, pp. 941-981, 1989.

[2] F. Hlawatsch and G. F. Boudreaux-Bartels, "Linear and Quadratic Time-Frequency Signal Representations," *IEEE SP Magazine*, April, 1992.

[3] P. M. Woodward, *Probability and information theory, with applications to radar*, Oxford: Pergamon Press, 1953.

[4] E. Wigner, " On the quantum correction for thermodynamic equilibrium," *Phys. Rev.*, vol. 40, pp. 749-759, 1932.

[5] H. L. Van Trees, *Detection, estimation, and modulation theory, Part I*, New York: Wiley, 1968.

[6] S. Kay and G. F. Boudreaux-Bartels, "On the optimality of the Wigner distribution for detection," in *Proc. IEEE Int. Conf. Acoust., Speech, Sig. Proc.*, 1985, pp. 1017-1020.

[7] G. F. Boudreaux-Bartels and T. W. Parks, "Time-varying filtering and signal estimation using Wigner distribution synthesis techniques," *IEEE Trans. Acoust., Speech, Signal Processing*, vol. ASSP-34, pp. 442-451, 1986.

[8] P. Flandrin, "A time-frequency formulation of optimum detection," *IEEE Trans. Acoust., Speech, Signal Processing*, vol. ASSP-36, pp. 1377-1384, 1988.

[9] B. Boashash and P. O'Shea, "A methodology for detection and classification of underwater acoustic signals using time-frequency analysis techniques," *IEEE Trans. Acoust., Speech, Signal Processing,* vol. ASSP-38, pp. 1829-1841, 1990.

[10] S. Barbarossa and A. Farina, "Detection and imaging of moving objects with synthetic aperture radar. Part 2: joint time-frequency analysis by Wigner-Ville distribution," *IEE Proc.-F,* vol. 139, no. 1, pp. 89-97, 1992.

[11] T. K. Bhattacharya and S. Haykin, "Application of time-frequency distributions for improved radar target detection," in *Proc. IEEE-SP Int. Symp. Time-frequency and time-scale analysis,* 1992, pp. 509-512.

[12] T. A. C. M. Claasen and W. F. G. Mecklenbrauker, "The Wigner distribution - a tool for time-frequency signal analysis," *Philips J. Res.,* vol. 35, part I: pp. 217-250; part II: pp. 276-300; part III: pp. 372-389, 1980.

[13] T. A. C. M. Claasen and W. F. G. Mecklenbrauker, "The aliasing problem in discrete-time Wigner distribution," *IEEE Trans. Acoust. Speech & Signal Processing,* vol. ASSP-31, pp.1067-1072, 1983.

[14] P. Peyrin and R. Prost, "A unified definition for the discrete-time, discrete-frequency, and discrete-time/frequency Wigner distributions," *IEEE Trans. Acoust., Speech, Signal Processing,* vol. ASSP-34, pp. 858-867, 1986.

[15] J. Jeong and W. J. Williams, "Alias-free generalized discrete-time time-frequency distributions," *IEEE Trans. Acoust., Speech, Signal Processing,* vol. ASSP-40, pp. 2757-2765, 1992.

[16] P. K. Varshney *et al., Analysis of ambiguity function for biststic radar,* Technical Report No. RL-TR-95-23, Rome Laboratory, 1995.

[17] R. Price and E. M. Hofstetter, "Bounds on the volume and height distributions of the ambiguity function," *IEEE Trans. Inform. Theory,* vol. IT-11, pp. 207-214, 1965.

[18] G. J. Iafrate, H. L. Grubin, and D. K. Ferry, "The Wigner Distribution Function," *Phys. Lett. A,* vol. 87, no. 4, pp. 145-148, 1982.

[19] M. Hillery, R. F. O'Connell, M. O. Scully, and E. P. Wigner, "Distribution Functions in Physics: Fundamentals," *Phys. Rep.,* vol. 106, no. 3, pp. 121-167, 1984.

[20] M. J. Bastiaans, "Use of the Wigner Distribution Function in Optical Problems," *Proc. Soc. Photo-Opt. Instrum. Eng.,* vol. 492, pp. 251-262, 1985.

[21] K. H. Brenner and A. W. Lohmann, "Wigner Distribution Function Display of Complex 1D Signals," *Opt. Commun.,* vol. 42, no. 5, pp. 310-314, 1982.

[22] B. V. K. V. Kumar, "Role of Wigner Distribution Function in Pattern-recognition," *Proc. Soc. Photo-Opt. Instrum. Eng.,* vol. 521, pp. 44-52, 1985.

[23] N. H. Morgan and A. S. Gevins, "Wigner Distributions of Human Event-related Brain Potentials," *IEEE Trans. Biomedical Eng.,* vol. BME-33, no. 1, pp. 66-70, 1986.

[24] B. Boashash and P. J. Black, "An efficient real-time implementation of the Wigner-Ville distribution," *IEEE Trans. Acoust., Speech, Signal Processing,* vol. ASSP-35, pp. 1611-1618, 1987.

[25] B. E. A. Saleh and N. S. Subotic, "Time-variant Filtering of Signals in the Mixed Time-Frequency Domain," *IEEE Trans. Acoust., Speech, Signal Processing,* vol. ASSP-33, pp. 1479-1485, 1985.

[26] D. Slepian, "On bandwidth," *Proc. IEEE,* vol. 64, pp. 292-300, 1976.

[27] I. S. Gradshteyn and I. M. Ryzhik, *Table of integrals, series, and products,* p. 718, San Diego, CA: Academic Press, 1980.

[28] A. V. Oppenheim, *Applications of digital signal processing,* Englewood Cliffs, NJ: Prentice-Hall, 1978.

[29] A. H. Nuttall, "Aliasing-free discrete-time Wigner distribution function and complex ambigutiy function," Naval Underwater Syst. Center, NUSC Tech. Rep., 8533, Apr. 1989.

[30] M. I. Skolnik, *Introduction to radar systems,* New York: McGraw-Hill, 1980.

[31] C. E. Cook and M. Bernfeld, *Radar signals,* New York: Academic Press, 1967.

[32] A. W. Rihaczek, *Principles of high-resolution radar*, New York: McGraw-Hill, 1969.

[33] S. Peleg and B. Porat, "Linear FM Signal Parameter Estimation from Discrete-Time Observations," *IEEE Trans. Aero. and Elec. Sys.,* vol. 27, no. 4, pp. 607-615, July 1991.

[34] A. V. Oppenheim and R. W. Schafer, *Discrete-time signal processing,* Englewood Cliffs, NJ: Prentice-Hall, 1989.

[35] M. F. Wagdy and W. Ng, "Validity of uniform quantization error model for sinusoidal signals without and with dither," *IEEE Trans. Instrum. Meas.* vol. IM-38, pp. 718-722, 1989.

[36] P. W. Wong, "Quantization noise, fixed-point multiplicative roundoff noise, and dithering," *IEEE Trans. Acoust., Speech, Signal Processing,* vol. ASSP-38, pp. 286-300, 1990.

[37] H. B. Kushner, M. Meisner, and A. V. Levy, " Almost uniformity of quantization errors," *IEEE Trans. Instrum. Meas.* vol. IM-40, pp. 682-687, 1991.

[38] J. D. Echard, "Quantization noise spectrum and radar MTI processing," *IEEE Tras. Aero. and Elec. Sys.,* vol. 28, no. 2, pp. 588-596, 1992.

[39] A. V. Oppenheim and C. J. Weinstein, "Effects of finite register length in digital filtering and fast Fourier transform," *Proc. IEEE,* vol. 60, no. 8, pp. 957-976, 1972.

MISSION

OF

ROME LABORATORY

Mission. The mission of Rome Laboratory is to advance the science and technologies of command, control, communications and intelligence and to transition them into systems to meet customer needs. To achieve this, Rome Lab:

    a. Conducts vigorous research, development and test programs in all applicable technologies;

    b. Transitions technology to current and future systems to improve operational capability, readiness, and supportability;

    c. Provides a full range of technical support to Air Force Materiel Command product centers and other Air Force organizations;

    d. Promotes transfer of technology to the private sector;

    e. Maintains leading edge technological expertise in the areas of surveillance, communications, command and control, intelligence, reliability science, electro-magnetic technology, photonics, signal processing, and computational science.

The thrust areas of technical competence include: Surveillance, Communications, Command and Control, Intelligence, Signal Processing, Computer Science and Technology, Electromagnetic Technology, Photonics and Reliability Sciences.